PMTurkeyCOLPEm Resource

From: Comar, Manny
Sent: Tuesday, April 29, 2014 3:04 PM
To: Jackson, Diane
Cc: Karas, Rebecca; Xi, Zuhan; Seber, Dogan; Stieve, Alice; Walsh, Lisa; Candelario, Luissette; Patel, Pravin; Thomas, Vaughn; Shams, Mohamed; Burkhart, Lawrence; Segala, John; Vega, Frankie; Comar, Manny
Subject: FW: L-2014-111 Revised Response to NRC Request for Additional Information Letter No. 040 (eRAI 6006) - Standard Review Plan Section 02.05.04 - Stability of Subsurface Materials and Foundations - Email 2 of 2
Attachments: L-2014-111 Signed 04-29-2014 Revised Response to NRC RAI Letter No. 040 (eRAI 6006) Part 2.pdf

4th and final e-mail

From: Burski, Raymond [mailto:RAYMOND.BURSKI@fpl.com]
Sent: Tuesday, April 29, 2014 11:02 AM
To: Comar, Manny
Cc: Franzone, Steve
Subject: L-2014-111 Revised Response to NRC Request for Additional Information Letter No. 040 (eRAI 6006) - Standard Review Plan Section 02.05.04 – Stability of Subsurface Materials and Foundations - Email 2 of 2

Manny,

Part 2 of signed letter L-2014-111

Ray Burski
NNP Licensing Engineer
Turkey Point Units 6&7 COLA Project
New Nuclear Projects
Florida Power & Light Company
700 Universe Blvd
Juno Beach, FL 33408

(O) 561-694-4496
(C) 504-909-6436

Hearing Identifier: TurkeyPoint_COL_Public
Email Number: 877

Mail Envelope Properties (377CB97DD54F0F4FAAC7E9FD88BCA6D00166D6972A26)

Subject: FW: L-2014-111 Revised Response to NRC Request for Additional Information Letter No. 040 (eRAI 6006) - Standard Review Plan Section 02.05.04 - Stability of Subsurface Materials and Foundations - Email 2 of 2
Sent Date: 4/29/2014 3:03:36 PM
Received Date: 4/29/2014 3:03:41 PM
From: Comar, Manny

Created By: Manny.Comar@nrc.gov

Recipients:
"Karas, Rebecca" <Rebecca.Karas@nrc.gov>
Tracking Status: None
"Xi, Zuhan" <Zuhan.Xi@nrc.gov>
Tracking Status: None
"Seber, Dogan" <Dogan.Seber@nrc.gov>
Tracking Status: None
"Stieve, Alice" <Alice.Stieve@nrc.gov>
Tracking Status: None
"Walsh, Lisa" <Lisa.Walsh@nrc.gov>
Tracking Status: None
"Candelario, Luissette" <Luissette.Candelario@nrc.gov>
Tracking Status: None
"Patel, Pravin" <Pravin.Patel@nrc.gov>
Tracking Status: None
"Thomas, Vaughn" <Vaughn.Thomas@nrc.gov>
Tracking Status: None
"Shams, Mohamed" <Mohamed.Shams@nrc.gov>
Tracking Status: None
"Burkhart, Lawrence" <Lawrence.Burkhart@nrc.gov>
Tracking Status: None
"Segala, John" <John.Segala@nrc.gov>
Tracking Status: None
"Vega, Frankie" <Frankie.Vega@nrc.gov>
Tracking Status: None
"Comar, Manny" <Manny.Comar@nrc.gov>
Tracking Status: None
"Jackson, Diane" <Diane.Jackson@nrc.gov>
Tracking Status: None

Post Office: HQCLSTR01.nrc.gov

Files	**Size**	**Date & Time**
MESSAGE	1297	4/29/2014 3:03:41 PM
L-2014-111 Signed 04-29-2014 Revised Response to NRC RAI Letter No. 040 (eRAI 6006) Part 2.pdf	4432972	

Options
Priority: Standard
Return Notification: No

Reply Requested: No
Sensitivity: Normal
Expiration Date:
Recipients Received:

~~Where,~~

~~q_t = the CPT corrected tip resistance~~

~~σ_v' = the effective overburden pressure at the depth of the CPT test interval~~

~~Recommended values of φ' derived from the different correlations/test methods (i.e., from SPT correlation, CPT correlation, and laboratory consolidated undrained triaxial testing), and for each stratum, are shown in Table 2.5.4-209. An effective friction value (φ') of 20 degrees is measured in triaxial testing on one tube sample of the lower Tamiami Formation sandy silt (Stratum 6) as presented in Table 2.5.4-208.~~

Triaxial testing was performed on a total of five samples from the Lower Tamiami Formation (including the sample from borehole B-630 of the initial investigation). A total of one sample from the Upper Tamiami Formation was tested and 15 from the Peace River Formation were tested.

The only sample tested from the Upper Tamiami Formation was taken from Borehole R-6-1b from the supplemental investigation, from El. −147.7 ft. to El. −149.8 ft.

Triaxial testing is summarized in Table 2.5.4-208.

The quantity of triaxial samples tested for the Lower Tamiami and the Peace River Formations is considered to be sufficient to characterize the shear strength parameters of these soils. For the Upper Tamiami Formation, the shear strength parameters are established by the analysis and corroborating data described below.

Cohesion of the Upper Tamiami Formation

The only triaxial test result for the Upper Tamiami Formation gives a cohesion value of zero. Atterberg testing on samples from the Upper Tamiami Formation indicates that the plasticity index (PI) of this material is lower than the PI for the Lower Tamiami (1.44 versus 3.53). Since the cohesion of the Lower Tamiami is relatively low (0.75 ksf), and considering the lower fines content of the Upper Tamiami, the effective cohesion of the Upper Tamiami is considered to be zero.

Friction Angle of the Upper Tamiami Formation

Correlated values established from standard penetration test (SPT) and cone penetrometer test (CPT) results are used to determine the effective friction angle φ' for this formation.

SPT Correlation for Friction Angle of the Upper Tamiami Formation

Average effective friction angle is determined using three correlations for the Upper Tamiami Formation.

SPT Correlation for Friction Angle – Method 1

The effective friction angle can be approximated using the following equation from Kulhawy and Mayne (Reference 292):

$$\varphi'_{tc} = \tan^{-1} \{[N / (12.2 + 20.3\ \sigma'_{vo}/p_a)]^{0.34}\}$$ **Equation 2.5.4-3a**

Where,

φ'_{tc}: = Triaxial Compression effective friction angle
σ'_{vo}: = Vertical effective stress (same units as p_a)
p_a: = Atmospheric pressure (i.e. 1 atm = 101.3 kPa or 2.1 ksf)
N: = Uncorrected SPT-N value

SPT Correlation for Friction Angle – Methods 2 and 3

The effective friction angle is approximated from the SPT N-values and relative densities using the correlation table below, obtained from Kulhawy and Mayne (Ref. 292):

SPT N-value	Relative Density	Approximate φ' (°)	
		Peck, Hansen, and Thornburn Approximation (Method 2)	Meyerhof Approximation (Method 3)
0 - 4	very loose	< 28	< 30
4 - 10	loose	28 - 30	30 - 35
10 - 30	medium	30 - 36	35 - 40
30 - 50	dense	36 - 41	40 - 45
> 50	very dense	> 41	> 45

CPT Correlation for Friction Angle

The effective friction angle is approximated from the CPT data using the correlation below from Mayne (2007) (Reference 293):

$$\varphi' = 29.5° B_q^{0.121}[0.256 + 0.336 B_q + \log Q]$$ **Equation 2.5.4-3b**

Where,

$$Q = \frac{q_t - \sigma_{v0}}{\sigma'_{v0}}$$ **Equation 2.5.4-3c**

$$B_q = \frac{u_2 - u}{q_t - \sigma_{v0}}$$ **Equation 2.5.4-3d**

The expression of φ' above is valid for values of $0.1 < B_q < 1.0$ and the results acceptable when are within 20 and 45 degrees. If $B_q < 0.1$, the following expression can be used, which is appropriate for clean sands.

$$\varphi' = 17.6^\circ + 11.0^\circ \log q_{t1}$$ **Equation 2.5.4-3e**

Where,

$$q_{t1} = \frac{q_t/\sigma_{atm}}{(\sigma'_{v0}/\sigma_{atm})^{0.5}}$$ **Equation 2.5.4-3f**

Summary for Upper Tamiami Formation

The table below presents the friction angle values for the Upper Tamiami Formation based on triaxial testing, CPT testing, and SPT testing. The average effective friction angle, 35°, obtained from correlations (SPT and CPT based) is in agreement with the result of one triaxial test.

Stratum	Effective Friction Angle: φ′(°)				
	Triaxial	SPT Correlation			CPT Correlation
		Method 1	Method 2	Method 3	
Upper Tamiami Formation	35 (1)	28	33	39	38

(1) **Based on one test result.**

Therefore, the friction angle of the Upper Tamiami Formation is recommended as 35 degrees.

Recommended values of φ' for each stratum are shown in Table 2.5.4-209.

The following references will be added FSAR Subsection 2.5.13 in a future revision:

292. Kulhawy, F.H., and P.W. Mayne, *Manual on Estimating Soil Properties for Foundation Design*, Electric Power Research Institute, Palo Alto, California, August 1990.

293. Mayne, P.W., *Cone Penetration Testing, A Synthesis of Highway Practice*, Transportation Research Board, 2007.

FSAR Table 2.5.4-208 will be replaced in a future revision:

Table 2.5.4-208
Summary of Triaxial Testing Results

Borehole	Sample	Elevation [ft]		c' (ksf)	φ' (°)	Conf Press 1 (psi)	Conf Press 2 (psi)	Conf Press 3 (psi)	E_{50} 1 (psi)	E_{50} 2 (psi)	E_{50} 3 (psi)	σ' (psi) (1)	y=mx+ b (2)	E_{50} at Effective Mean Stress at Mid Layer (ksf)	Engineering Layer
		From	To												
R-6-1b	ST-3	-147.7	-149.8	0.00	35	26.20	50.70	101.80	1903	6756	17186	41.63	4984	718	Upper Tamiami F.
B-630	UD 12	-180.4	–	1.70	20	34.70	69.40	104.20	2717	7058	20156	54.79	6302	907	Lower Tamiami F.
R-6-1b	ST-5	-162.5	-165.2	0.25	33	28.60	56.20	117.70	12317	14259	28104	50.18	15019	2,163	Lower Tamiami F.
R-6-1b	ST-11	-184.7	-187.4	0.46	31	32.70	62.90	127.40	9767	16451	43949	56.98	16946	2,440	Lower Tamiami F.
R-6-1b	ST-15	-199.5	-202.2	0.99	29	34.30	69.00	136.90	6815	19485	4458	61.51	11186	1,611	Lower Tamiami F.
R-7-1	ST-4	-189.9	-190.4	0.37	31	32.40	66.00	132.00	6778	15034	31813	58.29	13216	1,903	Lower Tamiami F.
R-6-1b	ST-22	-224.2	-226.3	0.69	35	37.80	77.40	–	6038	11010	–	66.33	9619	1,385	Peace River F.
R-6-1b	ST-31	-250.9	-253.3	0.08	33	45.10	89.00	172.60	6234	10253	20621	74.23	9169	1,320	Peace River F.
R-6-1b	ST-40	-279.8	-282.5	0.82	30	50.20	99.00	191.40	11361	21299	50563	82.79	19048	2,743	Peace River F.
R-6-1b	ST-46	-299.6	-302.3	0.38	33	51.40	103.10	204.80	6254	17212	34591	88.62	13658	1,967	Peace River F.
R-6-1b	ST-55	-325.9	-328.0	3.82	33	56.00	115.10	223.50	7430	10950	42573	96.27	12563	1,809	Peace River F.
R-6-1b	ST-66	-355.9	-358.6	1.12	33	62.40	123.10	241.70	6235	11395	22812	105.19	10021	1,443	Peace River F.
R-6-1b	ST-82	-401.0	-404.6	0.00	34	68.90	141.90	276.00	16006	22005	37844	118.61	20613	2,968	Peace River F.
R-7-1	ST-7	-231.8	-234.5	0.83	32	40.20	81.60	158.70	8509	13547	23277	68.71	12017	1,730	Peace River F.
R-7-1	ST-9	-254.8	-257.3	1.11	27	44.20	89.50	180.10	3002	15193	28240	75.45	10239	1,474	Peace River F.
R-7-1	ST-10	-265.8	-268.5	3.85	20	48.00	90.30	182.00	7926	15107	39592	78.72	14109	2,032	Peace River F.
R-7-1	ST-11	-276.8	-279.5	0.94	31	46.80	94.60	190.10	6924	23224	40022	81.96	17023	2,451	Peace River F.
R-7-1	ST-13	-297.8	-300.5	0.82	32	51.10	104.00	203.40	6483	24281	34612	88.15	16327	2,351	Peace River F.
R-7-1	ST-16	-319.5	-322.0	8.20	27	55.50	108.40	219.10	13804	16760	45636	94.51	18611	2,680	Peace River F.
R-7-1	ST-20	-353.8	-355.8	0.15	35	59.90	124.50	241.80	6759	7387	47221	104.53	11574	1,667	Peace River F.
R-7-1	ST-23	-389.8	-392.3	0.00	37	68.70	135.70	266.00	6796	13972	27451	115.21	11725	1,688	Peace River F.

(1) Effective mean stress (σ')

(2) m and b are linear correlation factors of Confining Pressure and E_{50} and x is the effective mean stress (σ')

FSAR Table 2.5.4-209 will be revised in a future revision:

Table 2.5.4-209 (Sheet 1 of 2)
Summary of Recommended Geotechnical Engineering Parameters

Stratum[a]	**1[a]**	**2**	**3**	**4**	**5**	**6**	**7**	**8**	**Fill**
Description	Muck	Miami	Key Largo	Ft. Thompson	Upper Tamiami	Lower Tamiami	Peace River	Arcadia	—
Elevation of top of layer (ft)	–1.2	–4.5	–26.7	–49.4	–115.1	–159.0	–215.2	–452.1	—
USCS symbol	ML, MH	GM, GP-GM, SM, SW-SM, SW, SP-SM	Limestone	Limestone	SM, SP-SM	ML	SM	Limestone	—
Total unit weight, γ (pcf)	80	125	136	139	120	120	120	130	130
Natural water content, w, (%)	>80	—	—	—	—	30	—	—	33
Fines content (%)	>60	18	—	—	28	62	16	—	15
Atterberg limits									
Liquid limit, LL	—	—	—	—	—	24	—	—	—
Plastic limit, PL	—	—	—	—	—	20	—	—	—
Plasticity index, PI	—	—	—	—	—	4	—	—	—
SPT N_{60}-value (blows/ft)	~0	20	—	—	40	32	75	—	30
Undrained properties									
Undrained shear strength, s_u (ksf)	—	—	—	—	—	4.0	—	—	—
Internal friction angle, φ, (deg)	—	—	—	—	—	—	—	—	—
Drained properties									
Effective cohesion, c' (ksf)	—	—	—	—	**0**	**0.75**	**1.52**	—	—
Effective friction angle, φ' (deg)	—	—	—	—	**35**	**29**	**31**	—	33
Average Rock core recovery (%)	—	—	83 to 96	41 to 98	—	—	—	63 to 100	—
Average RQD (%)	—	—	54 to 81	16 to 91	—	—	—	32 to 90	—
Unconfined compressive strength, U (psi)	—	200	1,500	2,000	—	—	—	100	—
Elastic modulus (high strain), E_H	—	630 ksi	2,600 ksi	1,500 ksi	1,500 ksf	2,500 ksf	2,700 ksf	980 ksi	1,100 ksf
Elastic modulus (low strain), E_L	—	950 ksi	2,600 ksi	1,500 ksi	19,700 ksf	25,750 ksf	27,400 ksf	980 ksi	9,100 ksf
Shear modulus (high strain), G_H	—	230 ksi	1,000 ksi	550 ksi	550 ksf	900 ksf	1,000 ksf	360 ksi	420 ksf

Table 2.5.4-209 (Sheet 2 of 2)
Summary of Recommended Geotechnical Engineering Parameters

Stratum[a]	1[a]	2	3	4	5	6	7	8	Fill
Shear modulus (low strain), G_L	—	350 ksi	1,000 ksi	550 ksi	7,300 ksf	9,500 ksf	10,150 ksf	360 ksi	3,500 ksf
Shear wave velocity, V_S, (ft/sec)	—	3,600	5,800	4,250	1,400	1,600	1,650	3,600	860
Compression wave velocity, V_C, (ft/sec)	—	8,000	11,000	8,700	2,900	3,300	3,450	7,850	1,600
Coefficient of sliding	—	0.6	0.7	0.7	0.4	0.3	—	—	0.5
Poisson's ratio, v′	—	0.37	0.31	0.34	0.35	0.35	0.35	0.36	0.3
Static earth pressure coefficients									
Active, K_a	—	0.3	—	—	0.27	0.5	—	—	0.3
At-rest, K_o	—	0.5	—	—	0.5	0.66	—	—	0.5

[a] Properties of Stratum 1 (muck) are not provided as this stratum was removed prior to construction.

ASSOCIATED ENCLOSURES:

None

NRC RAI Letter No. PTN-RAI-LTR-040

SRP Section: 02.05.04 - Stability of Subsurface Materials and Foundations

QUESTIONS from Geosciences and Geotechnical Engineering Branch 1 (RGS1)

NRC RAI Number: 02.05.04-8 (eRAI 6006)

Section 2.5.4.2.1.3.8 discusses the computation of effective (drained) friction angle in each sand stratum from corrected SPT, CPT and laboratory direct shear test results. However, previous discussion in the FSAR Section 2.5.4.2.1.3.2.1 indicates that the SPT data is suspect due to anomalies of sampling, only 4 CPT profiles are available for use and no direct shear testing results were provided. Correlations of these data to generate typical soil properties are expected to have a high degree of uncertainty. Laboratory tests of these material samples can be expected to be extremely disturbed considering the depth and behavior of materials. In accordance with NUREG-0800, Standard Review Plan, Chapter 2.5.4, "Stability of Subsurface Materials and Foundations," please justify the adequacy of the friction angle. Also, provide detailed information regarding your laboratory direct-shear test program and test results.

FPL RESPONSE:

The revised response to RAI 02.05.04-7 provides details on how the friction angles are determined. As stated in the revised response to RAI 02.05.04-7, during the supplemental geotechnical investigations, additional triaxial tests were performed on undisturbed soil samples from the upper Tamiami, lower Tamiami, and Peace River Formations. Detailed procedures and results are provided in FSAR 2.5.4 Reference 290.

For the lower Tamiami and Peace River formations, the total number of triaxial tests performed is 5 (including 1 test from the initial investigation) and 15, respectively. The number of triaxial tests for these formations is considered sufficient to estimate the effective friction angle.

Following the supplemental geotechnical investigations, the primary source of data used to interpret shear strength is the triaxial tests. The revised response to RAI 02.05.04-7 describes that SPT and CPT (locations and details for these tests are provided in the revised response to RAI 02.05.04-3) based correlations are also used to complement the triaxial test results and estimate the effective friction angles if the number of triaxial tests is not sufficient, as is the case in the upper Tamiami Formation.

No direct shear tests were performed.

This response is PLANT SPECIFIC.

References:

None

ASSOCIATED COLA REVISIONS:

Associated COL revisions are provided as part of the revised response to RAI 02.05.04-7.

ASSOCIATED ENCLOSURES:

None

NRC RAI Letter No. PTN-RAI-LTR-040

SRP Section: 02.05.04 - Stability of Subsurface Materials and Foundations

QUESTIONS from Geosciences and Geotechnical Engineering Branch 1 (RGS1)

NRC RAI Number: 02.05.04-9 (eRAI 6006)

In accordance with NUREG-0800, Standard Review Plan, Chapter 2.5.4, "Stability of Subsurface Materials and Foundations," please describe how shear and compressive wave velocity values are selected for design in Table 2.5.4- 209. Provide correlations for shear and compressive wave velocity between Table 2.5.4-209 and Table 2.5.4-215 to indicate what percentile is used for recommended values. Given the large deviations, especially on Key Largo and Fort Thompson formations (see Figures 2.5.4-218 and 2.5.4-19 and Table 2.5.4- 215), explain how the selected single value for each stratum statistically reflects the entire layer.

FPL RESPONSE:

The recommended shear wave velocities (V_s) provided in the revised FSAR Table 2.5.4-209 presented in the revised response to RAI 02.05.04-10 reflect the average velocity associated with each layer based on data obtained during the initial and supplemental investigations.

The shear wave velocities are used in the site response analysis and for determination of soil and rock stiffness.

As discussed in FSAR Subsection 2.5.2.5.2, 60 randomized V_s profiles were developed for the site response analyses, and as such, the site response analysis does not use a single V_s value within each layer. Revised FSAR Table 2.5.4-215 provided in the revised response to RAI 02.05.04-10 summarizes the average and standard deviation of shear and compressive wave velocities with depth.

Multiple methods (pressuremeter tests, triaxial tests, etc.), including but not limited to direct shear wave velocity measurements, were used to determine the rock and soil stiffness as described in revised responses to RAI 02.05.04-5 and RAI 02.05.04-6. The use of multiple methods addresses the inherent variability and the uncertainty involved in determining the stiffness value used for analysis, such as settlement analysis.

The remainder of this response is divided into two sections. The first section outlines the methodology followed to obtain the shear and compressive wave velocities presented in the revised FSAR Table 2.5.4-209 provided in the revised response to RAI 2.5.4-10. The second section provides evaluation of the site uniformity according to the DCD Revision 19 requirements.

<u>Methodology to Obtain Velocities in FSAR Table 2.5.4-209:</u>

The measured shear wave velocity (V_s) and compression wave velocity (V_p) values from each of the 12 suspension P-S velocity logging tests (includes data from both initial and supplemental investigations) are plotted against depth in revised FSAR Figures 2.5.4-218 and 2.5.4-219, updated in the revised response to RAI 02.05.04-03. Using these test results, V_s values were averaged over selected vertical depth intervals for the power block

area, and a mean V_s profile with low/high end boundaries (mean + standard deviation) was obtained, as shown in the revised FSAR Table 2.5.4-215 (updated in the revised response to RAI 02.05.04-10). The same approach was applied to the V_p measurements and the resulting mean V_p profile with low/high end boundaries is included in revised FSAR Table 2.5.4-215.

The elevation intervals for each formation are summarized as follows in Table 1. Note that all references to elevations in this RAI are consistent with those in Section 2.5.4 of FSAR, which are to the North American Vertical Datum of 1988 (NAVD 88).

Table 1
Top and Bottom Elevations for Rock and Soil Formations:

Formation	Top Elevation	Bottom Elevation
Miami Limestone	0	–30
Key Largo	–30	–50
Fort Thompson*	–50	–60
Fort Thompson	–60	–110
Upper Tamiami*	–110	–120
Upper Tamiami	–120	–170
Lower Tamiami	–170	–210
Peace River	–210	–450

* Interval is excluded from analysis. The mean V_S decreases by approximately 1200 ft/sec between –50 feet and –60 feet elevation and by approximately 2100 ft/sec between –110 feet and –120 feet elevation. The reason for such a decrease is the transition zone between the Key Largo and Fort Thompson and the transition between the Fort Thompson and upper Tamiami. For design purposes, it is reasonable to exclude the V_S measured in these transition zones for obtaining best estimate values.

As an example, a summary of the V_s model for the Key Largo Limestone is presented as follows in Table 2:

Table 2
Average Shear Wave Velocities for Key Largo Limestone

Elevation (ft)	V_s (ft/sec) Mean	V_s (ft/sec) Mean - Std. Dev.	V_s (ft/sec) Mean + Std. Dev.
-30 to -40	5770	4566	7575
-40 to -50	6751	4945	8104
Average	6260		

V_s readings were taken at 1.64-foot intervals in each boring, i.e., there were six readings per 10 feet depth. The depth interval between El. –30 feet and –40 feet in the above table is used here as an example to explain how the mean and standard deviations in the above table were derived. All 12 V_s borings covered this depth interval. Using the 12 V_s readings, a mean V_s value with plus/minus standard deviation was computed and was assigned at each 1.64-foot interval. By averaging the 6 mean V_s values that fall in the 10-foot increment from El. –30 feet to –40 feet, the mean V_s of 5770 feet per second (ft/sec) was obtained.

The minimum of the 6 mean minus standard deviation V_s values within the 10 foot layer was assigned as the low end V_s boundary (4566 ft/sec), whereas the maximum of the 6 mean plus standard deviation V_s values within the 10 foot layer is assigned as the high end V_s boundary (7575 ft/sec). The mean V_s of 6260 ft/sec for the Key Largo Limestone was computed by taking the average of these two mean V_s values, each corresponding to a 10-foot vertical depth interval.

A best estimate (BE) V_s, rounded down to the nearest multiple of 50, of 6250 ft/sec is recommended as shown in revised FSAR Table 2.5.4-209 (updated in the revised response to RAI 02.05.04-10). In the muck layer and in deeper strata (part of the Peace River Formation and all of the Arcadia Formation), where only one boring had measurements, the standard deviation was not computed because there was only a single V_s value measured at each 1.64-foot interval. In addition, for the overlying muck there was only one measurement in the entire layer. Therefore, this measurement is given as the layer average for V_s and V_p.

As mentioned earlier, for the Fort Thompson Formation, the V_s measurements were averaged between El. –60 feet and –110 feet. The top of the Fort Thompson Formation is at El. –49.4 feet and the bottom is at El. –115.4 feet. The mean V_s decreases by approximately 1200 ft/sec between –50 feet and –60 feet elevation and by approximately 2100 ft/sec between –110 feet and –120 feet elevation. The reason for such a decrease is the transition zone between the Key Largo and Fort Thompson and the transition between the Fort Thompson and upper Tamiami. For design purposes, it is reasonable to exclude the V_s measured in these transition zones for obtaining BE values.

The Poisson's ratios (ν) derived from the 12 P-S suspension velocity logs were analyzed using the layer averages as determined through the process explained above. Table 4-11 of FSAR 2.5.4. Reference 217 presents the values of ν in the range of 0.24 and 0.45 for limestone. We recommend using ν values equal to 0.37 for the Miami Limestone, 0.30 for the Key Largo Limestone, and 0.34 for the Fort Thompson Formation. These values are layer averages as obtained from P-S Suspension logs.

BE values for ν in rock and V_s, V_p for all formations, are presented in FSAR Table 2.5.4-209 (updated in the revised response to RAI 02.05.04-05 and RAI 02.05.04-10, respectively).

Uniformity Requirements as Provided in DCD Revision 19:

In Table 2-1 of AP1000 DCD, the "Lateral Variability" item reads:

> *Soils supporting the nuclear island should not have extreme variations in subgrade stiffness. This may be demonstrated by one of the following:*
>
> 1. *Soils supporting the nuclear island are uniform in accordance with Regulatory Guide 1.132 if the geologic and stratigraphic features at depths less than 120 feet below grade can be correlated from one boring or sounding location to the next with relatively smooth variations in thicknesses or properties of the geologic units, or*
> 2. *Site-specific assessment of subsurface conditions demonstrates that the bearing pressures below the nuclear island do not exceed 120% of those from the generic analyses of the nuclear island at a uniform site, or*
> 3. *Site-specific analysis of the nuclear island basemat demonstrates that the site-specific demand is within the capacity of the basemat.*

The following is an evaluation in terms of both stratigraphic uniformity and bearing pressure uniformity as defined in the first and second items in Table 2-1 of AP1000 DCD.

Stratigraphic Uniformity:

The calculated dip is less than 5 degrees in 95 percent of layer interfaces between adjacent borings, as shown in the cross sections in revised FSAR Figures 2.5.4-203 through 2.5.4-208 (updated in the revised response to RAI 02.05.04-03). In four places, the interfaces dip is between 5 degrees and 10 degrees at the top and bottom of the upper Tamiami layer. In one place, between borings B-718 and B-710, on Section A-A' (revised FSAR Figure 2.5.4-206) the interface between the upper and lower Tamiami formations dips steeper than 20 degrees due to interpretation of the interface in adjacent borings.

The termination depth of B-718 is limited to 150.8 feet, and the true interface may not have been reached in this boring, since the site-wide approximate average depth of the upper and lower Tamiami interface is between depths of 167 feet and 168 feet. The other adjacent boring B-719 is also a shallow boring with a termination depth of 126.7 feet and does not reach the interface. A portion of the revised FSAR Figure 2.5.4-206, with the relevant borings, is shown in Figure 1. If B-718 and B-719 are not considered in the interpretation of this interface due to their shallow termination depths, all layer interfaces dip less than 20 degrees, with more than 95 percent of the layer interfaces between adjacent borings dipping less than 5 degrees.

As a result, geologic and stratigraphic features at depths less than 120 feet below grade can be correlated from one boring or sounding location to the next with relatively smooth variations in thicknesses.

.

Figure 1 Geotechnical Cross-Section A-A'

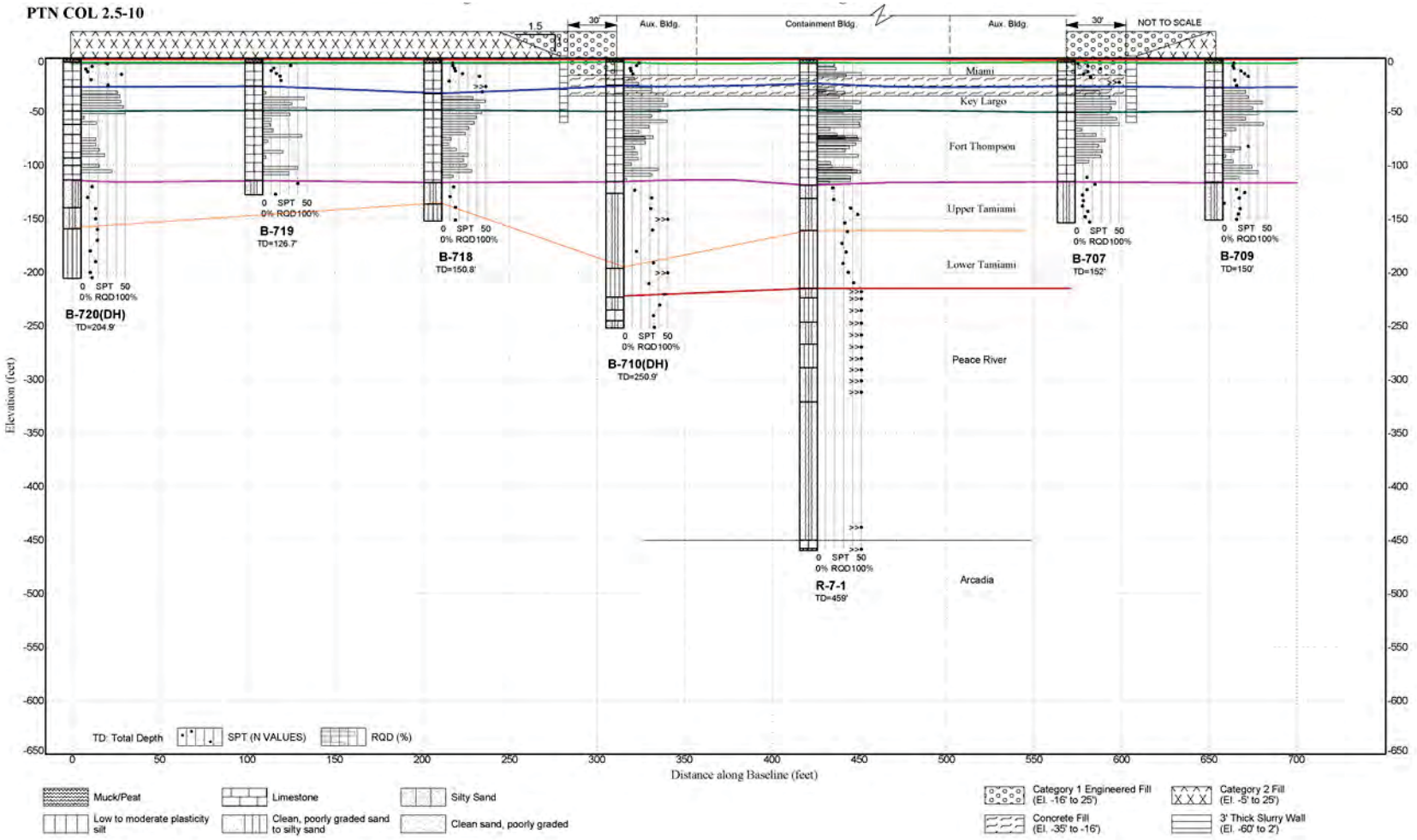

Bearing Pressure Uniformity:

To evaluate the bearing pressures for site-specific conditions, a two dimensional plane-strain PLAXIS 2D model is developed. The variability of the shear wave velocity and rock quality designation (RQD) are random in nature and do not have directional dependencies, as will be shown later in this response. Therefore, a 2D model is considered adequate.

Both a laterally uniform ground model and a laterally variable ground model are considered in the PLAXIS simulation. For the laterally uniform case, the BE stiffness for soil and rock strata are assigned for each stratum. For the laterally variable case, a worst-case scenario (extremely unlikely scenario) is considered, in which, half of the foundation rests on the softer soil/rock column and half of the foundation rests on the stiffer soil/rock column. The softer soil/rock column is assigned the lower bound (LB) parameters, whereas the stiffer soil/rock column is assigned the BE parameters. To avoid numerical issues with this contrast of stiffness, a transition zone (TZ) is assigned between the soft and stiff zones. The stiffness of the TZ is taken as the average of BE and LB stiffness for each stratum. The width of the transition zone is taken as one-third, one-fifth, and one-sixteenth of B = 160 feet, where B is the shorter foundation dimension, and these cases correspond to Case 2, 3, and 4, respectively, while Case 1 represents the laterally uniform case.

All cases involve constant layer thicknesses for each of the soil and rock strata. The foundation load is conservatively assumed as 9.2 kips per square foot (ksf). The layer thicknesses and the material properties are provided in Table 3. The soil/rock column underneath the foundation as well as the foundation are shown in Figure 2. All soil and rock layers are assumed to be Mohr-Coulomb materials.

The LB parameters are developed using two methodologies depending on the available data. If there are too few measurements, the LB is considered to be 16th percentile. Usually, a goodness-of-fit test is not performed for sample with size less than 5 (Reference 1), and this number (5) is adopted hereby as the quantitative criterion for determining the sufficiency of the sample size. If there are sufficient measurements, the minimum of the following four descriptors is used as the LB.

1. $\mu - \sigma$ where μ is sample mean and σ is sample standard deviation
2. 16th percentile
3. BE/(1+COV) where BE is the best estimated value, taken as the lower one of mean and median, and COV is coefficient of variation
4. $\exp(\ln(Median) - \sqrt{\ln(1 + COV^2)})$, which is analogous to the equation on Page 18 of the Standard Review Plan (SRP) 3.7.2

FSAR Table 2.5.4-221 presents the LB parameters. It is observed that the derived LB RMR (Rock Mass Rating) value for unfractured (FD1) Fort Thompson is lower than that for fractured (FD4) Fort Thompson. This may be against intuition. The reason is the variation of RMR for the FD1 Fort Thompson is greater than the variation of RMR for the FD4 Fort Thompson.

Table 3
Layer Thickness and Material Properties

Stratum	Thickness (ft)	γ (kcf)	c (ksf)	φ (°)	BE E (ksf)	TZ E (ksf)	LB E (ksf)
Concrete Fill	–	0.145	–	–	3.185E5		
Miami	22.3	0.137	6.2	56	3.42E4		
Key Largo	22.5	0.137	22.5	55	8.39E4	6.60E4	4.81E4
Fort Thompson	65.9	0.137	22.4	52	4.66E4	3.35E4	2.04E4
Upper Tamiami	51.2	0.119	0	35	1.15E3	9.27E2	7.04E2
Lower Tamiami	43.7	0.117	0.75	29	1.95E3	1.616E3	1.281E3
Peace River	241.7	0.121	1.52	31	2.70E3	2.193E3	1.685E3

Notes:
γ = unit weight
c = effective cohesion
φ = effective friction angle
E =Young's modulus

Figure 2 PLAXIS 2D Model, Soil, and Rock Column

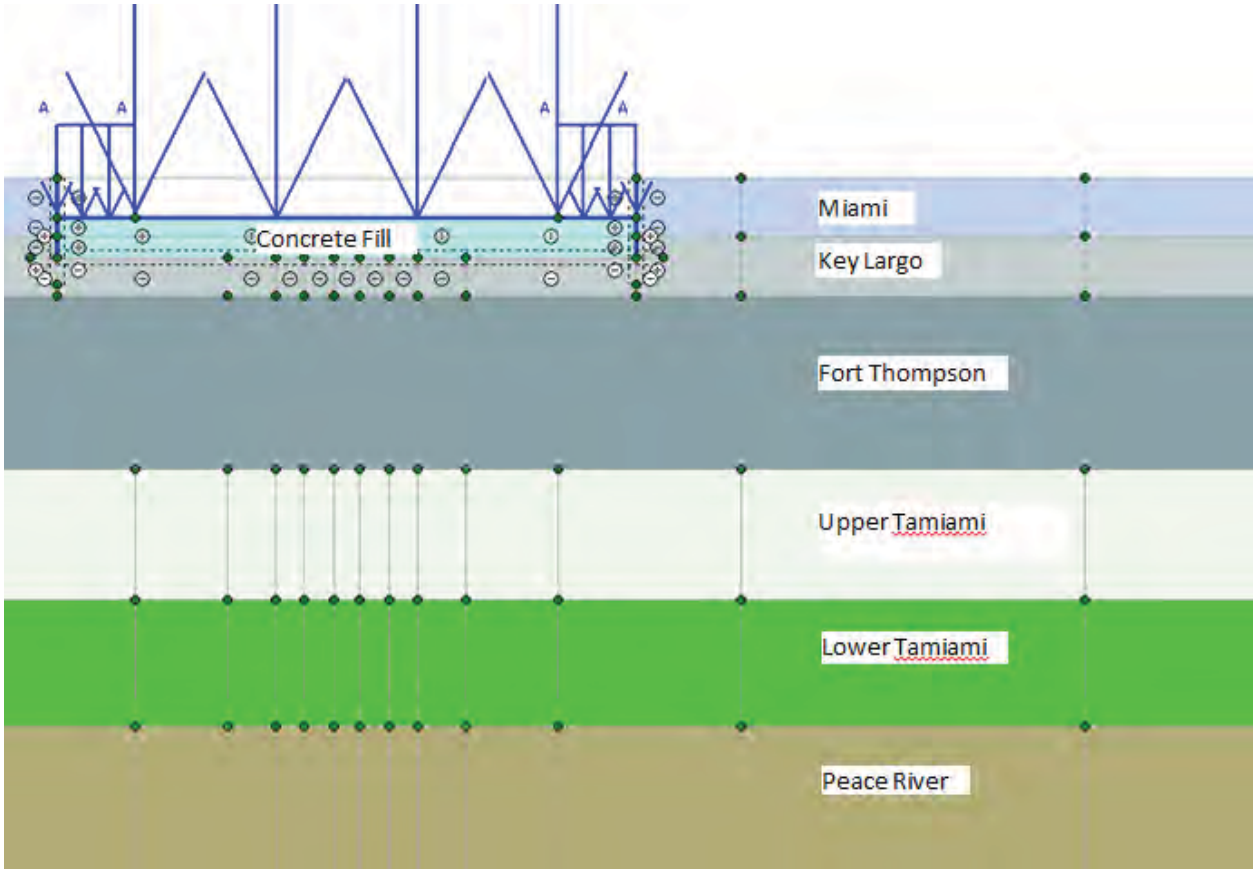

The bearing pressure distributions for Cases 1 through 4 are provided in Figure 3. The percent bearing pressure difference for Cases 2, 3, and 4, with respect to Case 1 (base case with laterally uniform foundation material) are presented in Figure 4. For all cases considered, the maximum bearing pressure difference is less than 5 percent. Therefore, the DCD Criterion 2 for lateral uniformity in AP1000 DCD as cited earlier is satisfied.

Figure 3 Bearing Pressure Distributions for the Cases 1 through 4

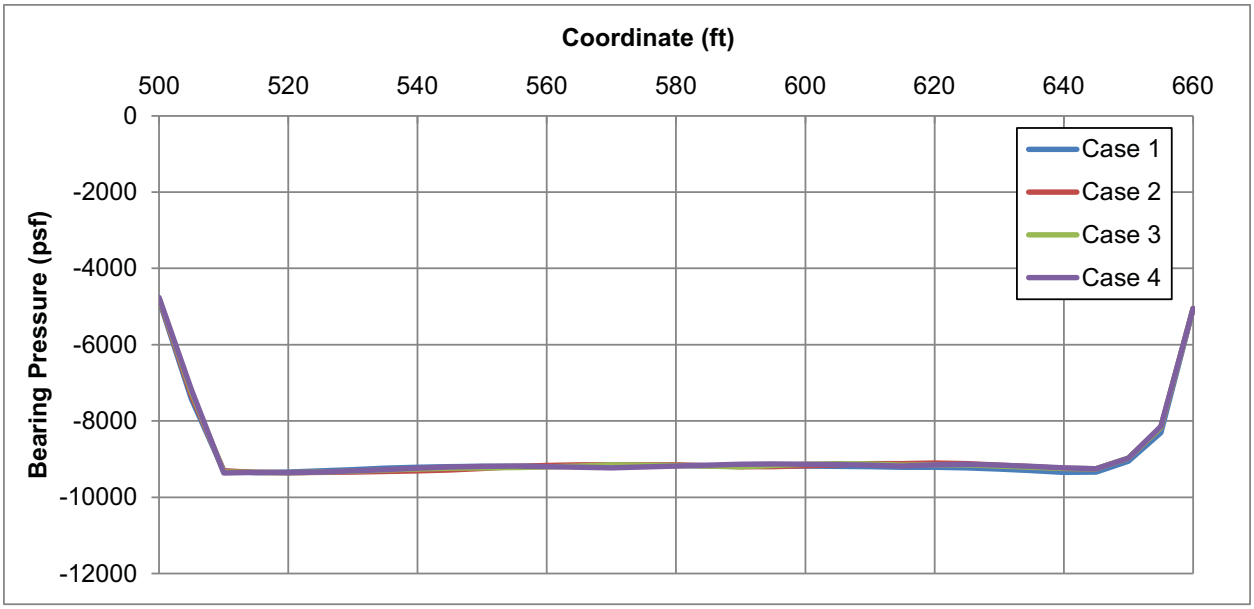

Figure 4 Percent Difference in Bearing Pressure Distribution of Cases 2, 3, and 4 relative to Case 1

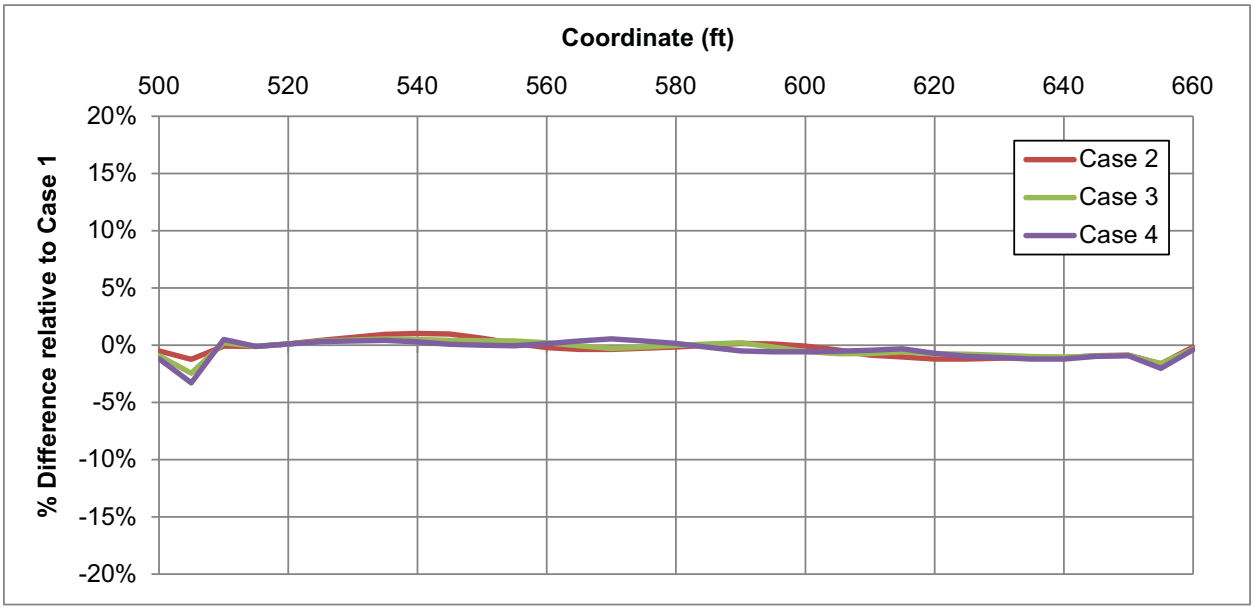

Conclusion for Uniformity:

In terms of both stratigraphic uniformity and bearing pressure uniformity, the Turkey Point Units 6 & 7 site meets the requirements given in Table 2-1 of the AP1000 DCD.

However, the variation in the shear wave velocity is still provided below for reference purposes.

Shear Wave Velocity Variability:

The Key Largo and Fort Thompson Limestone formations at the Turkey Point site consistently have V_s values well in excess of 2500 ft/sec. Shear wave velocities are evaluated and no extreme variations are found. However, V_s within the Fort Thompson Formation does vary from the average velocity in the stratum by more than 20 percent. Note that a variation of more than 20 percent from the mean value of V_s within a layer does not necessarily indicate a deviation from the DCD (please see the previous section on uniformity).

The coefficient of variation (COV) in V_s for each stratum (inclusive of both initial and supplemental investigations) is listed in Table 4. Note the Mean V_s values are taken over the entire data set in each stratum and these values are slightly different from those reported in FSAR Table 2.5.4-209.

To determine if the V_s variability is systematic in one or both of the horizontal directions, average shear wave velocities from different borings are compared. Figures 5 and 6 show the selected borings for Units 6 & 7 and the variation of shear wave velocity in different locations of Units 6 & 7, respectively. According to Figures 5 and 6, the variation in shear wave velocity does not depend on the horizontal location. The horizontal variability is instead random in nature.

Similar trend is shown for the RQD variation in the revised response to RAI 02.05.04-16. These trends are also presented in Figures 7 and 8.

Table 4

COV in V_s for Each Stratum

Stratum	Mean V_s (ft/s)	Std. Dev. of V_s (ft/s)	COV
Miami	3357.8	1022.7	0.30
Key Largo	6089.5	1105.9	0.18
Fort Thompson	4598.9	1275.6	0.28
Upper Tamiami	1538.0	343.1	0.22
Lower Tamiami	1718.0	212.5	0.12
Peace River	1712.9	360.3	0.21

Figure 5 Shear Wave Velocity Averages by Boring and Layer in Unit 6

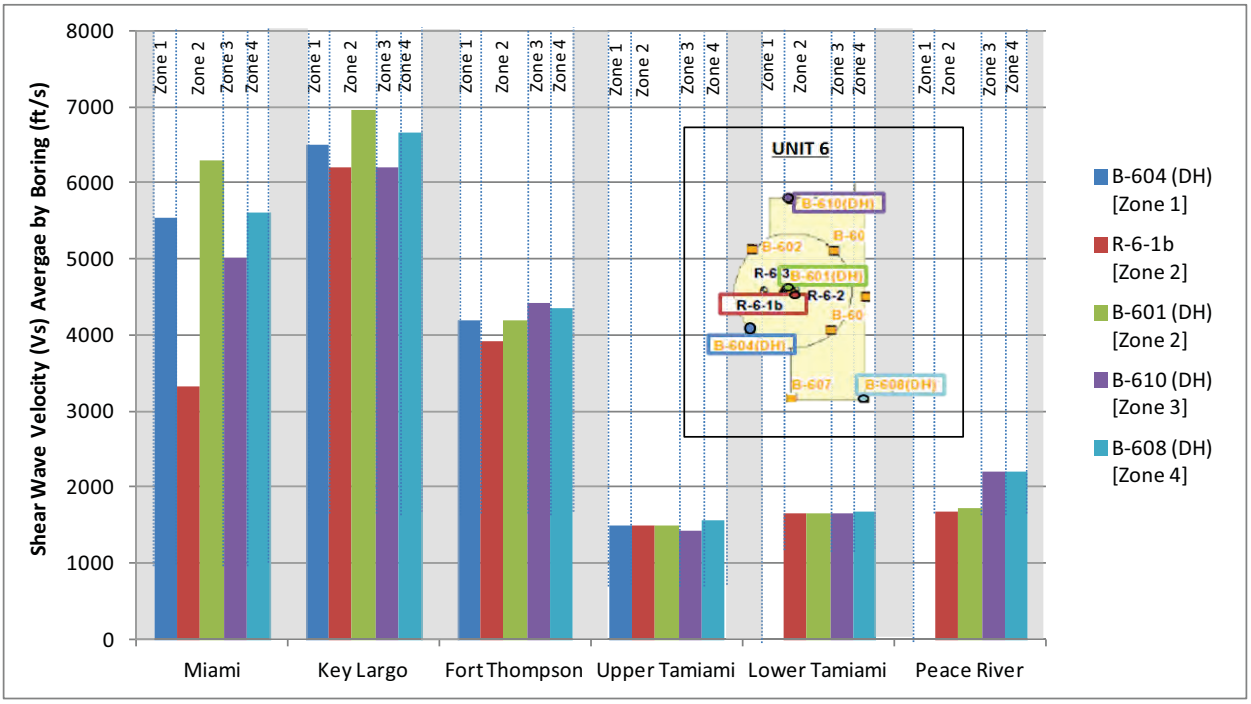

Figure 6 Shear Wave Velocity Averages by Boring and Layer in Unit 7

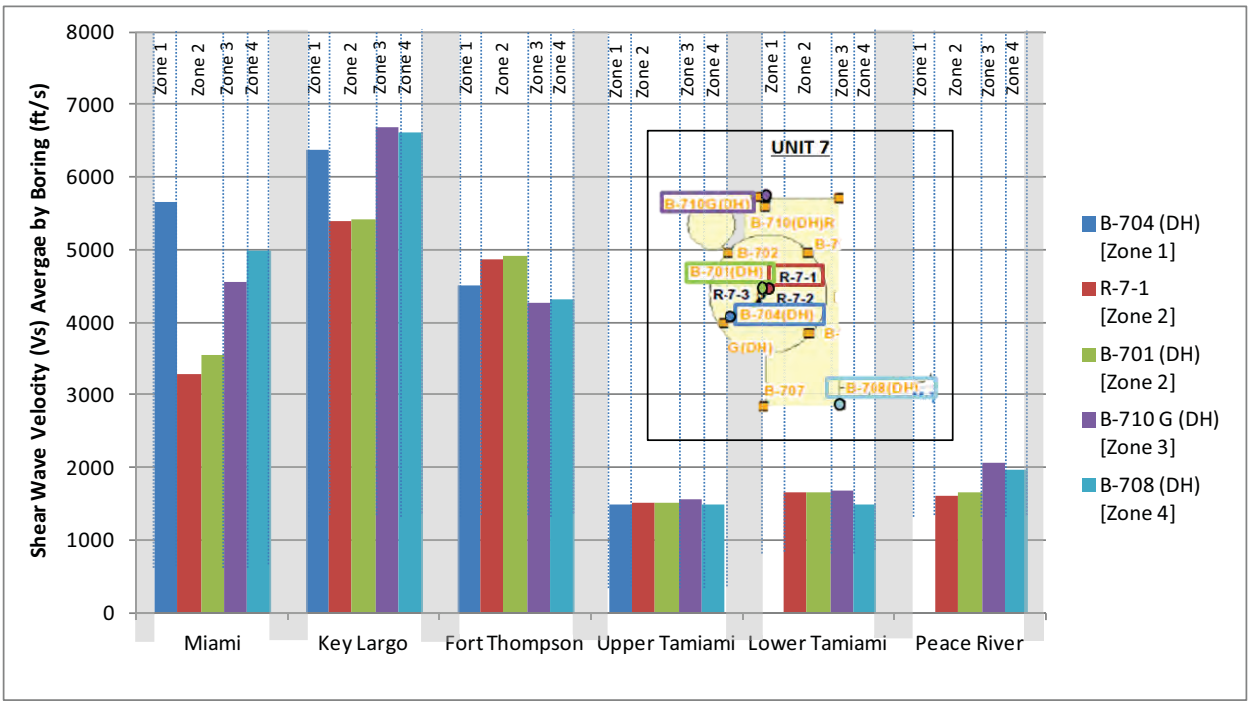

Figure 7 RQD Variation from South to North

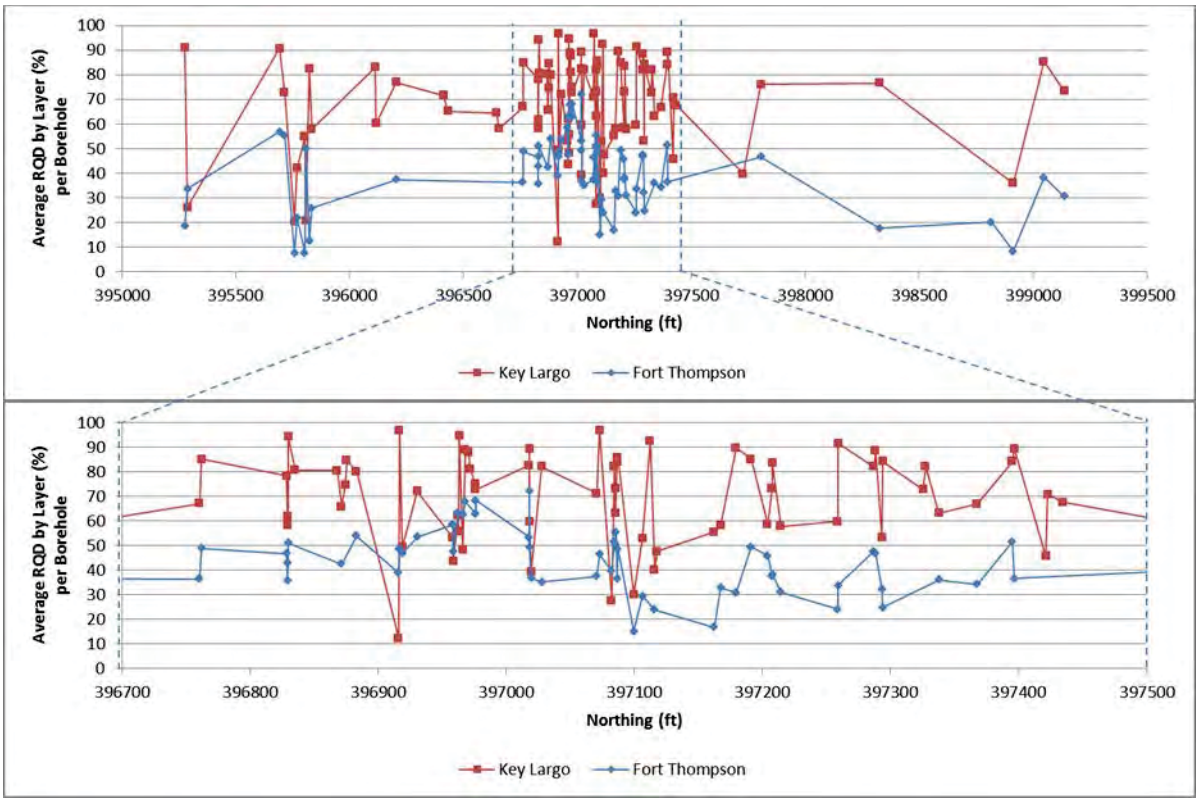

Figure 8 RQD Variation from West to East

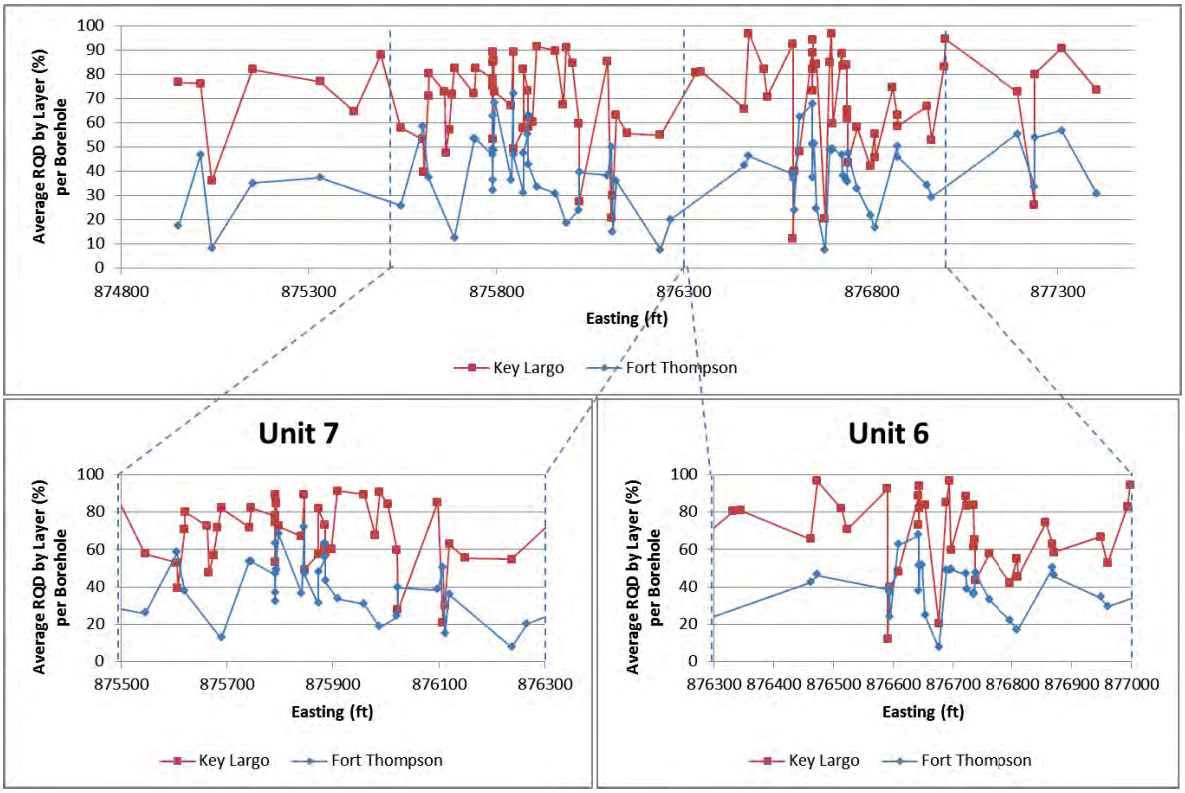

This response is PLANT SPECIFIC.

References:

1. Ang, A.H-S., W.H. Tang, *Probability Concepts in Engineering: Emphasis on Applications to Civil and Environmental Engineering*, 2nd Edition, John Wiley & Sons Inc., New Jersey, 2007.

ASSOCIATED COLA REVISIONS:

The third paragraph of FSAR Subsection 2.5.4.10.1 will be revised in a future revision as follows:

For foundation analysis purposes, the specific subsurface conditions/profiles associated with each of the Seismic Category I structures at both Unit 6 and Unit 7 are developed as shown on Figures 2.5.4-203 through 2.5.4-208. Associated strata depths and elevations for each of these structure-specific conditions/profiles are shown in Table 2.5.4-201. ~~As can be seen from these profiles and additional information in Subsection 2.5.4.2~~**As described in Subsection 2.5.4.10.7**, the subsurface conditions in the upper 120 feet can be considered uniform in accordance with RG 1.132, therefore, there is no extreme lateral variability in the subgrade stiffness.

A new Subsection will be added after Subsection 2.5.4.10.6 in a future revision as follows::

2.5.4.10.7 Lateral Variability

In Table 2-1 of the DCD, the "Lateral Variability" item reads:

> ***Soils supporting the nuclear island should not have extreme variations in subgrade stiffness. This may be demonstrated by one of the following:***
>
> 1. ***Soils supporting the nuclear island are uniform in accordance with Regulatory Guide 1.132 if the geologic and stratigraphic features at depths less than 120 feet below grade can be correlated from one boring or sounding location to the next with relatively smooth variations in thicknesses or properties of the geologic units, or***
> 2. ***Site-specific assessment of subsurface conditions demonstrates that the bearing pressures below the nuclear island do not exceed 120% of those from the generic analyses of the nuclear island at a uniform site, or***
> 3. ***Site-specific analysis of the nuclear island basemat demonstrates that the site-specific demand is within the capacity of the basemat.***

The following is an evaluation in terms of both stratigraphic uniformity and bearing pressure uniformity as defined in the first and second items of Table 2-1 of the DCD.

Following the AP1000 DCD criterion, the dip angles for all the layers along some predefined sections in Figure 2.5.4-209 are calculated using the layering and boring coordinates information. The calculated dip is less than 5 degrees in 95 percent of layer interfaces between adjacent borings (Figures 2.5.4-203 through 2.5.4-208). In four places, the interfaces dip between 5 degrees and 10 degrees, at the top and bottom of the upper Tamiami layer. In one place, between borings B-718 and B-710, on Section A-A' (Figure 2.5.4-206) the interface between the upper and lower Tamiami formations dips steeper than 20 degrees due to interpretation of the interface in adjacent borings. The termination depth of B-718 is limited to 150.8 feet, and the true interface may not have been reached in this boring. The other adjacent boring B-719 is also shallow boring with a termination depth of 126.7 feet, and does not reach the interface. If B-718 and B-719 are not considered in the interpretation of this interface due to their shallow termination depths, all layer interfaces dip less than 20 degrees and satisfy the AP1000 DCD dip criteria, with more than 95 of the layer interfaces between adjacent borings dipping less than 5 degrees.

As a result, geologic and stratigraphic features at depths less than 120 feet below grade can be correlated from one boring or sounding location to the next with relatively smooth variations in thicknesses.

To evaluate the bearing pressures for site-specific conditions, a two dimensional plane-strain PLAXIS 2D model is developed. Both a laterally uniform ground model and a laterally variable ground model are considered in the PLAXIS simulation. For the laterally uniform case, the best estimate (BE) stiffness for soil and rock strata are

assigned for each stratum. For the laterally variable case, a worst-case scenario (extremely unlikely scenario) is considered, in which, half of the foundation rests on the softer soil/rock column and half of the foundation rests on stiffer soil/rock column. The softer soil/rock column is assigned the lower bound (LB) parameters (as defined in Subsection 2.5.4.2.1.3.17), whereas the stiffer soil-rock column is assigned the BE parameters. To avoid numerical issues with this contrast of stiffness, a transition zone is assigned between the soft and stiff zones. The stiffness of the transition zone is taken as the average of BE and LB stiffness for each stratum. The width of the transition zone is taken as one-third, one-fifth, and one-sixteenth of B = 160 feet, where B is the shorter foundation dimension. For all cases considered, the maximum bearing pressure difference is less than 5 percent. Therefore, the DCD Criterion for lateral uniformity as cited earlier is satisfied.

A new Subsection will be added after Subsection 2.5.4.2.1.3.16 in a future revision as follows:

2.5.4.2.1.3.19 Lower Bound Soil/Rock Parameters

For sensitivity cases regarding settlement, bearing capacity and bearing pressure uniformity sensitivity analyses, lower bound parameters for soil and rock formations are developed using two methodologies depending on the available data. If there are too few measurements, the LB is considered to be 16th percentile. Usually, a goodness-of-fit test is not performed for sample with size less than 5 (Reference 318), and this number (5) is adopted hereby as the quantitative criterion for determining the sufficiency of the sample size. If there are sufficient measurements, the minimum of the following four descriptors is used as the LB.

1. **$\mu - \sigma$ where μ is sample mean and σ is sample standard deviation**
2. **16th percentile**
3. **BE/(1+COV) where BE is the best estimate or design value, the lower one of mean and median, as given in Table 2.5.4-209, and COV is coefficient of variation**
4. **$\exp(\ln(\text{Median}) - \sqrt{\ln(1+\text{COV}^2)})$, which is analogous to the equation on Page 18 of the Standard Review Plan (SRP) 3.7.2**

The following reference will be added FSAR Subsection 2.5.13 in a future revision:

318. Ang, A.H-S., W.H. Tang, *Probability Concepts in Engineering: Emphasis on Applications to Civil and environmental Engineering*, 2nd Edition, John Wiley & Sons Inc., New Jersey, 2007.

FSAR Table 2.5.4-221 will be added in a future revision as follows:

Table 2.5.4-221
Recommended Lower Bound Properties

Strata		Unit Weight (kcf)	Cohesion c' (ksf)	Friction Angle (degrees)	E (ksf)
Unfractured (FD1)	Key Largo	0.125	7.95	55	48,102
	Fort Thompson	0.125	2.59	48	20,483
Fractured (FD4)	Key Largo	0.125	2.38	55	18,100
	Fort Thompson	0.125	3.60	50	20,483
Upper Tamiami		0.116	0.00	34	704
Lower Tamiami		0.115	0.25	28	1,281
Peace River		0.117	0.00	33	1,685
Arcadia		0.125	0.00	33	108,442

ASSOCIATED ENCLOSURES:

None

NRC RAI Letter No. PTN-RAI-LTR-040

SRP Section: 02.05.04 - Stability of Subsurface Materials and Foundations

QUESTIONS from Geosciences and Geotechnical Engineering Branch 1 (RGS1)

NRC RAI Number: 02.05.04-10 (eRAI 6006)

FSAR Figures 203 through 209 indicate one boring for each of the two Units extending to a depth of about 450'. Most other borings taken at the site extend to depths of only about 150'. Figure 2.5.4-220 presents information on shear wave velocity, including best estimate (BE) and upper/lower bound (UB/LB) values down to a depth of about 600'. In accordance with NUREG-0800, Standard Review Plan, Chapter 2.5.4, "Stability of Subsurface Materials and Foundations," please indicate how you estimated variations in shear wave velocity based on only two readings over the deeper portion of the profile.

FPL RESPONSE:

Two additional P-S Suspension soundings were performed during the supplemental field investigation program in 2013, as outlined in the revised Response to RAI 02.05.04-3. The locations of these soundings, R-6-1b and R-7-1, are near B-601(DH) and B-701(DH), respectively (see Figure 1 of the revised response to RAI 02.05.04-3).

From the initial (Reference 1) and supplemental (Reference 2) investigations, shear wave velocity (V_s) readings through P-S Suspension soundings were taken in 12 locations as follows (see Figure 1 of the revised response to RAI 02.05.04-3):

- Two borings (B-604[DH] and B-704G[DH]) to a depth of 150 feet
- Two borings (B-620[DH] and B-720G[DH]) to a depth of 200 feet
- Four borings (B-608[DH], B-610[DH], B-708[DH], and B-710G[DH]) to a depth of 250 feet
- One boring (B-601[DH]) to a depth of 400 feet
- One boring (R-7-1) to a depth of 440 feet
- One boring (R-6-1b) to a depth of 450 feet
- One boring (B-701[DH]) to a depth of 600 feet

Approximate depths, descriptions, and the number of P-S Suspension soundings for deeper formations including upper Tamiami, lower Tamiami, Peace River, and Arcadia formations are provided in Table 1.

Table 1
Number of P-S Suspension Loggings in Deeper Formations

Formation	Predominant Material Type	Approximate Top Depth (ft) [1]	Approximate Bottom Depth (ft) [1]	Number of P-S Suspension Loggings	Remarks
Upper Tamiami	Dense silty sand	115	167	12	- two V_s profiles down to 150 feet
Lower Tamiami	Stiff to hard sandy silt	167	218	10	- two V_s profiles down to 200 feet
Peace River	Very dense silty sand	218	455	4	- one V_s profile down to 400 feet - one V_s profile down to 440 feet - two V_s profiles down to the base of the Peace River formation
Arcadia	Limestone	455	No boring available [2]	1	- one V_s profile down to 600 feet

[1] Based on approximate surface elevation of 0 feet.

[2] None of the borings reached the bottom depth of the Arcadia Formation.

Figure 1 and the revised FSAR Figure 2.5.4-220 presents the mean shear wave velocity (V_s) profile with upper and lower bounds (calculated as mean ± standard deviation) as a function of depth for all 12 P-S Suspension velocity data sets.

For the upper and lower Tamiami formations, V_s profiles are obtained from at least ten P-S Suspension soundings, which is an adequate sample size from which to estimate a mean and standard deviation.

For the deeper portion of the soil profile, i.e., Peace River Formation, the mean shear wave velocity and its variation are estimated based on four V_s profiles (Table 1). The estimations of the mean V_s and its corresponding variations based on four V_s profiles within the Peace River Formation are sufficient for soil modeling and analysis purposes.

Additionally, V_s measurements beyond the required investigation depth of approximately 450 feet (required investigation depth is per RG 1.132, assuming unit weight of 0.13 kcf, and considering the embedment depth) were taken for the Arcadia Formation at boring B-701(DH) down to a depth of 600 feet. The standard deviation is not computed for the Arcadia Formation in the original FSAR Figure 2.5.4-220, the updated FSAR Figure 2.5.4-220, or Figure 1, since only one P-S Suspension sounding is available below 440 feet depth.

.

Figure 1 Plot of Recommended Shear Wave Velocity with Elevation

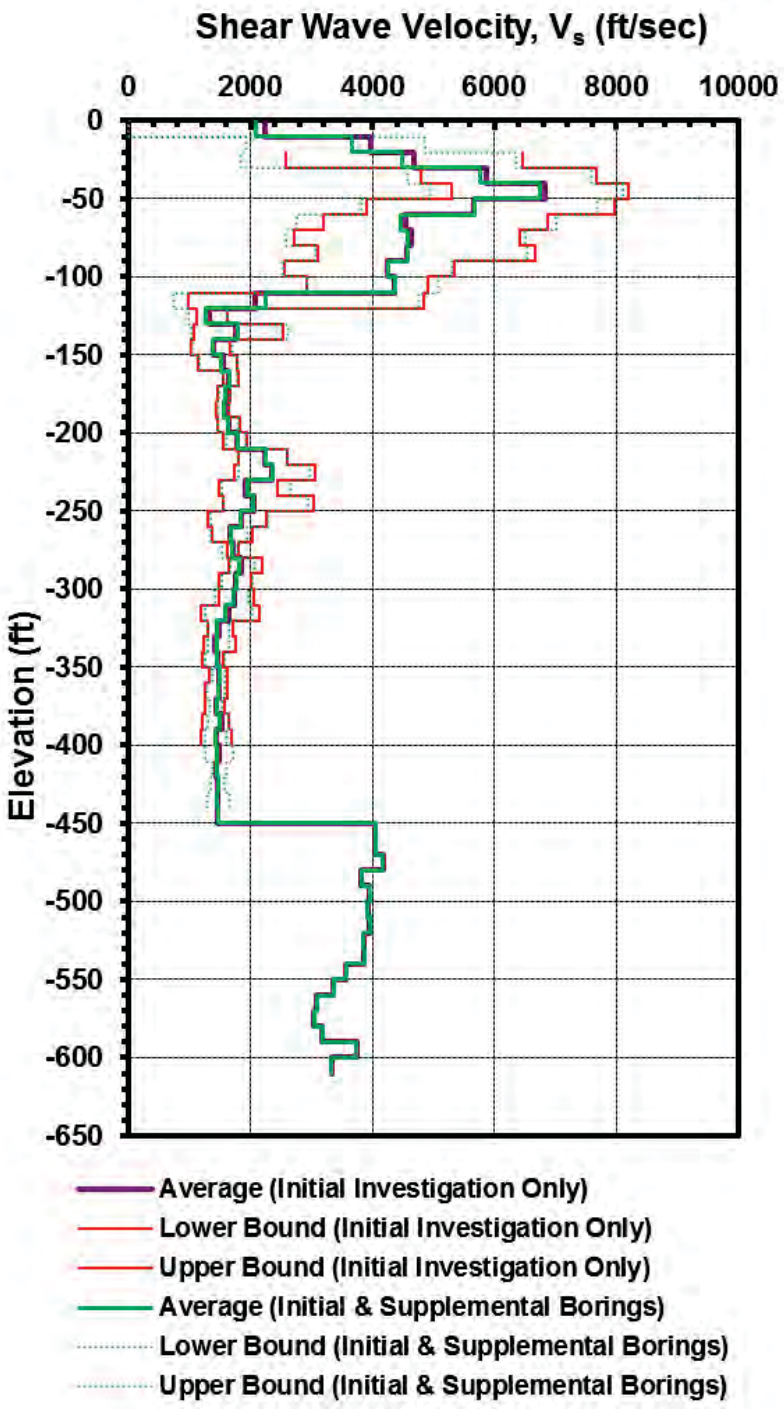

Note: Averages and boundary values above contain both Unit 6 and Unit 7 measurements.

This response is PLANT SPECIFIC.

References:

1. MACTEC Engineering and Consulting, Inc., *Final Data Report – Geotechnical Exploration and Testing: Turkey Point COL Project Florida City, Florida*, Revision 2, included in COL Application Part 11, October 6, 2008.

2. Paul C. Rizzo Associates, Inc., *Field Investigation Data Report, Turkey Point Nuclear Power Plant Units 6 & 7*, Revision 1, RIZZO, Pittsburgh, Pennsylvania, January 31, 2014.

ASSOCIATED COLA REVISIONS:

Revisions associated with Subsections 2.5.4.1.1, 2.5.4.2.1.3.14, 2.5.4.2.2, 2.5.4.4, 2.5.4.4.2.1, and 2.5.4.13 of this revised RAI response are presented in the revised response to RAI 02.05.04-3.

FSAR Subsection 2.5.4.4 will be revised in a future revision as follows:

2.5.4.4.4 S-Wave and P-Wave Velocity Profile Selection

Suspension P-S velocity logging results summarized in Table 2.5.4-215 are used to develop the recommended V_s velocity profiles shown in Figure 2.5.4-220. The data collected at individual suspension P-S velocity logging borings and at individual seismic CPTs are sorted by stratum and averaged and presented in Table 2.5.4-209~~. In this table, the measured Vc values in the saturated sand strata (Strata 5, 6, and 7) are adjusted to account for the high readings due to measuring the Vc of water.~~ The average thickness and elevation of each stratum is also determined at each of the boring test locations and averaged. The V_s profiles given in Figure 2.5.4-218 plot measured shear wave versus depth~~, and indicate strata thicknesses and depths~~. Figure 2.5.4-220 illustrates the design V_s profile (average) for materials at the site from ground surface to approximately **450** ~~600~~ feet depth **from data measured at Units 6 and 7**. **Figure 2.5.4-220 includes the V_s data of one reading from 450−600 feet measured at Unit 7.** ~~As previously noted, Unit 7 V_s data are collected to a depth of approximately 600 feet, while at Unit 6 V_s data are collected to a depth of approximately 400 feet.~~

The third paragraph of FSAR Subsection 2.5.4.7.2.1 will be revised in a future revision as follows:

2.5.4.7.2.1 Seismic Velocities in the Upper 600 Feet

Suspension P-S velocity logging is performed in ~~10~~**12** dedicated borings (~~five~~**six** borings in each of the two power blocks), with depths ranging from 150 feet to 600 feet, and at the locations shown on Figure 2.5.4-202. Downhole geophysical testing including gamma, caliper, resistivity, spontaneous potential, and caliper measurements extend as deep as 400 feet bgs. The suspension P-S logging data and the downhole geophysical data are contained in Appendix B of Reference**s** 257 **and 290**.

FSAR Table 2.5.4-209 will revised in a future revision as follows:

Table 2.5.4-209
Summary of Recommended Geotechnical Engineering Parameters

Stratum[(a)]	1[(a)]	2	3	4	5	6	7	8	Fill
Description	Muck	Miami	Key Largo	Ft. Thompson	Upper Tamiami	Lower Tamiami	Peace River	Arcadia	—
Elevation of top of layer (ft)	–1.2	–4.5	–26.7	–49.4	–115.1	–159.0	–215.2	–452.1	—
USCS symbol	ML, MH	GM, GP-GM, SM, SW-SM, SW, SP-SM	Limestone	Limestone	SM, SP-SM	ML	SM	Limestone	—
Total unit weight, γ (pcf)	80	125	136	139	120	120	120	130	130
Natural water content, w, (%)	>80	—	—	—	—	30	—	—	33
Fines content (%)	>60	18	—	—	28	62	16	—	15
Atterberg limits									
Liquid limit, LL	—	—	—	—	—	24	—	—	—
Plastic limit, PL	—	—	—	—	—	20	—	—	—
Plasticity index, PI	—	—	—	—	—	4	—	—	—
SPT N_{60}-value (blows/ft)	~0	20	—	—	40	32	75	—	30
Undrained properties									
Undrained shear strength, s_u (ksf)	—	—	—	—	—	4.0	—	—	—
Internal friction angle, φ, (deg)	—	—	—	—	—	—	—	—	—
Drained properties									
Effective cohesion, c′ (ksf)	—	—	—	—	0	1.7	0	—	—
Effective friction angle, φ′ (deg)	—	—	—	—	35	20	40	—	33
Average Rock core recovery (%)	—	—	83 to 96	41 to 98	—	—	—	63 to 100	—
Average RQD (%)	—	—	54 to 81	16 to 91	—	—	—	32 to 90	—
Unconfined compressive strength, U (psi)	—	200	1,500	2,000	—	—	—	100	—
Elastic modulus (high strain), E_H	—	630 ksi	2,600 ksi	1,500 ksi	1,500 ksf	2,500 ksf	2,700 ksf	980 ksi	1,100 ksf
Elastic modulus (low strain), E_L	—	950 ksi	2,600 ksi	1,500 ksi	19,700 ksf	25,750 ksf	27,400 ksf	980 ksi	9,100 ksf
Shear modulus (high strain), G_H	—	230 ksi	1,000 ksi	550 ksi	550 ksf	900 ksf	1,000 ksf	360 ksi	420 ksf
Shear modulus (low strain), G_L	—	350 ksi	1,000 ksi	550 ksi	7,300 ksf	9,500 ksf	10,150 ksf	360 ksi	3,500 ksf
Shear wave velocity, V_S, (ft/sec)	850	3,400~~3,600~~	6,250~~5,800~~	4,450~~4,250~~	1,500~~1,400~~	1,600~~1,600~~	1,600~~1,650~~	3,650~~3,600~~	860
Compression wave velocity, V_C, (ft/sec)	4,900	7,450~~8,000~~	11,750~~11,000~~	9,000~~8,700~~	5,650~~2,900~~	5,700~~3,300~~	5,850~~3,450~~	7,950~~7,850~~	1,600
Coefficient of sliding	—	0.6	0.7	0.7	0.4	0.3	—	—	0.5
Poisson's ratio, *v′*	—	0.37	0.31	0.34	0.35	0.35	0.35	0.36	0.3
Static earth pressure coefficients									
Active, K_a	—	0.3	—	—	0.27	0.5	—	—	0.3
At-rest, K_o	—	0.5	—	—	0.5	0.66	—	—	0.5

(a) Properties of Stratum 1 (muck) are not provided as this stratum was removed prior to construction.
The values tabulated for use as design guideline only. Refer to specific boring logs, CPT logs, and laboratory test results for appropriate modifications at specific design locations.
USCS = Unified Soil Classification System (ML = silt; MH = silt of high plasticity; GM = silty gravel; GP = poorly graded gravel; SM = silty sand; SW = well graded sand; SP = poorly graded sand).

FSAR Table 2.5.4-215 will be replaced with the following revised table in a future revision:

Table 2.5.4-215 (Sheet 1 of 2)
Summary of Measured Shear Wave Velocity and Compressive Wave Velocities

		Shear Wave Velocity, V_s (ft/s)			Compressive Wave Velocity, V_p (ft/s)		
Top Elevation (ft)	Bottom Elevation (ft)	Average	Upper Bound	Lower Bound	Average	Upper Bound	Lower Bound
0	-10	2097	-	-	5566	-	-
-10	-20	3659	4853	1903	7568	9825	4851
-20	-30	4480	6348	1850	9249	12114	6086
-30	-40	5770	7575	4566	11004	14256	9002
-40	-50	6751	8104	4945	12540	15158	9405
-50	-60	5684	7663	3818	10742	13769	7894
-60	-70	4472	7011	2749	9349	12679	6382
-70	-80	4575	6509	2586	9379	12425	6558
-80	-90	4579	6538	3049	9142	12238	7283
-90	-100	4261	5294	2529	8706	10702	6674
-100	-110	4381	5065	2926	8565	9380	7667
-110	-120	2246	4739	725	6553	8882	5074
-120	-130	1271	1610	982	5491	5814	5183
-130	-140	1794	2597	1021	5938	6795	5159
-140	-150	1383	1676	1048	5526	5828	5254
-150	-160	1524	1773	1162	5621	5864	5237
-160	-170	1644	1770	1555	5724	5860	5586
-170	-180	1590	1661	1476	5694	5783	5607
-180	-190	1562	1642	1452	5681	5825	5564
-190	-200	1636	1800	1468	5738	5865	5570
-200	-210	1778	1923	1591	5787	6000	5641
-210	-220	2236	2592	1809	6390	6983	5832
-220	-230	2354	2976	1796	6465	7019	5991
-230	-240	1950	2652	1535	6058	6640	5550
-240	-250	2045	2932	1553	6079	6771	5554
-250	-260	1835	2273	1344	6003	6311	5612
-260	-270	1668	1940	1354	5856	6073	5587
-270	-280	1696	1785	1525	5844	6109	5577
-280	-290	1823	2051	1656	5954	6192	5775
-290	-300	1757	2023	1523	5980	6217	5729
-300	-310	1713	1963	1409	5866	6101	5662
-310	-320	1572	2026	1243	5732	5916	5560
-320	-330	1444	1636	1298	5816	5971	5679
-330	-340	1436	1632	1299	5682	5958	5523
-340	-350	1436	1566	1262	5754	5947	5549
-350	-360	1481	1571	1377	5787	5940	5563
-360	-370	1470	1570	1285	5811	6032	5559

Table 2.5.4-215 (Sheet 2 of 2)
Summary of Measured Shear Wave Velocity and Compressive Wave Velocities

		Shear Wave Velocity, V_s (ft/s)			Compressive Wave Velocity, V_p (ft/s)		
Top Elevation (ft)	Bottom Elevation (ft)	Average	Upper Bound	Lower Bound	Average	Upper Bound	Lower Bound
-370	-380	1439	1521	1318	5718	6098	5446
-380	-390	1492	1630	1299	5755	5930	5527
-390	-400	1430	1606	1261	5727	5929	5497
-400	-410	1450	1717	1242	5690	5916	5488
-410	-420	1449	1587	1363	5736	5979	5538
-420	-430	1469	1566	1338	5786	6025	5514
-430	-440	1449	1657	1273	5716	6031	5479
-440	-450	1460	-	-	5565	-	-
-450	-460	4046	-	-	8842	-	-
-460	-470	4046	-	-	8842	-	-
-470	-480	4171	-	-	8247	-	-
-480	-490	3818	-	-	7739	-	-
-490	-500	3953	-	-	8021	-	-
-500	-510	3917	-	-	8118	-	-
-510	-520	3961	-	-	8256	-	-
-520	-530	3843	-	-	7743	-	-
-530	-540	3860	-	-	8088	-	-
-540	-550	3569	-	-	7873	-	-
-550	-560	3364	-	-	7627	-	-
-560	-570	3083	-	-	7275	-	-
-570	-580	3040	-	-	7398	-	-
-580	-590	3174	-	-	7453	-	-
-590	-600	3741	-	-	8307	-	-
-600	-610	3331	-	-	7847	-	-

FSAR Figure 2.5.4-220 will be replaced with the following revised figure in a future revision:

Figure 2.5.4-220. Plot of Recommended Shear Wave Velocity with Elevation~~Depth~~

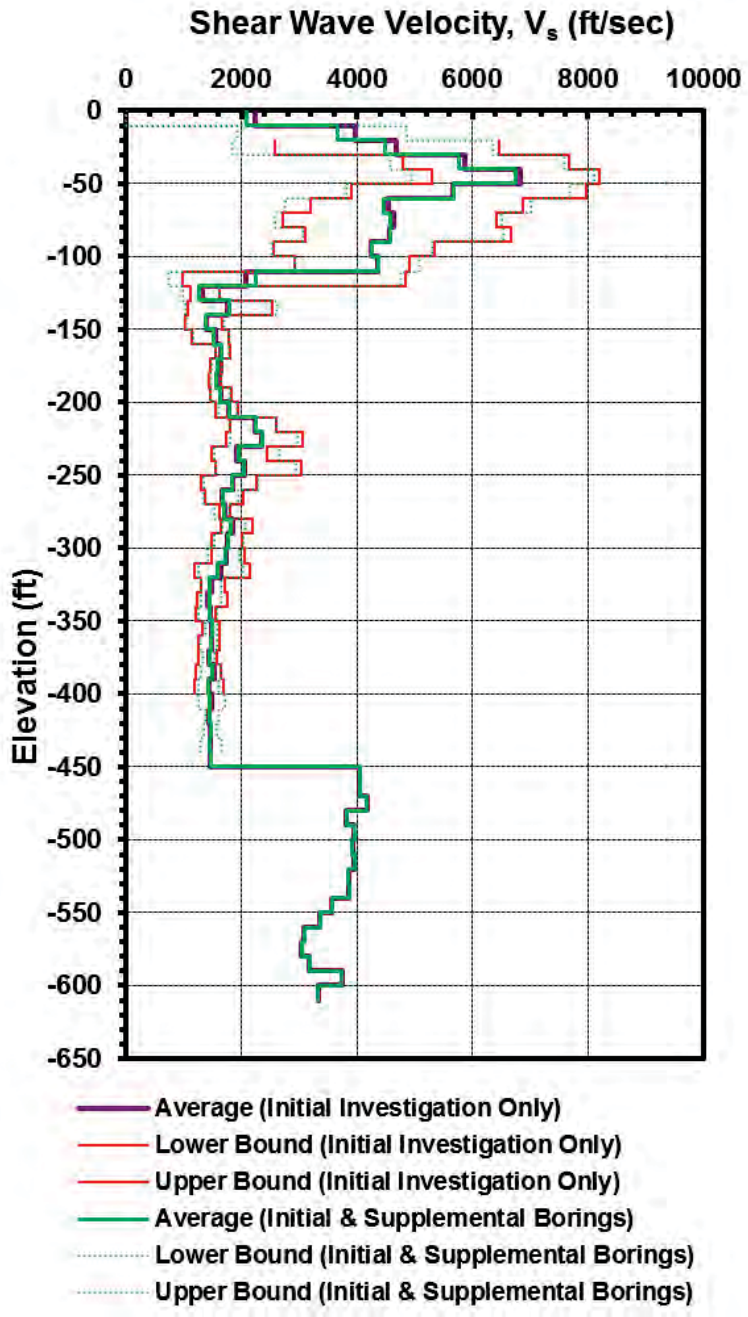

Data from Reference**s** 257 **and 290.**
Note: Average and boundary values above contain both Unit 6 and Unit 7 measurements.

ASSOCIATED ENCLOSURES:

None

NRC RAI Letter No. PTN-RAI-LTR-040

SRP Section: 02.05.04 - Stability of Subsurface Materials and Foundations

QUESTIONS from Geosciences and Geotechnical Engineering Branch 1 (RGS1)

NRC RAI Number: 02.05.04-11 (eRAI 6006)

Figure 2.5.4-218 presents a plot of shear wave velocity measurements. Below the Fort Thompson formation, the soils are variously described as silty sands or silts and clays. However, the velocities do not show any change with depth. In accordance with NUREG-0800, Standard Review Plan, Chapter 2.5.4, "Stability of Subsurface Materials and Foundations," please indicate the data that was used to construct this figure and explain the uniformity in shear wave velocity below the Fort Thompson formation.

FPL RESPONSE:

A supplemental field investigation was conducted in 2013, which involved two additional P-S Suspension soundings at locations R-6-1b and R-7-1 around the center of each reactor building for Units 6 & 7, respectively. The scope of the supplemental field investigation is outlined in the revised response to RAI 02.05.04-3.

This revised response includes description and analysis of all the data collected during the initial investigation in 2008 and the supplemental investigation in 2013. The list of borings and the exploration depths are shown in Figure 1 of the revised response to RAI 02.05.04-3 and are provided below:

- Two borings (B-604[DH] and B-704G[DH]) to a depth of 150 feet
- Two borings (B-620[DH] and B-720G[DH]) to a depth of 200 feet
- Four borings (B-608[DH], B-610[DH], B-708[DH], and B-710G[DH]) to a depth of 250 feet
- One boring (B-601[DH]) to a depth of 400 feet
- One boring (R-7-1) to a depth of 440 feet
- One boring (R-6-1b) to a depth of 450 feet
- One boring (B-701[DH]) to a depth of 600 feet

The shear wave velocity profile for the upper Tamiami, lower Tamiami, and Peace River formations obtained from all of these borings is shown in Figure 1. A shear wave velocity profile extending from ground surface to approximately 600 feet depth is presented in the revised response to RAI 02.05.04-10.

The Tamiami Formation, including both the upper and lower Tamiami, exhibits a slightly increasing V_s profile with depth up to a depth of approximately 215 feet. This correlation of the shear wave velocity with depth is expected for the shallower sections of the soil formations. An example of this trend is provided in the Electric Power Research Institute (EPRI) Seismic Evaluation Guidance (Reference 1), where shear wave velocity profiles for various soil formations with V_{s30} = 400 meter/second (1312 ft/second) and V_{s30} = 560 meter/second (1837 ft/second) are provided as shown in Figure 2 (V_{s30} is the average

shear wave velocity for the top 30 feet). These profiles also show the similar trend of increasing shear wave velocity with depth for the depth interval of 115 feet to 215 feet.

At the interface of the lower Tamiami and Peace River formations, at a depth of approximately 220 feet, an abrupt increase (occurring within 5−10 feet) in shear wave velocity is evident. This variation is attributed to the soil formation change and particularly to the decrease in fines content at the transition to the Peace River Formation (Figure 3). The variability in shear wave velocity between the depths of 220 feet and about 290 feet is again attributed to changes in fines content (Figure 3).

For the relatively uniform Peace River Formation, especially for sections deeper than 300 feet, the shear wave velocity variation with depth is minimal. This is also anticipated, since the rate of shear wave velocity increase with depth decreases for deeper sections of the soil formations. This behavior is also consistent with the template of soil shear wave velocity profiles provided by EPRI Seismic Evaluation Guidance (Reference 1) for the same depth interval (Figure 2).

In summary, the shear wave velocity profile for upper Tamiami, lower Tamiami, and Peace River formations does not necessarily indicate a constant shear wave velocity. Some variations, even though not significant, are observed as a function of depth at shallow depths, and as a function of fines content at the contact of lower Tamiami and Peace River Formation. The dependency of shear wave velocity to depth diminishes after 300 feet.

Figure 1 Variation of Shear Wave Velocity with Elevation

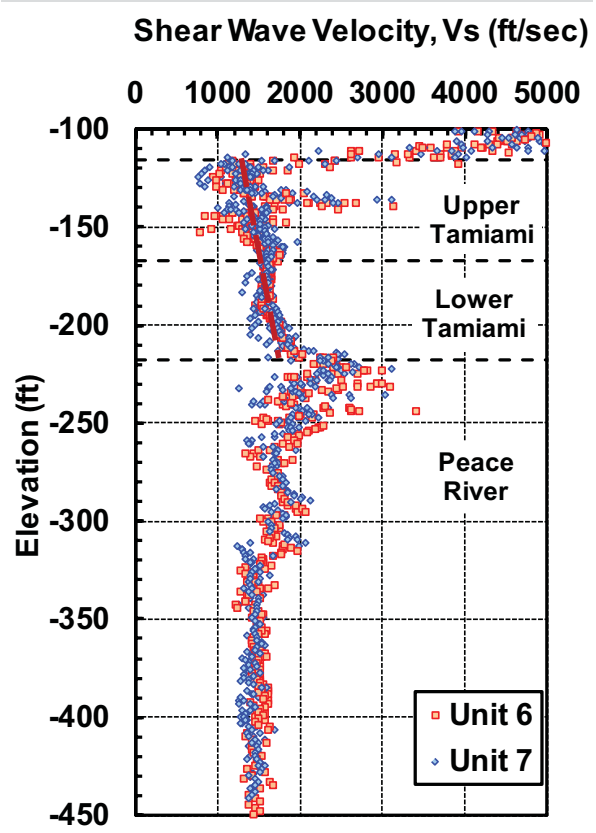

Figure 2 Template Shear Wave Velocity Profiles for Soils, Soft Rock, and Firm Rock

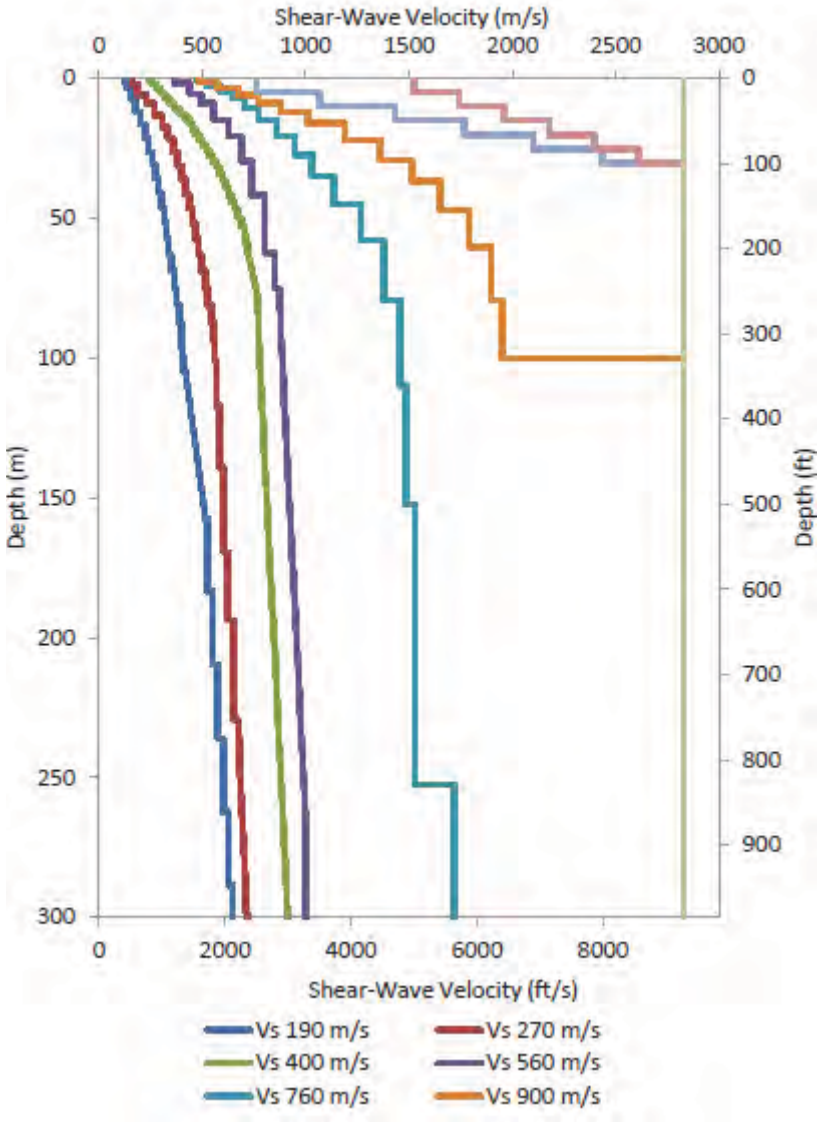

Note : Rock Profiles Include Shallow Weathered Zone. Indicated velocities are for V_{s30}.

Source: Reference 1

Figure 3 Variation of Fines Content with Elevation

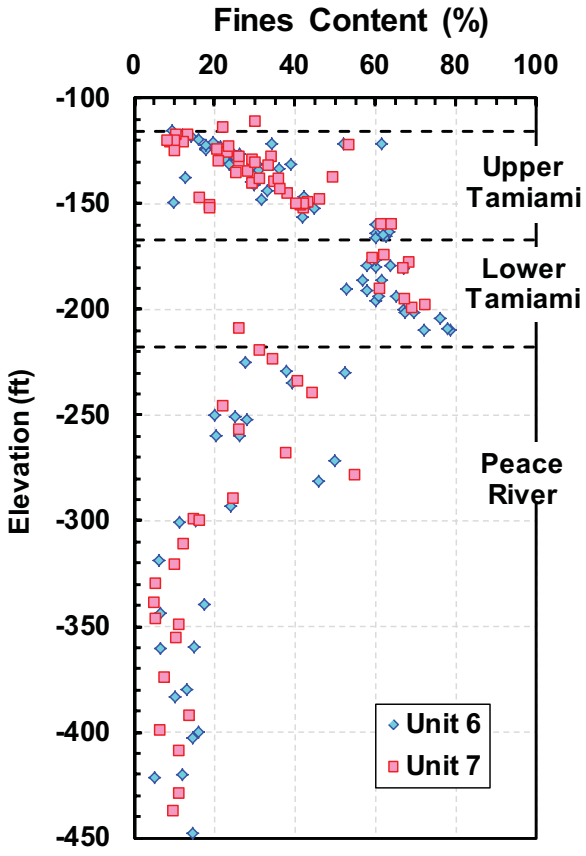

This response is PLANT SPECIFIC.

References:

1. EPRI, 2012, Seismic Evaluation Guidance, Screening, Prioritization, and Implementation Details (SPID) for the Resolution of Fukushima Near-Term Task Force Recommendation 2.1: Seismic, Electric Power Research Institute Palo Alto, California, 2012.

ASSOCIATED COLA REVISIONS:

Associated revisions are provided as part of the revised response to RAI 02.05.04-3.

ASSOCIATED ENCLOSURES:

None

NRC RAI Letter No. PTN-RAI-LTR-040

SRP Section: 02.05.04 - Stability of Subsurface Materials and Foundations

QUESTIONS from Geosciences and Geotechnical Engineering Branch 1 (RGS1)

NRC RAI Number: 02.05.04-12 (eRAI 6006)

Section 2.5.4.5.2 “Extent of Excavations, Fills, and Slopes”, states that the TPNPP Units 6 and 7 nuclear islands will be founded directly on a 20 ft thick lean-concrete layer above a competent rock stratum (Key Largo Formation). In accordance with NUREG-0800, Standard Review Plan, Chapter 2.5.4, "Stability of Subsurface Materials and Foundations," please address the following:

a. Define “Lean Concrete” and clarify if CLSM is used. Also specify which ACI standard(s) will be followed.

b. Given the load path, how is the potential for cracking of the lean concrete evaluated? Also discuss your plan to control thermal cracking of the fill materials.

c. Describe the load transfer mechanism between the base of the NI structures and the lean fill concrete as well as the load transfer between the lean concrete and the surrounding supporting soils.

d. Your chemical tests of soil and rock indicated that that the chemistry of soil and rock is considered to be aggressive towards cementitious materials. Please provide test results on groundwater chemistry including pH, chlorides, and sulfates. Evaluate the potential aging effects and address the concrete durability for lean concrete backfill and sub- foundation due to aggressive soil and groundwater conditions. Also provide a description on how potential settlement and differential settlement due to erosion of cement from porous lean concrete backfill will be addressed.

FPL RESPONSE:

a. Lean concrete is unreinforced concrete with lower cement to aggregate ratio than typical concrete. Controlled Low Strength Material (CLSM) will not be used. In the remainder of the response, the term “lean concrete fill” will be shortened to “concrete fill.” The American Concrete Institute (ACI) standard that will be followed is ACI 207, Guide to Mass Concrete prepared by ACI Committee 207 (FSAR Subsection 2.5.4.13, Reference 281).

b. FSAR Subsection 2.5.4.12 indicates the concrete fill will have an estimated compressive strength of 1500 pounds per square inch (psi). The design bearing capacity of this strength of concrete is over 100 kips per square feet (ksf). According to the AP1000 DCD (Reference 1), the maximum applied bearing pressure (from the reactor building) is 8.9 ksf, less than 9 percent of the bearing capacity of the concrete. Thus, cracking of the concrete due to loading/overstressing is not expected.

   A comprehensive bearing capacity analysis involving hand calculations, limit equilibrium analysis, and finite element methods indicates that the allowable bearing capacity of the foundation medium is 39 ksf (refer to the revised response to RAI 02.05.04-18), which is

well above the applied stress of 8.9 ksf. The analysis determined that overstressing is not an issue for the concrete fill.

ACI 207 defines mass concrete as “any volume of concrete with dimensions large enough to require that measures be taken to cope with generation of heat from hydration of the cement and attendant volume change to minimize cracking.” The approximately 19-foot thick layer of concrete fill qualifies as mass concrete. As such, a thermal control plan will be developed during detailed design to minimize thermal cracking of the concrete fill.

The thermal control plan would include the following elements as outlined in ACI 207 (FSAR 2.5.4 Reference 281) and detailed below:

- Controls on cementitious material content:

  Choosing the type and amount of cementitious material can lessen the heat-generating potential during concrete curing. Since the strength of the concrete fill and, therefore, the amount of cementitious materials will be relatively low, the heat of hydration will be less than with higher strength mixes. Furthermore, the use of pozzolans (such as fly ash) will reduce the heat generated during the curing process.

- Precooling:

  The precooling of aggregates and mixing water can enable a lower placement temperature, thereby reducing the potential for cracking. This can be achieved, for example, with shades over the aggregate, sand chillers, water chillers, and ice.

- Construction management:

  Construction scheduling and procedures can be optimized for concrete placement to reduce the risk of cracking. These methods include the placement of concrete at night and placement of the concrete in properly sized lift thicknesses and blocks determined in advance with thermal analysis.

c. The strength of the concrete fill (1500 psi) and the underlying rock of the Key Largo Formation (2689 psi) are approximately the same. Thus, during vertical load transfer from the foundation to the concrete fill and from the concrete fill to the underlying rock, stress levels will remain low in these materials and well within the elastic range.

   For transfer of lateral loading, the coefficient of friction against sliding between mass concrete and the clean sound rock of the Key Largo Formation is 0.7. This coefficient value gives the resistance to sliding of the concrete fill bearing on the Key Largo Formation. The 0.7 value also gives the resistance to sliding of the base of the nuclear island concrete foundation mat bearing on the mudmat, and the mudmat bearing on the concrete fill.

   The mudmat provides a working surface for the construction of the concrete foundation mat. The mudmat has a minimum thickness of 12 inches and is comprised of un-reinforced concrete. As noted in FSAR Subsection 3.8.5.1, a sheet type high-density polyethylene (HDPE) waterproofing material will be used for both the horizontal and vertical surfaces under Seismic Category I structures. The material will be qualified by

test, with commercial grade dedication and laboratory testing, to achieve a minimum coefficient of friction against sliding of 0.55, as shown in FSAR Subsection 3.8.5.1. This waterproof membrane is sandwiched within the mudmat.

Because of the low seismic forces (and hence lateral loading) at the Turkey Point Units 6 & 7 site, the friction between the foundation and the mudmat, the friction within the mudmat (waterproofing material), the friction between the mudmat and the concrete fill, and the friction between the concrete fill and the underlying rock will be sufficient to prevent sliding movement. Thus, the surrounding structural backfill and in situ soils and rock will not be required to resist lateral loading from the building.

d. The measured values of chemical tests on groundwater samples from observation wells on the site are presented in FSAR Tables 2.4.12-210 (pH) and 2.4.12-211 (chloride and sulfate).

   The pH values measured from 24 water samples range from 6.65 to 7.29, resulting in a median of 7.06, i.e., essentially neutral. The pH of the water will therefore not affect the concrete fill.

   The chloride values measured from 24 water samples range from 16,300 parts per million (ppm) to 37,500 ppm, resulting in a median value of about 29,000 ppm. This level of chloride concentration can affect the reinforcing steel used in structural concrete. However, since the concrete fill is non-structural and unreinforced, the chloride concentration will not affect the concrete fill.

   The sulfate values measured from 24-water samples range from 2280 ppm to 4400 ppm, resulting in a median value of about 3800 ppm, or close to 0.4 percent by weight. This classifies the concrete exposure to sulfate attack as severe, according to the ACI Manual of Concrete Practice, Part 1. One (of several) potential solution to this situation is to make the first lift of concrete fill (bottom lift) from sulfate resisting Type V cement with maximum C3A content of 5 percent as specified in ACI 318-05/318R-05 (Reference 2). In addition, fly ash can be used as an additive to the concrete to improve the sulfate resistance. Fly ash will also contribute to the thermal control. The use of sulfate resisting Type V concrete in combination with fly ash will minimize the aging effects.

   The concrete fill will be placed on top of the Key Largo Limestone layer that will have been extensively grouted to significantly reduce the quantity of groundwater to be removed during the dewatering process. During construction dewatering, permanent diaphragm cut-off walls will also be installed surrounding the perimeter of the nuclear island. Furthermore, the Freshwater Limestone, a layer of limestone between the Key Largo Formation and the Fort Thompson Formation, has significantly lower permeability than either of these layers. This will reduce the amount of vertical inflow into the area. Thus, there will be limited exposure of the concrete fill to aggressive groundwater and soil.

   The approximate plan dimensions of the approximately 19-foot thick mass of concrete fill are 240 feet x 290 feet, including 30-foot width of concrete extending beyond the perimeter of the nuclear island. The concrete fill will be placed on top of Key Largo Limestone that will have been extensively grouted to enable dewatering. The concrete

fill will be placed against the perimeter concrete diaphragm wall that extends down to El. –60 feet. The majority of the surface of the concrete fill will be covered by the nuclear island, and the remainder will be covered by structural fill. Thus, there will be limited exposure of the concrete fill to aggressive groundwater and soil. On the perimeter, there is a 30-foot wide buffer of concrete fill placed against a concrete diaphragm wall, and on the surface, most of the concrete fill is covered by structures. The only plausible potential for exposure is on the base of the concrete fill.

Based on the conditions described above and the potential solution for combating the effects of high sulfate content, erosion, or leaching of the cement will have no impact on total or differential settlement.

This response is PLANT SPECIFIC.

References:

1. Westinghouse Electric Company, *AP1000 Design Control Document (DCD)*, Revision 19, June 21, 2011.
2. American Concrete Institute, *Building Code Requirements for Structural Concrete* (ACI 318-05) and Commentary (ACI 318R-05) ACI 318-05.

ASSOCIATED COLA REVISIONS:

The second paragraph of FSAR Subsection 2.5.4.5.1 will be revised in a future revision as follows:

The deepest excavation is **to** approximately El. –35 feet. Structural fill is placed around but not below the power block structures extending to as deep as El. –14 feet. Lean concrete fill is placed between **the bottom of the mudmat at** El. –14 feet and the bottom of excavation. **Lean concrete is unreinforced concrete with a lower ratio of cement to aggregate than structural concrete.** The final grade is shown on Figure 2.5.4-201. The grade in profile is shown in Figure 2.5.4-221.

New text will be added after the third paragraph of FSAR Subsection 2.5.4.5.1.2 in a future revision as follows:

Structural fill consisting of excavated fill material is placed around but not below any nuclear island structure. Replacement material below the nuclear island consists of lean concrete fill. The selection of lean concrete mix design is made at project detailed design. The compressive strength of 1.5 ksi is estimated for lean concrete fill.

The approximately 19-foot thick layer of lean concrete fill qualifies as mass concrete. As such, a thermal control plan will be developed during detailed design to minimize thermal cracking of the lean concrete fill.

The thermal control plan will include the following elements as outlined in ACI 207 (Reference 281) and detailed below:

- **Controls on cementitious material content:**

Choosing the type and amount of cementitious material can lessen the heat-generating potential during concrete curing. Since the strength of the lean concrete fill, and therefore the amount of cementitious materials, will be relatively low, the heat of hydration will be less than that found in higher strength mixes. Furthermore, the use of pozzolans (such as fly ash) will reduce the heat generated during the curing process.

- **Precooling:**

  The precooling of aggregates and mixing water can enable a lower placement temperature, thereby reducing the risk of cracking during the curing process. This can be achieved by shading the aggregate, sand chillers, water chillers, and ice.

- **Construction management:**

  Construction scheduling and procedures can be optimized for concrete placement to reduce the risk of cracking. These methods include the placement of concrete at night and placement of the concrete in properly sized lift thicknesses and blocks determined in advance with thermal analysis.

ASSOCIATED ENCLOSURES:

None

NRC RAI Letter No. PTN-RAI-LTR-040

SRP Section: 02.05.04 - Stability of Subsurface Materials and Foundations

QUESTIONS from Geosciences and Geotechnical Engineering Branch 1 (RGS1)

NRC RAI Number: 02.05.04-14 (eRAI 6006)

FSAR Figure 2.5.4-222 shows a general conceptual excavation cross-section. In accordance with NUREG-0800, Standard Review Plan, Chapter 2.5.4, "Stability of Subsurface Materials and Foundations," please describe the procedures that will be followed during site excavation and construction activity to ensure that the appropriate strata for the proposed foundation locations are confirmed through objective measures and the exposed foundation laying surface is uniform. Also, please provide the vertical and horizontal extent of all seismic categories I excavations, fills, and slopes, including the locations and limits of excavations, fills, and backfills on plot plans and geologic sections and profiles.

FPL RESPONSE:

Excavation to support construction of the nuclear island (NI) safety-related foundations will involve the removal of the top layer of surficial sediments or “muck” followed by removal of all the underlying Miami Limestone down to approximate El. –35 feet to expose the Key Largo Limestone. In all areas at the site to be excavated for safety-related foundations, the Key Largo Limestone begins at an elevation above El. –35 feet. The Key Largo Limestone will be excavated from that elevation down to El. –35 feet. Part A of the response addresses field procedures for ensuring proper foundation strata and uniformity through objective measures. Part B of the response provides figures and a discussion on the extent of excavations, slopes and backfills, both horizontal and vertical.

Part A

FSAR Subsection 2.5.4.2.1.2 Description of Soil and Rock Strata, updated in the revised response to RAI 02.05.04-03 provides a description of each soil and near-surface rock stratum encountered in the subsurface investigation for the power block areas and what is expected to be observed during the excavation process. The stratum elevation and thickness indicated in each description for the power block is the calculated average from the entire site because the layering encountered in the subsurface boring program is relatively uniform. The sections and profiles from the power block subsurface investigations show that the subsurface strata to support foundations are nearly horizontal (refer to revised FSAR Figures 2.5.4-203 through 2.5.4-209, updated in the revised response to RAI 02.05.04-03). As seen in the cross sections in FSAR Figures 2.5.4-203 through 2.5.4-208 the dip of rock layer interfaces between adjacent borings is less than 5 degrees in all sections. Descriptions of the upper three strata at the site are as follows:

- Stratum 1: Muck consists primarily of light gray to black silty clay with varying amounts of sand and peat. Typically, this stratum contains trace organics near the surface, and 5 percent to 30 percent organics lower in the deposits. This stratum has a very soft to medium-stiff consistency. The thickness of Stratum 1 ranges from 2 feet to 11 feet, with an average of 3.6 feet. The top of this layer is typically at El. –1.1 feet. The average base elevation of this stratum is –4.7 feet.

- Stratum 2: The top of the Miami Limestone (or the Miami Oolite, as it is referred to in some publications) is encountered at elevations (top of the layer) ranging from –3.3 feet to –12.2 feet. The range in thickness for the Miami Limestone varies from 13 feet to 30 feet with an average of 22.3 feet. This stratum consists of pale yellow, light brownish gray, and white limestone. It has a porous, sometimes fossiliferous texture, comprising oolite grains with varying carbonate cementation. Observed fossils include mollusks, bryozoans, and corals. This stratum has soft to very hard consistency, depending on the degree of cementation. A more detailed description of the structure and content of the Miami Limestone is provided in FSAR Subsection 2.5.1.1.1.2.1.1.
- Stratum 3: The top of the Key Largo Limestone is encountered between El. –23.1 feet and El. –35.3 feet, at an average of El. –26.9 feet. The thickness varies between 14.6 feet and 26.9 feet in the borings, with an average thickness of 22.5 feet. The Key Largo Limestone is a coralline, porous formation with recrystallized calcite infill visible in core samples. The color varies between white, pale yellow, light brownish gray, and gray. A more detailed description of the structure and content of the Key Largo Limestone is provided in FSAR Subsection 2.5.1.1.1.2.1.1.

The Miami Limestone is considerably softer than, and has a quite different structure from, the coralline Key Largo Limestone, as described above. During the excavation process, onsite geotechnical engineers and geologists will verify complete removal of the Miami Limestone to the Key Largo Limestone layer by visual inspection (texture difference).

As stated in FSAR Subsection 2.5.1.1.1.2.1.1, the Miami Limestone is considerably softer than the Key Largo Limestone due, in part, to a higher degree of weathering. Figure 1 (Reference 1) provides rock hardness/strength descriptors. Based on analysis of the results of the geotechnical investigation, it was determined that the Miami Limestone is moderately soft (H5), and the Key Largo Limestone Formation is moderately hard to hard (H4 to H3). The hardness value for this index property is an average for each of these two rock formations found on the site. The foundation bearing layer should be the Key Largo Limestone formation with moderately hard to hard consistency. Within the Key Largo formation, zones may be encountered that are softer than moderately hard (H4). These zones are to be identified by the onsite geotechnical engineers and geologists and removed.

Figure 1 Rock Hardness/Strength Descriptors

Alpha-numeric descriptor	Descriptor	Criteria
H1	Extremely hard	Core, fragment, or exposure cannot be scratched with knife or sharp pick; can only be chipped with repeated heavy hammer blows.
H2	Very hard	Cannot be scratched with knife or sharp pick. Core or fragment breaks with repeated heavy hammer blows.
H3	Hard	Can be scratched with knife or sharp pick with difficulty (heavy pressure). Heavy hammer blow required to break specimen.
H4	Moderately hard	Can be scratched with knife or sharp pick with light or moderate pressure. Core or fragment breaks with moderate hammer blow
H5	Moderately soft	Can be grooved 1/16 inch (2 mm) deep by knife or sharp pick with moderate or heavy pressure. Core or fragment breaks with light hammer blow or heavy manual pressure.
H6	Soft	Can be grooved or gouged easily by knife or sharp pick with light pressure, can be scratched with fingernail. Breaks with light to moderate manual pressure.
H7	Very soft	Can be readily indented, grooved or gouged with fingernail, or carved with a knife. Breaks with light manual pressure.
Any bedrock unit softer than H7, very soft, is to be described using USBR 5000 consistency descriptors.		

Note: Although "sharp pick" is included in these definitions, descriptions of ability to be scratched, grooved, or gouged by a knife is the preferred criteria

Source: Reference 1

In addition, surveying during excavation will ensure the proper depth is reached and excavation into the Key Largo is accomplished across the foundation site. Based on all borings in the initial and supplemental site investigations, the top of the Key Largo Limestone is never encountered at or below El. –35 feet within the power block boundary. In a few borings, the top of the Key Largo approaches El. –35 feet, but these locations are not under either NI and are therefore not foundation bearing materials. Figure 2 illustrates a contour plot of the elevation of the Miami and Key Largo interface.

The natural variation in physical properties of the Key Largo Formation is addressed through the randomization process for the site response analysis. For the settlement and bearing capacity analyses, the geotechnical properties of the Key Largo Formation are determined based on both in situ tests (P-S Suspension, pressuremeter tests), laboratory tests (resonant column torsional shear [RCTS] and unconfined compressive strength tests [UCS]), and rock mass classification as outlined in the revised response to RAI 02.05.04-06, which addresses the natural variability that exists in the Key Largo Formation. In addition, in the area for the safety-related structures, the foundation bearing Key Largo Formation will be grouted as part of the dewatering efforts. As a by-product of this process, a more uniform foundation bearing strata will be established by filling the vugs with grout that will reduce the variability in shear wave velocity.

Figure 2 Top Elevation of Key Largo Limestone

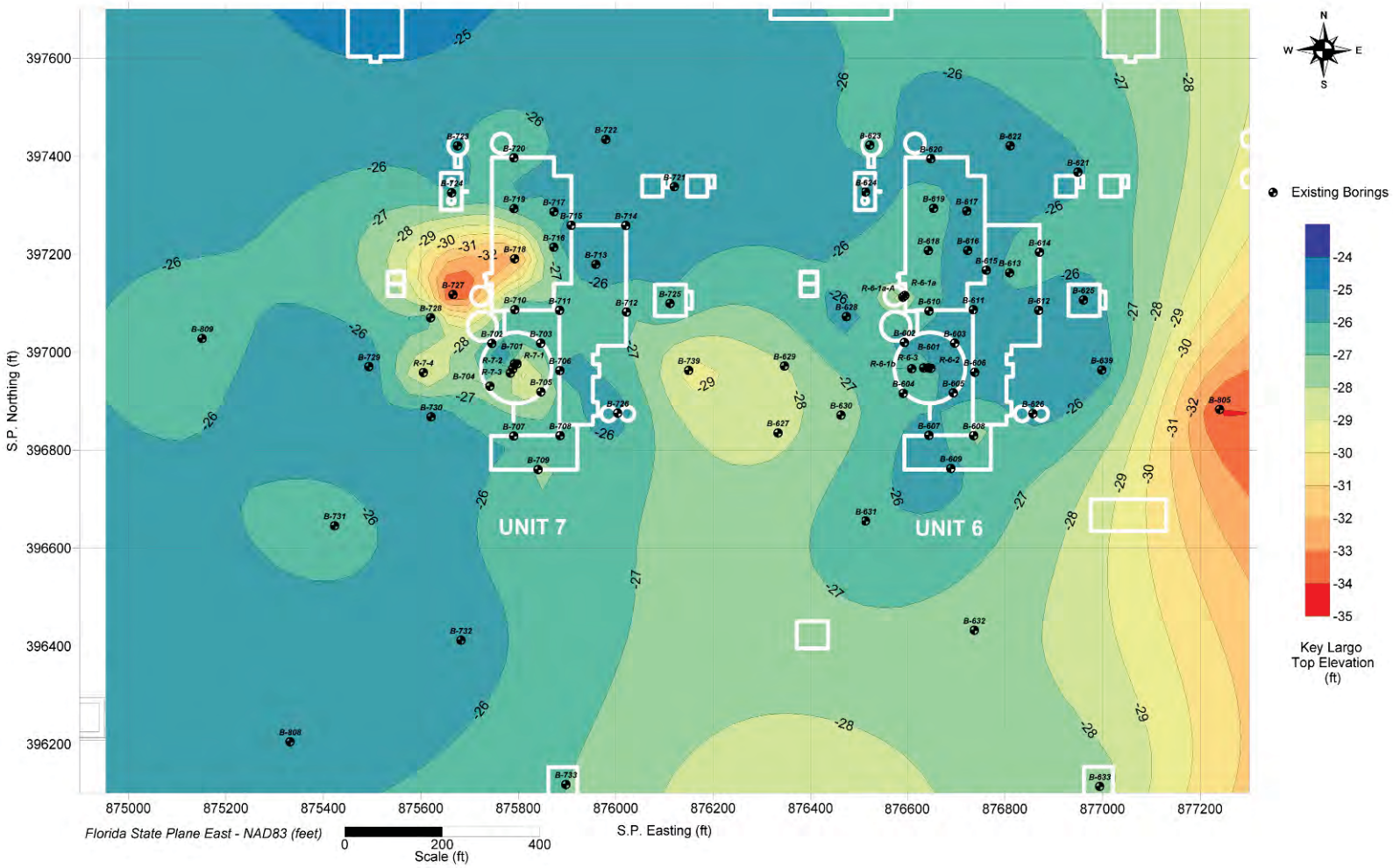

Part B

The vertical and horizontal extent of all Seismic Category I excavations, fills, and slopes, including the locations and limits of excavations, fills, and backfills on plot plans and geologic sections and profiles are shown in the revised FSAR Figures 2.5.4-203 through 2.5.4-209, which are updated in the revised response to RAI 02.05.04-03. The revised FSAR Figure 2.5.4-222 shows the extent of excavation in plan view.

This response is PLANT SPECIFIC.

References:

1. U.S. Department of Interior Bureau of Reclamation*, Engineering Geology Field Manual*, 2001.

ASSOCIATED COLA REVISIONS:

FSAR Figures 2.5.4-203 through 2.5.4-209 were updated in the revised response to RAI 02.05.04-03 to show the vertical and horizontal extent of the excavation, fill locations, and slopes. Note that dimensions and slopes on figures as shown are preliminary pending final design.

Figure 2.5.4-222 is revised in this response to include section lines according to the sections shown.

FSAR Figure 2.5.4-222 will be replaced with the following revised figure in a future revision:

Figure 2.5.4-222 Excavation at Power Block

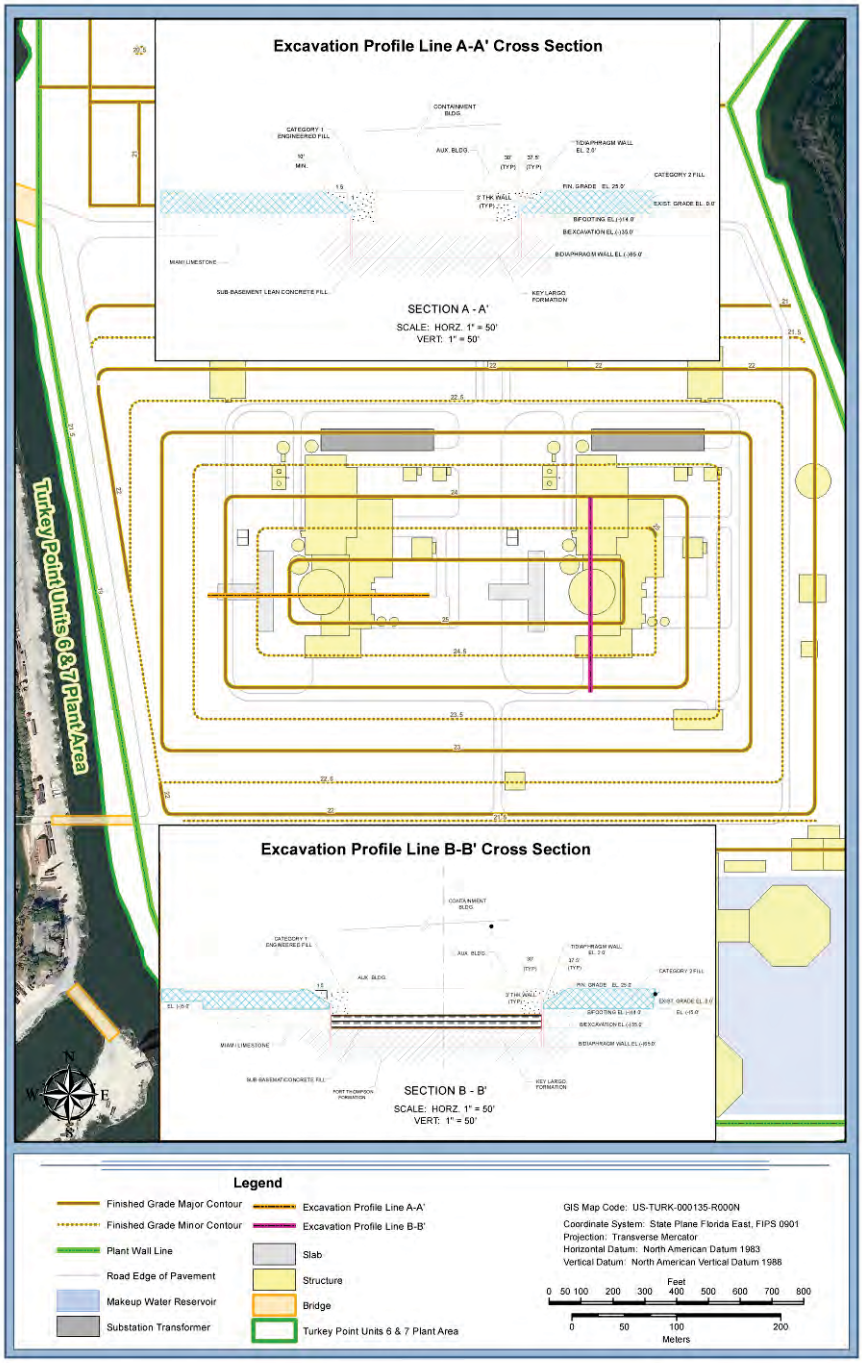

ASSOCIATED ENCLOSURES:

None

NRC RAI Letter No. PTN-RAI-LTR-040

SRP Section: 02.05.04 - Stability of Subsurface Materials and Foundations

QUESTIONS from Geosciences and Geotechnical Engineering Branch 1 (RGS1)

NRC RAI Number: 02.05.04-15 (eRAI 6006)

FSAR Section 2.5.4.7.3.4 provides a justification for use of generic curves for the dynamic properties of the crushed limestone backfill. The nature of this material is unique and potentially not conducive to dynamic testing. In accordance with NUREG-0800, Standard Review Plan, Chapter 2.5.4, "Stability of Subsurface Materials and Foundations," and Regulatory Guide (RG) 1.138, "Laboratory Investigations of Soils and Rocks for Engineering Analysis and Design of Nuclear Power Plants" and in order for the staff to review this issue, please provide additional evaluations, possibly through other types of testing, to justify the use of these generic curves.

FPL RESPONSE:

As stated above in the Request for Additional Information (RAI), dynamic tests such cyclic triaxial and/or Resonant Column Torsional Shear (RCTS) tests in this crushed limestone backfill material are not suitable. Thus, the dynamic properties of this material are based on comparison with dynamic properties of similar materials documented in the literature. As part of this revised response, a further literature review was conducted to evaluate the assumptions made for the dynamic properties and assigned uncertainty through randomization.

The specification of the crushed limestone backfill material for Turkey Point Units 6 & 7 will be prepared during detailed design. For the analysis, the generic curves from Seed et al., (Reference 1) for gravelly soils were considered representative for the backfill. Figure 1 shows the selected curve as “Structural Fill” along with the boundaries considered in the randomization conducted for the site response analysis.

As a result of the literature review, curves proposed by Menq (Reference 2) were selected. These curves are normalized curves based on parameters of the material that include the coefficient of uniformity (C_u), and the effective confining pressure for calculating the shear modulus ratio, the average particle size (D_{50}), and number of testing cycles for calculating the damping ratio.

Structural fill to be used at Turkey Point Units 6 & 7 will be limestone fill (limerock) obtained from onsite Miami Limestone and offsite sources. The use of this material for structural fill is standard practice in Florida. As an example, the Florida Department of Transportation (DOT) Standard Specification (Reference 3) Section 911-5.2.1 for limestone base states, “At least 97% (by weight) of the material shall pass a 3 1/2 inch sieve and the material shall be graded uniformly down to dust. The fine material shall consist entirely of dust of fracture.” The requirement that the material be “graded uniformly down to dust” indicates a material that is well graded. Although the specification for gradation and size requirements for this project will be prepared during detailed design, they are anticipated to be similar to the Florida DOT specifications.

Uniformly graded granulometric curves with at least 97 percent (by weight) of the material passing the 3 1/2 inch sieve, and 5 percent to 10 percent (by weight) of fines (as is typically found in backfills) are simulated (i.e., the curves are generated based on the assumptions stated), which yield coefficients of uniformity around 60 and mean particle sizes around 2.5 millimeters (mm). The number of cycles selected was ten, as typically reported in RCTS.

In order to validate the simulated granulometric curves, they were compared to granulometric curves obtained from testing performed on crushed Miami Limestone in the initial subsurface investigation program from test pits (Reference 4). Despite the curves obtained in the initial investigation lacking fines, there is good agreement for diameters above D_{10} when compared with the simulated granulometric curves. The D_{10} parameter is necessary in order to make use of Menq's equations (Reference 2), thus, the curves obtained in the initial investigation were not deemed sufficient.

The effective overburden pressure is calculated considering a total unit weight of 137 pounds per cubic foot (pcf), an at-rest pressure coefficient of 0.5 and a depth of 20 feet, which is half the thickness of the backfill layer. The mean effective stress at this depth is approximately 1000 psf.

Figure 1 depicts the shear modulus ratio against strain of the generic curve taken from Seed et al. (Reference 1), which is labeled as "Structural Fill" along with two curves obtained using Menq's equations (Reference 2) and the parameters discussed above (i.e., the coefficient of uniformity [C_u], the effective confining pressure for calculating the shear modulus ratio, the average particle size [D_{50}], and number of testing cycles for calculating the damping ratio). These two curves are labeled after the coefficient of uniformity obtained from the simulated well-graded and uniformly distributed granulometric curves representing the backfill ($C_u = 60$ and $C_u = 50$). Moreover, bounding curves of the structural fill randomization are provided as dashed lines, where the highest strain from site response analysis in the structural fill is less than 0.02 percent as seen in FSAR Figure 2.5.2-248 (Sheet 2 of 2). The shear modulus ratio curves $C_u = 50$ and $C_u = 60$ are in good agreement with the structural fill curve at low strains (less than 0.001 percent), and at higher strains, up to 0.02 percent, these curves are enveloped by the randomization boundaries.

Table 1 shows the shear modulus ratio against strain values for backfill and for $C_u = 50$ using Meng's equations (Reference 2).

Figure 1 G/G_{max} Curves for Backfill

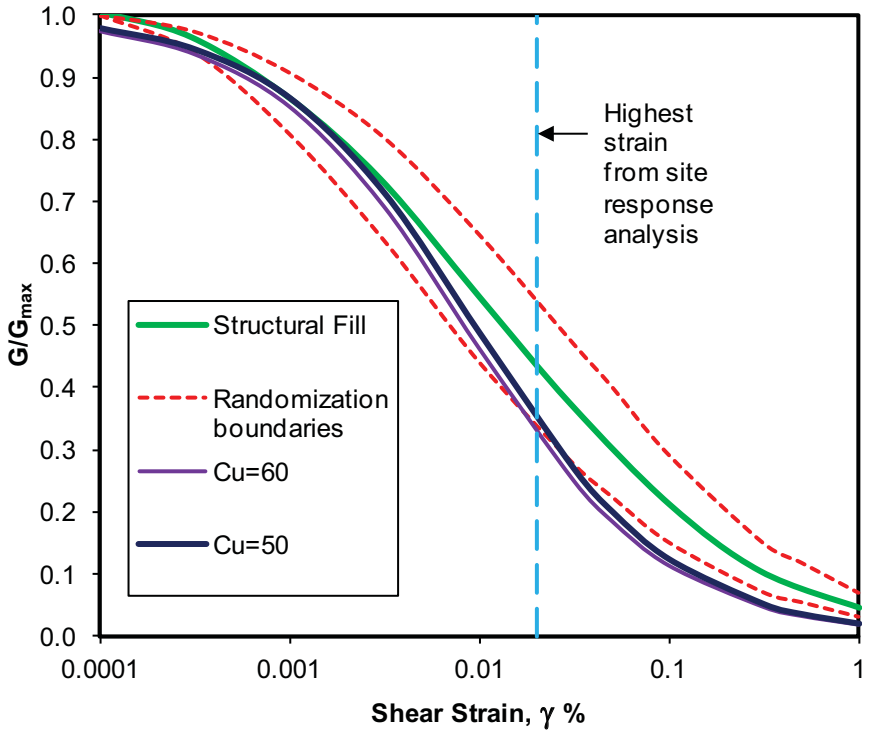

Figure 2 shows the damping against strain of the generic curve taken from Seed et al., (Reference 1) along with two curves obtained using Menq's equations (Reference 2) and the parameters discussed above (i.e., the coefficient of uniformity [C_u], the effective confining pressure for calculating the shear modulus ratio, the average particle size [D_{50}], and number of testing cycles for calculating the damping ratio). Bounding curves of the structural fill randomization are provided as dashed lines, where the highest strain in the structural fill is reported to be less than 0.02 percent as obtained from the site response analysis. The damping curves $C_u = 50$ and $C_u = 60$ are in good agreement with the structural fill curve at low strains, and at higher strains these curves are enveloped by the randomization boundaries.

Table 2 shows the damping against strain values for backfill and for $C_u = 50$ using Menq's equations (Reference 2).

The prior shows that the selected generic dynamic properties from Seed et al. (Reference 1) and the assigned randomized profiles represent the backfill behavior well in absence of final backfill design and laboratory testing.

Figure 2 Damping Curves for Backfill

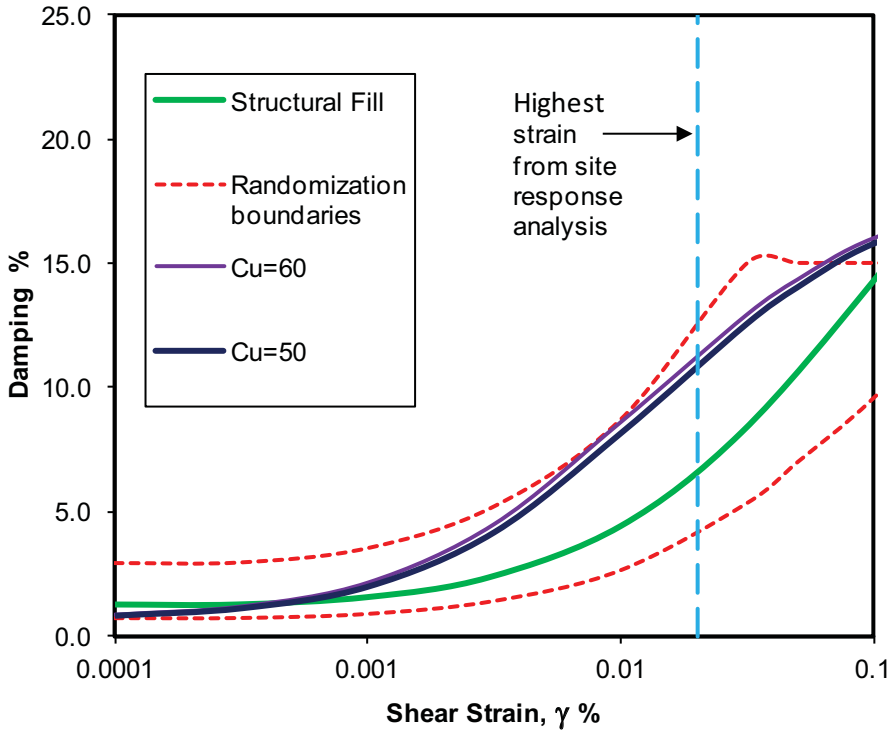

Table 1

G/G_{max} for Backfill (Structural Fill & C_u = 50)

Structural Fill

G/G_{max}	1.00	0.96	0.87	0.74	0.55	0.37	0.21	0.11	0.05
γ (%)	0.0001	0.0003	0.001	0.003	0.01	0.03	0.1	0.3	1

C_u = 50

G/G_{max}	0.98	0.94	0.86	0.71	0.49	0.27	0.12	0.05	0.02
γ (%)	0.0001	0.0003	0.001	0.003	0.01	0.03	0.1	0.3	1

Table 2

Damping for Backfill (Structural Fill & C_u=50)

Structural Fill

D (%)	1.3	1.3	1.6	2.4	4.4	8.2	14.3	20.6	27.9
γ (%)	0.0001	0.0003	0.001	0.003	0.01	0.03	0.1	0.3	1

C_u = 50

D (%)	0.8	1.1	2.0	4.2	8.2	12.6	15.8	17.5	17.7
γ (%)	0.0001	0.0003	0.001	0.003	0.01	0.03	0.1	0.3	1

Under large strain (between 0.001 and 0.02 percent), the G/G_{max} curves for the backfill and for C_u = 50 using Menq's equations (Reference 2) are reasonably close and are within the randomized profiles. Therefore, the G/Gmax curves for backfill as provided in FSAR Table 2.5.4-216 are considered appropriate after additional literature review.

Similarly, damping curves for backfill as reported in FSAR Table 2.5.4-216 and for C_u = 50 using Menq's equations are within the randomized profiles. Even though there is difference between these two curves, particularly for strains between 0.001 percent and 0.02 percent, the assigned values in FSAR Table 2.5.4-216 are lower and more conservative. More importantly, damping curves for backfill as reported in FSAR Table 2.5.4-216 and for C_u = 50 using Menq's equations (Reference 2) are within the randomized profiles. Therefore, the damping curves given in the current FSAR Table 2.5.4-216 are considered appropriate.

This response is PLANT SPECIFIC.

References:

1. Seed, H., R. Wong, I. Idriss, and K. Tokimatsu, *Moduli and Damping Factors for Dynamic Analyses of Cohesionless Soils*, Earthquake Engineering Research Center, Report EERC 84/14, University of California, Berkeley, 1984.
2. Menq, F.Y., *Dynamic Properties of Sandy and Gravelly Soils*, Ph.D. Thesis, University of Texas at Austin, 2003.
3. Florida Department of Transportation, *Standard Specifications for Road and Bridge Construction*, 2010.
4. MACTEC Engineering and Consulting, Inc., *Field Data Report - Geotechnical Exploration and Testing Turkey Point COL Project Florida City, Florida, MACTEC Job No. 6468-07-1950*, October 6, 2008.

ASSOCIATED COLA REVISIONS:

None

ASSOCIATED ENCLOSURES:

None

NRC RAI Letter No. PTN-RAI-LTR-040

SRP Section: 02.05.04 - Stability of Subsurface Materials and Foundations

QUESTIONS from Geosciences and Geotechnical Engineering Branch 1 (RGS1)

NRC RAI Number: 02.05.04-16 (eRAI 6006)

Section 2.5.4.7.3.3 “Shear modulus and Damping for Rock”, indicates that the damping for rock is taken as 1%. The damping shown in Figure 2.5.2-249, which describes the soil properties used to develop the GMRS, indicates that a damping value of 0.5% was used in the analyses. In accordance with NUREG- 0800, Standard Review Plan, Chapter 2.5.4, "Stability of Subsurface Materials and Foundations," please provide clarification as to the actual level of damping used in the analyses and provide a basis for its selection considering the large variability in RQD shown in Figure 2.5.4-215.

FPL RESPONSE:

As part of the supplemental field investigation as discussed in the revised response to RAI 02.05.04-3, four resonant column torsional shear tests (RCTS) were conducted on the Key Largo and Fort Thompson formations. Three samples were extracted from initial borings B-615, B-714, B-728, and one sample was extracted from supplemental boring R-6-1b. The sample descriptions are provided in Table 1. The sample locations are shown in Figure 1 of the revised response to RAI 02.05.04-3. The supplemental field investigation also involved three additional RCTS tests.

This response provides clarification on the actual levels of damping used in the analysis. In addition, this response outlines if the additional test results on the rock and soil samples impact the conclusions of the previously conducted site response analysis.

Table 1
RCTS Tests on Rock Samples

Boring Number	Sample Designation	Material Type	Specimen Midpoint Depth (Feet)
B-728	728-CS-04	Fort Thompson Limestone	54.0
B-615	615-CS-01	Key Largo Limestone	32.9
B-714	714-CS-01	Key Largo Limestone	29.7
R-6-1b	R-6-1b-SC-3	Fort Thompson Limestone	47.9

The following discussion provides a basis for the selection of damping ratio values for the various rock strata considering the large variability in rock quality designation (RQD).

The variability in RQD within each stratum is generally random in nature and does not have directional trends (e.g., high RQD at the top of the stratum and low RQD at the bottom), thus, the strata are not sub-divided within each formation. Figure 1 shows vertical RQD variability in the boreholes of cross-section A-A (see Figure 2. The lateral variability for the Key Largo and Fort Thompson formations is presented in Figures 2 and 3. The natural

variability, which is evident in Figures 1, 3 and 4, is addressed through a randomization process for site response analysis as described in FSAR Subsection 2.5.2.5.2.

For the purpose of this response, the rock strata will be classified as either “strain dependent” or “not strain dependent.” The strain dependent strata have a variable G/G_{max} and damping ratios as a function of shear strain. The rock strata contained in the Key Largo and Fort Thompson formations are not strain dependent; whereas the Miami and Arcadia Limestone are strain dependent.

Key Largo and Fort Thompson Formations:

The RCTS results, as obtained from the supplemental field investigation testing, are used to create the best fit damping curve labeled “Key Largo and Fort Thompson” in Figure 4. The maximum shear strain that these strata experience is much smaller than 0.005 percent (Figure 5). For this strain interval, the damping ratio is first constant around 0.8 percent, and then increases towards 1 percent as the shear strain approaches 0.005 percent. Even though, the assumed damping ratio of 1 percent is slightly higher than the measured value, the test results can be considered in good agreement with the assumptions made for this layer and the difference is within the uncertainty involved in determining the damping ratio from the test results.

Miami Limestone:

In FSAR Subsection 2.5.4.7.3.3 the Miami Limestone is designated as strain dependent. The recommended damping curve in Figure 4, labeled “Miami Limestone,” shows that damping remains constant at 0.6 percent from 0.0001 to 0.03 percent shear strain.

Arcadia Formation:

Although the Arcadia Formation is reported in FSAR Subsection 2.5.4.2.1.1 along with the Miami Limestone, Key Largo, and Fort Thompson formations as being rock strata, the Arcadia Formation is much weaker than the Key Largo and Fort Thompson formations as indicated by the unconfined compressive strengths in revised FSAR Table 2.5.4-209 provided in the revised response to RAI 02.05.04-4. Additionally, the strain-dependent Miami Limestone has double the strength of the Arcadia Formation. Thus, for the Arcadia Formation the recommended damping curve from the overlying Peace River Formation (natural soil) was used, as they both belong to the Hawthorn Group (FSAR Subsection 2.5.1.1.1.2.1.1).

The uncertainties and variation in the damping ratios (reflected in the variations in parameters such as RQD) were taken into account in the randomization process. FSAR Figure 2.5.2-238 shows the variation assumed in the randomization process for the damping ratio versus strain for the Arcadia Formation.

The constant damping ratio of the material below the Arcadia Formation, i.e., below about 640 feet depth in FSAR Figure 2.5.2-249, is 0.32 percent based on the median value of kappa and associated uncertainty.

Sensitivity Analysis for New (2013) RCTS Test Results:

During supplemental field investigation, three additional RCTS tests were conducted on soil formations (samples collected from the center of the NI from borings R-6-1b and R-7-1), and four additional RCTS were conducted on Key Largo and Fort Thompson formations.

For the soil formations, The G/Gmax and damping ratio curves as a function of shear strain are provided in Figures 7 and 8, respectively. Both damping ratio and G/Gmax curves include the 2008 data and the aggregated 2008 and 2013 data.

In the case of the Key Largo and Fort Thompson formations, the existing site response analysis assumes linear behavior with strain-independent shear modulus and damping ratios for the range of shear strains induced in site response analysis. A damping ratio of 1 % was adopted for both the Key Largo and Fort Thompson formations. Figures 9 and 10 presents the laboratory measured (2013) G/Gmax and damping ratio curves, respectively, for the two formations. The figure shows a damping ratio of 0.76% at low-strain, smaller than the assumed value of 1%, as well as shear modulus reduction at higher shear strains, as opposed to no degradation in the existing analysis.

For the sensitivity analysis, seismic site amplification analysis is performed for two sets of dynamic soil properties. The first set includes the two Best Estimate (BE) "original" dynamic soil profiles, i.e. the existing dynamic soil profiles, representing the near nuclear island (NI) site conditions and the far from nuclear island (FAR) conditions, respectively. These profiles were used as the basis for the seismic amplification at the Turkey Point site as documented in the FSAR. For the sensitivity analysis, a site response analysis using random vibration theory is conducted, which is similar to the analysis documented in the FSAR Subsection 2.5.2.5. Lower bound (LB) and upper bound (UB) profiles for the NI and FAR site conditions are also used in the study. The shear wave velocity profiles for the LB and UB cases are calculated as the BE profile -/+ one standard deviation. All other dynamic properties including strain-dependent property curves are the same as for the BE profiles. All profiles have low-strain dynamic properties (shear-wave velocity and damping) and corresponding strain-dependent property curves.

The site-specific rock Uniform Hazard Response Spectra (UHRS) at 1E-4 and 1E-5 hazard levels for low frequency (LF) and high frequency (HF) motions are propagated through all soil columns and the site response is calculated at the ground surface (EI. +25.5, depth of 0 feet) and at the bottom of foundation of the nuclear island (EI. –16, depth of 41.5 feet).

To estimate the effect of the new strain-dependent property curves on the design level earthquake, the design response spectrum level motion is calculated for the “Original” and “New” response based on the lower bound (LB), best estimate (BE), and upper bound (UB) profiles. These design level ARS are compared to the true foundation input response spectra (FIRS) and the Turkey Point safe shutdown earthquake (SSE) (i.e., the envelope of FIRS and RG 1.60, respectively) in Figure 11 for FAR site conditions. Note that the limited differences between “FIRS FAR” and “Design Level ARS FAR Original” are due to the reduced number of used profiles (LB, BE, and UB profiles only) in the case of the latter, when compared with the complete set of analysis using 60 randomized profiles in the case of the former. The general agreement between the two responses demonstrate the adequacy of the three selected profiles (LB, BE, and UB) for representing the site

amplification at Turkey Point for the purpose of this sensitivity study. Comparing the "Design Level ARS FAR Original" to the "Design Level ARS FAR New" shows some increase in the response. This increase is nevertheless enveloped by the Turkey Point SSE at all frequencies, except at around 0.5 Hz. At this frequency, the "Design Level ARS FAR New" spectral acceleration is larger than the spectral acceleration of the "Design Level ARS FAR Original" by less than 2 percent. This exceedance is expected to be of similarly negligible magnitude for the Turkey Point SSE at around 0.5 Hz. These same observations apply to the NI site conditions in Figure 12.

It should be noted that if the differences were to be calculated from a fully randomized soil column profile, they would be expected to be even smaller than those observed in the current study.

The conclusions of the sensitivity study are as follows:

- The newly acquired data has a small effect on the site amplification results, which were used to calculate the site-specific design response spectra for Turkey Point Units 6 & 7, resulting in an increased response.
- A large margin exists between the site-specific motions and the adopted broadband SSE response spectrum, adopted as the envelope of the RG 1.60 horizontal motion with a peak ground acceleration of 0.1 g and the site-specific FIRS. The increase in seismic response is enveloped by the SSE at all frequencies, except at around 0.5 Hz, where the SSE exceedance is negligible (less than 2 percent).
- It is concluded that the Turkey Point Units 6 & 7 SSE is not impacted by the new data, and no further analyses are required. In conclusion, the results of the existing site response analysis in FSAR Section 2.5.2 are still valid

Figure 1 Vertical RQD Variation

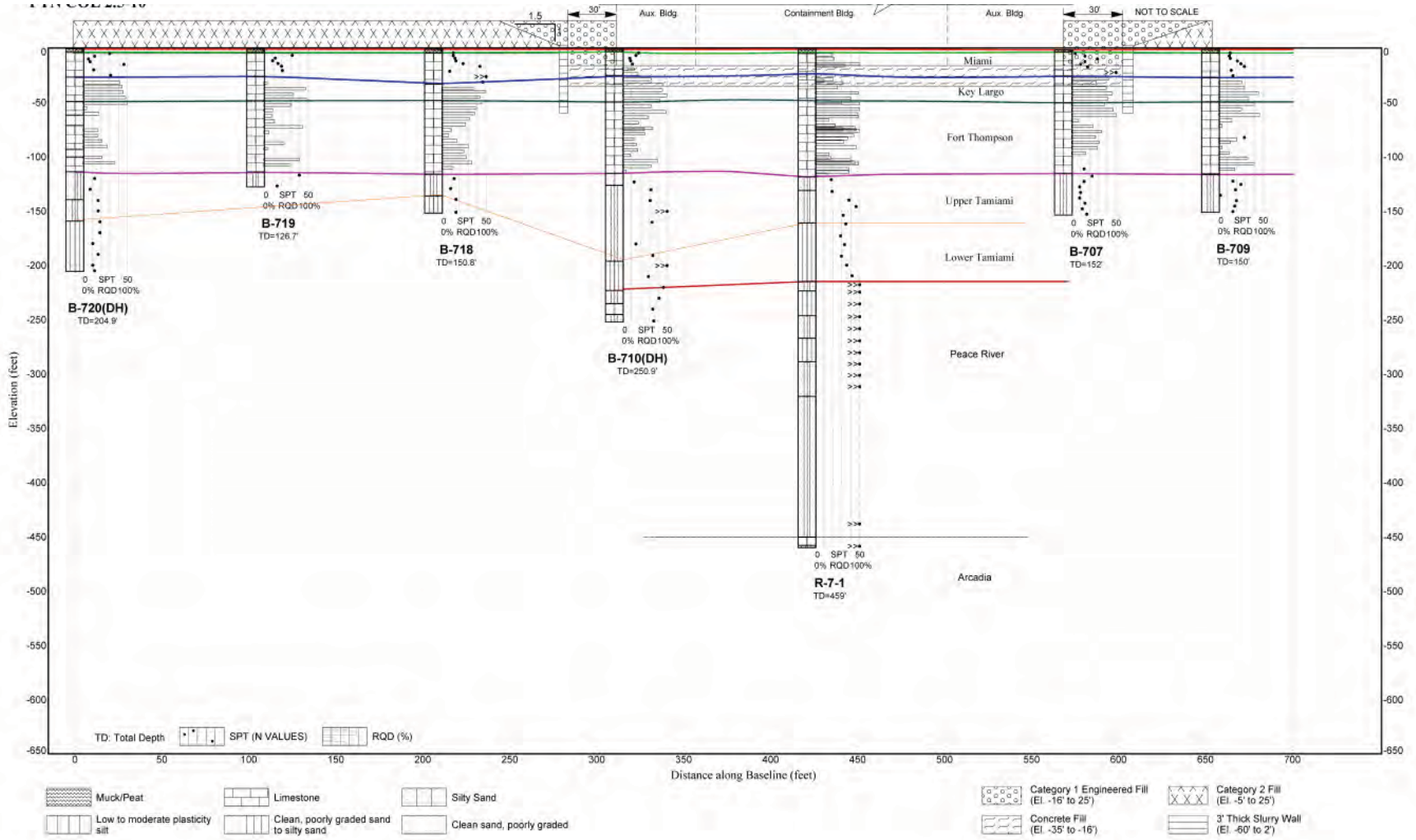

Figure 2 Plan Showing Geotechnical Cross Section Locations

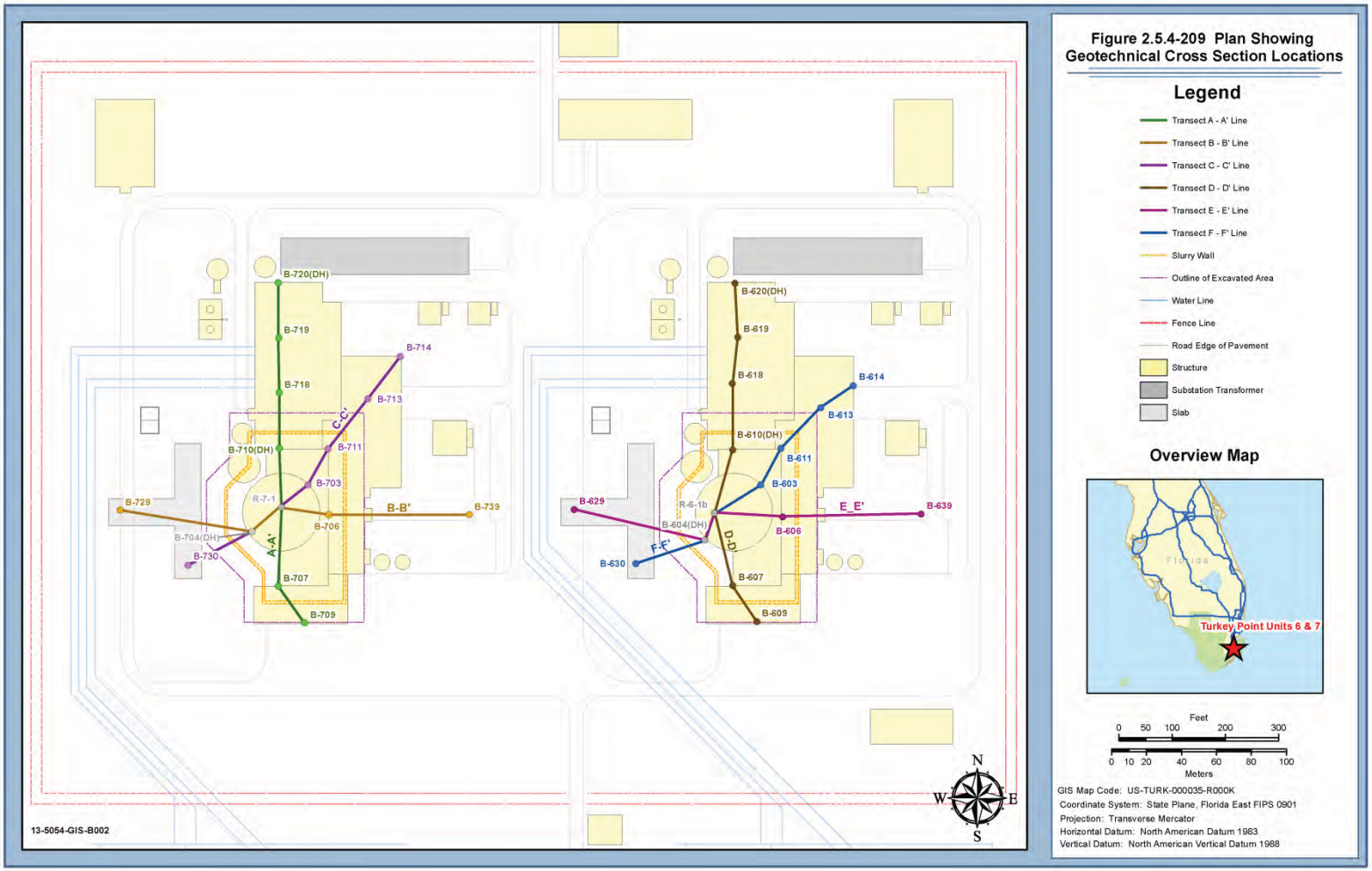

Figure 3 RQD Variation from South to North

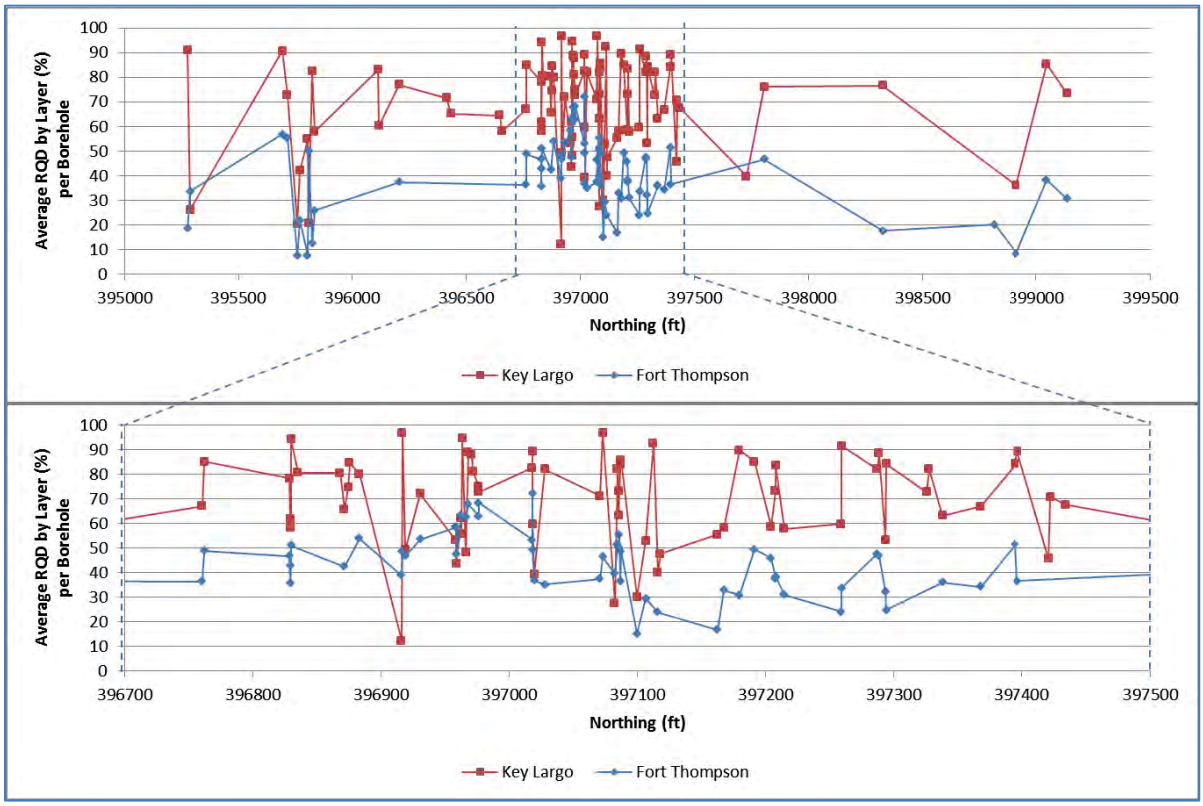

Figure 4 RQD Variation from West to East

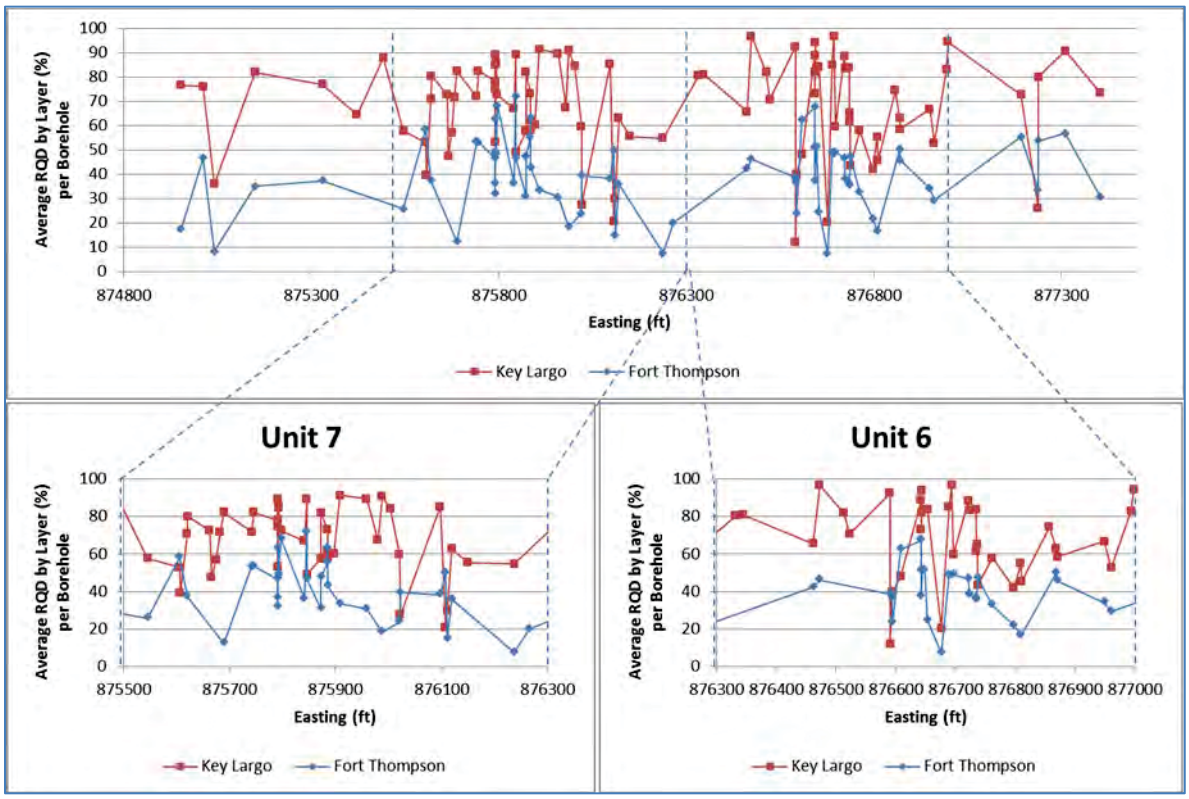

Figure 5 Recommended Damping Curves

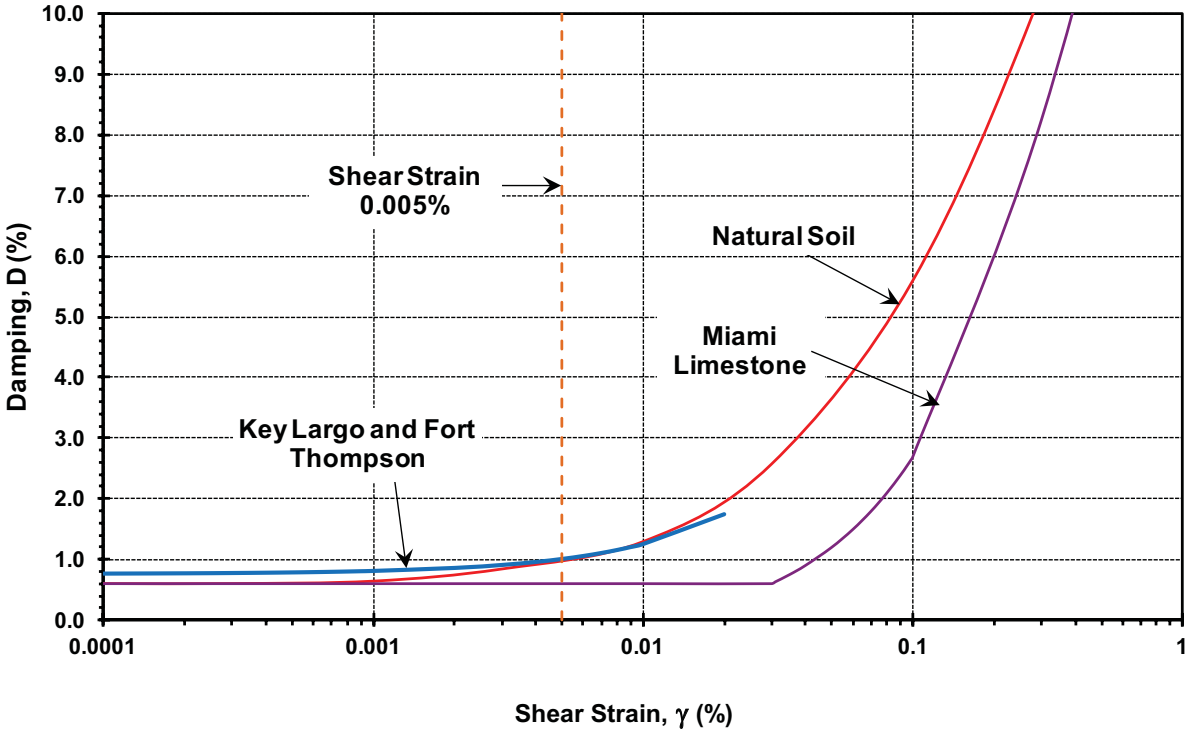

Figure 6 Median Strain-Compatible Soil Profiles (Upper 800 feet)

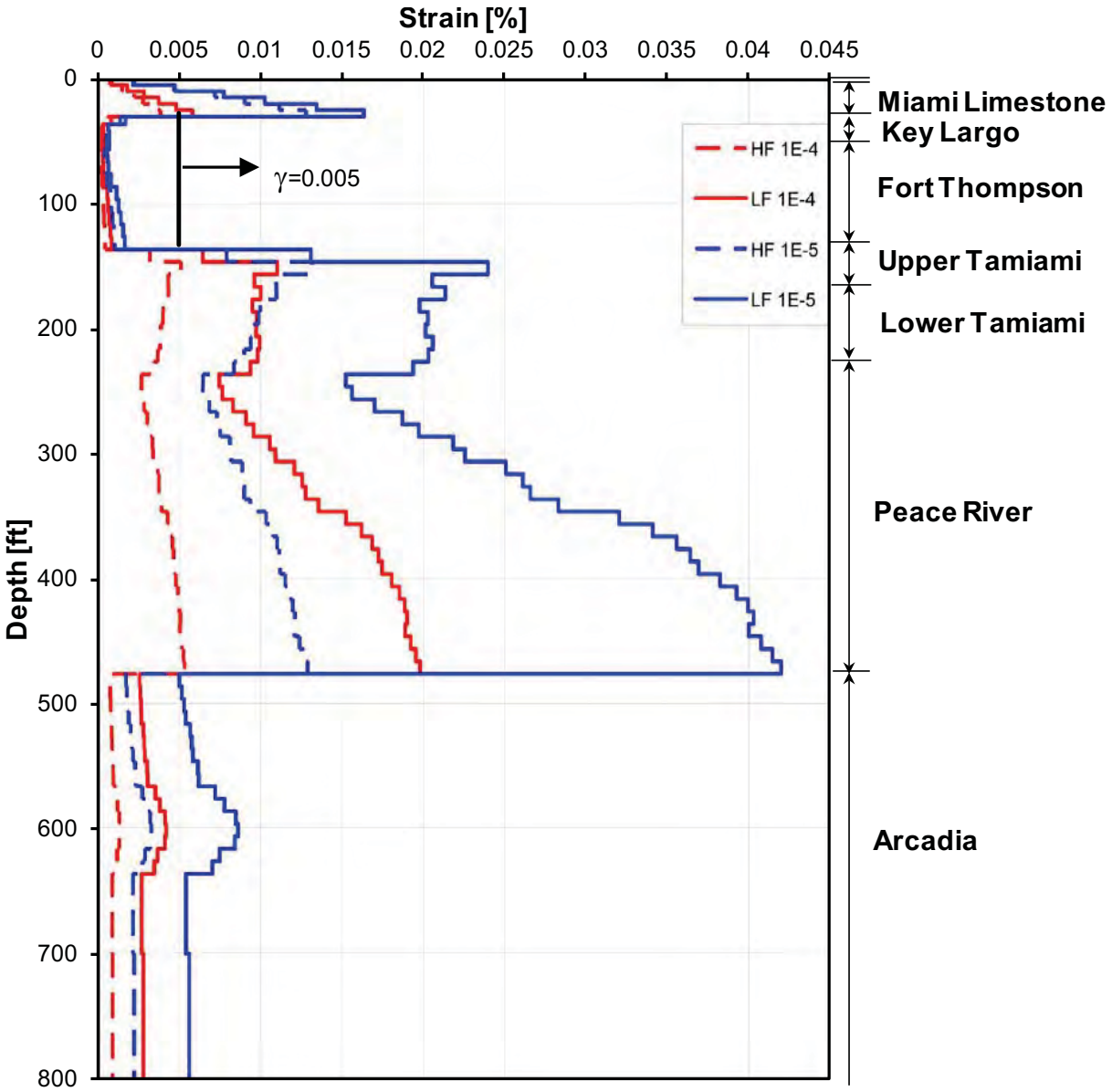

Figure 7 Comparison of Shear Modulus Reduction Curves for Natural Soil

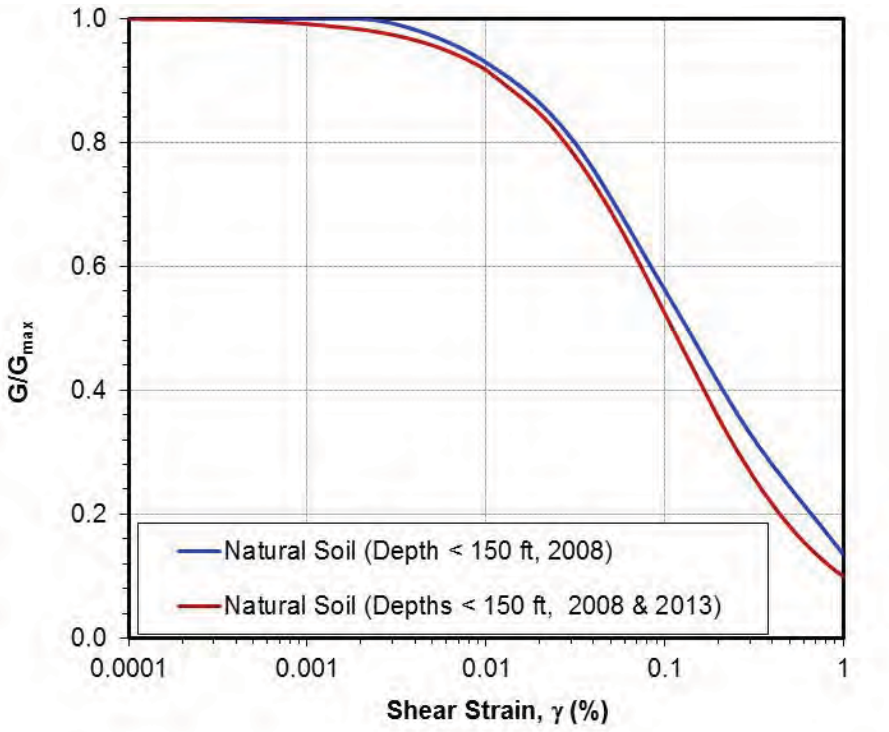

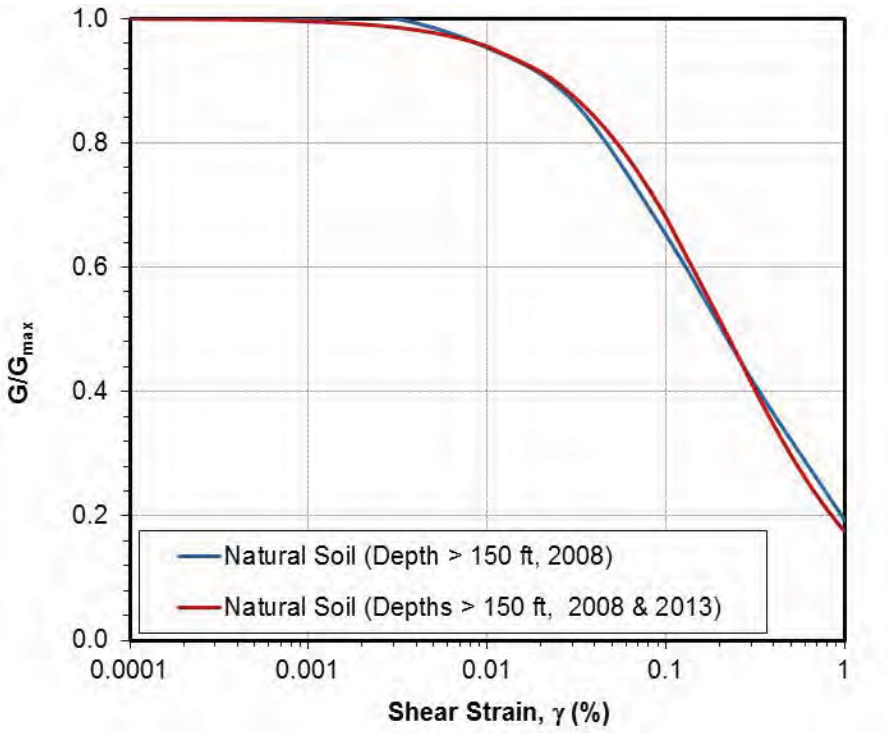

Figure 8 Comparison of Damping Ratio for Natural Soil

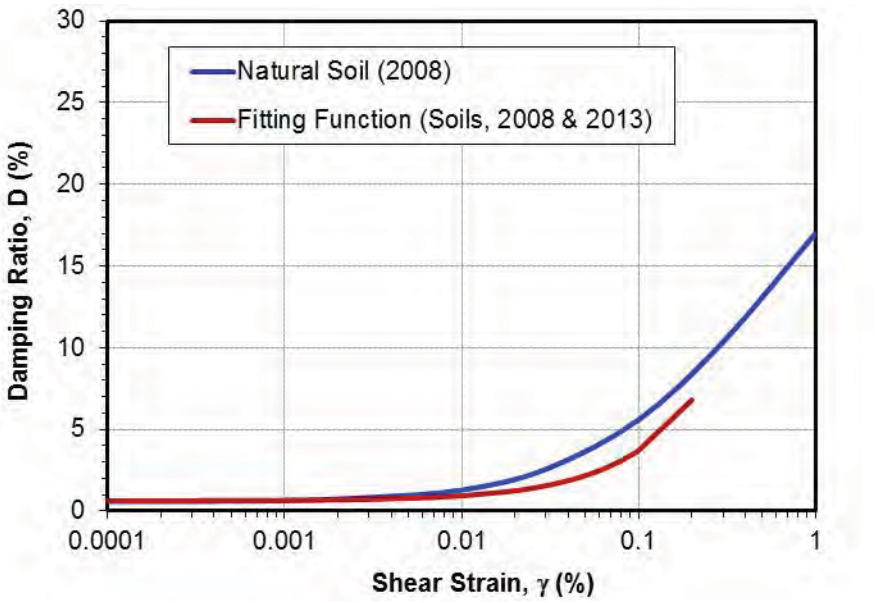

Figure 9 Shear Modulus Reduction and Key Largo and Fort Thompson Formations

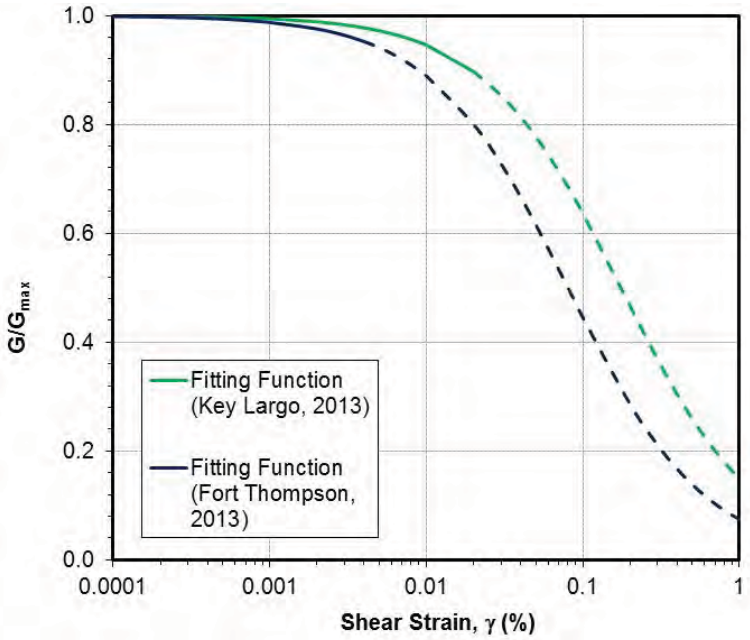

Note: Solid G/Gmax lines indicate fitted curves based on laboratory data; dashed G/Gmax lines indicate extrapolated curves based on the laboratory data fitting function. Calculated shear strain levels in the conducted study are smaller than 0.01 %

Figure 10 Damping Ratio Curves for Key Largo and Fort Thompson Formations

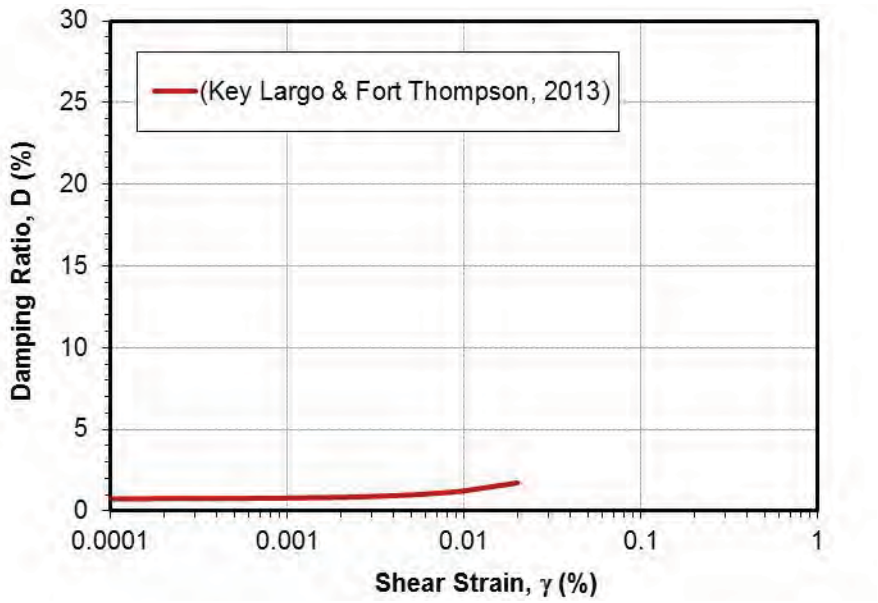

Figure 11 Design Level Response Spectra – FAR Site Conditions

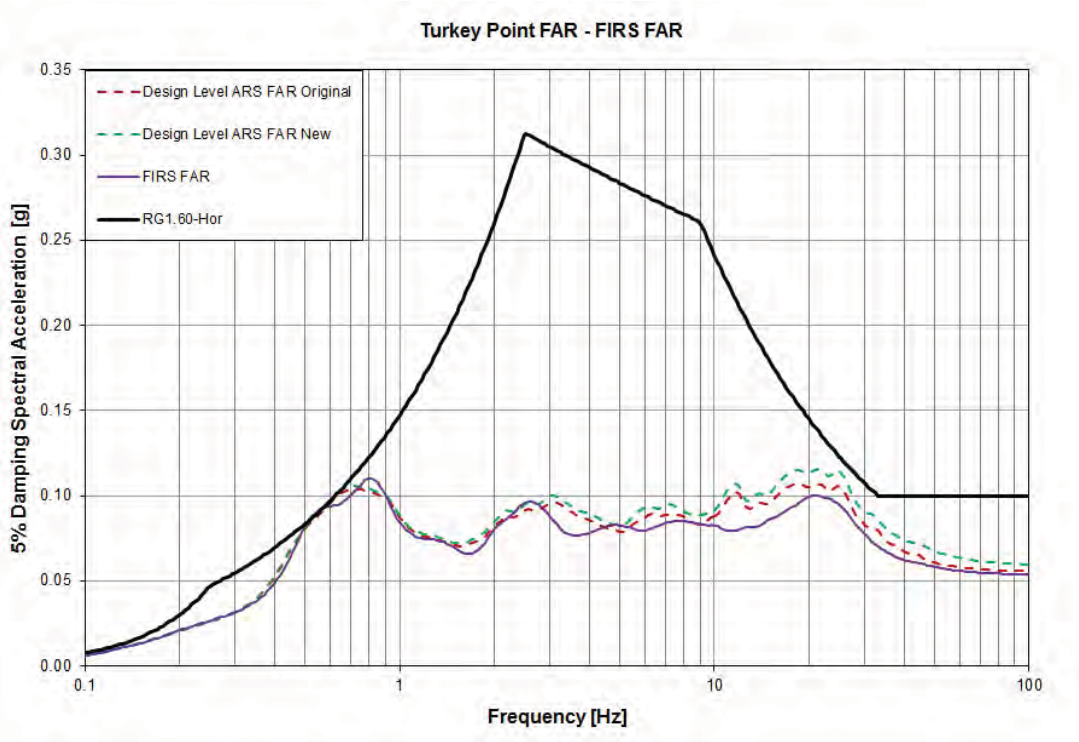

Figure 12 Design Level Response Spectra – NI Site Conditions

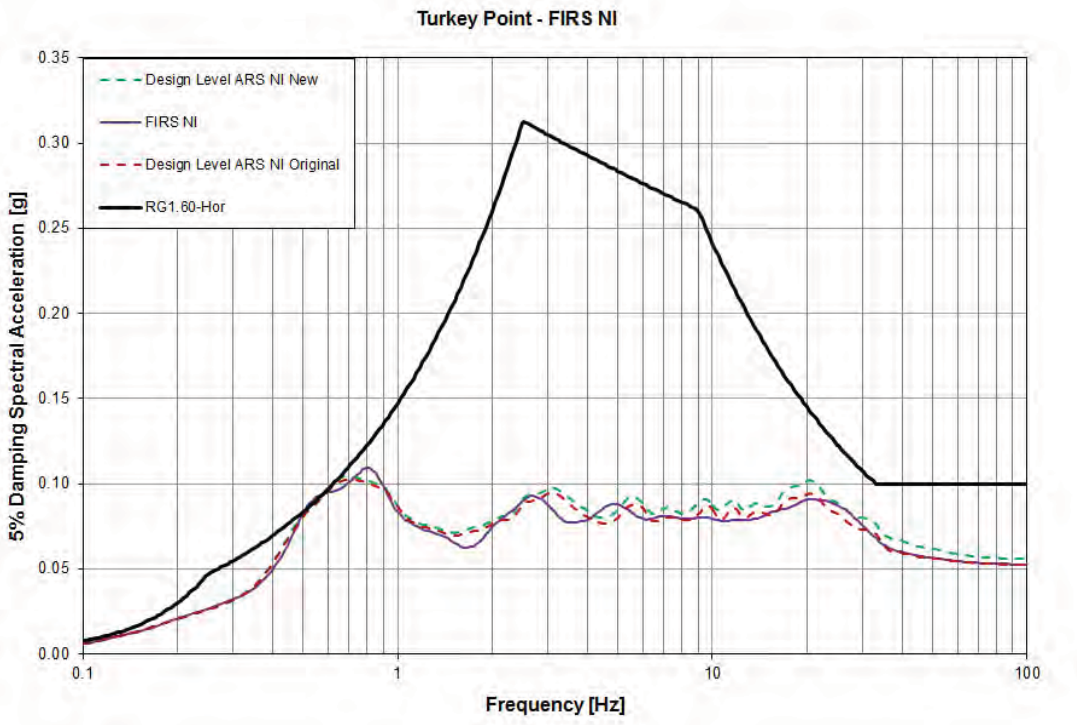

This response is PLANT SPECIFIC.

References:

None

ASSOCIATED COLA REVISIONS:

Revisions to the first paragraph of FSAR Section 2.5.4.2.1.3.16, Shear Modulus Degradation and Damping Ratio are provided as part of the revised response to: RAI 02.05.04-4.

Revisions to FSAR Section 2.5.4.7.3, Static and Dynamic Laboratory Testing are provided as part of the revised response to RAI 02.05.04-4.

The third paragraphs of FSAR Subsection 2.5.4.2.1.3.16 will be revised in a future revision as follows:

Table 2.5.4-216 summarizes the selected values of G/G_{max} versus shear strain for each stratum investigated. Each RCTS test also provides measured values of damping ratio (D) at increasing shear strain levels. The same procedure used for G/G_{max} is employed to obtain a best-fit D versus shear strain curve from the literature. Table 2.5.4-216 shows the selected values of D versus shear strain for each test. This is described further in Subsection 2.5.4.7.3.2. RCTS test results are tabulated in Appendix F of Reference 257 **and Appendix B of Reference 290**.

FSAR Subsection 2.5.4.7.3.1 will be revised in a future revision o as follows:

2.5.4.7.3.1 Selected Shear Modulus Degradation Curves for Site Strata

As described in Subsection 2.5.4.2.1.3.16, **fourteen**~~seven~~ RCTS tests are performed on intact samples collected from Strata **3, 4,** 5, 6, and 7. Each of these intact samples is from the power block area. In each RCTS test, values of shear modulus (G) measured at increasing strain levels are obtained. These values are compared to the value of G_{max}, the shear modulus measured at 10^{-4} percent shear strain. The shear modulus degradation (ratio of G/G_{max}) is plotted against shear strain, and a curve of G/G_{max} from the literature that best fits the test data is selected. Literature curves are used rather than an actual best-fit curve through the test data because the literature curves typically extend over a greater range of shear strain than the test data. Curves recommended by the Electric Power Research Institute (EPRI) for non-cohesive soils are employed (Reference 258).

The modulus degradation curves (plots of G/G_{max} versus shear strain) from actual RCTS tests are presented on Figure 2.5.4-232 **for the Key Largo Formation, Figure 2.5.4-246 for the Fort Thompson Formation, Figure 2.5.4-247 for natural soils less than 150 feet deep, and Figure 2.5.4-248 for natural soils greater than 150 feet deep**. Figure 2.5.4-233 shows the selected values of G/G_{max} versus shear strain for the ~~two~~**five** strata tested in the power block in addition to the other site strata addressed in this evaluation. The selected G/G_{max} versus strain values for each stratum are also presented in Table 2.5.4-216.

Stratum 1 is removed from the site so the shear modulus degradation properties of that stratum are not relevant.

Stratum 2 is a weak rock stratum described in Subsection 2.5.4.7.3.3.

Due to the similarity of the grain size distribution and the materials, the recommended shear modulus degradation for Stratum 7 is the same as for Stratum 6, i.e., natural soil deeper than **150**~~159~~ feet depth in Figure 2.5.4-233. This modulus degradation curve is also selected for Stratum 8 which consists of very weak rock and is part of the same geological formation (Hawthorn Group) as Stratum 7.

Rock Strata 3 and 4 are considered not subject to modulus degradation **in the shear strain range of 10^{-4} percent to 0.005 percent**, as described in Subsection 2.5.4.7.3.3. **The recommended shear modulus degradation curves for rock Strata 3 and 4 are provided on Figure 2.5.4-233.**

Dynamic properties of compacted structural fill are described in Subsection 2.5.4.7.3.4.

For soil/rock beneath 600 feet, strain levels are so small that it can be reasonably assumed that there is no shear modulus degradation.

FSAR Subsection 2.5.4.7.3.2 will be revised in a future revision as follows:

2.5.4.7.3.2 Selected Damping Curves for Soils

Each RCTS test also provides measured values of damping ratio (D) at increasing shear strain levels. The damping data for tests performed **on natural soils** are shown on ~~Figure~~

~~2.5.4-234~~ **Figure 2.5.4-249.**The same procedure used for shear modulus degradation (G/G_{max} versus shear strain) is employed to obtain a ~~best-fit~~ D versus shear strain **best-fit** curve from the literature. Figure 2.5.4-235 shows the selected values of D versus shear strain for tested **Strata 3, 4,** 5, 6, and 7, i.e., the **rock curve for Strata 3 and 4 and the** natural soil curve used for **the remaining**~~all three~~ soil strata. Th**e natural soil** ~~is~~ D versus shear strain curve is also selected for Stratum 8.

FSAR Subsection 2.5.4.7.3.3 will be revised in a future revision as follows:

2.5.4.7.3.3 Shear Modulus and Damping for Rock

Rock strata are encountered at several depths at the site. For Strata 3 and 4, **RCTS test results were used to find best-fit shear modulus degradation and damping curves. The modulus degradation curves (plots of G/G_{max} versus shear strain) from actual RCTS tests are presented on Figure 2.5.4-232 for the Key Largo Formation and Figure 2.5.4-246 for the Fort Thompson Formation. Recommended shear modulus degradation curves are presented on Figure 2.5.4-233. Based on these results,** ~~F~~for Strata 3 and 4 **(Key Largo and Fort Thompson formations)**, the shear modulus is considered non-strain dependent based upon the competency of the rock. **The damping data for tests performed on the Key Largo and Fort Thompson formations are shown on Figure 2.5.4-234. The recommended damping curve for the Key Largo and Fort Thompson formations is shown on Figure 2.5.4-235. Below a shear strain of 0.01 percent, the damping ratio varies between 0.8 percent and 1.2 percent. Considering the small variation in damping in the shear strain range of interest, the damping ratio is considered as constant at 1 percent.** For the Miami Limestone (Stratum 2), the limestone is considered sufficiently weak as to have a strain-dependent shear modulus. A recommended shear modulus degradation for this stratum based on literature (Reference 259) for mudstones/shales is provided in Figure 2.5.4-233. Similarly, a recommended damping curve for Stratum 2 is provided in Figure 2.5.4-235.

See Subsection 2.5.4.1 for a brief description of geologic conditions at depths greater than 600 feet based upon regional data. See Subsection 2.5.4.7.2.2 for a description of deep shear wave velocity profiles pertinent to the site derived from sonic logging data.

~~It should be noted that hard rock is considered to have damping, but is not strain dependent. For site-specific work, damping of 1 percent is adopted for Strata 3 and 4, and bedrock shear modulus is considered to remain constant (i.e., no degradation) in the shear strain range of 10-4 percent to 1 percent.~~

FSAR Table 2.5.4-216 will be revised in a future revision as follows:

Table 2.5.4-216
Summary of Recommended Shear Modulus Degradation and Damping Curves

	Shear Strain, γ (%)	0.0001	0.0003	0.001	0.003	0.01	0.03	0.1	0.3	1
G/G_{max}	Natural Soil (Depth > ~~159~~ 150 ft)	1.00	1.00	1.00	1.00	0.95	0.87	0.65	0.42	0.19
	Natural Soil (Depth < ~~159~~ 150 ft)	1.00	1.00	1.00	0.99	0.93	0.81	0.56	0.33	0.14
	Miami Limestone	1.00	1.00	1.00	1.00	1.00	0.98	0.87	0.63	0.33
	Key Largo [1]	1.00	1.00	0.99	0.98	0.95	0.85	0.64	0.37	0.15
	Fort Thompson[1]	1.00	1.00	0.99	0.96	0.89	0.73	0.45	0.21	0.07
	Structural Fill	1.00	0.96	0.87	0.74	0.55	0.37	0.21	0.11	0.05
D (%)	Natural Soil	0.6	0.6	0.6	0.8	1.3	2.6	5.6	10.4	17.0
	Miami Limestone	0.6	0.6	0.6	0.6	0.6	0.6	2.7	8.2	17.0
	Key Largo & Fort Thompson [2]	0.8	0.8	0.8	0.9	1.2	–	–	–	–
	Structural Fill	1.3	1.3	1.6	2.4	4.4	8.2	14.3	20.6	27.9

[1] Up to the strain level of 0.005 percent, the rocks are considered non strain-dependent
[2] The damping is assumed to be constant at 1 percent.

Data from References 257, 258, 259, and 260.

FSAR Figure 2.5.4-232 will be replaced with the following figure in a future revision:

Figure 2.5.4-232 Shear Modulus Degradation for Key Largo Based on RCTS Testing

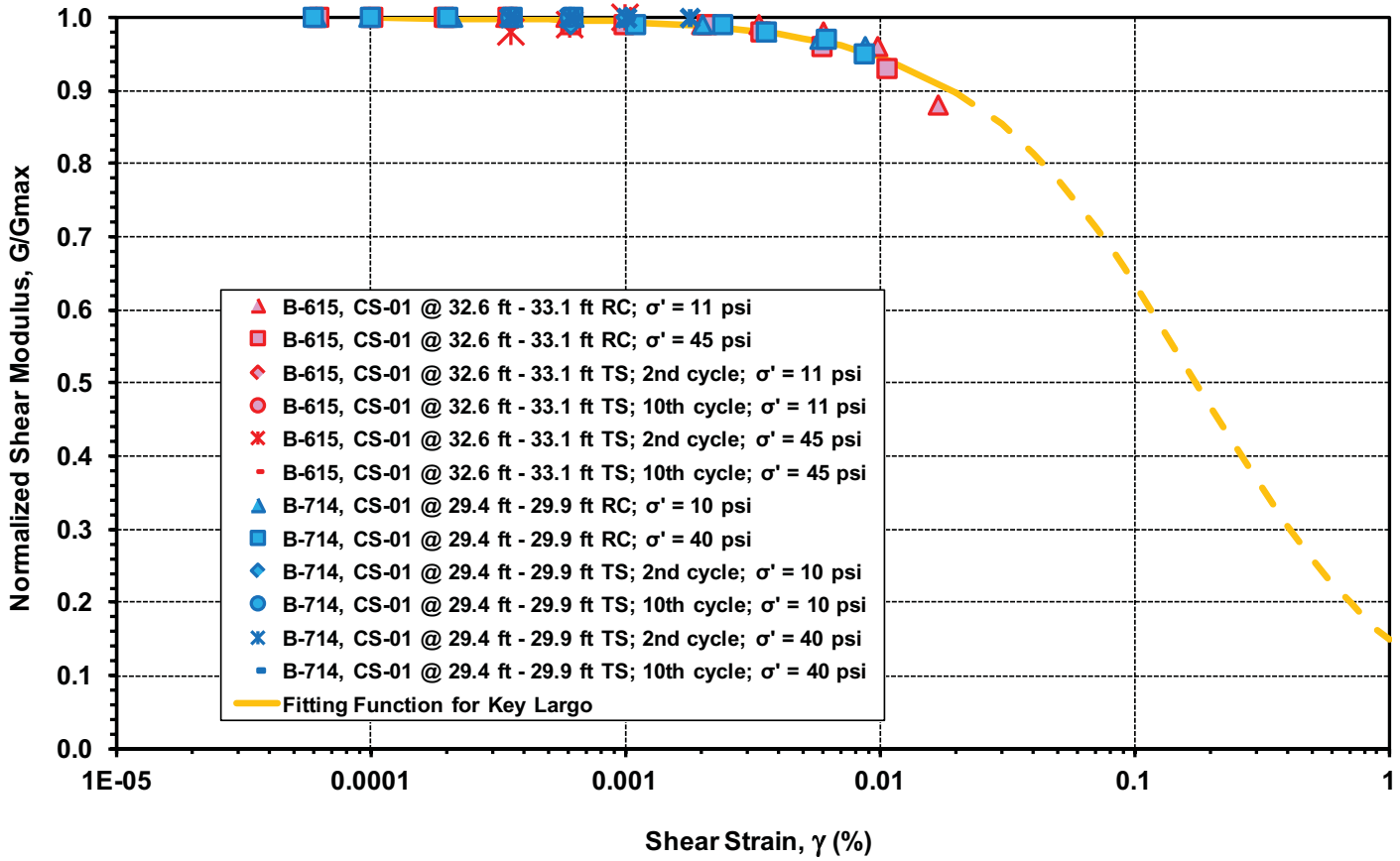

Data from References 257 and 290.

FSAR Figure 2.5.4-233 will be replaced with the following figure in a future revision:

Figure 2.5.4-233 Recommended Shear Modulus Degradation Curves

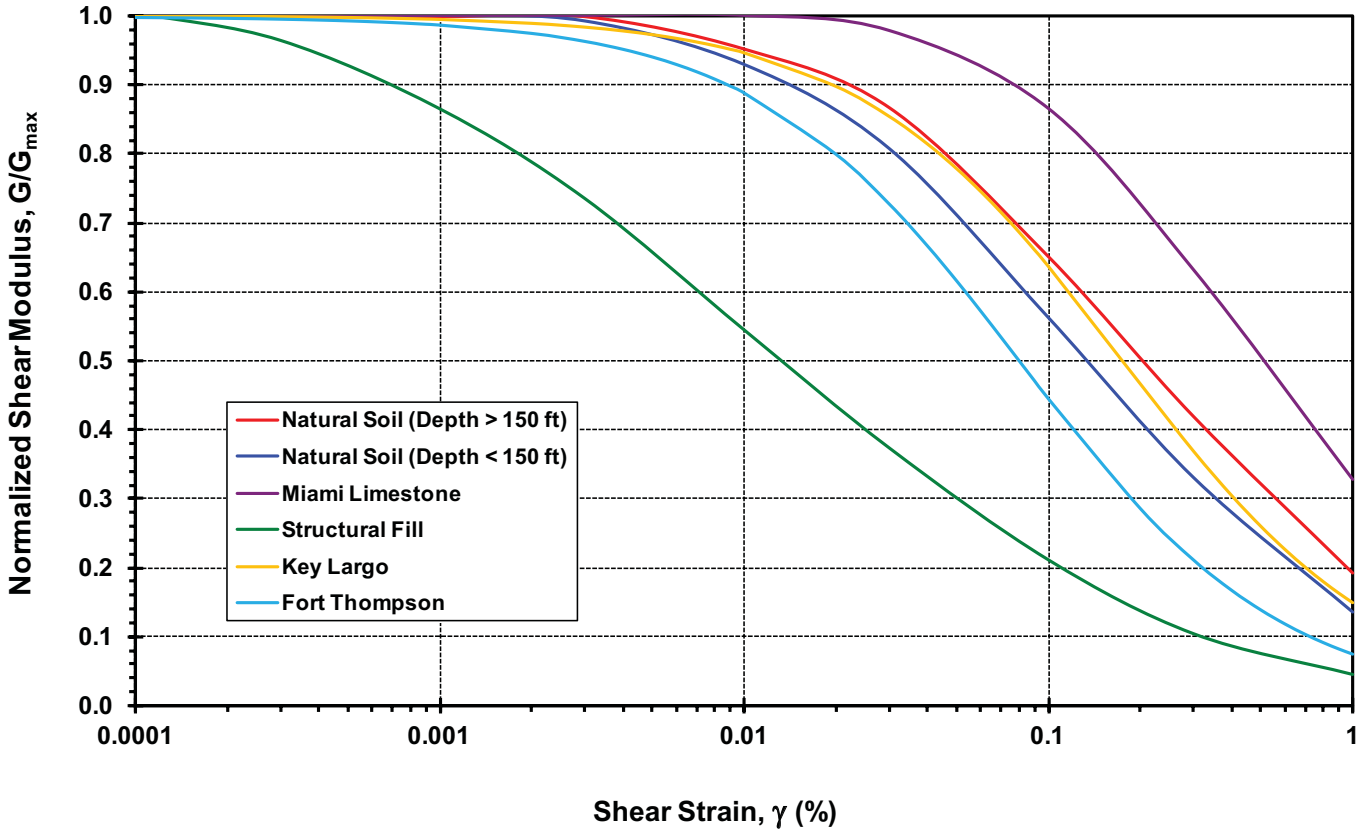

Data from Reference**s** 257, ~~for Miami Limestone and References~~ 258, 259, ~~and~~ 260**, and 290**.

FSAR Figure 2.5.4-234 will be replaced with the following figure in a future revision:

Figure 2.5.4-234 Damping Curve Measurements for Key Largo and Fort Thompson Based on RCTS Testing

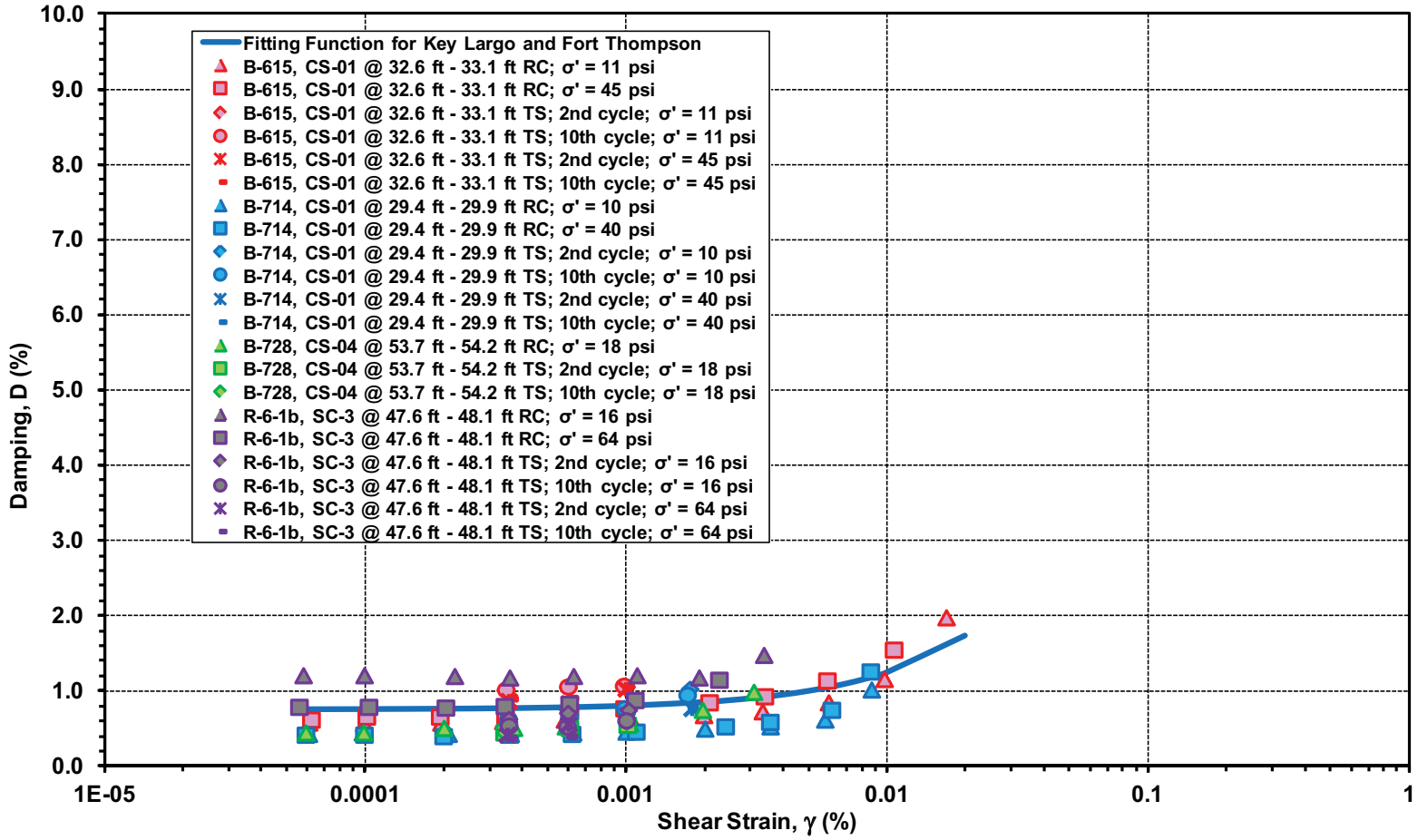

Data from References 257 and 290.

FSAR Figure 2.5.4-235 will be replaced with the following figure in a future revision:

Figure 2.5.4-235 Recommended Damping Curves

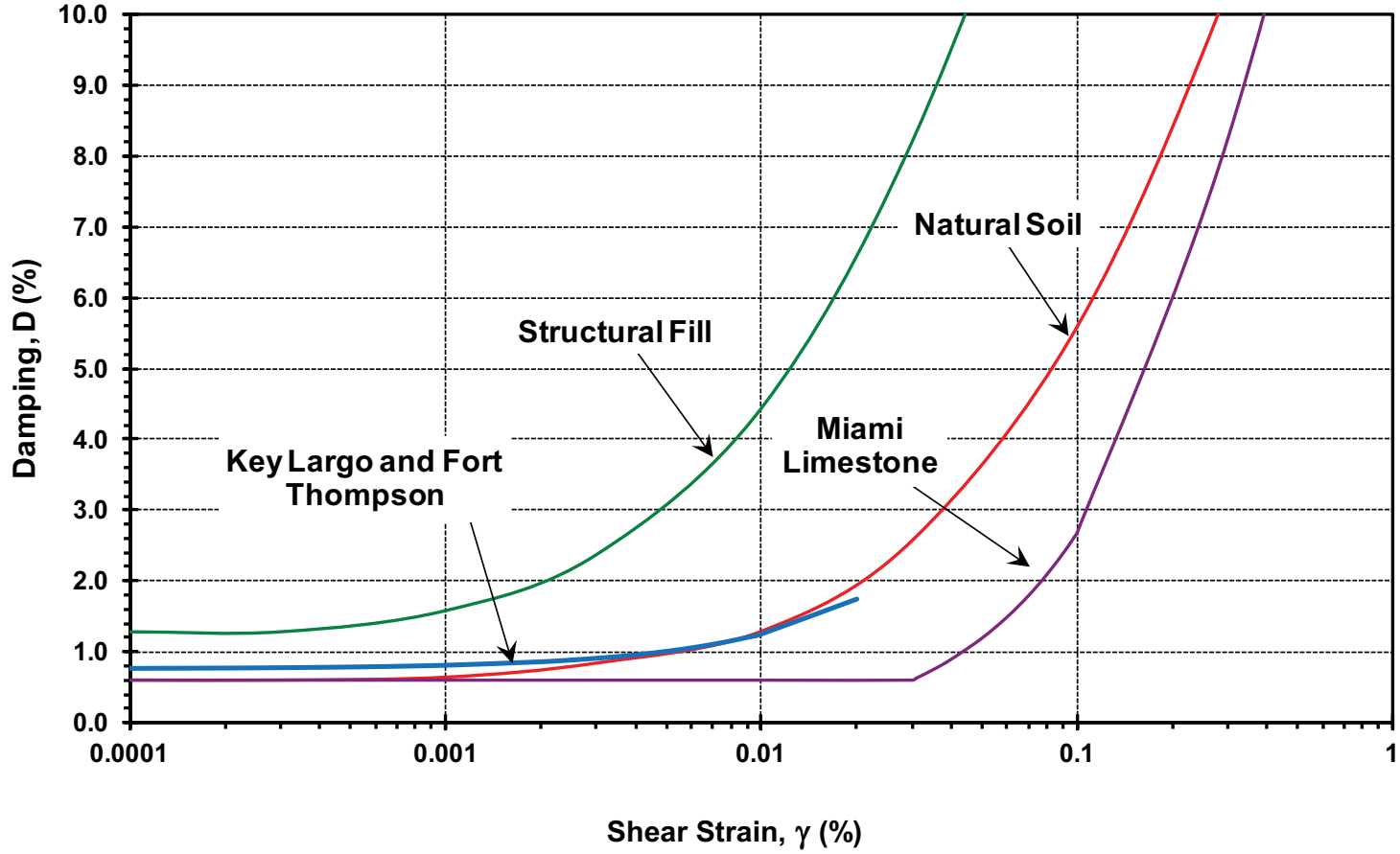

Data from Reference**s** 257, ~~for Miami Limestone and References~~ 258, 259, ~~and~~ 260**, and 290**.

The following figures will be added in a future revision:

Figure 2.5.4-246 Shear Modulus Degradation for Fort Thompson Based on RCTS Testing

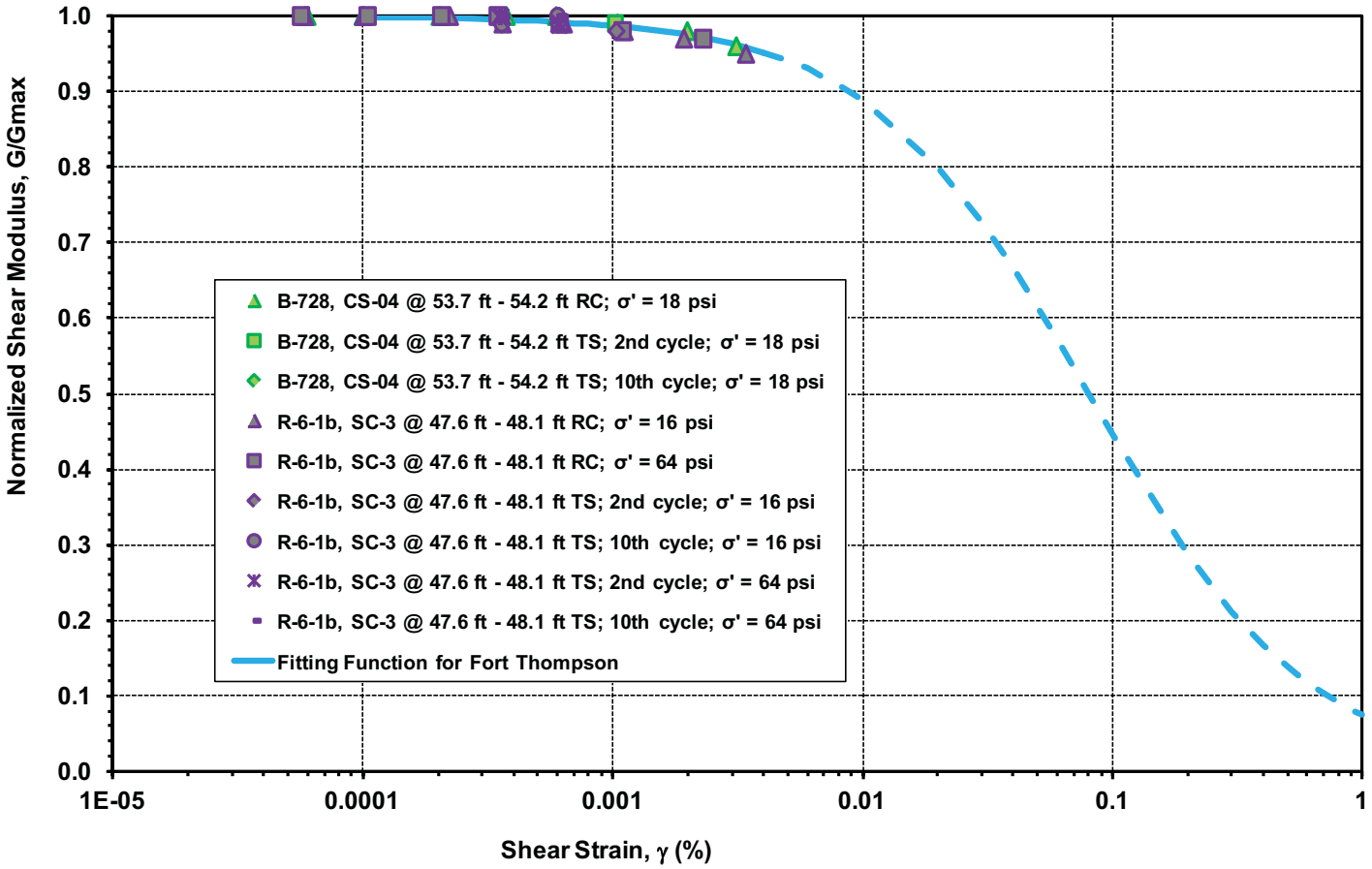

Data from References 257 and 290.

Figure 2.5.4-247 Shear Modulus Degradation for Natural Soil (Depth < 150 ft) Based on RCTS Testing

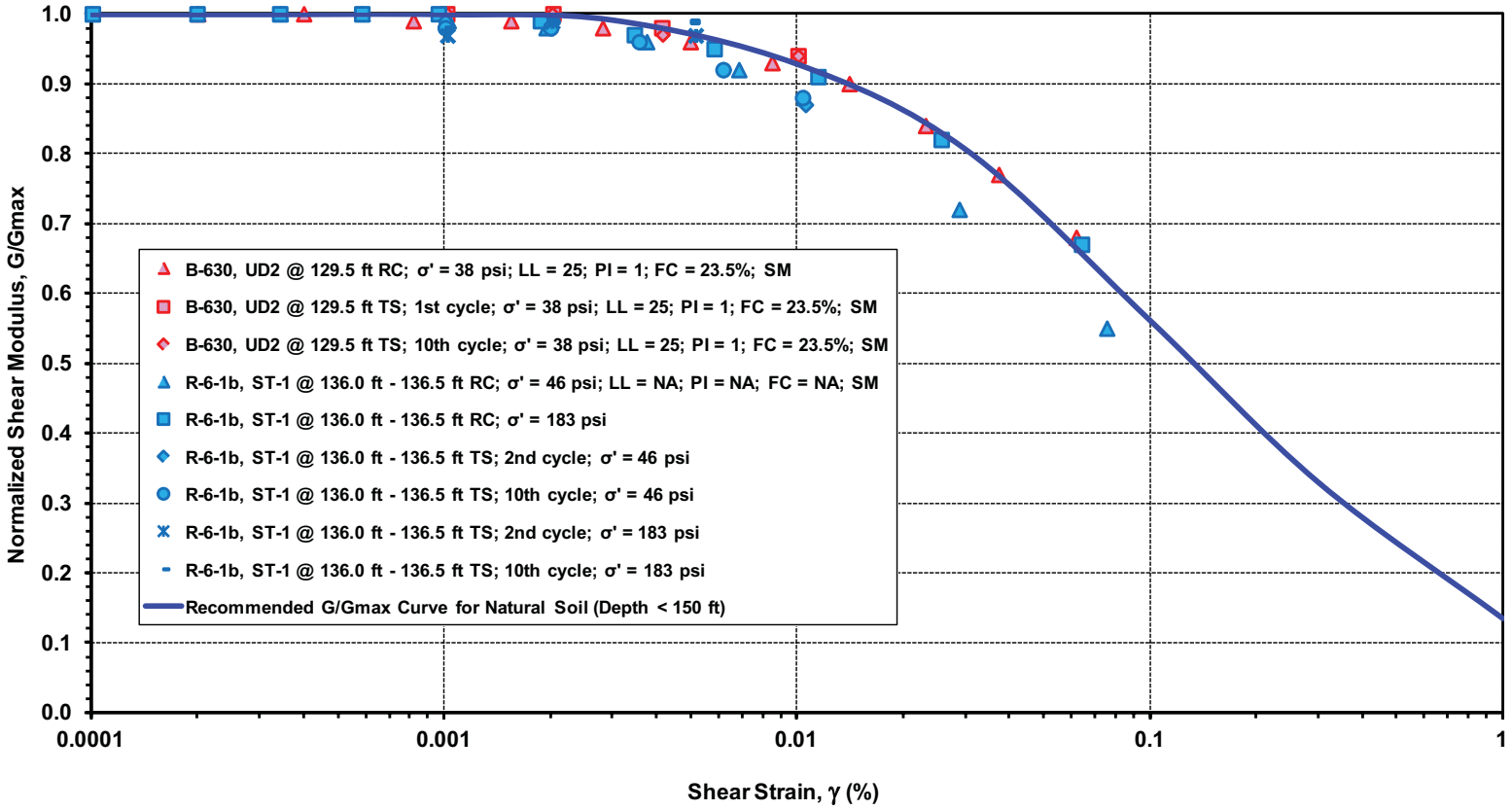

Data from References 257, 258, and 290.

Figure 2.5.4-248 Shear Modulus Degradation for Natural Soil (Depth > 150 ft) Based on RCTS Testing

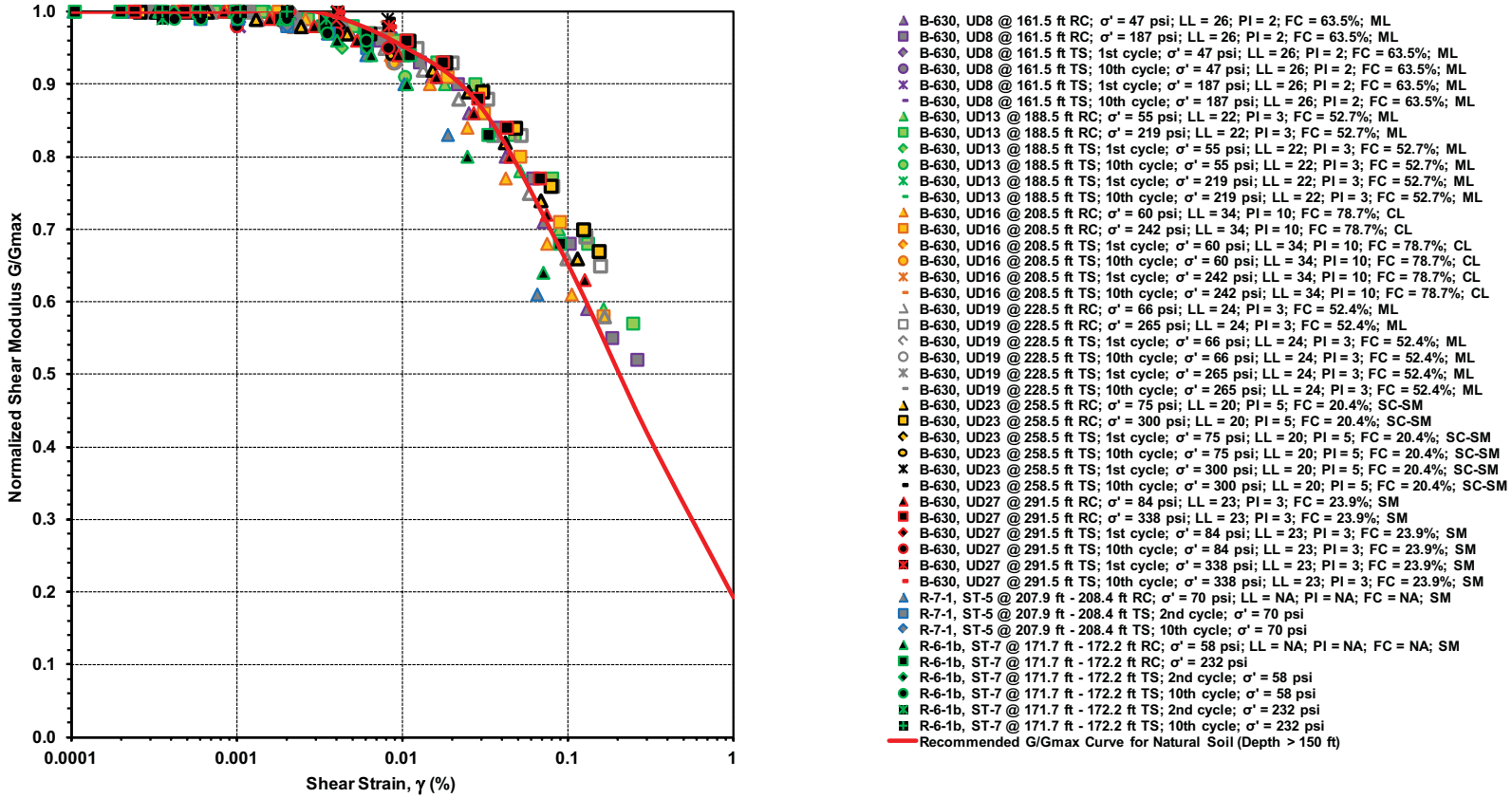

Data from References 257, 258, and 290.

Figure 2.5.4-249 Damping Curve Measurements for Natural Soil Based on RCTS Testing

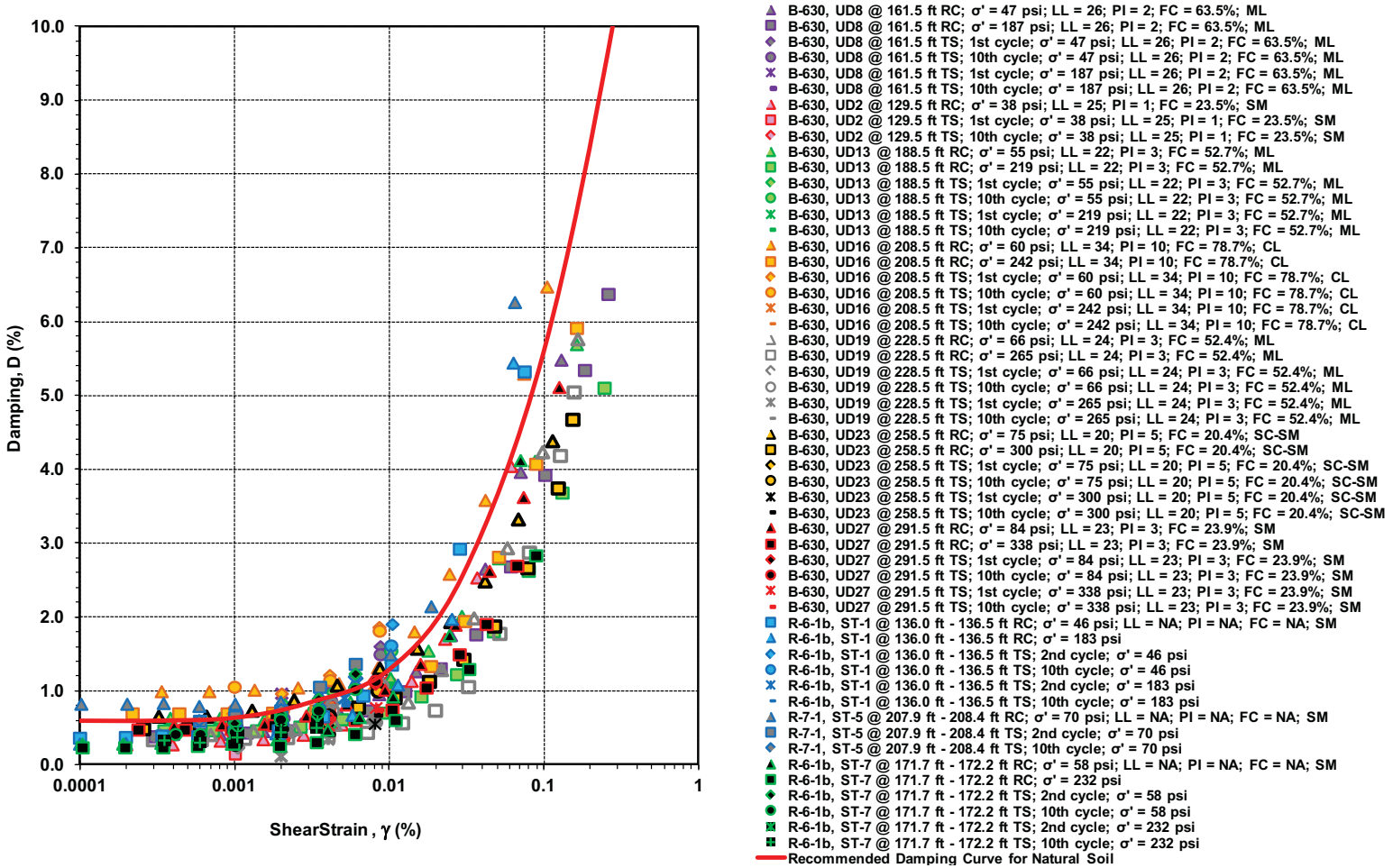

Data from References 257, 258, and 290.

ASSOCIATED ENCLOSURES:

None

NRC RAI Letter No. PTN-RAI-LTR-040

SRP Section: 02.05.04 - Stability of Subsurface Materials and Foundations

QUESTIONS from Geosciences and Geotechnical Engineering Branch 1 (RGS1)

NRC RAI Number: 02.05.04-17 (eRAI 6006)

The calculation for "Site Response and Strain Compatible Properties Calculation" Rev. 001 describes the procedure used to calculate stresses in the liquefaction analysis. In accordance with NUREG-0800, Standard Review Plan, Chapter 2.5.4, "Stability of Subsurface Materials and Foundations," and Regulatory Guide (RG) 1.198, "Procedures and Criteria for Assessing Seismic Soil Liquefaction at Nuclear Power Plant Sites" please clarify the following regarding the methodology used to calculate the CSR (cyclic stress ratio):

a. Clarify how the method used for determining SR_{DRS} meets the ground motion level requirements for liquefaction analysis per 10 CFR 50, Appendix S. The *GRMS* initially resulted in a *PGA* of less than 0.1g and was scaled upwards per RG 1.208. Since the method used for determining the *SRDRS* is the same as the *GRMS*, describe how this method provides stress ratio values that are comparable to those calculated using a *PGA* value of at least 0.1g.

b. Describe how the amplitude ratio $A_R(f)$, defined by ($ARS_{10\text{-}5}$)/($ARS_{10\text{-}4}$) and used in the determination of the weighting factor w, correlates to the ratio of the in-situ *stress ratios* resulting from site response analysis using the $ARS_{10\text{-}5}$ and $ARS_{10\text{-}4}$ as input spectrums.

c. The weighting factor *w* applied to the stress ratios $SR_{10\text{-}4}$ and $SR_{10\text{-}5}$ for the determination of SR_{DRS} is based on the average of the weighting factor *W(f).* Justify using an average value of *W(f)* over all frequencies, and describe how this is a conservative approach.

d. Describe how $ARS_{10\text{-}5}$ and $ARS_{10\text{-}4}$ are used as input to the *RVT* for site response, and how this approach correctly accounts for duration effects as compared to time series inputs for the determination of Cyclic Stress Ratio (*CSR)*. Please justify and provide the technical basis of this approach, including any assumptions.

e. Justify use of equations (77) and (78) from Idriss and Boulanger (2008) for determining q_{c1Ncs} values, and how the resulting values are conservative compared to the methods outlined in RG 1.198 using your calculated I_c values.

FPL RESPONSE:

The methodology for the liquefaction analysis of the Turkey Point Units 6 & 7 site has been revised using field data obtained from both the initial (Reference 1) and the supplemental field investigations (Reference 2). The potential for soil liquefaction at the Turkey Point Units 6 & 7 site was evaluated following RG 1.198 (Reference 3) which corresponds to the methodology found in Youd et al., (FSAR Reference 219). The evaluation did not include the site response analysis or any additional literature sources, e.g., Idriss and Boulanger

(Reference 4). Therefore, the responses to parts a through d are no longer relevant, and are not included in the response.

A revised response describing the revised analyses per RG 1.198 (Reference 3) recommendations is provided in part e of this response.

Part e:

Justify use of equations (77) and (78) from Idriss and Boulanger (2008) for determining q_{c1Ncs} values, and how the resulting values are conservative compared to the methods outlined in RG 1.198 using your calculated I_c values.

As discussed in the first paragraph of this response, the liquefaction analysis for the Turkey Point Units 6 & 7 site has been revised using field data obtained from both the initial (Reference 1) and the supplemental field investigations (Reference 2). The potential for soil liquefaction at the Turkey Point Units 6 & 7 site was evaluated following RG 1.198 (Reference 3) which corresponds to the methodology found in Youd et al., (FSAR Reference 219). The evaluation did not include any additional literature sources, e.g., Idriss and Boulanger (Reference 4).

Liquefaction Evaluation Methodology

This liquefaction analysis employs state-of-the-art methods of Youd et al., (FSAR Reference 219) for evaluating the liquefaction potential of soils at the Turkey Point Units 6 & 7 site.

The state-of-the-art methodology considers the evaluation of data from CPT, shear wave velocity (V_s), and SPT data. Initially, a measure of stress imparted to the soils by the ground motion is calculated, referred to as the Cyclic Stress Ratio (CSR) following the methodology outlined by Youd et al., (FSAR Reference 219). The stress reduction factor, r_d, used in the calculation of CSR is based on Reference 5. A constant value equal to 0.5 is used for depths equal to and larger than 98.4 feet (30 meters). A measure of resistance of soils to the ground motion is then calculated, referred to as the Cyclic Resistance Ratio (CRR). Finally, FOS against liquefaction is calculated as a ratio of CRR and CSR. A magnitude scaling factor (MSF) of 1.07 corresponding to $M_w = 7.3$ was used in the calculations based on the adopted earthquake magnitude and guidelines in Youd et al., (FSAR Reference 219). The following provides the results of the liquefaction resistance calculations using the available CPT, V_s, and SPT data from the Turkey Point Units 6 & 7 site. The earthquake acceleration and magnitude levels adopted for the liquefaction analysis are conservative (Mw=7.3 and PGA = 0.1g). The earthquake magnitude of 7.3 selected is the highest earthquake magnitude among the controlling magnitudes from deaggregation (FSAR Table 2.5.2-225). The PGA associated with the ground motion response spectra (GMRS) was less than 0.1g (FSAR Figure 2.5.2-253) and had to be scaled up per RG 1.208 (Reference 6) so that the PGA was 0.1g.

FOS Against Liquefaction Based on CPT Data

The CPT testing at the Turkey Point Units 6 & 7 site included the measurement of commonly measured cone parameters, namely tip resistance and sleeve friction. The evaluation of soil resistance for liquefaction analysis is based on those two parameters. The equivalent clean-sand $CRR_{7.5}$ value, based on CPT measurements, was calculated following recommendations in Youd, et al., (FSAR Reference 219), based on normalized clean sand cone penetration resistance (q_{c1Ncs}) and other parameters such as the soil behavior type index, I_c. Cone tip resistance values from CPT soundings are shown in Figure 1 for the power block area. The deepest CPT soundings (C-701, R-6-3, and R-7-3) penetrated up to 289 feet below the ground surface, encountering refusal at that depth. Tip resistance measurements were made at 2 centimeter (cm) intervals (0.79 inches) during the initial investigation (Reference 1) and at 5 cm intervals (2 inches) during the supplemental investigation (Reference 2). The results showing FOS against liquefaction using the CPT data are provided in Figure 2 for the power block area. The value of FOS is consistently higher than 1.1 across the full depth of testing at the site. Based on CPT data, there is no potential for liquefaction for the Turkey Point Unit 6 & 7 power block area.

Figure 1 CPT results of Cone Resistance (q_t), Friction Sleeve Resistance (f_s), Friction Ratio (R_f) and dynamic pore pressure (u_2)

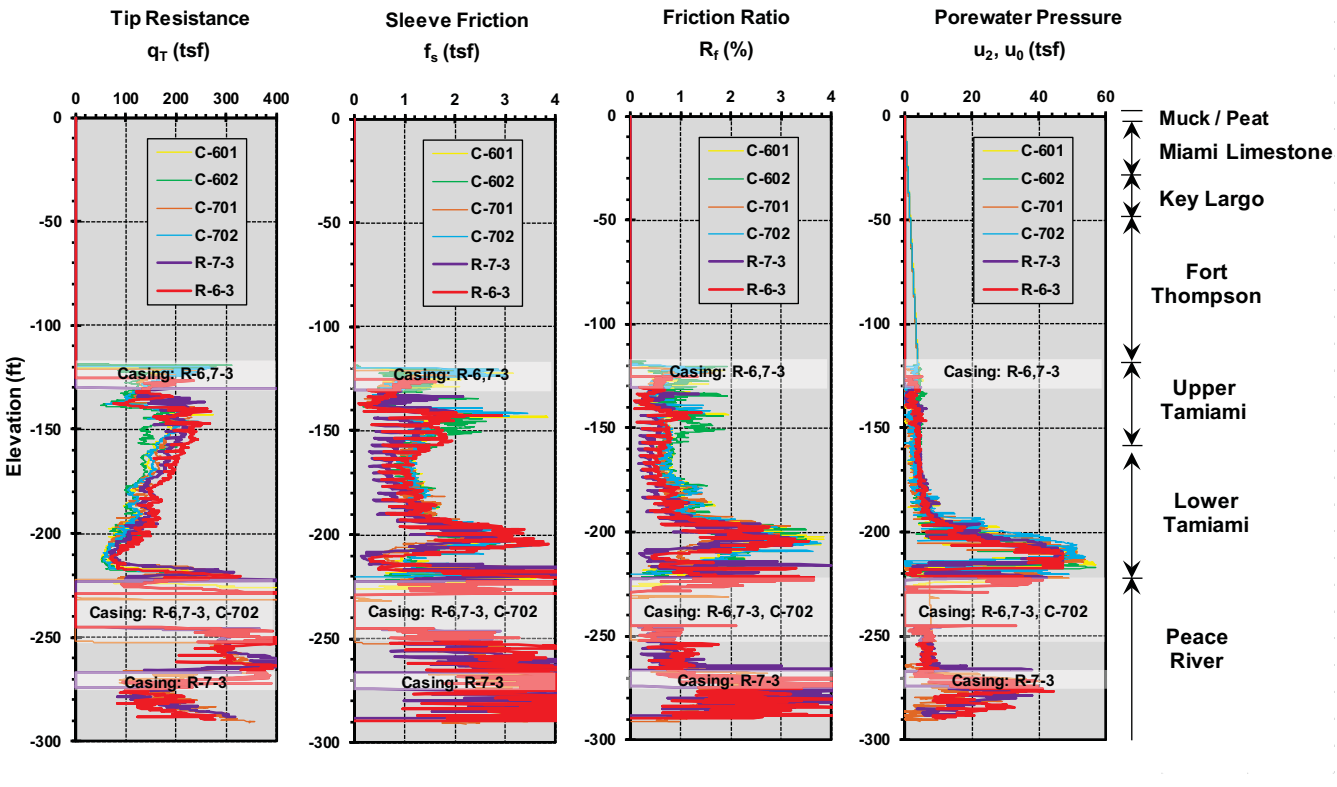

Figure 2 Factor of Safety Against Liquefaction with Depth Based on CPT Results

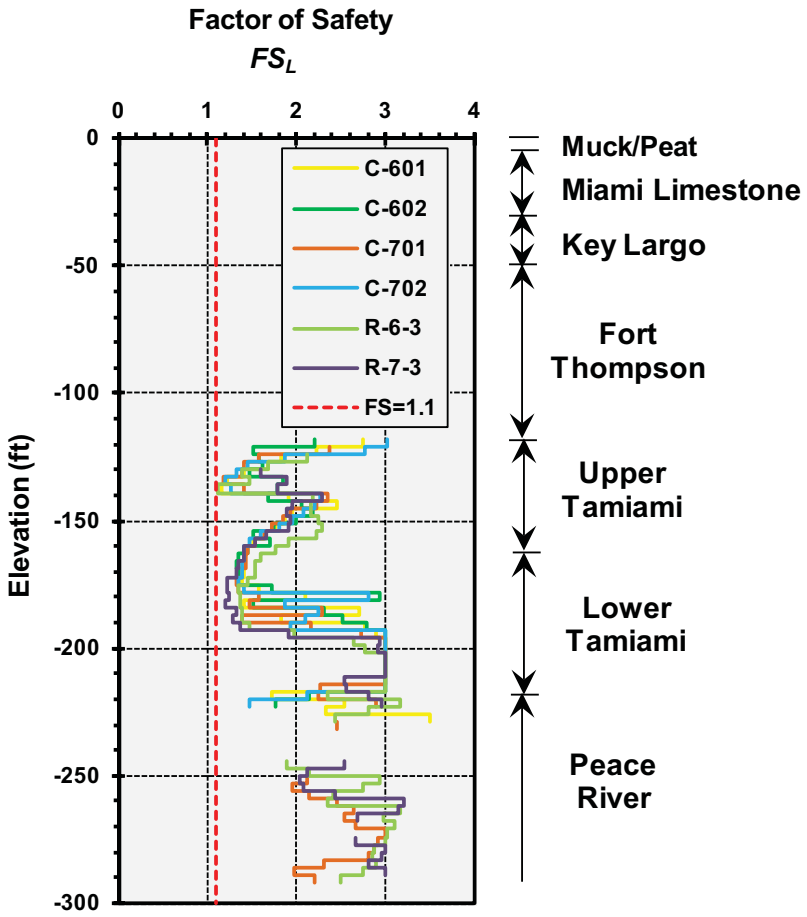

FOS Against Liquefaction Based on Shear Wave Velocity Data

Similar to the FOS calculations for the CPT values, equivalent clean-sand $CRR_{7.5}$ values based on V_s measurements were calculated following recommendations in Youd, et al., (FSAR Reference 219). The curve proposed by Andrus and Stokoe (FSAR Reference 219) that relate CRR to V_s was used. Shear wave velocity data from P-S Suspension logging and downhole measurements were used for the FOS calculations. The collected raw (uncorrected) V_s data are shown in Figure 3 for the power block area. P-S Suspension velocity logging measurements were made at 1.64 foot intervals (0.5 meters). The deepest measurements (B-701) extended to about 600 feet below the ground surface. A total of 1247 V_s data points from the upper Tamiami, lower Tamiami, and Peace River formations were used for the FOS calculations. The results showing FOS against liquefaction using the shear wave velocity data are provided in Figure 4. The limiting upper value of V_{S1} for liquefaction resistance is referred to as V_{S1}*; a conservative value for fines content of 20 percent was used resulting in a V_{S1}* equal to 680.6 fps (207.5 m/s). A cutoff value of 647.5 fps (197.4 m/s) for V_{S1} was used such that the maximum CRR was set equal to 0.35. Almost all (99.8 percent) of the FOS calculated among the 1247 measurement points (1244 out of 1247) are above 1.4. Of the three remaining values, two values fall in the intermediate zone between 1.1 and 1.4, namely 1.20 at El.−124.47 and 1.27 at El. −127.75

at CPT R-7-1 (Unit 7), and one FOS is equal to 1.06 at El. −152.32 in CPT B-601 (Unit 6). This value of 1.06 corresponds to a tributary thickness to its measurement point equal to 1.64 feet. If the FOS is calculated as an average over adjacent measured points, it is equal to 2.36 (among the central point and 1 adjacent point on each side [top and bottom] for a total of 3 points), 2.91 (5 points), and 3.15 (7 points); this shows that the low value of 1.06 for the single point at El. −152.32 is a localized exception, and does not represent a weak zone. Based on shear wave velocity data, there is no potential for liquefaction for the Turkey Point Unit 6 & 7 power block area.

Figure 3 Shear Wave Velocities of B-601, B-701, R-6-1b, and R-7-1

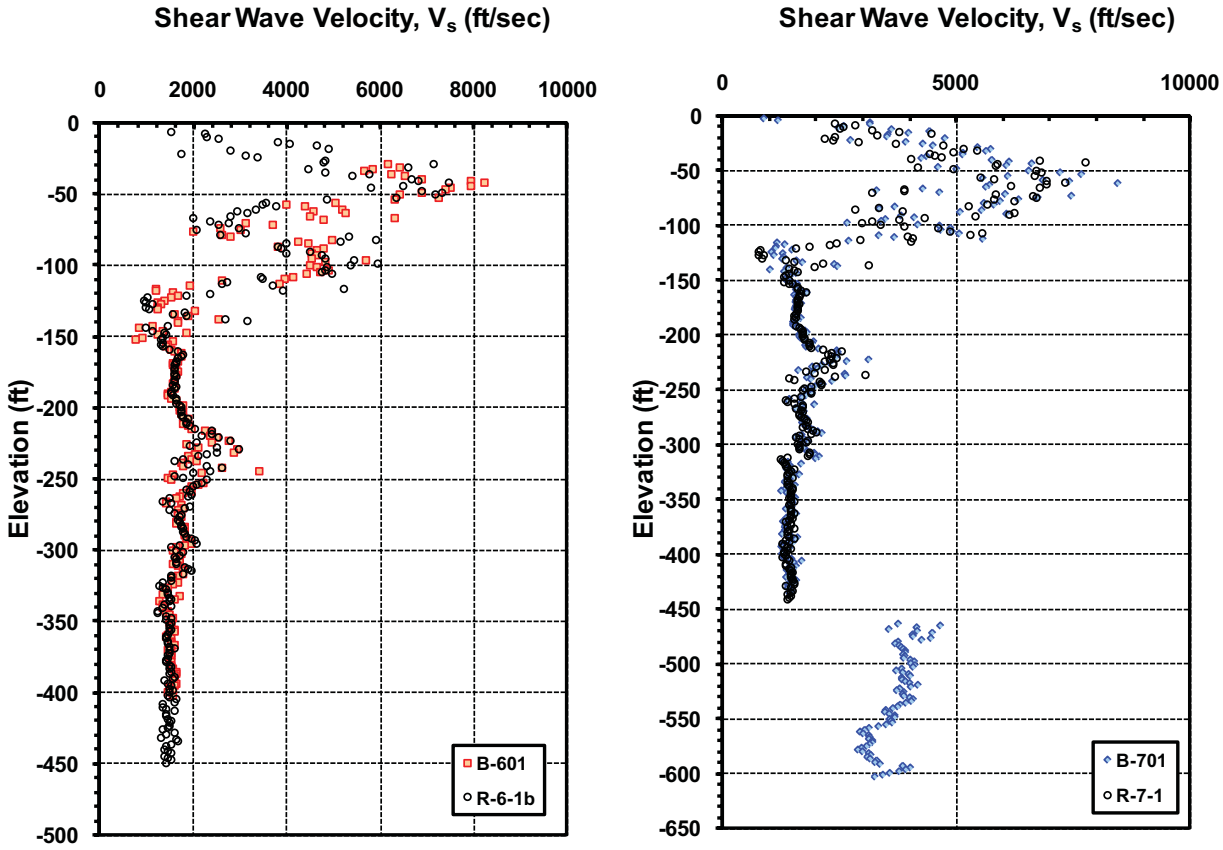

Figure 4 Factor of Safety against Liquefaction using Shear Wave Velocity

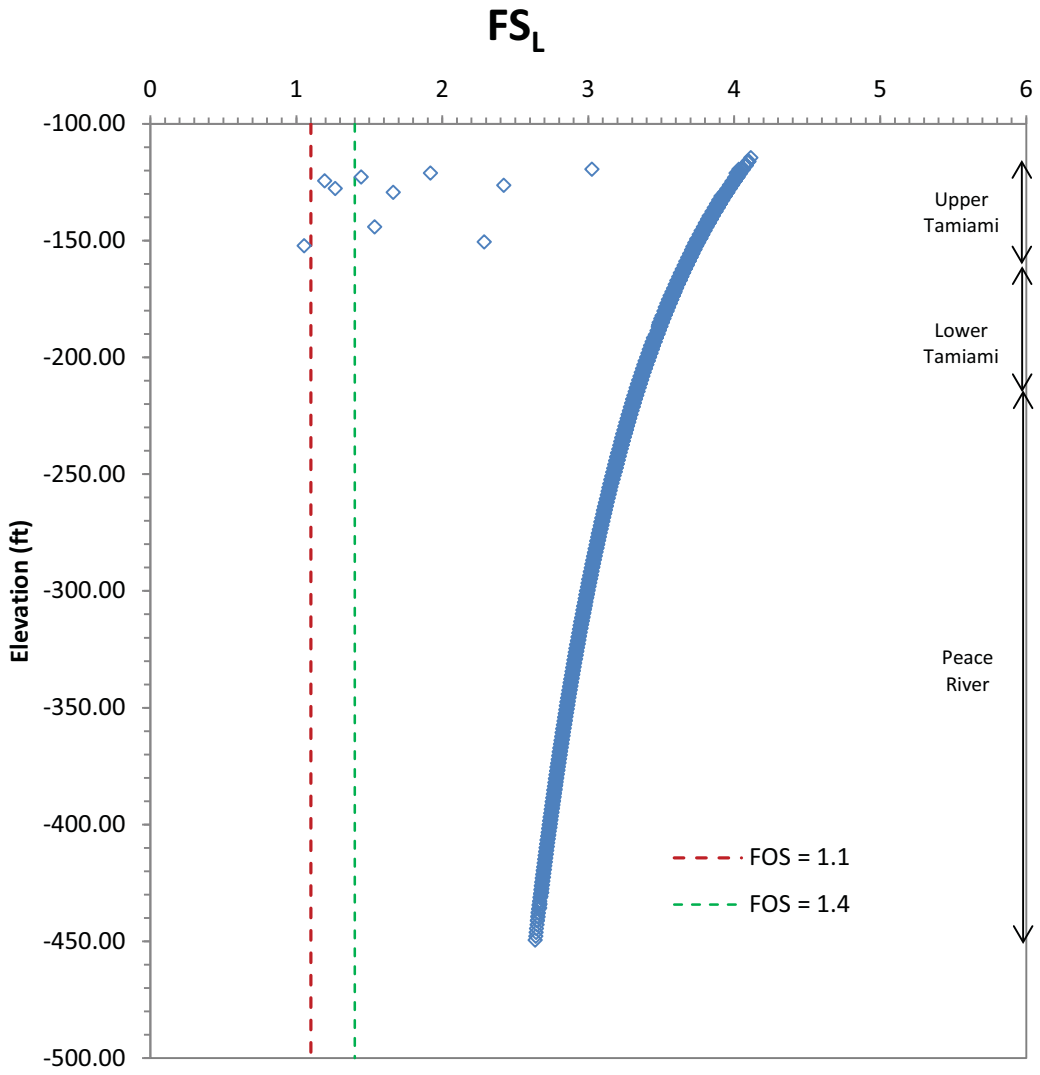

FOS Against Liquefaction Based on Standard Penetration Test (SPT) Data

As discussed in the revised response to RAI Question No. 02.05.04-2, the blow counts obtained from the initial site investigation (Reference 1) turned out to be lower than anticipated. At the time, this was assumed to be associated with artesian conditions. The blow counts from the initial investigation were based on the second and third (2+3) 6 inch increments of penetration from an 18 inch long sampler. The lower blow counts were further examined during the supplemental field investigation (Reference 2). For this purpose, the sampler type used was the 24 inch long type, rather than the 18 inch long sampler. With a longer sampler, an additional set of blow counts can be obtained (last 6 inches of the 24 inch long sampler), allowing the observation of both blow counts, namely the blow counts for the second and third (2+3) 6 inch increments in penetration, and the blow counts for the third and fourth (3+4) 6 inch increments in penetration.

The summations of 3+4 blow counts are consistently and substantially higher than the summations of 2+3, as discussed in the revised response to RAI 02.05.04-2. The low value of the 2nd blow count directly impacts the “SPT N” value, since the “SPT N” is based on 2+3 blow counts per ASTM D 1586 (Reference 7). The 3+4 blow counts are at least 1 foot away from the last drilled location (bottom of borehole) before the initiation of the SPT. The soil zone penetrated by 3+4 blow counts is considered to be less influenced by overwashing as defined in Table 13 of NAVFAC DM 7.1 (Reference 8) associated with the upper half of the sampler length (as evidenced by the low 1st and 2nd blow count readings) and drilling conditions that affect the first two 6 inch increments.

Due to the effect of overwashing, as discussed in the revised response to RAI 02.05.04-2, the original SPT-N values are too low and not representative of the actual soil conditions at the Turkey Point Units 6 & 7 site. The current liquefaction analysis based on SPT data considers only the results of the supplemental investigation (Reference 2), which are believed to best represent the actual soil conditions at the Turkey Point Units 6 & 7 site.

The equivalent clean-sand $CRR_{7.5}$ value based on SPT measurements was calculated following recommendations in Youd, et al., (FSAR Reference 219), based on corrected SPT N-values $(N_1)_{60}$, including corrections based on hammer-rod combination energy measurements at the site and corrections made based on average fines content.

The SPT liquefaction analysis is based on both blow counts 2+3 and 3+4 of the supplemental investigation (Reference 2). It is noted that for the more likely conditions of the soil in situ, represented by the blow counts 3+4, 70 points out of 79 points are directly classified as non-liquefiable given that the parameter $(N_1)_{60}$ results in values equal to or higher than 30. The nine remaining points have factors of safety ranging between 1.15 and 4.07. The value of 1.15 (at El. −119.78) is the only value under 1.4, and corresponds to the transition between the Fort Thompson and upper Tamiami formations. The graphical results of FOS are given in Figure 5. Based on SPT data, there is no potential for liquefaction for the Turkey Point Units 6 & 7 power block area.

In addition to the three approaches followed, namely CPT, V_s, and SPT based liquefaction analyses, it is noted that liquefaction resistance increases markedly with geologic age. Youd et al., (FSAR Reference 219) indicate that pre-Pleistocene sediments (sediments older than 1.6 million years) are generally immune to liquefaction. The Tamiami Formation is Pliocene (1.6 to 5.3 million years old) and the Peace River Formation is Pliocene-Miocene (1.6 to 23.7 million years old).

Figure 5 Comparison between Liquefaction Analysis Results using SPT N Values and the Sum of the 3rd and 4th Blow Counts from the Supplemental Investigations

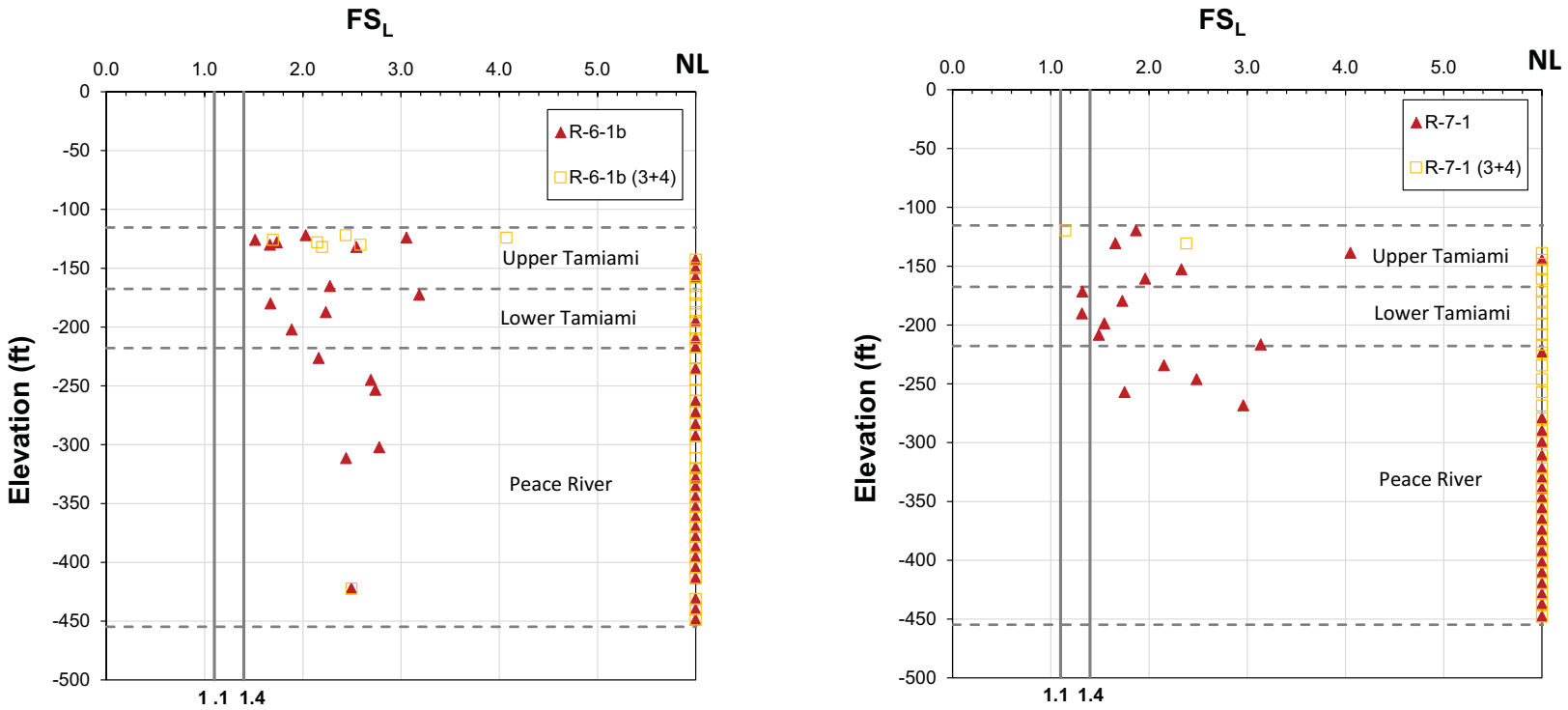

Note: NL corresponds to Non-Liquefiable locations, $(N_1)_{60} \geq 30$. No numerical FS value is obtained.

Conclusion for Liquefaction Analysis

From the collective results obtained following the methodology outlined by Youd et al., (FSAR Reference 219), it is concluded that soils at the Turkey Point Units 6 & 7 site are not likely to liquefy given the ground motion level for the site.

A negligible portion of the data at isolated locations indicated potentially liquefiable soils. The state-of-the-art methodology used for the liquefaction evaluation was intended to be conservative, not necessarily to encompass every data point; therefore, the presence of a few data points beyond the CRR base curve is acceptable (FSAR Reference 219). Additionally, in the liquefaction evaluation, the effects of age, overconsolidation, and cementation were ignored. These factors tend to increase resistance to liquefaction. Finally, the earthquake acceleration and magnitude levels adopted for the liquefaction analysis are conservative (M_w=7.3 and PGA = 0.1g). The earthquake magnitude of 7.3 selected is the highest earthquake magnitude among the controlling magnitudes from deaggregation (FSAR Table 2.5.2-225). The PGA associated with the ground motion response spectra (GMRS) was less than 0.1g (FSAR Figure 2.5.2-253) and had to be scaled up per RG 1.208 so that the PGA was 0.1g. Therefore, it is concluded that liquefaction is not a concern for the Turkey Point Units 6 & 7 site.

This response is PLANT SPECIFIC.

References:

1. MACTEC Engineering and Consulting, Inc., *Final Data Report – Geotechnical Exploration and Testing: Turkey Point COL Project Florida City, Florida*, Revision 2, included in COL Application Part 11, October 6, 2008.
2. Paul C. Rizzo Associates, Inc., *Supplemental Field Investigation Data Report, Turkey Point Nuclear Power Plant Units 6 & 7*, Revision 2, April 15, 2014.
3. U.S. Nuclear Regulatory Commission, *Procedures and Criteria for Assessing Seismic Soil Liquefaction at Nuclear Power Plant Sites*, Regulatory Guide 1.198,NRC, Washington, DC, November 2003.
4. Idriss, I.M. and Boulanger, R.W., *Soil Liquefaction during Earthquakes,* Earthquake Engineering Research Institute, 2008.
5. U.S. Army Corps of Engineers, *Technical Bases for Regulatory Guide for Soil Liquefaction*, NUREG/CR-5741, March 2000.
6. U.S. Nuclear Regulatory Commission, A Performance-Based Approach to Define the Site-Specific Earthquake Ground Motion, Regulatory Guide 1.208, NRC, Washington, DC, March 2007.
7. ASTM International, Standard Test Method for Standard Penetration Test (SPT) and Split-Barrel Sampling of Soils, Standard D 1586-11, DOI: 10.1520/D 1586-11, ASTM International, West Conshohocken, Pennsylvania, 2011.
8. Naval Facilities Engineering Command, Soil Mechanics, Design Manual 7.01, Alexandria, Virginia, 1986.

ASSOCIATED COLA REVISIONS:

FSAR Subsection 2.5.4.7.5 will be revised in a future revision as follows:

2.5.4.7.5 Seismic Parameters for Liquefaction Evaluation

The site-specific soil column extending to the proposed ground surface is developed for evaluation of liquefaction potential. ~~The development of the design response spectra (DRS) calculated based on consideration of the design earthquake and the soil column dynamic properties is described Subsection 2.5.2. The seismic acceleration as a function of elevation is used to develop the Cyclic Stress Ratio (CSR).~~ **The Cyclic Stress Ratio (CSR) is calculated following the methodology given in Reference 219. The stress reduction factor, r_d, used in the calculation of CSR is based on Reference 313. A constant value equal to 0.5 is used for depths equal to and larger than 98.4 feet (30 meters).** The CSR is used to evaluate liquefaction potential as described in Subsection 2.5.4.8.

The last paragraph of FSAR Subsection 2.5.4.8 will be revised in a future revision as follows:

Unconsolidated soil deposits at the site are Pliocene (at least 1.6 million years old) or older. Additionally, the overburden of rock from Strata 2, 3, and 4 should preclude development of liquefaction-induced features, such as lateral spreading and settlement, from propagation to the ground surface. To be complete and conservative, a comprehensive liquefaction analysis for all CPT, ~~and~~ shear wave velocity**, and SPT** data is made. ~~SPT results are also considered, but are discounted due to artesian conditions causing inconsistent and some unrealistically low SPT N- values.~~

The first, fifth, and eighth paragraphs of FSAR Subsection 2.5.4.8.1 will be revised in a future revision as follows:

Liquefaction is the transformation of a granular soil material from a solid to a liquefied state as a consequence of increased pore water pressure and reduced effective stress. Soil liquefaction occurrence (or lack thereof) depends on geologic age, state of soil saturation, density, gradation, plasticity, and earthquake intensity and duration. The liquefaction analysis presented here employs state-of-the-art deterministic methods (References ~~and 268~~ 219).

As addressed above, only the soil strata of the upper and lower Tamiami Formation and Peace River Formation (Strata 5, 6, and 7) are considered for liquefaction potential analysis. As noted above, the Tamiami and Peace River formations are attributed to the Pliocene and Miocene ages, respectively. Conventionally, only younger deposits, especially Holocene age and, to a lesser extent, Pleistocene age deposits, are considered potentially liquefiable. As the unconsolidated soil deposits at the site below rock are Pliocene (at least 1.6 million years old) or older, the probability of liquefaction is considered extremely low. Reference 269 proposes an age correction factor, C_A, that accounts for the low probability of liquefaction of older deposits. Although this factor is not applied in this calculation, it would be approximately 2 to 2.5; therefore, use of this factor would increase the calculated factors of safety against liquefaction by **a factor of** 2 to 2.5.

For completeness, calculations to evaluate the factor of safety (FOS) against liquefaction are performed. The measured CPT values, ~~and~~ the shear wave velocity, V_s, **and SPT data** are used for liquefaction analysis. These evaluations are performed separately, using the state-of-art approaches summarized in References~~s~~ 219 ~~and 268~~. SPT results **from Reference 257** are not used in the liquefaction calculations~~, as explained in the following subsection.~~**; the liquefaction assessment based on SPT data considers only the data obtained from Reference 290, as explained in Subsection 2.5.4.8.2.**

FSAR Subsection 2.5.4.8.2 will be revised in a future revision as follows:

2.5.4.8.2 Liquefaction Resistance Based on SPT Data

~~As indicated on Figures 2.5.4-212 and 2.5.4-213, there is a very wide scatter of uncorrected and corrected N-values. The N60-values vary from 0 to 100 blows/ foot in the upper Tamiami Formation and from 3 to around 100 blows/foot in the lower Tamiami Formation. Where SPT sampling encountered refusal, the N-value is capped at 100, so the actual range of penetration resistance is higher than these values indicate. There is no obvious correlation between N-value and elevation in these strata. Silty sands and sandy silts that range in depth from 120 to 220 feet would normally be dense to very dense with consistently high N60- values. Blow counts of less than 20 blows/foot and particularly less than 5 blows/ foot (including the zero values) are most probably due to sample disturbance. Subsection 2.4.12 describes the upward vertical hydraulic gradient observed in the water level measurements. It seems likely that this hydraulic gradient has contributed to at least partial blowout of the bottom of the hole prior to/during SPT sampling on many if not most of the samples. To evaluate where N-values are not representative of actual in situ density conditions, the corrected N-values are compared to the CPT corrected tip resistance. The ratio of qc1/N1 for clean sands is typically 4 to 5 and for silty sands 3.5 to 4.5 based on the work presented in Reference 282. Figure 2.5.4-237 indicates the N-values relative to the predicted range based on the ratio of qc1/N1. As can be seen in the figure, very few of the N-values fall into the predicted range, supporting the theory that these blow counts are significantly affected by the hydraulic gradient. Therefore, the measured N- values are not used in the calculation of liquefaction potential in favor of the measured CPT and Vs results that are more consistent with each other and with expected values for deposits of similar age, depth, and overburden.~~

As discussed in Subsection 2.5.4.2.1.3.2.1, the blow counts obtained from the initial site investigation (Reference 257) are lower than anticipated. The blow counts from the initial investigation are based on the second and third (2+3) 6 inch increments in penetration of an 18 inch long sampler. The lower blow counts are further examined during the supplemental field investigation (Reference 290). For this purpose, the sampler type used is the 24 inch long type, rather than the 18 inch long sampler. With a longer sampler, an additional blow count can be obtained (last 6 inches of the 24 inch long sampler), allowing the observation of both blow counts, namely the blow counts for the second and third (2+3) 6 inch increments in penetration, and the blow counts for the third and fourth (3+4) 6 inch increments in penetration.

The summations of 3+4 blow counts are consistently and substantially higher than the summations of 2+3, as discussed in Subsection 2.5.4.2.1.3.2.1. The low value of

the 2nd blow count directly impacts the "SPT N" value, since the "SPT N" is based on 2+3 blow counts per Reference 302. The 3+4 blow counts are at least 1 foot away from the last drilled location (bottom of borehole) before the initiation of the SPT. The soil zone penetrated by 3+4 blow counts is considered to be less influenced by overwashing as defined in Table 13 of NAVFAC DM 7.1 (Reference 301) associated with the upper half of the sampler length (as evidenced by the low 1st and 2nd blow count readings) and drilling conditions that affect the first two 6 inch increments.

Due to the effect of overwashing as discussed in Subsection 2.5.4.2.1.3.2.1, the original SPT-N values are too low and not representative of the actual soil conditions at the Turkey Point Units 6 & 7 site. The liquefaction analysis based on SPT considers only the results of the supplemental investigation (Reference 290), which are believed to best represent the actual soil conditions at the Turkey Point Units 6 & 7 site.

The equivalent clean-sand $CRR_{7.5}$ value based on SPT measurements is calculated following recommendations provided in Reference 219, based on corrected SPT N-values $(N_1)_{60}$, including corrections based on hammer-rod combination energy measurements at the site and corrections made based on average fines content.

The SPT based liquefaction analysis considers both blow counts 2+3 and 3+4 of the supplemental investigation (Reference 290). It is noted that for the more representative conditions of the soil in situ, represented by the blow counts 3+4, 70 points out of 79 points are directly classified as non-liquefiable given that the parameter $(N_1)_{60}$ results in values equal to or higher than 30. The nine remaining points have factors of safety ranging between 1.15 and 4.07. The value of 1.15 (at El. −119.78 in borehole R-7-1) is the only value under 1.4 and corresponds to the transition between the Fort Thompson and upper Tamiami formations. The graphical results of FOS are given in Figure 2.5.4-250. Based on SPT data, there is no potential for liquefaction for the Turkey Point Units 6 & 7 power block area.

FSAR Subsection 2.5.4.8.3 will be revised in a future revision as follows:

2.5.4.8.3 FOS Against Liquefaction Based on CPT ~~and Vs~~ Data

~~The CPT measurements are much less susceptible to soil disturbance from hydraulic gradients, and Vs measurements are not affected at all. The CPT measurements are taken at approximately 0.07 foot depth intervals, where CPT could be probed (no rock coring), from approximately 120 to 290 feet depth. Considering a total of 7304 points, a FOS is calculated if the material is considered potentially liquefiable based on tip resistance and fines content. The Vs measurements, taken at depth intervals generally 1.6 to 1.7 feet, are used for the FOS against liquefaction with a total of 878 points considered.~~

~~Table 2.5.4-218 is a summary of the results of the calculations. The native soils that indicate the lowest FOS values are those in the upper Tamiami Formation. However, the FOS values calculated indicate adequate resistance to liquefaction based on published criteria (FOS > 1.25). The FOS as a function of elevation for the CPT-based calculations is presented in Figure 2.5.4-238. As described above, even if liquefaction occurs, the~~

~~thickness and stiffness of the overlying rock, lean concrete fill, and compacted limerock fill precludes the effects of liquefaction from reaching near the ground surface.~~

CPT testing at the Turkey Point Units 6 & 7 site includes the measurement of commonly measured cone parameters (tip resistance and sleeve friction). The evaluation of liquefaction based on commonly measured parameters is discussed herein. The equivalent clean-sand $CRR_{7.5}$ value, based on CPT measurements, is calculated following recommendations found in Reference 219, based on normalized clean sand cone penetration resistance (q_{c1Ncs}) and other parameters such as the soil behavior type index, I_c. Cone tip resistance values from CPT soundings are shown in Figure 2.5.4-214 for the power block area. The deepest CPT soundings (C-701, R-6-3 and R-7-3) penetrate 289 feet below the ground surface, encountering refusal at that depth. Tip resistance measurements are made at 2 centimeter (cm) intervals (0.79 inches) during the initial investigation (Reference 257) and at 5 cm intervals (2 inches) during the supplemental investigation (Reference 290). The results showing FOS against liquefaction using the CPT data are provided in Figure 2.5.4-238 for the power block area. The value of FOS is consistently higher than 1.1 across the full depth of testing at the site. Based on CPT data, there is no potential for liquefaction for the Turkey Point Unit 6 & 7 power block area.

New FSAR Subsections 2.5.8.4 and 2.5.8.5 will be added in a future revision as follows:

2.5.4.8.4 FOS Against Liquefaction Based on V_s Data

Similar to the FOS calculations for the SPT and CPT values, equivalent clean-sand $CRR_{7.5}$ values based on V_s measurements are calculated following recommendations provided in Reference 219. The curve proposed by Andrus and Stokoe (Reference 219) relating V_s to CRR is used. Shear wave velocity data from P-S logging and downhole measurements are used for the FOS calculations. The collected raw (uncorrected) V_s data are shown in Figure 2.5.4-218 for the power block area. Suspension P-S velocity logging measurements were made at 1.64-feet intervals (0.5-m). The deepest measurements (B-701) extend to about 600 feet below the ground surface. A total 1247 V_s data points from the upper Tamiami, lower Tamiami, and Peace River formations are used for the FOS calculations. The results showing FOS against liquefaction using the shear wave velocity data are provided in Figure 2.5.4-251. The limiting upper value of V_{S1} for liquefaction resistance is referred to as V_{S1}*; a conservative value for fines content of 20 percent is used resulting in a V_{S1}* equal to 680.6 fps (207.5 m/s). A cutoff value of 647.5 fps (197.4 m/s) for V_{S1} is used such that the maximum CRR is set equal to 0.35. Almost all (99.8 percent) of the FOS calculated among the 1247 measurement points (1244 out of 1247) are above 1.4. Of the three remaining values, two values fall in the intermediate zone between 1.1 and 1.4, namely 1.20 at El.−124.47 and 1.27 at El. −127.75 at borehole R-7-1 (Unit 7), and one FOS is equal to 1.06 at El. −152.32 at CPT B-601 (Unit 6). This value of 1.06 corresponds to a tributary thickness to its measurement point equal to 1.64 feet. If the FOS is calculated as an average over adjacent measured points, it is equal to 2.36 (among the central point and 1 adjacent point on each side [top and bottom] for a total of 3 points), 2.91 (5 points), and 3.15 (7 points); this shows that the low value

of 1.06 of the single point at El. −152.32 is a localized exception, and does not represent a weak zone. Based on shear wave velocity data, there is no potential for liquefaction for the Turkey Point Unit 6 & 7 power block area.

2.5.4.8.5 Conclusions for Liquefaction Analysis

From the collective results obtained following the methodology outlined in Reference 219, it is concluded that soils at the Turkey Point Units 6 & 7 site are not likely to liquefy given the ground motion level for the site.

A negligible portion of the data at isolated locations indicates potentially liquefiable soils. The state-of-the-art methodology used for the liquefaction evaluation is intended to be conservative, not necessarily to encompass every data point; therefore, the presence of a few data points beyond the CRR base curve is acceptable (Reference 219). Additionally, in the liquefaction evaluation, the effects of age, overconsolidation, and cementation are ignored. These factors tend to increase resistance to liquefaction. Finally, the earthquake acceleration and magnitude levels adopted for the liquefaction analysis are conservative (M_w=7.3 and PGA = 0.1g). The earthquake magnitude of 7.3 selected is the highest earthquake magnitude among the controlling magnitudes from deaggregation (Table 2.5.2-225). The PGA associated with the ground motion response spectra (GMRS) is less than 0.1g (Figure 2.5.2-253) and has to be scaled up per RG 1.208 so that the PGA is 0.1g. Therefore, it is concluded that liquefaction is not a concern for the Turkey Point Units 6 & 7 site.

FSAR Subsection 2.5.4.13 will be revised in a future revision as follows:

2.5.4.13 References

~~268. Idriss, I., and R. Boulanger, *Soil Liquefaction During Earthquakes,* Earthquake Engineering Research Institute Engineering Monograph MNO-12, Oakland, California, 2008.~~

313. U.S. Army Corps of Engineers, *NUREG/CR-5741, Technical Bases for Regulatory Guide for Soil Liquefaction,* March 2000.

Table 2.5.4-218 will be deleted in a future revision:

Table 2.5.4-218
Summary of Liquefaction Resistance Calculation Results

Subsurface Data Source	Lowest Calculated Factor of Safety (FOS)	Elevation in feet of Lowest FOS
CPT C-601	1.92	–137.7
CPT C-602	2.06	–137.3
CPT C-701	2.11	–231.5
CPT C-702	1.95	–137.3
SWV B-601	1.50	–152.3
SWV B-620	3.76	–144.2
SWV B-701	4.03	–393.2
SWV B-708	2.14	–121.2

Notes:
SWV = Shear Wave Velocity
CPT = Cone Penetration Test
Calculated Safety Factors Using Shear Wave Velocity Measurements in borings B-604, B-608, B-610, B-704, B-710, and B-720 were greater than 10 or too large to calculate.

Figure 2.5.4-238 will be replaced in a future revision as follows:

Figure 2.5.4-238 Factor of Safety against Liquefaction Based on CPT Values

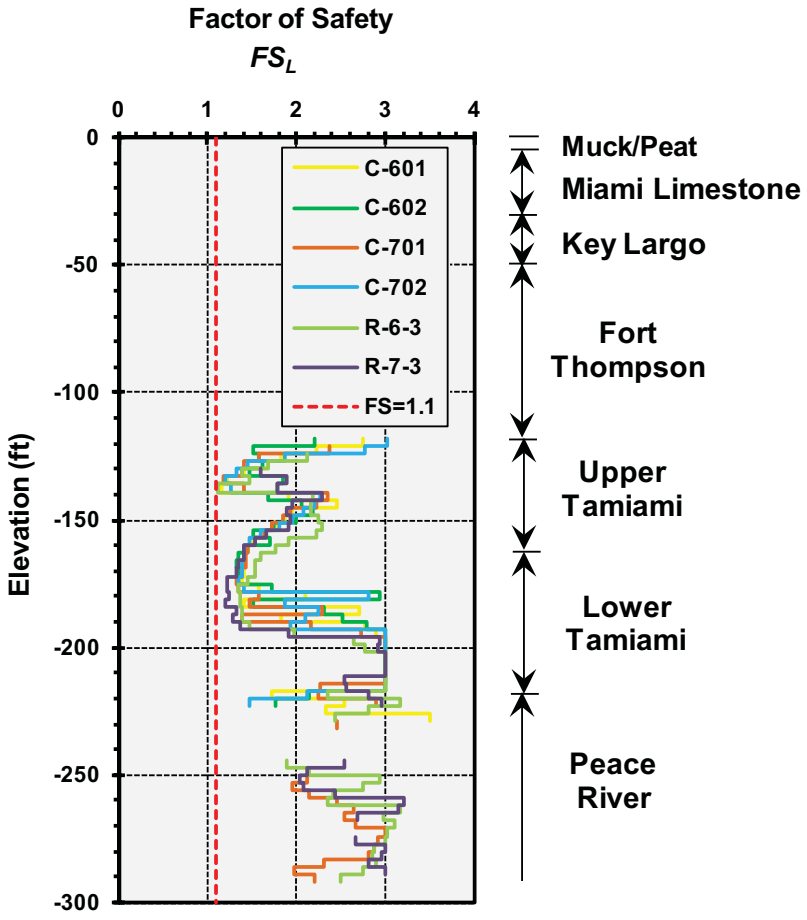

The following figures will be added in a future revision as follows:

Figure 2.5.4-250 Comparison between Liquefaction Analysis Results using SPT N Values and the Sum of the 3rd and 4th Blow Counts from the Supplemental Investigations

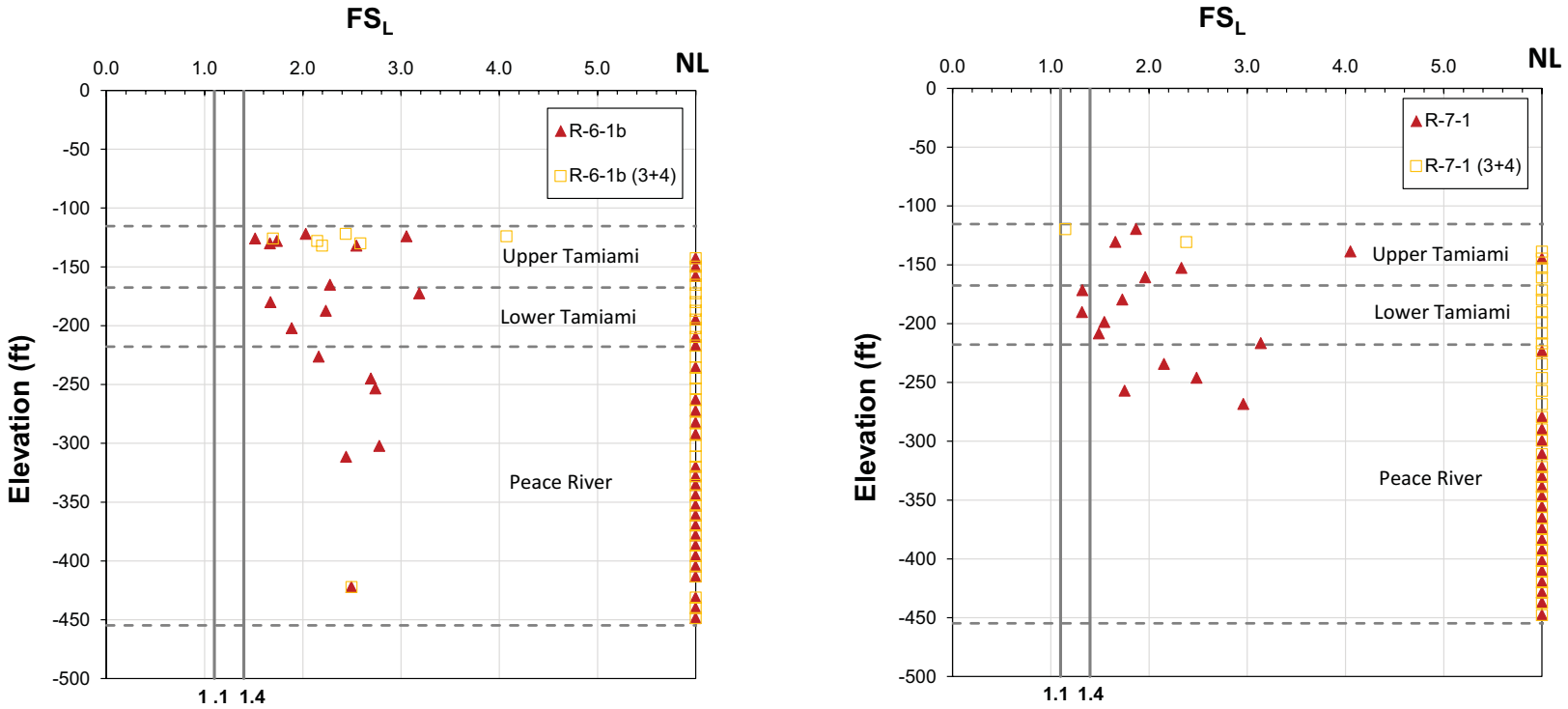

Note: NL corresponds to Non-Liquefiable locations, $(N_1)_{60} \geq 30$. No numerical FS value is obtained.

Figure 2.5.4-251 Factor of Safety against Liquefaction using Shear Wave Velocity

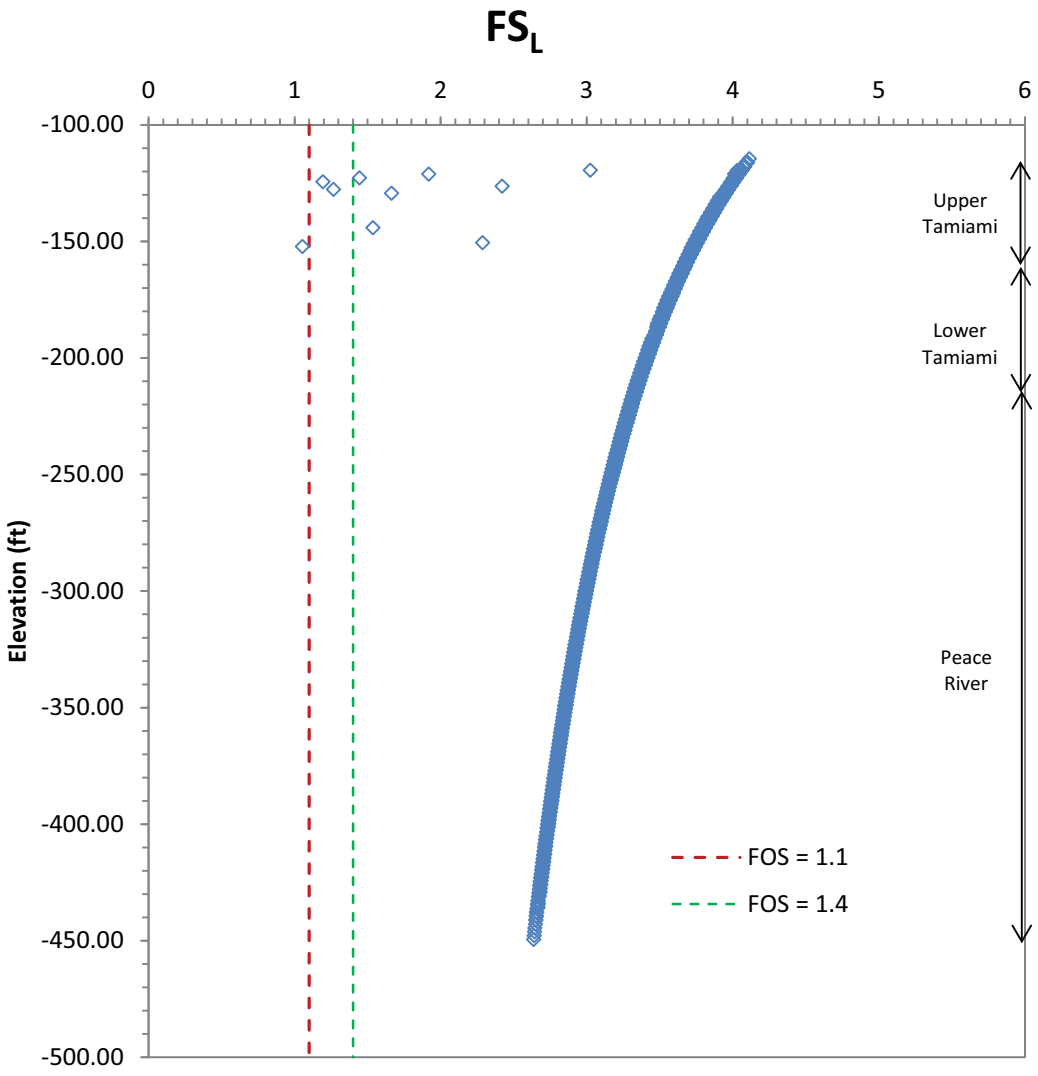

ASSOCIATED ENCLOSURES:

None

NRC RAI Letter No. PTN-RAI-LTR-040

SRP Section: 02.05.04 - Stability of Subsurface Materials and Foundations

QUESTIONS from Geosciences and Geotechnical Engineering Branch 1 (RGS1)

NRC RAI Number: 02.05.04-18 (eRAI 6006)

FSAR Section 2.5.4.10.2 describes bearing capacity calculations for the nuclear island foundation. This section states that FSAR Equation 2.5.4-15 was used to calculate the ultimate bearing capacity of the reactor and auxiliary buildings. Also the calculation for COL bearing capacity and settlement analyses states that 20 % of the unconfined compressive strength was used instead. In accordance with NUREG-0800, Standard Review Plan, Chapter 2.5.4, "Stability of Subsurface Materials and Foundations," please clarify on the actual methodology used to calculate the ultimate bearing capacity and justify its applicability. Also, please explain how the unconfined compressive strength parameter values in Table 2.5.4-209 were selected given the large range of values presented in FSAR Figure 2.5.4-217 and Table 2.5.4-207.

FPL RESPONSE:

As part of this response, the methodology to determine the bearing capacity has been revised. The new methodology includes:

- local shear failure checks using Vesic's methodology and EM 1110-1-2908,
- punching failure check,
- beam tension check, and
- limit equilibrium and finite element two dimensional (2D) models (SLOPE/W and PLAXIS 2D).

The response is divided into two parts:

- Part A describes the methodologies used to obtain the bearing capacity of the foundation media underlying the nuclear island (NI).
- Part B discusses unconfined compressive strength (UCS) parameter selection.

Part A

The NI at Turkey Point Units 6 & 7 bears on two rock layers that overlie three soil formations.

Application of classical bearing capacity hand calculations, such as Vesic et al., (described in Reference 1), or methods outlined in USACE EM 1110-1-2908 (Reference 2), to obtain the bearing capacity of the foundation media underlying the NI is not straightforward due to the strength difference between rock and soil formations as shown in Table 1. Therefore, this response includes not only hand calculations, but also limit-equilibrium and finite element 2D models.

Table 1

Summary of Layer Properties

Layer	Cohesion, c (ksf) [1]	Internal Friction, ϕ (deg) [1]	Unit Weight, γ (kcf)	Thickness (ft) [2]
Key Largo	22.5	55	0.137	14
Fort Thompson	22.4	52	0.137	66
Upper Tamiami	0.00	35	0.119	52
Lower Tamiami	0.75	29	0.117	50
Peace River	1.52	31	0.121	237

[1] FD1 properties for rock layers
[2] Top of Key Largo is set at bottom of lean concrete fill
ksf = kips per square foot

The following simplified configurations of both isolated and averaged contributions from rock and soil layers are considered in the hand calculations:

1. Only the rock formations using Hoek-Brown methodology (described in Reference 3), USACE EM 1110-1-2908 (Reference 2) and Reference 6 for rock failure modes.
2. Rock and soil formations together using the same methodologies from Reference 2.
3. Only the soil formations using the traditional Vesic methodology (described in Reference 1).

For all three configurations, dynamic bearing capacity is determined using Soubra's bearing capacity factors for shear failure modes (Reference 4).

To adequately consider both rock and soil formations, bearing capacity is additionally obtained using SLOPE/W software (limit-equilibrium method) and justified using PLAXIS 2D (finite element method). In SLOPE/W the applied load (bearing demand) is increased until the failure is observed. The allowable bearing capacity from SLOPE/W can be obtained in two ways:

1. Increase the load in increments up to the ultimate bearing capacity (i.e., failure with FS = 1.0 as obtained from SLOPE/W) and divide it by three (FS = 3.0) to obtain the allowable bearing capacity, or
2. Increase the load until FS = 3.0 as output from SLOPE/W to obtain the allowable bearing capacity.

Using results from hand calculations and SLOPE/W, a conservative allowable bearing capacity is obtained with a factor of safety FS = 3.0 for static conditions and FS = 2.0 for dynamic conditions.

Dynamic bearing capacity is obtained using only Soubra's methodology (Reference 4).

Bearing capacity calculated as 20 percent of UCS is not considered in favor of more comprehensive methodologies that consider the rock mass behavior.

Rock Failure Modes:

Bearing capacity for rock failure modes is evaluated primarily using the procedures described in the USACE EM 1110-1-2908 (Reference 2) and Carter- Kulhawy (Reference 3). Supplementary evaluations are based on the Hoek-Brown criterion (described in Reference 3 and Reference 5) or presented by Wyllie (Reference 6). Considered failure modes include:

- General shear (wedge) failure (Figure 1)
- Local shear failure
- General shear failure without cohesion
- Compressive failure (Figure 1)
- Splitting failure (Figure 1)
- Hoek-Brown evaluation
- Punching failure
- Beam tension failure

General shear failure is a generic wedge failure as shown in Figure 1. Bearing capacity for this type of failure includes resistance from rock mass cohesion, depth of embedment, and self-weight of the rock mass. For this analysis to be valid, all three contributions should be addressed which is not always realistic. This failure mode is not included in bearing capacity analysis reported here in favor of a more conservative variation, local shear failure, that includes only two contributions (resistance from cohesion and self-weight). General shear failure is the typical failure mode for soils and rock of moderate to high strength, as seen at Units 6 & 7.

Local shear failure represents a conservative variation of general shear failure where failure surfaces begin to develop but do not propagate to the surface. Therefore, the depth of embedment does not contribute to the total bearing capacity. By excluding depth of embedment, the modeled ground surface is dropped to foundation level so weight of surcharge above the foundation does not resist movement of the failure wedge. This case is included in the bearing capacity analysis reported here.

General shear failure without cohesion considers a case where failure develops along discontinuities in highly fractured rock masses and the contribution from cohesion is neglected. Since the limestone under the NIs of Units 6 & 7 is predominantly massive (described as very slightly fractured), this case is not included in bearing capacity analysis reported here.

Compressive failure as shown on Figure 1 occurs where the foundation rests on poorly constrained columns of rock, similar to an unconfined compression failure. Compressive failure assumes open vertical discontinuities that are more closely spaced than the width of the foundation. This failure mode is not probable at Units 6 & 7, since fractures are very

widely spaced. Additionally, discontinuities are generally only moderately open and are rough which is more conducive to a general shear type failure where stress is able to be transmitted across the vertical discontinuity Carter- Kulhawy (Reference 3).

Splitting failure as shown on Figure 1 occurs in rock where widely spaced, open, vertical discontinuities cause tensile failures to generate splitting beneath the foundation in the foundation media. In this failure, vertical fracture spacing is assumed to be greater than the width of the foundation. This is the case at Units 6 & 7, but the discontinuities are only moderately open which does not promote significant movement in the rock to close the discontinuities. In addition, discontinuities are rough which promotes the stress transfer between the faces precluding the occurrence of a split failure. Therefore, splitting failure is not likely at Units 6 & 7 and not included in the bearing capacity analysis reported here.

Figure 1 Bearing Capacity Failure Modes

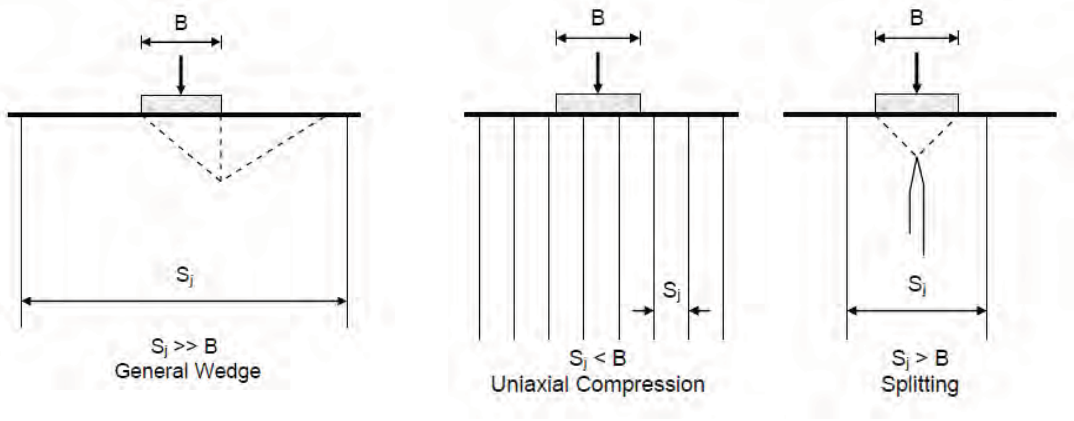

Source: Reference 7

In addition to the bearing capacity checks listed in USACE EM 1110-1-2908 (Reference 2), the Hoek-Brown methodology, punching failure and beam tension failure checks are considered. Punching failure and beam tension failure are generally considered when a thin rigid layer overlies a more compressible layer, as is the case at Units 6 & 7.

The Hoek-Brown methodology (described in References 3 and 5) utilizes the strength criterion for jointed rock masses, assumes a strip footing, but does not take foundation dimensions into account. Instead, the method relies on rock description as well as UCS (discussed in Part B).

Punching failure describes a case where the overlying rock layers fail in shear on all sides of the foundation due to the concentrated force on the thin rock layers. This failure is considered in the bearing capacity analysis reported here.

Beam tension failure occurs when the rock layers bend and fail due to the moment applied from the foundation.

Wyllie (Reference 6) cites a study by Kaderabek and Reynolds that states that there has been no reported beam tension failure in the south Florida area. That study was not able to induce a failure after exceeding the theoretical beam tension failure stress by a factor of 2. However, beam tension failure is checked using the PLAXIS 2D finite element model.

In summary, the bearing capacity determined for rock failure checks reported here is based on the following failure modes:

- Local shear failure
- Hoek-Brown evaluation
- Punching failure
- Beam tension failure

Vesic's Methodology for Soil Failures:

Traditional soil bearing capacity as proposed by Vesic (described in Reference 1) requires only shape and depth factors, but not inclination factors because the load is applied vertically and the foundation is on level ground. The NI basemat foundation is evaluated using Vesic's methodology, accounting for only soil properties as if it were founded on the upper Tamiami formation. To be conservative, and to be consistent with the rock failure checks, only the bearing capacity from local shear failure is considered.

SLOPE/W Analysis of Rock and Soil Combined:

A 2D SLOPE/W model is created to include contributions from both soil and rock layers since the contrast between stiff rock and soft soil layers is not adequately accounted for in weighted averages for the hand calculation.

SLOPE/W uses limit equilibrium following the Morgenstern-Price method to test multiple prescribed circular failure surfaces GEO-SLOPE (Reference 8). The factor of safety against failure is determined on the most critical failure surface. The ultimate bearing capacity is estimated by increasing the bearing demand until this factor of safety reaches approximately FS = 1.0. Similarly, the allowable bearing capacity is estimated when FS = 3.0. The critical failure surfaces are shown in Figures 2 and 3.

Figure 2 Failure Surface from SLOPE/W, when FS=3.0

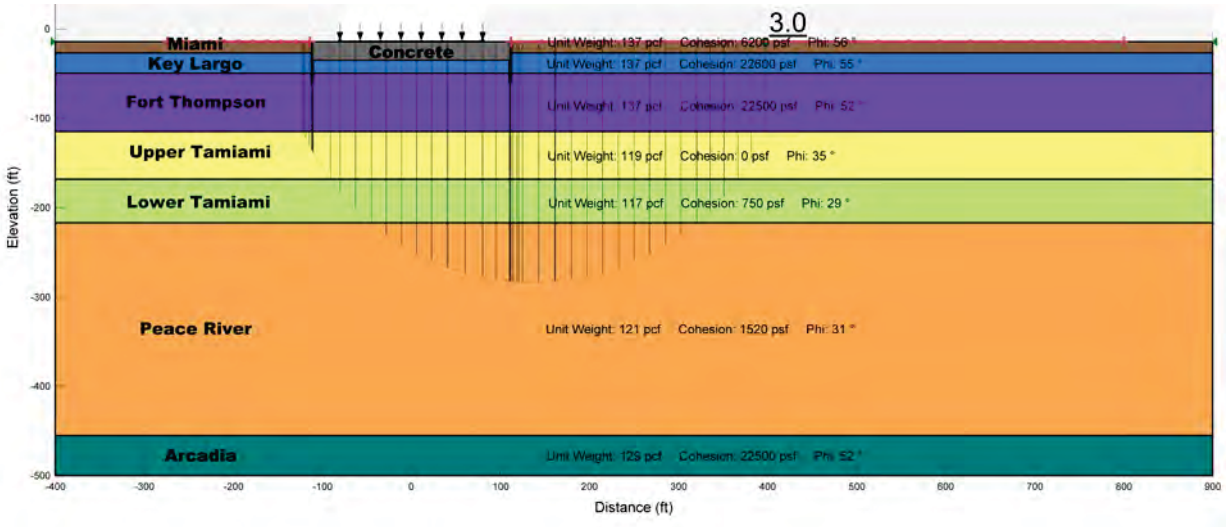

Figure 3 Failure Surface from SLOPE/W, when FS=1.0

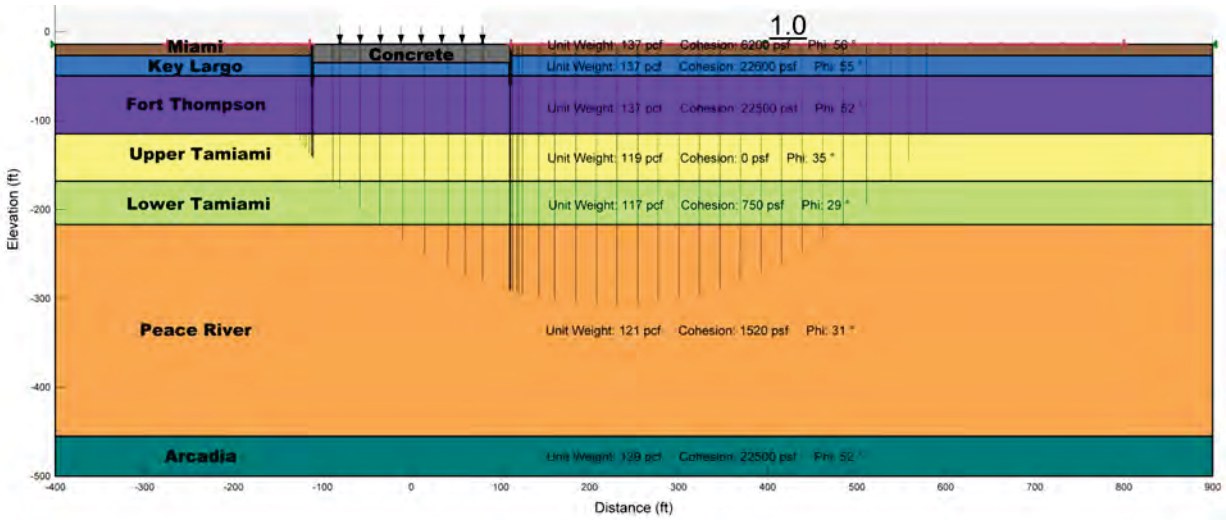

PLAXIS 2D Analysis of Rock and Soil Combined:

PLAXIS 2D is a finite element model used to verify the failure surface from SLOPE/W using the unique solution found from increasing the bearing demand to failure. As seen in a plot of plastic points (i.e., points reaching Mohr-Coulomb failure) (Figure 4), the ultimate failure surface becomes evident and reaches a depth approximately one third below the top of the Peace River Formation. This is the same depth reached by the prescribed failure surface from SLOPE/W (Figures 2 and 3).

This model is also used to check the beam tension failure. The tension cutoff for the rock layers (i.e., tensile strength of rock) is determined according to equation 3.20 in Reference 6.

Figure 4 Failure Surface from PLAXIS 2D

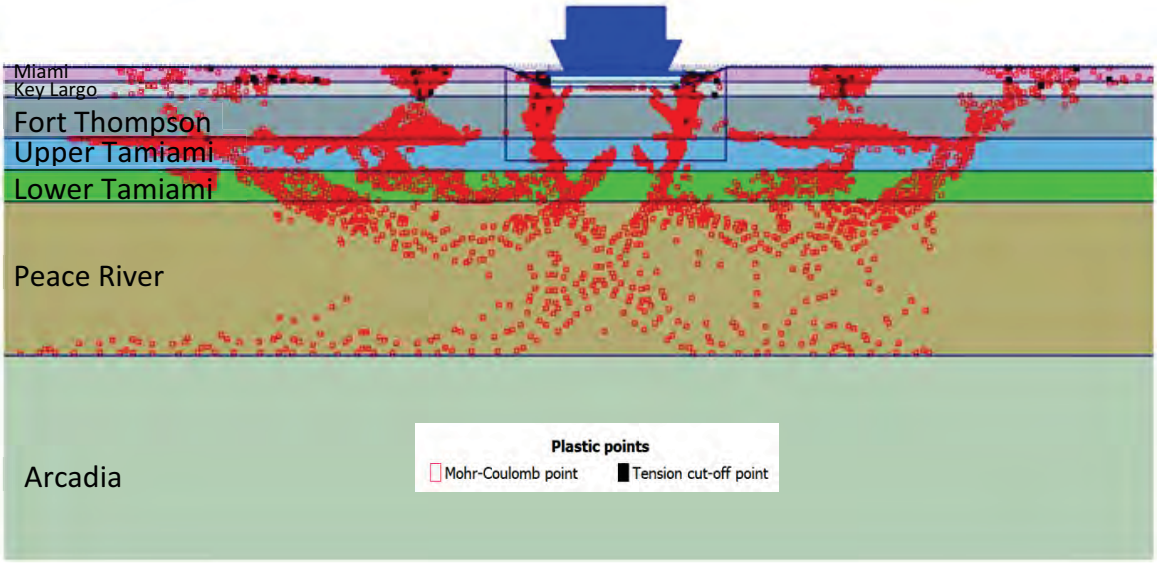

Foundation and Material Configurations:

Foundation and material configurations are summarized in Table 3.

Bearing capacity is evaluated for two extreme foundation widths (B); the shortest east-west dimension on the south edge of the building (B = 88 feet), and the longest east-west dimension (shown on Figure 5) through the shield building and the auxiliary building (B = 160 feet). Rock and soil properties (c', φ', γ) are determined by an arithmetic average weighted by thickness of the underlying strata.

Rock-only bearing capacity is evaluated using a weighted average with properties of the Key Largo and Fort Thompson formations only. An additional case using weighted averages to a depth of 2B, including soil layers, is evaluated for rock and soil together in local shear failure evaluation. Soil-only bearing capacity is evaluated using weighted averages of the upper Tamiami, lower Tamiami, and Peace River to a depth of 2B.

Properties for rock are varied between assumptions of very slightly fractured rock (fracture density = 1, FD1), slightly to moderately fractured rock (FD4), and lower bound rock (as discussed in the revised response to RAI 02.05.04-09, provided here, and included in FSAR Table 2.5.4-221, which is updated in the revised response to RAI 02.05.04-09). Soil is varied between best estimate properties and lower bound properties. For lower bound properties in soil, the upper Tamiami is reduced to the properties in FSAR Table 2.5.4-221 while lower Tamiami and Peace River properties remain as best estimate properties. It is unrealistic to assign lower bound properties to all layers, so the upper Tamiami was reduced, as it is the bearing layer in soil-only calculations.

To obtain static bearing capacity according to Hoek-Brown methodology, Table 1 from Reference 9 is followed (see Table 2). The rock mass at Units 6 & 7 is tightly interlocking undisturbed carbonate rock and is classified as very good quality rock. The material parameters m and s (Reference 9) are interpolated accordingly into the methodology described in Reference 3. To be conservative, the average UCS value of the two rock layers is adopted, this is approximately equal to 17 megapascals (MPa). Foundation configuration is not considered in Hoek-Brown methodology.

Punching failure also uses the average UCS of the Key Largo and Fort Thompson formations. This failure is determined for the two foundation configurations (88 feet and 160 feet) instead of the two rock strengths (FD4 and FD1) since UCS is not determined for FD4 conditions.

In SLOPE/W, a case is considered where zones representing open discontinuities are placed beneath and to the side of the NI to represent zones of FD4 material as shown in Figure 5. This case is unrealistic because joints in FD4 rock are only moderately open, but is presented to show an extreme case that still meets the bearing demand criteria.

In SLOPE/W, the extreme case of simulated FD4 zones is evaluated differently than the other SLOPE/W cases, by finding the factor of safety when the bearing demand pressure of 8.9 ksf is applied instead of finding the allowable bearing capacity for a prescribed factor of safety. The following failures are found for configurations with and without simulated FD4 zones (Figures 6 and 7).

The factor of safety with simulated FD4 zones (FS = 6.2) is almost half of the factor of safety with no FD4 zones (FS = 11.6). This low factor of safety is still more than double the required FS=3.0

In PLAXIS 2D, the beam tension failure is checked for the required bearing demand (8.9 ksf) as well as three times the required bearing demand (26.7 ksf). In Figures 8 and 9, points in tension are shown with black circles. As evident in both cases, there are minimal black circles, i.e., no tensile failure is observed.

If the load is increased high enough, the failure pattern observed from PLAXIS 2D (Figure 4)resembles the one obtained from SLOPE/W. PLAXIS 2D also shows that at the interface of Fort Thompson and Upper Tamiami formations, series of points go into the plastic zone (Mohr Coulomb shear failure). These points are in addition to the typical general shear failure shape, and are attributed to the strength and stiffness contrast between the two formations. The plastic points at the Fort Thompson and Upper Tamiami formations do not preclude the general failure pattern from forming all the way to the surface. In other words, series of points at this interface experience shear failure while the general shear failure is also fully developed. Nevertheless, the load to reach this type of failure is at least 20 times the foundation bearing demand.

.

Figure 5 Estimated Locations of FD4 Zones

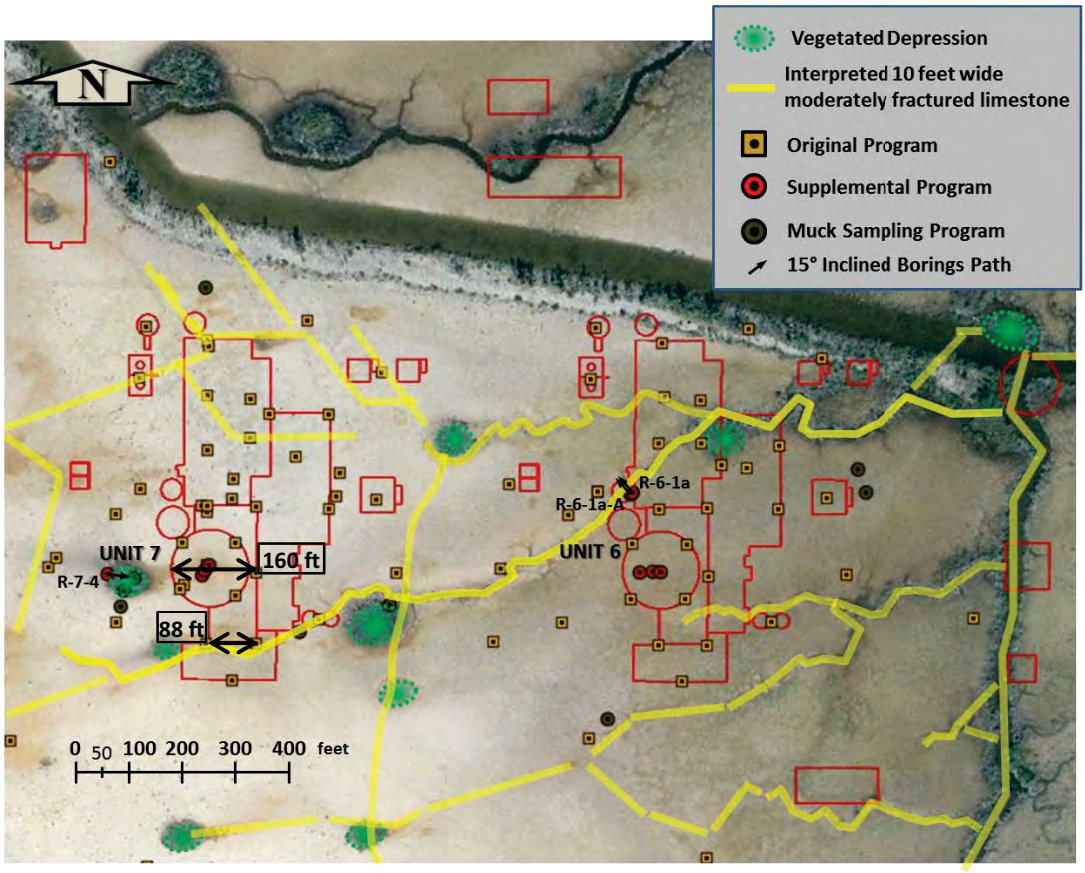

Google earth image 1/30/2005 U.S. Geological Survey

Figure 6 No Discontinuities, 1x Required Bearing Demand

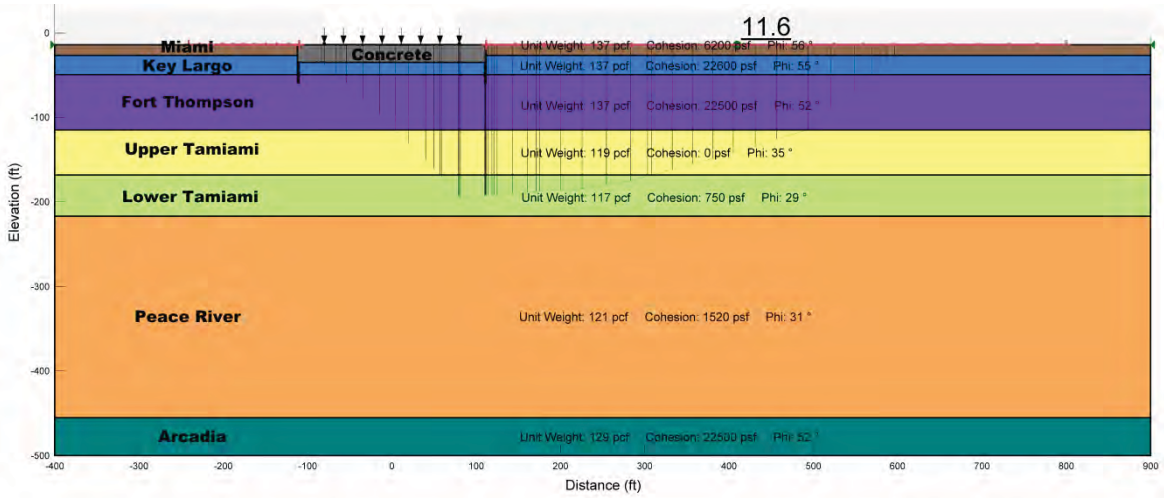

Figure 7 Simulated Discontinuities, 1x Required Bearing Demand

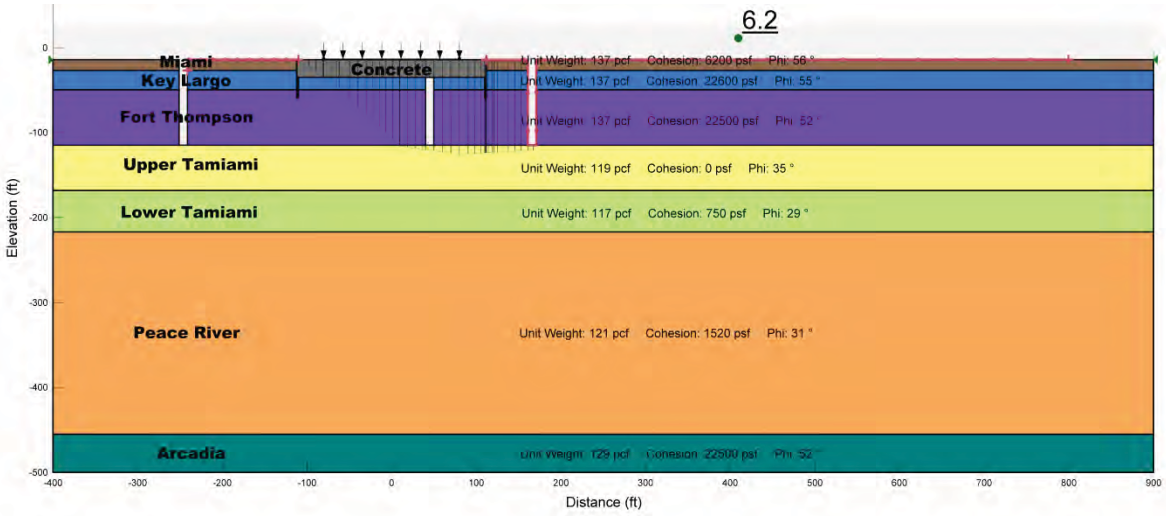

Figure 8 Plastic Deformation from PLAXIS 2D Analysis, 1x Required Bearing Demand

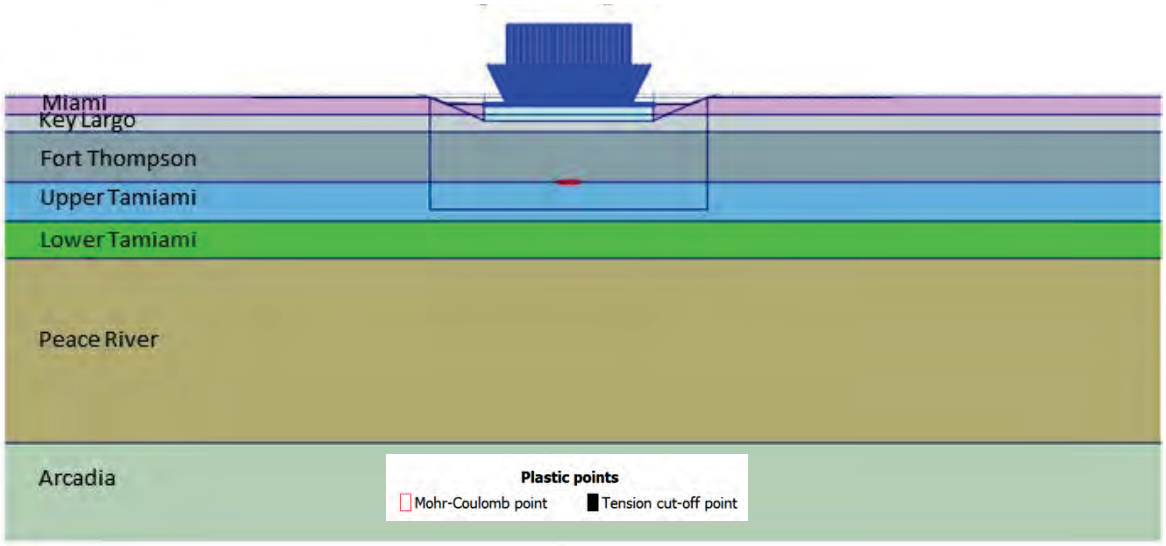

Figure 9 Plastic Deformation from PLAXIS 2D Analysis, 3x Required Bearing Demand

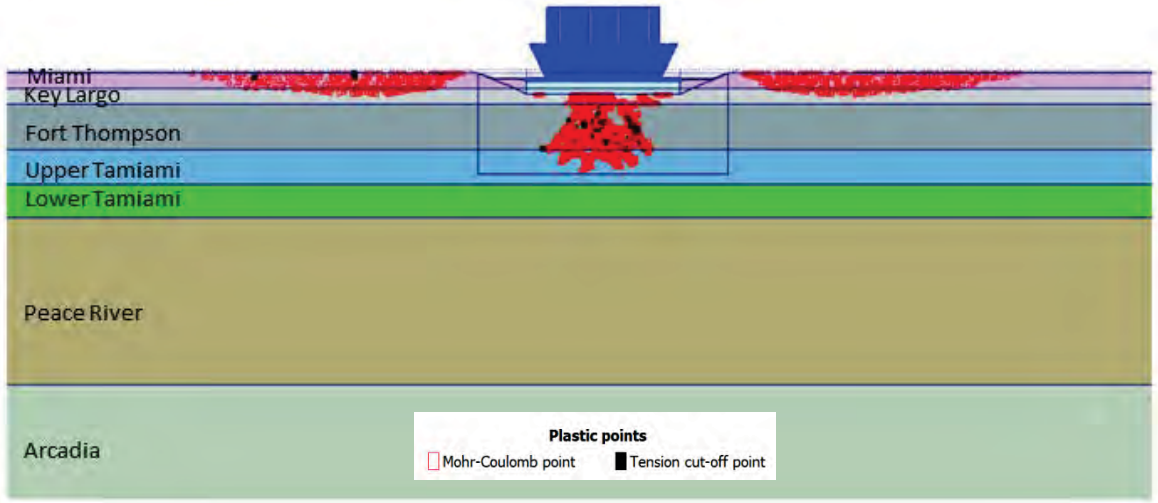

Table 2

Hoek-Brown Material Constants

Table 1 : Approximate relationship between rock mass quality and material constants

Disturbed rock mass m and s values — *undisturbed rock mass m and s values*

EMPIRICAL FAILURE CRITERION

$$\sigma'_1 = \sigma'_3 + \sqrt{m\sigma_c\sigma'_3 + s\sigma_c^2}$$

σ'_1 = major principal effective stress
σ'_3 = minor principal effective stress
σ_c = uniaxial compressive strength of intact rock, and
m and s are empirical constants.

		CARBONATE ROCKS WITH WELL DEVELOPED CRYSTAL CLEAVAGE *dolomite, limestone and marble*	LITHIFIED ARGILLACEOUS ROCKS *mudstone, siltstone, shale and slate (normal to cleavage)*	ARENACEOUS ROCKS WITH STRONG CRYSTALS AND POORLY DEVELOPED CRYSTAL CLEAVAGE *sandstone and quartzite*	FINE GRAINED POLYMINERALLIC IGNEOUS CRYSTALLINE ROCKS *andesite, dolerite, diabase and rhyolite*	COARSE GRAINED POLYMINERALLIC IGNEOUS & METAMORPHIC CRYSTALLINE ROCKS – *amphibolite, gabbro gneiss, granite, norite, quartz-diorite*
INTACT ROCK SAMPLES						
Laboratory size specimens free	m	7.00	10.00	15.00	17.00	25.00
from discontinuities	s	1.00	1.00	1.00	1.00	1.00
CSIR rating: RMR = 100	*m*	*7.00*	*10.00*	*15.00*	*17.00*	*25.00*
NGI rating: Q = 500	*s*	*1.00*	*1.00*	*1.00*	*1.00*	*1.00*
VERY GOOD QUALITY ROCK MASS						
Tightly interlocking undisturbed rock	m	2.40	3.43	5.14	5.82	8.56
with unweathered joints at 1 to 3m.	s	0.082	0.082	0.082	0.082	0.082
CSIR rating: RMR = 85	*m*	*4.10*	*5.85*	*8.78*	*9.95*	*14.63*
NGI rating: Q = 100	*s*	*0.189*	*0.189*	*0.189*	*0.189*	*0.189*
GOOD QUALITY ROCK MASS						
Fresh to slightly weathered rock, slightly	m	0.575	0.821	1.231	1.395	2.052
disturbed with joints at 1 to 3m.	s	0.00293	0.00293	0.00293	0.00293	0.00293
CSIR rating: RMR = 65	*m*	*2.006*	*2.865*	*4.298*	*4.871*	*7.163*
NGI rating: Q = 10	*s*	*0.0205*	*0.0205*	*0.0205*	*0.0205*	*0.0205*
FAIR QUALITY ROCK MASS						
Several sets of moderately weathered	m	0.128	0.183	0.275	0.311	0.458
joints spaced at 0.3 to 1m.	s	0.00009	0.00009	0.00009	0.00009	0.00009
CSIR rating: RMR = 44	*m*	*0.947*	*1.353*	*2.030*	*2.301*	*3.383*
NGI rating: Q = 1	*s*	*0.00198*	*0.00198*	*0.00198*	*0.00198*	*0.00198*
POOR QUALITY ROCK MASS						
Numerous weathered joints at 30-500mm,	m	0.029	0.041	0.061	0.069	0.102
some gouge. Clean compacted waste rock	s	0.000003	0.000003	0.000003	0.000003	0.000003
CSIR rating: RMR = 23	*m*	*0.447*	*0.639*	*0.959*	*1.087*	*1.598*
NGI rating: Q = 0.1	*s*	*0.00019*	*0.00019*	*0.00019*	*0.00019*	*0.00019*
VERY POOR QUALITY ROCK MASS						
Numerous heavily weathered joints spaced	m	0.007	0.010	0.015	0.017	0.025
<50mm with gouge. Waste rock with fines.	s	0.0000001	0.0000001	0.0000001	0.0000001	0.0000001
CSIR rating: RMR = 3	*m*	*0.219*	*0.313*	*0.469*	*0.532*	*0.782*
NGI rating: Q = 0.01	*s*	*0.00002*	*0.00002*	*0.00002*	*0.00002*	*0.00002*

Source: Reference 9

Table 3
Foundation and Material Configurations for Bearing Capacity Analysis

Evaluation Method	Foundation Width, B (feet)	Properties[1]	Local Shear Failure	Hoek-Brown [2]	Punching Failure[3]	Beam Tension Failure
Rock-Only Hand Calculation	88	FD1 Rock	X	X	X	–
Rock-Only Hand Calculation	160	FD1 Rock	X	X	X	–
Rock-Only Hand Calculation	88	FD4 Rock	X	–	–	–
Rock-Only Hand Calculation	160	FD4 Rock	X	–	–	–
Rock-Only Hand Calculation	88	LB FD4 Rock	X	–	–	–
Rock-Only Hand Calculation	160	LB FD4 Rock	X	–	–	–
Rock & Soil Hand Calculation	88	FD4 Rock & BE Soil	X	–	–	–
Rock & Soil Hand Calculation	160	FD4 Rock & BE Soil	X	–	–	–
Rock & Soil Hand Calculation	88	LB FD4 Rock & BE Soil	X	–	–	–
Rock & Soil Hand Calculation	160	LB FD4 Rock & BE Soil	X	–	–	–
Soil-Only Hand Calculation	88	BE Soil	X	–	–	–
Soil-Only Hand Calculation	160	BE Soil	X	–	–	–
Soil-Only Hand Calculation	88	LB Soil	X	–	–	–
Soil-Only Hand Calculation	160	LB Soil	X	–	–	–
SLOPE/W	88	FD1 Rock & BE Soil	X	–	–	–
SLOPE/W	160	FD1 Rock & BE Soil	X	–	–	–
SLOPE/W	160	LB FD4 Rock & LB Soil	X	–	–	–
SLOPE/W	160	FD1 Rock with open joints	X	–	–	–
PLAXIS 2D	160	FD1 Rock & BE Soil	X	–	–	X

(1) LB Soil includes LB properties of upper Tamiami and BE properties for lower Tamiami and Peace River
(2) Hoek-Brown methodology is dimension independent
(3) Punching failure is based on lowest average UCS of rock layers
BE = Best Estimate
LB = Lower Bound, as defined in the revised response to RAI 02.05.04-09

Summary and Recommendation:

Ultimate and allowable bearing capacities for the failures marked in Table 2 are presented in Table 3, with the exception of two cases. The SLOPE/W model with simulated FD4 zones and the PLAXIS 2D model do not produce allowable bearing capacities to populate Table 3. They are included for visual inspection of the failure surface.

For static analyses, the lowest allowable bearing capacity of 39 ksf results from the Lower Bound configuration in SLOPE/W (Table 3). This static bearing capacity is acceptable according to the 8.9 ksf static bearing demand required by the AP1000 DCD.

For dynamic analyses, the minimum allowable bearing capacity using Soubra's methodology (Reference 4) is 43 ksf, resulting from the soil-only analysis using lower bound properties for the upper Tamiami layer. This dynamic bearing capacity is acceptable according to the 35 ksf bearing demand required by the DCD.

Recommended static bearing capacity at Units 6 & 7 is 39 ksf and recommended dynamic bearing capacity is 43 ksf.

Table 4

Summary of Calculated Bearing Capacities (ksf)

Evaluation Method	Foundation Width, B (ft)	Properties	Local Shear Failure				Hoek-Brown[1]		Punching[2]	
			Static, q_{ULT}	Static, q_{ALL}	Dynamic, q_{ULT}	Dynamic, q_{ALL}	Static, q_{ULT}	Static, q_{ALL}	Static, q_{ULT}	Static, q_{ALL}
Rock-Only Hand Calculation	88	FD1 Rock	2,623	874	3,701	1,851	1629	543	408	136
Rock-Only Hand Calculation	160	FD1 Rock	3,603	1,201	4,640	2,320			273	91
Rock-Only Hand Calculation	88	FD4 Rock	1,790	597	2,104	1,052	–	–	–	–
Rock-Only Hand Calculation	160	FD4 Rock	2,771	924	2,999	1,500	–	–	–	–
Rock-Only Hand Calculation	88	LB FD4 Rock	1,063	354	1,411	706	–	–	–	–
Rock-Only Hand Calculation	160	LB FD4 Rock	1,748	583	2,214	1,107	–	–	–	–
Rock & Soil Hand Calculation	88	FD4 Rock & BE Soil	386	129	658	329	–	–	–	–
Rock & Soil Hand Calculation	160	FD4 Rock & BE Soil	329	110	401	201	–	–	–	–
Rock & Soil Hand Calculation	88	LB FD4 Rock & BE Soil	279	93	485	243	–	–	–	–
Rock & Soil Hand Calculation	160	LB FD4 Rock & BE Soil	280	93	339	170	–	–	–	–
Soil-Only Hand Calculation	88	BE Soil	165	55	87	44	–	–	–	–
Soil-Only Hand Calculation	160	BE Soil	251	84	138	69	–	–	–	–
Soil-Only Hand Calculation	88	LB Soil	157	52	87	43	–	–	–	–
Soil-Only Hand Calculation	160	LB Soil	244	81	138	69	–	–	–	–
SLOPE/W	88	FD1 Rock & BE Soil	–	81	–	–	–	–	–	–
SLOPE/W	160	FD1 Rock & BE Soil	–	51	–	–	–	–	–	–
SLOPE/W	160	LB FD4 Rock & LB Soil	–	39	–	–	–	–	–	–
Minimum/Recommended			**157**	**39**	**87**	**43**	**694**	**231**	**273**	**91**

(1) LB Soil includes LB properties of upper Tamiami and BE properties for lower Tamiami and Peace River
(2) Hoek-Brown methodology is dimension independent
(3) Punching failure is based on lowest average UCS of rock layers
q_{ULT} = ultimate bearing capacity
q_{ALL} = allowable bearing capacity
BE = Best Estimate
LB = Lower Bound as defined in the revised response to RAI 02.05.04-09

Part B

Recommended bearing capacity does not implement UCS. UCS is only used in calculation of Hoek-Brown bearing capacity and tensile strength as the average of Key Largo and Fort Thompson data.

Values for UCS are discussed in the revised response to RAI 02.05.04-04. In this RAI response, the average values for each rock layer are updated in Tables 2.5.4-207 and 2.5.4-209 to include data from the supplemental investigation. These averages are determined arithmetically.

This response is PLANT SPECIFIC.

References:

1. Bowles, J. E., *Foundation Analysis and Design*, The McGraw-Hill Companies, Inc., 1997, pp. 219-228.
2. USACE, *Rock Foundations*, Engineering Manual EM 1110-1-2908, Ch. 6, 1994.
3. Carter, J.P. and Kulhawy, F.H., *Analysis and Design of Drilled Shaft Foundations Socketed into Rock*, Report EL-5918, Electric Power Research Institute, Palo Alto, CA, pp. 3-2 through 3-6, 1988.
4. Soubra, A. H., *Upper-Bound Solutions for Bearing Capacity of Foundations*, J. Geotechnical and Geoenvironmental Engineering, January, V. 125, No. 1, p. 59, 1999.
5. Hoek, E., C. Carranza-Torres, and B. Corkum, *Generalized Hoek-Brown Failure Criterion - 2002 Edition,* 5th North American Rock Mechanics, 2002.
6. Wyllie, D., *Foundations on Rock*, 2nd Edition, pp 143 and 144, 1999.
7. Prakoso, W.A. and F.H. Kulhawy, *Capacity of Foundations on Discontinuous Rock*, Golden Rocks 2006 (Proceedings of the 41st US Symposium of Rock Mechanics), Ed. DP Yale et al., Paper 06-972, page 3-2, 2006.
8. GEO-SLOPE International Ltd., *Stability Modeling with SLOPE/W 2007 Version: An Engineering Methodology*, Fourth Edition, p. 54, February 2010.
9. Hoek, E, and E.T. Brown, “The Hoek-Brown Failure Criterion – a 1988 Update,” Proceedings of the 15th Canadian Rock Mechanics Symposium, Toronto, 1988

ASSOCIATED COLA REVISIONS:

FSAR Subsection 2.5.4.10.2 will be revised in a future revision as follows:

Application of classical bearing capacity hand calculations, such as Vesic's methodology (Reference 225) or methods outlined in Reference 272, to obtain the bearing capacity of the foundation media underlying the NI is not straightforward due to the strength difference between rock and soil formations as seen in Table 2.5.4-209. Therefore, simplified configurations are assumed to calculate bearing capacity on:

1. **Rock only, using Hoek-Brown's methodology (described in Reference 314), local shear failure for rock (References 272 and 316), and punching failure (Reference 272).**
2. **Rock and soil together, using local shear failure for rock (Reference 272).**
3. **Soil only, using local shear failure from Vesic's methodology (described in Reference 225), as if the NI basemat was founded on the upper Tamiami layer.**

Due to the predominantly massive nature of rock layers at Units 6 & 7, as well as the rough condition of observed discontinuities, jointed rock failure modes are not considered in this bearing capacity analysis. Without open joints, stress is permitted to transmit continuously through the foundation media promoting a general shear failure mode.

The ultimate bearing capacity, q_{ult}, of a foundation **on soil** is calculated using **Vesic's methodology for general shear failure from** Reference 225:

$$q_{ult} = c\, N_c\, \zeta c + q\, Nq\, \zeta q + 0.5\, \gamma'\, B\, N\gamma\, \zeta_\gamma \qquad \text{Equation 2.5.4-14}$$

~~Category I seismic structures bear on lean concrete placed on the rock of Key Largo Limestone (Stratum 3).~~ For foundations bearing on rock, Reference**s** 272 **and 316 equations** ~~is used~~ calculate bearing capacity **from general shear failure**.

Using Reference 272, the ultimate bearing capacity (q_{ult}) formula for a footing on weak rocks with little fracturing is calculated as:

$$q_{ult} = c\, N_c\, C_{f1} + \gamma\, D_f\, N_q + 0.5\gamma\, B\, N_\gamma C_{f2} \qquad \text{Equation 2.5.4-15}$$

Where,

c = rock mass cohesion
γDf = effective overburden pressure at base of foundation
γ = effective unit weight of rock
Df = depth from ground surface to base of foundation
B = width of foundation
Nc, Nq, and Nγ are bearing capacity factors for rock

Cf1 and Cf2 are shape factors that replace the ζ shape factor in Equation 2.5.4-14.

From Table 5.4 of Reference 272,

Cf1 = Cf2 = 1.0 for L/B>6 strip foundation	Equation 2.5.4-16a
Cf1 = 1.12, Cf2 = 0.9 for L/B=2	Equation 2.5.4-16b
Cf1 = 1.05, Cf2 = 0.95 for L/B=5	Equation 2.5.4-16c
Cf1 = 1.25, Cf2 = 0.85 for square foundation	Equation 2.5.4-16d
Cf1 = 1.2, Cf2 = 0.7 for circular foundation	Equation 2.5.4-16e

Where,

L = length of footing

From Equation 5.8 of Reference 272,

Nφ = tan2(45+φ/2)	Equation 2.5.4-17
Nc = 2 N φ 0.5 (Nφ+1)	Equation 2.5.4-18
Nγ = 0.5 Nφ0.5(N2φ–1)	Equation 2.5.4-19
Nq = N φ 2	Equation 2.5.4-20

Equations 2.5.4-14 and 2.5.4-15 can be simplified to a local shear failure mode:

$$q_{ult} = c\,N_c\,\zeta_c + 0.5\,\gamma\,B\,N_\gamma\,\zeta_\gamma$$ Equation 2.5.4-14a

$$q_{ult} = cN_cC_{f1} + 0.5\,\gamma\,B\,N_\gamma\,C_{f2}$$ Equation 2.5.4-15a

This simplification is conservative because it neglects the contribution of the second ~~two~~ terms~~.~~**relating to surcharge resistance. Therefore, local shear failure evaluation is used in bearing capacity analysis instead of the general shear failure assumption.**

~~Since there were no laboratory test results available to derive rock mass cohesion or friction angle for Miami Limestone, a generic value was used from Reference 272. For limestones with 10 to 20 mm clay infillings, c = 2.3 ksf and φ = 14°. Using Equation 2.5.4-215a gives an allowable bearing capacity of 5.8 ksf, including a factor of safety of 3.~~

~~Alternatively, an allowable bearing capacity of not more than 20 percent of the unconfined compressive strength (U) of the rock can be used, according to Reference 221. For the Miami Limestone, a U of 200 psi is given in Table 2.5.4-209. Twenty percent of this strength is 40 psi (5.76 ksf). The results of the two methods compare favorably.~~

~~The foundation bearing capacities of the Category 1 seismic structures are considered similarly. The design U for the Key Largo Limestone is 1.5 ksi from Table 2.5.4-209 with 20 percent of 1.5 ksi = 300 psi ~ 43 ksf. This allowable capacity compares favorably to the value of 54.5 ksf which is calculated using Equation 2.5.4-15a (conservatively assuming a friction angle that is the same as for the Miami Limestone = 14° and a cohesion of 10 percent of the U, i.e., 21.6 ksf); the lower value of 43 ksf is recommended.~~

In addition to Equation 2.5.4-15a for a local shear failure in rock, the Hoek-Brown methodology considers the strength criterion for jointed rock masses to calculate ultimate bearing capacity. The Hoek-Brown methodology assumes a strip footing, but does not take foundation dimensions into account. Instead, the method relies on

rock descriptions and unconfined compressive strength, shown in Equation 3-6 of Reference 314:

$$q_{ult} = \left[\sqrt{s} + m\right] \times U \qquad \text{Equation 2.5.4-20a}$$

Where,

q_{ult} = ultimate bearing capacity,
U = unconfined compressive strength of a rock mass, and
m and s = empirically-determined strength parameters according to rock type, and rock condition, listed in Reference 274.

Punching failure describes a case where the overlying rock layers fail in shear on all sides of the foundation due to the concentrated force on thin rock layers. This failure is also applicable to bearing capacity analysis of Units 6 & 7. Punching failure bearing capacity is defined as the rock layer shear strength multiplied by the shearing surface area. The shearing surface area is equal to the loading perimeter multiplied by the thickness of the rock layer.

$$q_{ult} = \frac{U}{2} * (2B + 2L) * H / (B * L) \qquad \text{Equation 2.5.4-20a}$$

Where,

q_{ult} = ultimate bearing capacity,
U = unconfined compressive strength of a rock mass,
B = width of foundation,
L = length of foundation, and
H = thickness of Key Largo plus Fort Thompson beneath the bearing surface (Table 2.5.4-209).

To adequately consider both rock and soil formations, bearing capacity is additionally obtained using SLOPE/W software (limit-equilibrium method) and justified using PLAXIS 2D. In SLOPE/W the foundation bearing demand is increased until the desired factor of safety is observed (FS = 3.0). Allowable bearing capacity is obtained at FS = 3.0. When the load is further increased, the ultimate failure surface is observed at FS = 1.0. These conditions are presented in Figures 2.5.4-256 and 2.5.4-257. These surfaces are checked with PLAXIS 2D (finite element method) to obtain a unique solution independent of the prescribed failure surfaces in SLOPE/W.

PLAXIS 2D is used to verify the validity of failure surfaces from SLOPE/W using the unique solution found from increasing the bearing demand to failure. As seen in a plot of plastic points (i.e., points reaching Mohr-Coulomb failure), this unique surface becomes evident (Figure 2.5.4-268). This is the same depth reached by the prescribed failure surface from SLOPE/W (Figures 2.5.4-256 and 2.5.4-257).

The PLAXIS 2D model is also used to check for beam tension failure. The tension cutoff for the rock layers (i.e., tensile strength of rock) is determined according to equation 3.20 in Reference 272.

$$\sigma_t = 0.5\,\sigma_u\,(m - \sqrt{m^2 + 4s})$$ **Equation 2.5.4-20b**

In PLAXIS 2D, the beam tension failure is checked for the required bearing demand (8.9 ksf) as well as three times the required bearing demand (26.7 ksf). In Figures 2.5.4-266 and 2.5.4-267, points in tension are shown with black circles. As evident in both cases, there are minimal black circles, i.e., no significant tensile failure, is observed, even for loads three times the required bearing demand.

Bearing capacity is evaluated for two extreme foundation widths (B): the shortest east-west dimension on the south edge of the building (B = 88 feet) and the longest east-west dimension through the shield building and the auxiliary building (B = 160 feet). Rock and soil properties (c', φ', γ) are determined by an arithmetic average weighted by thickness of the underlying strata (Table 2.5.4-209). These properties are determined for the following cases:

1. **Rock-only bearing capacity is evaluated using a weighted average with properties of the Key Largo and Fort Thompson formations only.**
2. **Soil and rock together uses weighted averages to a depth of 2B, including soil layers.**
3. **Soil-only bearing capacity is evaluated using weighted averages of the upper Tamiami, lower Tamiami, and Peace River to a depth of 2B.**

Properties for rock are varied between assumptions of very slightly fractured rock (fracture density of = 1, FD1), slightly to moderately fractured rock (FD4), and lower bound rock (Table 2.5.4-221).

Soil is varied between best estimate properties and lower bound properties. For lower bound properties in soil, the upper Tamiami is reduced to the properties in Table 2.5.4-221 while lower Tamiami and Peace River properties remain as best estimate properties. It is unrealistic to assign lower bound properties to all layers, so the upper Tamiami was reduced as it is the bearing layer in soil-only calculations.

To obtain static bearing capacity according to Hoek-Brown methodology, material properties are estimated from Reference 319. The rock mass at Units 6 & 7 is tightly interlocking undisturbed carbonate rock, classified as very good quality. These material properties are used in Hoek-Brown bearing capacity and calculation of tensile strength for the beam tension failure check in PLAXIS 2D. The average UCS value of the two rock layers is adopted.

Punching failure also uses the average UCS of the Key Largo and Fort Thompson formations. This failure is determined for the two foundation configurations (88 feet and 160 feet).

In SLOPE/W, a case is considered where zones representing open discontinuities are placed beneath and to the side of the NI to represent zones of FD4 material as shown in Figure 2.5.4-254. This case is unrealistic because joints in FD4 rock are only moderately open, but the comparison to no simulated joints is presented in Figures 2.5.4-258 and 2.5.4-259.

Foundation bearing capacities are calculated using ~~the average material properties in Table 2.5.4-209 and~~ Equations 2.5.4-14**a, 2.5.4-15a and 2.5.4-16a** through 2.5.4-20**b**. A summary of the **cases evaluated and** allowable bearing capacities (using FOS = 3.0) of Seismic Category I structures (nuclear island) is given in Table 2.5.4-217. Analysis results show that for the Seismic Category I structures (including both units), the **minimum** allowable static bearing capacity is ~~43~~**39** ksf **from the lower bound SLOPE/W analysis**, which greatly exceeds the ~~anticipated~~ average required bearing capacity of 8.9 ksf specified in the DCD.

~~The above bearing capacity formulation is based on the assumption that the strata within the zone of foundation deformation are uniform with depth in terms of shear strength properties. While recognizing that the site strata are interlayered, the properties of the soil and rock are conservatively selected to provide for a representative bearing capacity.~~

FSAR Subsection 2.5.4.10.2.1 will be revised in a future COLA revision as follows:

2.5.4.10.2.1 Dynamic Bearing Capacity

Dynamic bearing capacity is determined using Soubra's bearing capacity factors (Reference 315), N_{cE} and $N_{\gamma E}$, in Equations 2.5.4-14a and 2.5.4-15a, replacing N_c and N_γ, respectively. These factors are chosen from Soubra's Tables 6 and 8 based on horizontal acceleration K_H = 0.1g and the friction angle according to the foundation media rounded down to the nearest 5.

The maximum dynamic bearing capacity required is 35 ksf (DCD). This total load includes normal loading plus seismic conditions with a 0.3g peak ground acceleration, which greatly exceeds the seismicity in Florida. Using the calculated allowable bearing capacity of 43 ksf for rock and lean concrete overlying the rock, this condition is satisfied even with the 0.3g peak ground acceleration.

Note that for concrete, no guidance is given in ACI 349-06 (Reference 273) for increasing or decreasing the design bearing strength for dynamic loading.

FSAR Subsection 2.5.4.11 will be revised in a future revision as follows:

2.5.4.11 Design Criteria and References

Table 2.5.4-217 contains calculated **allowable** bearing capacities, both static and dynamic, for Units 6 & 7 Seismic Category I structures. In the case of static bearing capacity, a minimum FOS = 3.0 is ~~applied against the calculated ultimate bearing capacity in evaluating the~~ **used to evaluate allowable** static bearing capacity of a structure. **For the Units 6 & 7 Category I structures, the computed allowable bearing capacity (including FOS = 3.0) of 39 ksf exceeds the DCD maximum static loading of 8.9 ksf.** In the case of dynamic bearing capacity, **an FOS = 2.0 is applied against** the calculated ultimate bearing capacity **in evaluating** ~~is typically compared directly against~~ the required **allowable** dynamic bearing capacity of a structure (i.e., the calculated allowable bearing capacity of subsurface materials for normal loads plus the SSE as per the DCD). ~~(~~Because the SSE in the DCD has a 0.3g peak ground acceleration that is much higher than that anticipated for South Florida, the dynamic bearing capacity in the DCD is substantially higher than the maximum dynamic loading that would be realized at the site~~)~~. For the Units 6 & 7 Category I

structures, the computed allowable bearing capacity (including FOS = ~~3.0~~**2.0**) of 43 ksf exceeds the DCD maximum dynamic loading of 35 ksf.

The following references will be added FSAR Subsection 2.5.13 in a future revision:

2.5.4-13 References

314. Carter, J.P. and Kulhawy, F.H., *Analysis and Design of Drilled Shaft Foundations Socketed into Rock*, Report EL-5918, Electric Power Research Institute, Palo Alto, California, 1988.

315. Soubra, A. H., *Upper-Bound Solutions for Bearing Capacity of Foundations*, J. Geotechnical and Geoenvironmental Engineering, V. 125, No. 1, January 1999.

319. Hoek, E, and E.T. Brown, "The Hoek-Brown Failure Criterion – a 1988 Update," Proceedings of the 15th Canadian Rock Mechanics Symposium, Toronto, 1988.

Table 2.5.4-217 will be replaced with the following in a future revision:

Table 2.5.4-217
Summary of Bearing Capacity

Evaluation Method	Foundation Width, B (ft)	Properties[1]	Local Shear Failure		Hoek-Brown[2]	Punching[3]
			Static, q_{ALL}	Dynamic, q_{ALL}	Static, q_{ALL}	Static, q_{ALL}
Rock-Only Hand Calculation	88	FD1 Rock	874	1851	67	136
Rock-Only Hand Calculation	160	FD1 Rock	1201	2320		91
Rock-Only Hand Calculation	88	FD4 Rock	597	1052	21	–
Rock-Only Hand Calculation	160	FD4 Rock	924	1500		–
Rock-Only Hand Calculation	88	LB FD4 Rock	354	706	–	–
Rock-Only Hand Calculation	160	LB FD4 Rock	583	1107	–	–
Rock & Soil Hand Calculation	88	FD4 Rock & BE Soil	129	329	–	–
Rock & Soil Hand Calculation	160	FD4 Rock & BE Soil	110	201	–	–
Rock & Soil Hand Calculation	88	LB FD4 Rock & BE Soil	93	243	–	–
Rock & Soil Hand Calculation	160	LB FD4 Rock & BE Soil	93	170	–	–
Soil-Only Hand Calculation	88	BE Soil	55	44	–	–
Soil-Only Hand Calculation	160	BE Soil	84	69	–	–
Soil-Only Hand Calculation	88	LB Soil	52	43	–	–
Soil-Only Hand Calculation	160	LB Soil	81	69	–	–
SLOPE/W	88	FD1 Rock & BE Soil	81	–	–	–
SLOPE/W	160	FD1 Rock & BE Soil	51	–	–	–
SLOPE/W	160	LB FD4 Rock & LB Soil	39	–	–	–
		Minimum:	39	43	21	91

Notes:
[1] LB Soil includes LB properties of Upper Tamiami and BE properties for Lower Tamiami and Peace River
[2] Hoek-Brown methodology is dimension independent
[3] Punching failure is based on lowest average UCS of rock layers
q_{ALL} = allowable bearing capacity
BE = Best Estimate LB = Lower Bound

The following figures will be added in a future revision

Figure 2.5.4-256
SLOPE/W Analysis of Bearing Capacity, where FS = 3.0

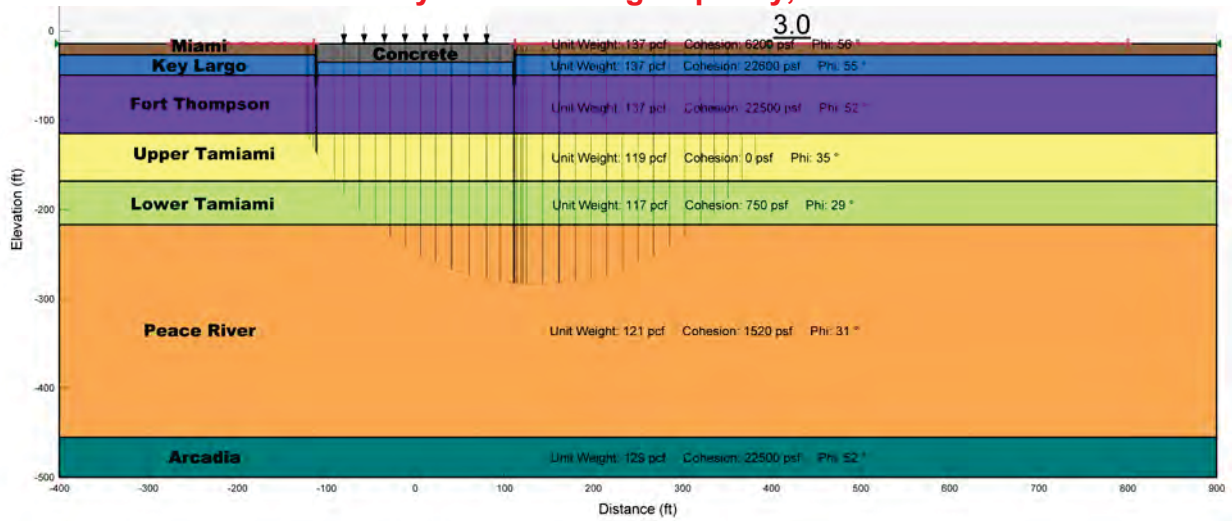

Figure 2.5.4-257
SLOPE/W Analysis of Bearing Capacity, where FS = 1.0

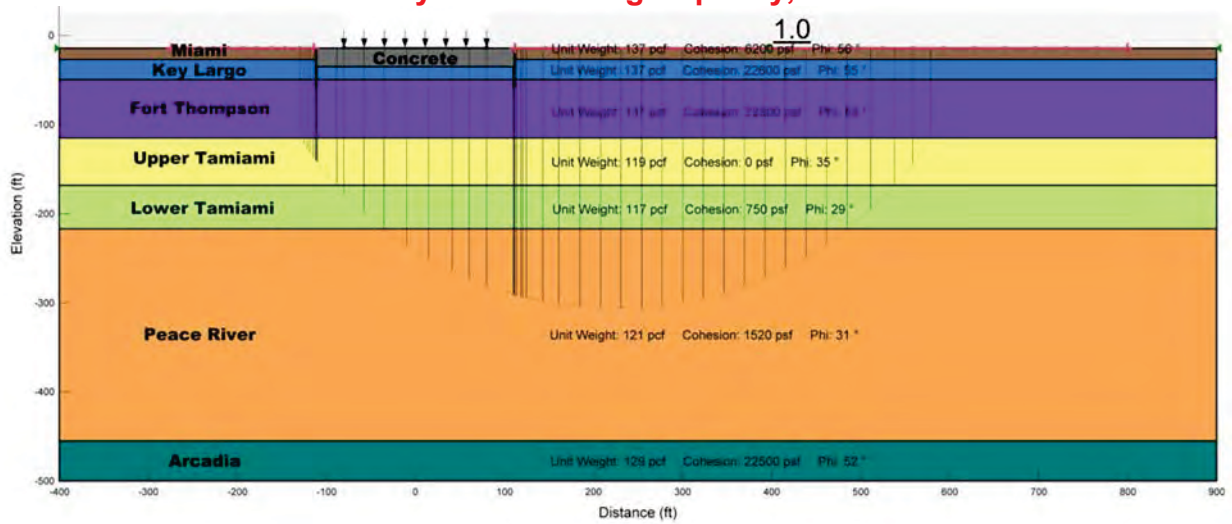

Figure 2.5.4-258
SLOPEW Analysis, 1x Required Bearing Demand

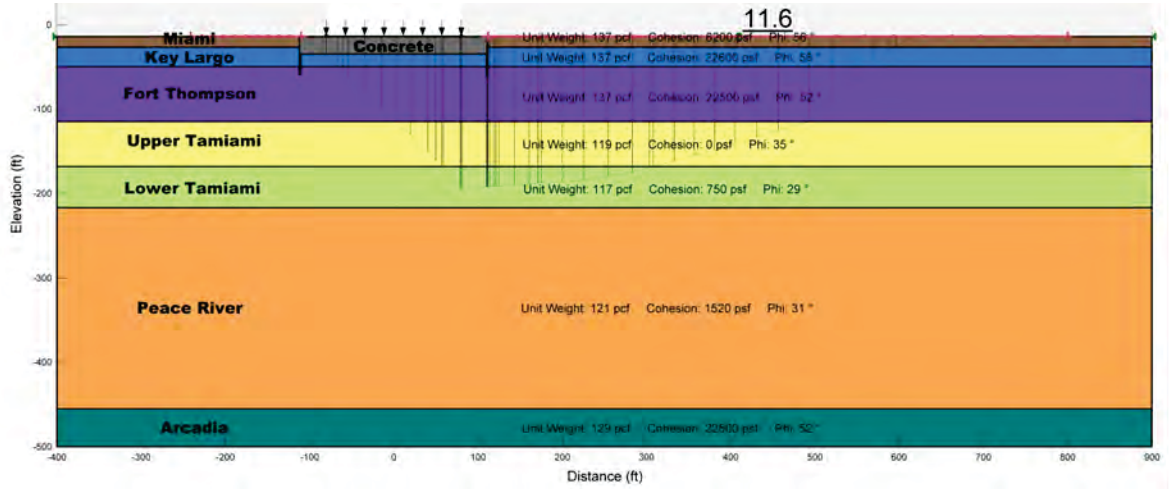

Figure 2.5.4-259
SLOPEW Analysis with Simulated FD4 Zones, 1x Required Bearing Demand

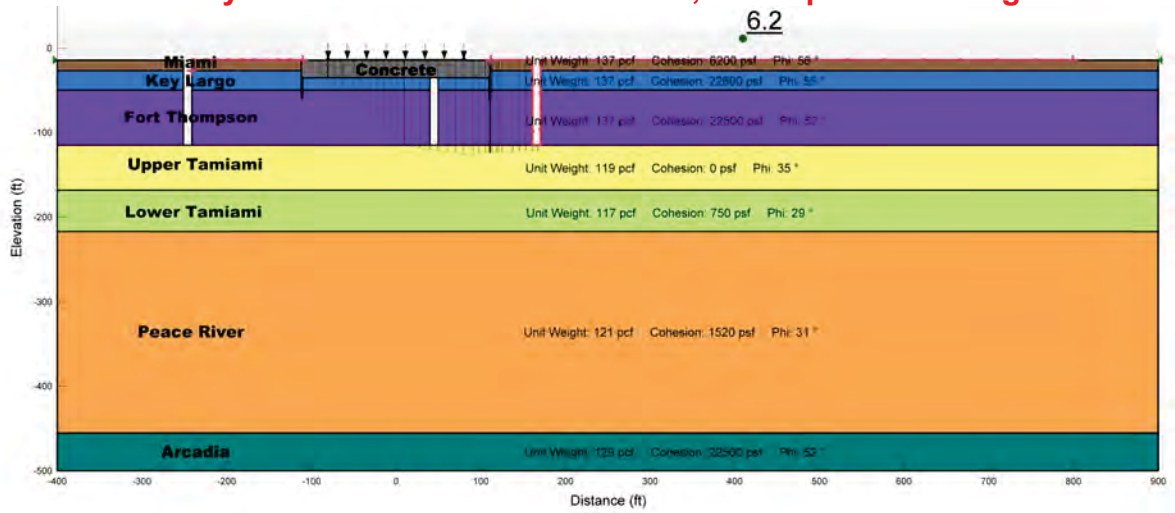

Figure 2.5.4-266
Plastic Deformation from PLAXIS 2D Analysis, 1x Required Bearing Demand

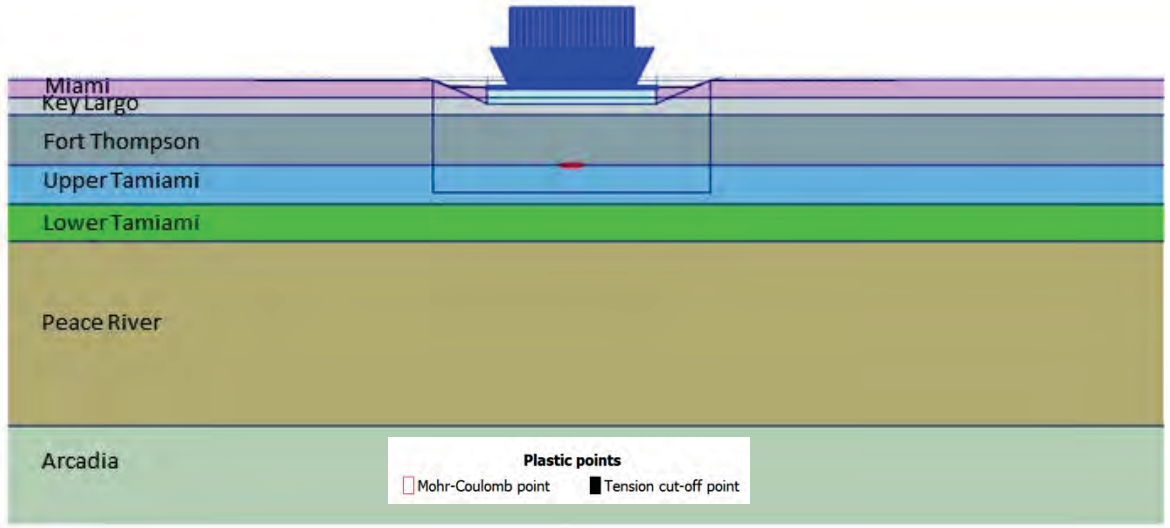

Figure 2.5.4-267
Plastic Deformation from PLAXIS 2D Analysis, 3x Required Bearing Demand

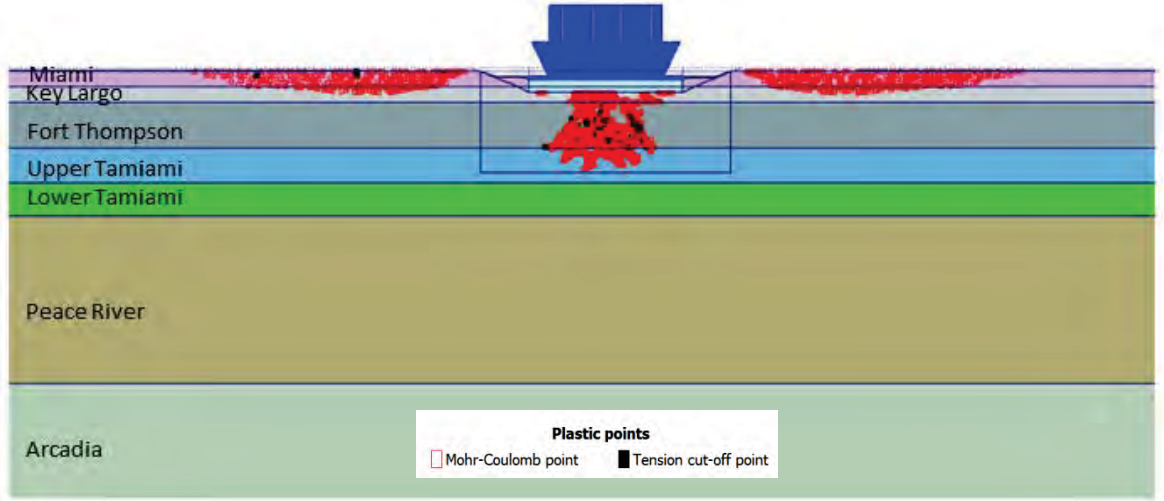

Figure 2.5.4-268
Failure Surface from PLAXIS 2D Analysis, 60.8x Required Bearing Demand

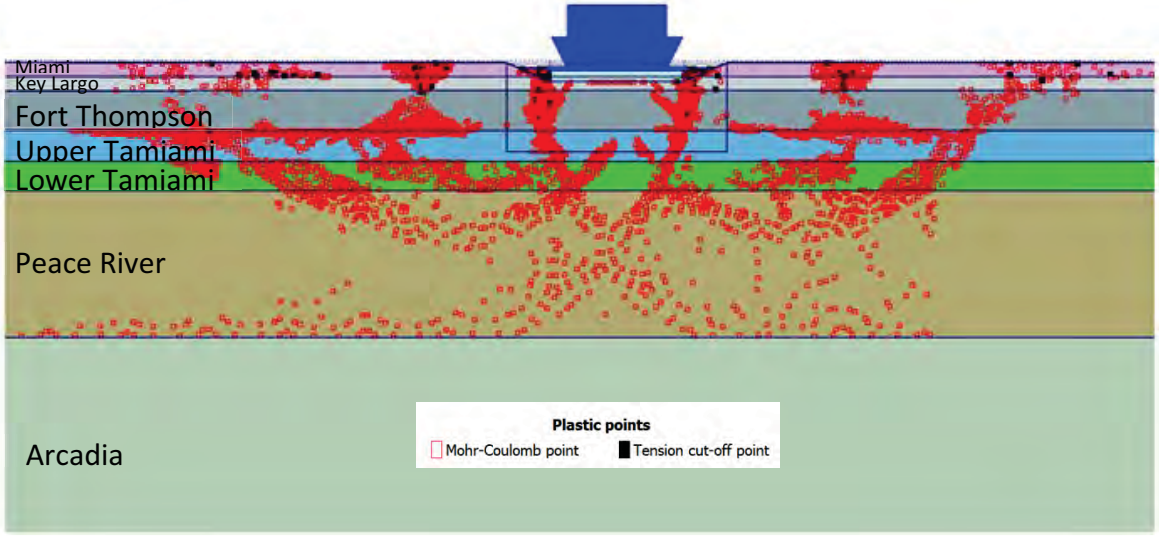

ASSOCIATED ENCLOSURES:

None

NRC RAI Letter No. PTN-RAI-LTR-040

SRP Section: 02.05.04 - Stability of Subsurface Materials and Foundations

QUESTIONS from Geosciences and Geotechnical Engineering Branch 1 (RGS1)

NRC RAI Number: 02.05.04-19 (eRAI 6006)

AP 1000 DCD, Revision 17, Table 2.5-1 provides the total- and differential- settlement limits. The table states that the total settlement limit for the nuclear island foundation mat is 3 inches and the differential settlement limit across the nuclear island foundation mat is 0.5 inch in 50 ft. Rev.18 revised Table 2.5-1, to state that the total settlement for the nuclear island foundation mat is limited to 6 inches; however, the differential settlement limit across the nuclear island foundation mat remained 0.5 inch in 50 ft . In accordance with NUREG-0800, Standard Review Plan, Chapter 2.5.4, "Stability of Subsurface Materials and Foundations,":

a. Please update the settlement calculations based on the DCD Rev.18 applied contact pressure for Reactor Building of 8.9 ksf instead of the 8.6 ksf stated in FSAR Rev. 2.
b. Provide additional information describing the differential settlement calculations across the nuclear island foundation mat since values appears to exceed the acceptable limits in DCD Table 2.5-1.
c. Provide a description of the monitoring program that will implemented to ensure that the actual settlements and differential settlements of the structures relative to the nuclear island do not exceed the DCD settlement criteria.
d. Provide additional explanation on why and how a dynamic shear modulus degradation curve was used to compute static unidirectional settlements.

FPL RESPONSE:

The methodology for the settlement analyses of the Turkey Point Units 6 & 7 site has been revised. The settlement analyses now consist of a hand calculation that uses stress distributions appropriate for layered systems as well as a three-dimensional finite element model using PLAXIS 3D Foundation (PLAXIS 3D). Settlement analyses use the revised best estimate material properties. These updated material properties are based on laboratory data from both the initial (FSAR Section 2.5.4 Reference 257) and supplemental (FSAR Section 2.5.4 Reference 290) field investigations.

Part a:

Please update the settlement calculations based on the DCD Rev.18 applied contact pressure for Reactor Building of 8.9 ksf instead of the 8.6 ksf stated in FSAR Rev. 2.

In the revised settlement analysis, the finite element model utilizes specific foundation pressures for the shield (11.8 ksf) and auxiliary buildings (5.1 ksf for north and 7.7 ksf for south), rather than assuming one value for the entire NI. In the finite element settlement model, the areas are slightly smaller than the as-built area of the NI. The loading in the finite element model is equivalent to the average NI foundation pressure of 9.2 ksf (conservative), where the total load is equal to the uniform 8.9 ksf pressure across the NI

for as-built geometry. For consistency, the same average contact pressure of 9.2 ksf is used in the hand calculation so that the results of the two analyses are comparable.

Part b:

Provide additional information describing the differential settlement calculations across the nuclear island foundation mat since values appears to exceed the acceptable limits in DCD Table 2.5-1.

The AP1000 DCD Table 2.5-1 allows for a differential settlement across the NI foundation mat of one-half inch in 50 feet. The revised settlement hand calculation and PLAXIS 3D analyses (described in further detail below) both predict differential settlement of 0.2 inches in 50 feet. The results of the revised settlement calculations are within the acceptable limits without additional evaluation.

Part c:

Provide a description of the monitoring program that will implemented to ensure that the actual settlements and differential settlements of the structures relative to the nuclear island do not exceed the DCD settlement criteria.

A settlement monitoring program is given as one of the alternatives for the additional evaluation of settlement in DCD Section 2.5.4.3. Based on the estimated settlements of the NI, no additional evaluation is anticipated. If additional evaluation is deemed necessary, and if the settlement monitoring alternative is selected, then the program will follow the guidelines provided in the DCD regarding settlement monuments (i.e., “settlement monuments placed directly on concrete, preferably on the mudmat for early construction monitoring and on the corners of structures at grade once the mudmat monuments have been covered by backfill to be used for long-term monitoring. Monuments at grade are to be accessible with conventional surveying equipment”). The DCD also notes that there should be piezometers to measure pore pressures in a soil layer prone to consolidation type settlement. Since the soils at the Turkey Point site are not prone to consolidation type settlement, piezometers will not be used.

Part d:

Provide additional explanation on why and how a dynamic shear modulus degradation curve was used to compute static unidirectional settlements.

The dynamic shear modulus degradation curve is no longer used to compute static unidirectional settlements. A description of the revised settlement methodology and results is provided below.

Methodology of Revised Settlement Analyses:

Hand Calculation

The settlement calculation has been revised to use stress distributions appropriate for layered systems, instead of the Boussinesq distribution. For the NI, the stress distribution from Milovic (Reference 2) for a two-layered system is used. For the remaining buildings (turbine, first bay, annex, and radwaste), a stress distribution from Poulos and Davis

(Reference 3) for a three-layered system is used. The revised response to RAI 02.05.04-20 provides further information regarding the stress distributions used for the hand calculation and a comparison to the stress distributions obtained from PLAXIS 3D.

Two cases are considered in the settlement hand calculation. The first is a best estimate case using the design stiffness for each layer. The second case acts as a sensitivity analysis by using the lower bound stiffness for two layers (the upper Tamiami and Peace River). The lower bound stiffness is defined as the 16th percentile, indicating a 16 percent probability of that or a lower stiffness occurring. Therefore, the probability of having two layers with lower bound stiffness is approximately 2.5 percent. The upper Tamiami and Peace River layers are chosen for the lower bound case because they are the layers that impact settlement the most.

In the hand calculation, vertical incremental strains are calculated assuming linear elastic properties. The resulting settlement is obtained by integrating the vertical incremental strains over the soil/rock column using Equations 1 through 5 from Bowles (Reference 4).

$$\Delta\sigma_z = P I_z \qquad \text{Equation 1}$$

Where,

σ_z= the vertical stress,
P= the building pressure,
and I_z = the percentage of building pressure at depth z

$$\Delta\sigma_h = \Delta\sigma_z * K_0 \qquad \text{Equation 2}$$

Where,

σ_h= the horizontal stress,
and K_0= the at rest earth pressure coefficient

$$K_0 = 1 - \mathrm{Sin}(\varphi) \qquad \text{Equation 3}$$

Where,

φ= the friction angle

$$\Delta\varepsilon = \frac{1}{E}\left(\Delta\sigma_z - 2v'\Delta\sigma_h\right) \qquad \text{Equation 4}$$

Where,

Δε= the vertical strain,
E= the Young's modulus,
and v'= Poisson's ratio

$\Delta S = \Delta\varepsilon^* \Delta z$ Equation 5

Where,

ΔS= the settlement,
and Δz= the thickness

Heave is considered for the excavation below the NI. Dewatering will occur prior to the construction process to an elevation of -38 feet under the NI. Up to the construction of the lean concrete layer, pumping rates are assumed to create conditions of zero pressure in the bottom of the foundation (no buoyancy). Conservatively, these conditions are assumed during loading, i.e., the buoyancy forces acting to reduce settlement are neglected. The effects of buoyancy are calculated and reported separately.

Lastly, consolidation settlement is also considered using Equation 6 (Reference 4) for the lower Tamiami and Peace River layers. Consolidation settlement is found to be negligible, as expected, because the soil types at the site (upper Tamiami, lower Tamiami, and Peace River) are silty sands and are therefore not considered to be prone to consolidation type settlement. Any secondary consolidation (creep) would be even smaller than consolidation settlement, and is therefore not considered in this analysis.

$$\Delta\varepsilon = \frac{C_r}{1+e_0} * \log \frac{\sigma'_v + \Delta\sigma_z}{\sigma'_v}$$ Equation 6

Where,

$\Delta\varepsilon$= the strain,
C_r = the recompression index,
e_0= the void ratio,
σ'_v= the in-situ effective stress,
and $\Delta\sigma_z$= the vertical stress

PLAXIS 3D

In addition to the settlement hand calculation, settlement is determined using PLAXIS 3D, a Finite Element Method (FEM)-based computer code designed for geotechnical analyses. The program calculates displacements with the use of numerical integration methods. In addition to the typical capabilities of a general FEM application for elastic solids, PLAXIS 3D incorporates advanced constitutive models (stress vs. strain relationship) that are capable of simulating the response of soils to external loading.

The PLAXIS 3D model includes the following phases:

1. Initial Conditions: Initial effective stresses for the soil column are obtained. The structural fill from El. -5 feet to El. 25.5 feet is already in place in this phase.
2. Dewatering: The water level, initially assumed to be at the ground surface (El. –1 feet) is lowered to El. –38 feet in the footprint of the NI. The vertical effective stresses across the depth of the soil column increase due to dewatering, causing incremental settlement.

3. Excavation and Lean Concrete Placement: Upon dewatering down to El. –38 feet, the material between El. 25.5 feet and El. –35 feet is removed in the footprint of the NI and a lean concrete backfill is installed from El. –35 feet up to El. –14 feet. In the PLAXIS 3D model, the net effect of the removal of soil/rock and the addition of the lean concrete is an incremental heave due to the drop in effective stresses across the depth. In the excavation phase, the area of the Turbine Building that is founded on El. 8.25 feet is also excavated.
4. Construction of power block structures (excluding the NI): Loads on the footprints of the turbine, first bay, radwaste, annex, and diesel generator buildings and water tanks are applied. Effective stresses increase causing incremental settlement in this stage.
5. Construction of the NI: Loads are applied on the footprint of the NI. Effective stresses increase causing incremental settlement in this stage. It is important to note that the loads on the footprint of the NI are applied while the pore pressure is assumed to be zero at the bottom of the foundation.
6. Rewatering: The water table is redefined in the PLAXIS model to be back at El.–1 foot for the NI footprint, which has the effect of generating the hydrostatic pressures acting on the bottom of the NI foundation from the stage where pumping for dewatering purposes ceased. The net effect of buoyant forces is to reduce settlements as calculated in the previous phase. However, for conservative purposes, this effect is neglected.

The actual construction sequence may involve simultaneous dewatering and excavation as well as simultaneous building construction and rewatering. The phases modeled in PLAXIS allow for determining settlements/heaves associated with each activity. Furthermore, initial conditions in the model include the backfill in place up to El. 25.5 feet. The excavation prediction, thus, includes slightly more material removal (larger heave number reported).

Nuclear Regulatory Commission RG 1.132 Appendix D states that, “Where soils are very thick, the maximum required depth for engineering purposes, denoted d_{max}, may be taken as the depth at which the change in the vertical stress during or after construction for the combined foundation loadings is less than 10% of the effective in situ overburden stress.” The analysis depth of El.–450 feet, which is greater than 2B (B = the least dimension of the foundation), was assumed to be adequate to meet the aforementioned criterion. In situ initial overburden effective vertical stress at the bottom of the model is 31,303 pounds per square foot (psf). The vertical effective stress at the bottom of the model becomes: 32,299 psf at the end of excavation, 32,694 psf at the end of loading other buildings, 33,262 psf at the end of loading the NI, and 31,781 psf at the end of rewatering. The changes in effective vertical stresses are less than 10 percent of the effective in situ stress for each phase, demonstrating that the model depth is appropriate.

The plan dimensions considered in the model are 1724 feet by 1396 feet. The total displacement at the corner of the model is less than 0.1 inches, confirming that the horizontal extent of the model is appropriate.

The foundations are considered as plate elements with a thickness corresponding to the basemat thickness. The plate elements have no self weight, as the building is assumed to be inclusive of the foundation weight.

The analysis uses 15-node wedge elements. Total number of elements is 70,152 for the design mesh. The boundary conditions for the sides of the model are set to allow for the vertical displacement, and restrain the two horizontal displacement components in the x- and z- directions. The bottom of the model is restrained in the vertical and horizontal directions.

The four following sensitivity analyses are included in the PLAXIS 3D calculation:

1. Mesh Sensitivity:

   Four models with the following numbers of elements are considered: Very Coarse – 11,514, Moderately Coarse – 25,650, Design – 70,152 and Finest – 115,810. The change in mesh density for these models is focused on the loaded areas. Both vertical and horizontal meshes are varied. These models have the best estimate material properties (slightly fractured [FD1], for rock). Figure 1 shows the design mesh.

Figure 1. PLAXIS 3D Design Mesh

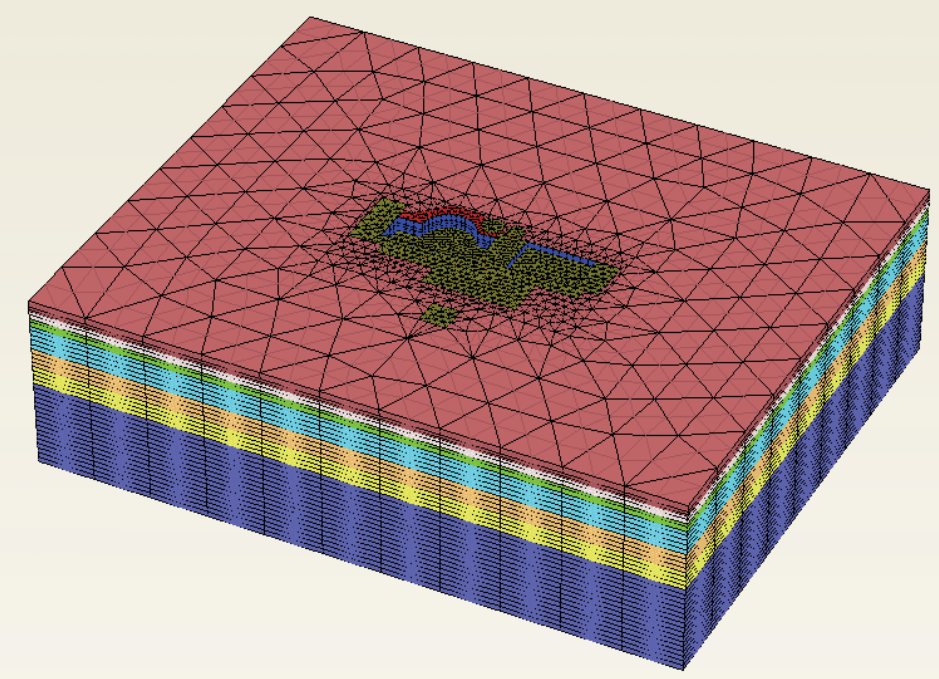

2. Fracture Density:

Two main fracture zones are identified: slightly fractured (FD1) and moderately fractured (FD4). The zone of moderately fractured rock is significantly smaller than the zone of slightly fractured rocks as shown in Figure 2. The stiffness of the FD4 zone is less than the FD1 zone. However, the effect of including FD4 zone in the 3D settlement model is anticipated to be negligible, since the settlement is governed by the lower stiffness of the soil layers. An additional sensitivity run is conducted to check this assumption. FD4 zones are incorporated into the model, assuming FD4 zones for Unit 6, since an FD4 zone extends below the Unit 6 NI, and the fracture density is higher for Unit 6 than for Unit 7 (Figure 2). Best estimate material properties are used for soil, and FD1 properties are used for the remaining rock.

Figure 2 Estimated Location of Moderately Fractured (FD4) Zones

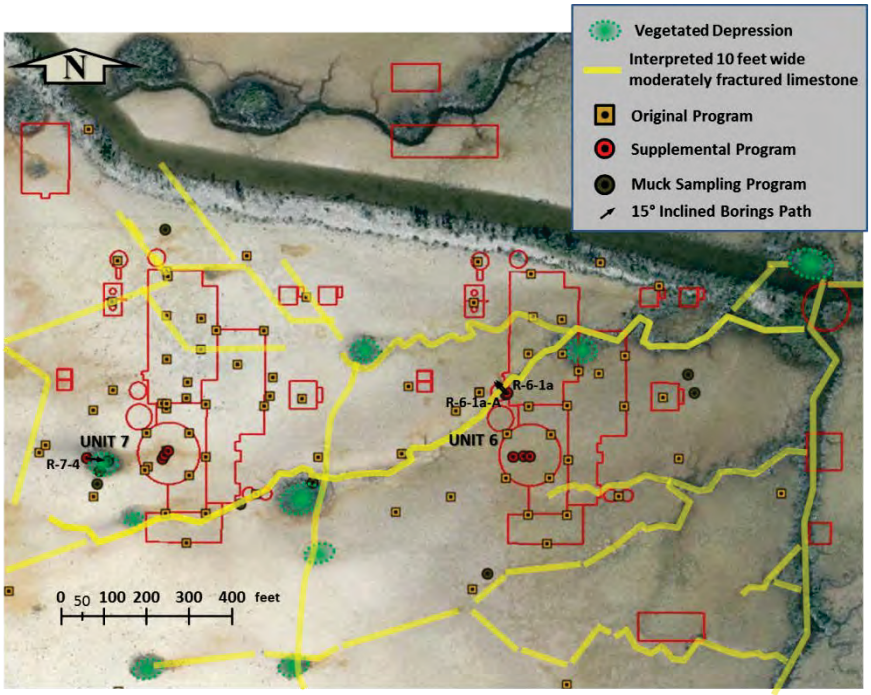

Google earth image 1/30/2005 U.S. Geological Survey

Note: Locations not marked as moderately fractured (FD4) are considered to be slightly fractured (FD1)

3. Soil Constitutive Behavior

Soil layers are modeled using an elasto-plastic Mohr-Coulomb model, since the strain levels are expected to be low and within the relatively elastic range. The use of a Mohr-Coulomb model also dictates the use of the constant stiffness throughout soil layers. This assumption is justified based on the insensitivity that the shear wave velocity shows against depth for the soil layers, particularly for the upper and lower Tamiami formations. To check this assumption, a more comprehensive Hardening Soil model is adopted for the soil layers.

The hardening soil model is a hyperbolic model developed based on the theory of plasticity. The hardening soil model accounts for the stress-dependency of the soil stiffness by increasing stiffness with increasing pressure. When the soil experiences reloading, such as foundation loading after excavation, the hardening soil model will account for the previous stress history. This is because the reloading stiffness is typically about three to five times higher than the loading stiffness. Unlike the loading portion of the stress-strain curve, the reloading portion of the stress-strain curve is linear. The reloading stiffness is used during the reloading until the stresses induced by the applied load exceed the stresses that the soil has previously experienced; at that point, PLAXIS 3D automatically switches to using the reloading portion of the hyperbolic curve.

To determine the material properties to use in the Hardening Soil model (triaxial stiffness E_{50}, triaxial unloading stiffness E_{ur}, and the oedometer loading stiffness E_{oed}), a calibration was done varying the material parameters, while keeping the E_u/E_i ratio constant, until the stress-strain plot from PLAXIS 3D matches the stress-strain plots from the triaxial testing results. Figures 3 through 5 shows the plots of the hardening soil calibration, where all the triaxial test results from each layer are shown, along with the soil hardening based PLAXIS 3D curves at the mid-depth, top, and bottom of each layer. In addition, Figures 3 through 5 show the Mohr-Coulomb stress-strain curves obtained from PLAXIS 3D best estimate model.

Figure 3 Plot of Soil Hardening Calibration for the Upper Tamiami

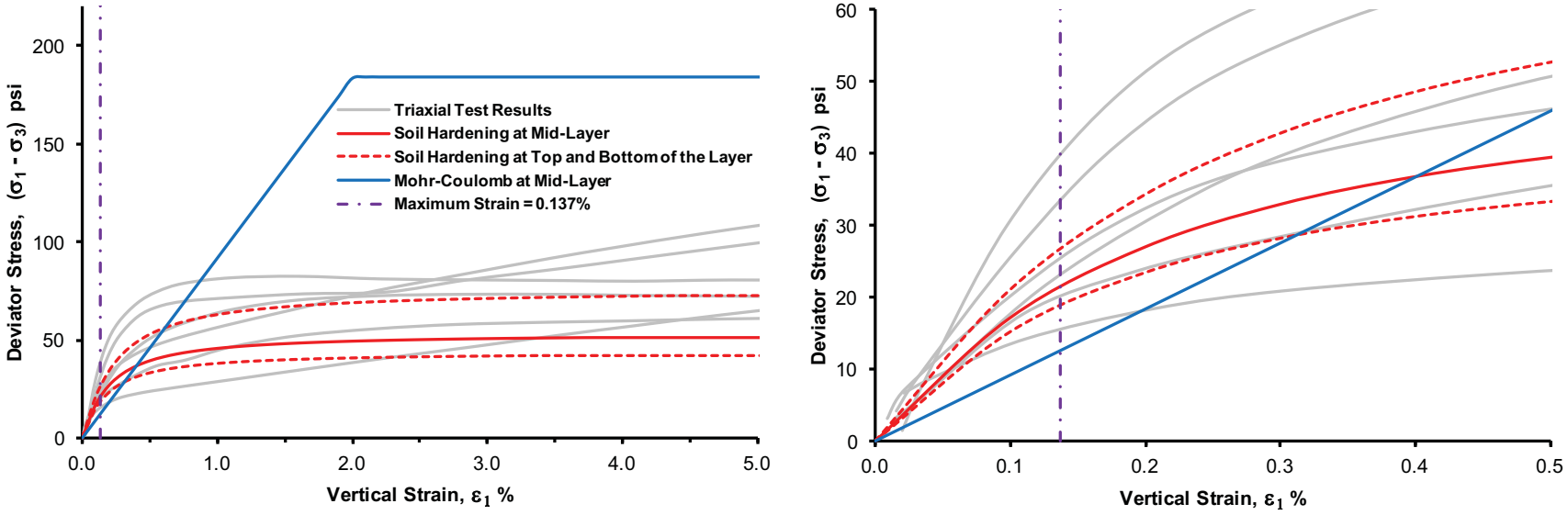

Figure 4 Plot of Soil Hardening Calibration for the Lower Tamiami

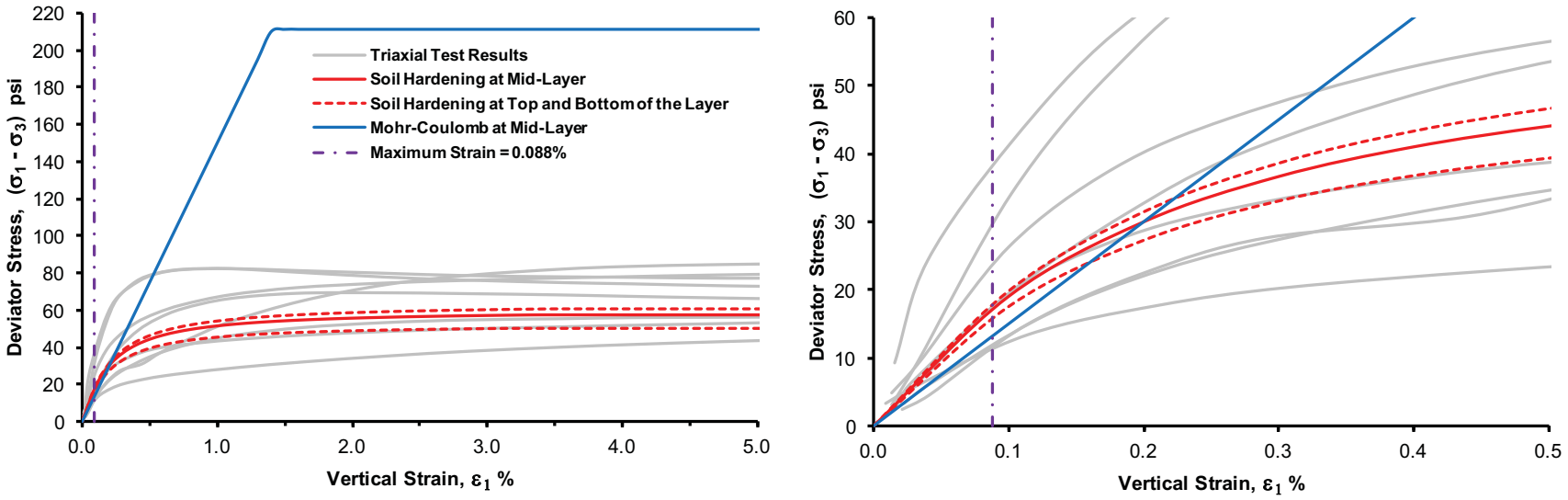

Figure 5 Plot of Soil Hardening Calibration for the Peace River

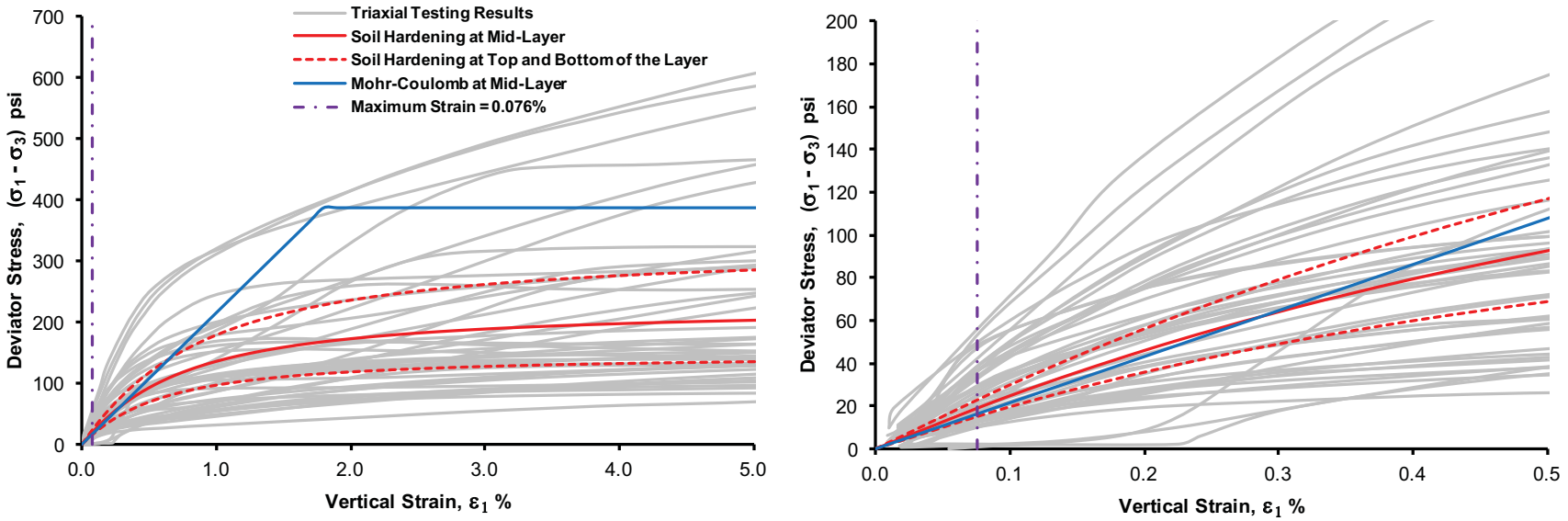

4. Lower Bound

For the lower bound model, soil layers (upper Tamiami, lower Tamiami, and Peace River) are given lower bound stiffness values, defined as the 16th percentile, indicating a 16 percent probability of that or a lower stiffness occurring. The details of how to obtain lower bound soil parameters are provided in the revised response to RAI 02.05.04-09. The rock layers are given FD1 stiffness values.

Results of the Revised Settlement Analyses:

The following PLAXIS 3D results do not include the excavation and dewatering phases because the basemat is expected to be placed and leveled before the structural loads are applied, and excess pore pressures generated prior to basemat placement are considered to be dissipated. Therefore, monitored settlements on the basemat will not reflect the effects of dewatering and excavation. In the PLAXIS 3D model, the average heave of the NI due to excavation is estimated to be 0.5 inches.

Table 1 shows the results of the mesh sensitivity analysis. Maximum settlement predicted for the NI varies from the design mesh by 0.10 percent, 0.05 percent, and 0.14 percent for the coarse, moderately coarse, and finest meshes, respectfully. Based on these results, the design mesh is confirmed to be appropriate for the settlement analysis.

Table 1

Comparison of Mesh Sensitivity Results in the Loading Phases

Maximum Settlement (in)		Nuclear Island	Turbine Building Interior	Turbine Building Exterior	Annex Building	First Bay Building	Radwaste Building	Ancillary Water Tank	Condensate Water Tank	Diesel Generator
Load Other Buildings	Design	----	2.03	2.05	2.04	1.92	1.02	1.86	1.89	0.86
	Coarse	----	2.02	2.04	2.04	1.93	0.99	1.92	1.92	0.84
	Moderately Coarse	----	2.03	2.05	2.04	1.93	1.01	1.88	1.90	0.84
	Finest		2.04	2.05	2.04	1.92	1.02	1.84	1.88	0.86
Load NI[(1)]	Design	2.52	2.89	3.02	2.99	2.99	2.15	3.09	2.93	1.35
	Coarse	2.52	2.89	3.00	3.00	2.97	2.12	3.16	2.95	1.33
	Moderately Coarse	2.52	2.89	3.01	2.99	3.00	2.16	3.12	2.94	1.33
	Finest	2.52	2.90	3.01	2.98	2.98	2.15	3.07	2.92	1.35

(1) The loading NI phase is inclusive of the previous phase.

Table 2 shows the results of the fracture density, hardening soil, and lower bound sensitivity analyses for the PLAXIS 3D models. Maximum settlement predicted for the NI varies by 1.4 percent between the model without fractures and the model with FD4 fractures. This confirms that the effect of including FD4 zone in the 3D settlement model is negligible, since the settlement is governed by the lower stiffness of the soil layers. Maximum settlement predicted for the NI varies by 1.6 percent based on the type of model (Mohr-Coulomb or hardening soil), confirming that the Mohr-Coulomb best estimate model is appropriate. The maximum settlement predicted for the NI varies by 29.9 percent between the lower bound and best estimate cases, again confirming that the settlement is governed by the lower stiffness of the soil layers.

Table 2
Fracture Density, Hardening Soil, and Lower Bound Sensitivity Analyses

Maximum Settlement (in)		Nuclear Island	Turbine Building Interior	Turbine Building Exterior	Annex Building	First Bay Building	Radwaste Building	Ancillary Water Tank	Condensate Water Tank	Diesel Generator
Load Other Buildings	Best Estimate	----	2.0	2.0	2.0	1.9	1.0	1.9	1.9	0.9
	Lower Bound	----	2.5	2.5	2.5	2.4	1.3	2.3	2.3	1.2
	Soil Hardening	----	1.9	1.9	1.9	1.8	0.9	1.7	1.7	0.8
	Fractured Zone	----	2.1	2.1	2.1	2.0	1.0	1.9	1.9	0.9
Load NI[(1)]	Best Estimate	2.5	2.9	3.0	3.0	3.0	2.1	3.1	2.9	1.3
	Lower Bound	3.4	3.7	3.9	3.8	3.9	2.9	3.9	3.8	2.0
	Soil Hardening	2.5	3.0	3.1	3.0	3.0	2.1	3.1	3.0	1.5
	Fractured Zone	2.6	3.0	3.1	3.0	3.0	2.2	3.1	3.0	1.4
Rewatering	Best Estimate	2.1	2.6	2.7	2.7	2.7	1.8	2.7	2.6	1.1
	Lower Bound	2.9	3.3	3.4	3.4	3.4	2.4	3.4	3.3	1.6
	Soil Hardening	2.3	2.8	2.9	2.9	2.9	2.0	2.9	2.8	1.4
	Fractured Zone	2.2	2.6	2.7	2.7	2.7	1.8	2.8	2.6	1.1

(1) The loading NI phase is inclusive of the previous phase.

The sensitivity analyses presented in Tables 1 and 2 demonstrate that the best estimate model used is appropriate. Figure 6 shows the PLAXIS 3D total displacement output for the best estimate model after the loading of the NI. Figure 7 shows the PLAXIS 3D total displacement output for the best estimate model after rewatering.

Figure 6 PLAXIS 3D Best Estimate Model Total Settlement After Loading

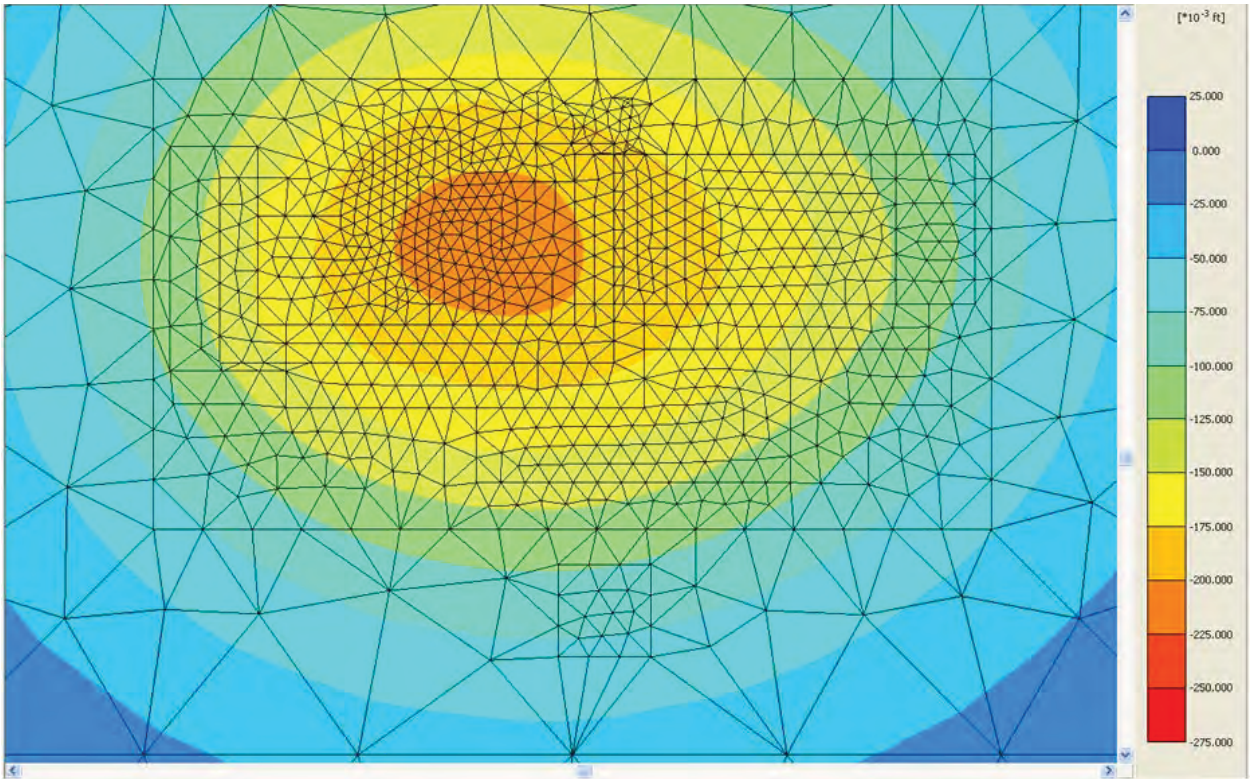

Figure 7 PLAXIS 3D Best Estimate Model Total Settlement After Rewatering

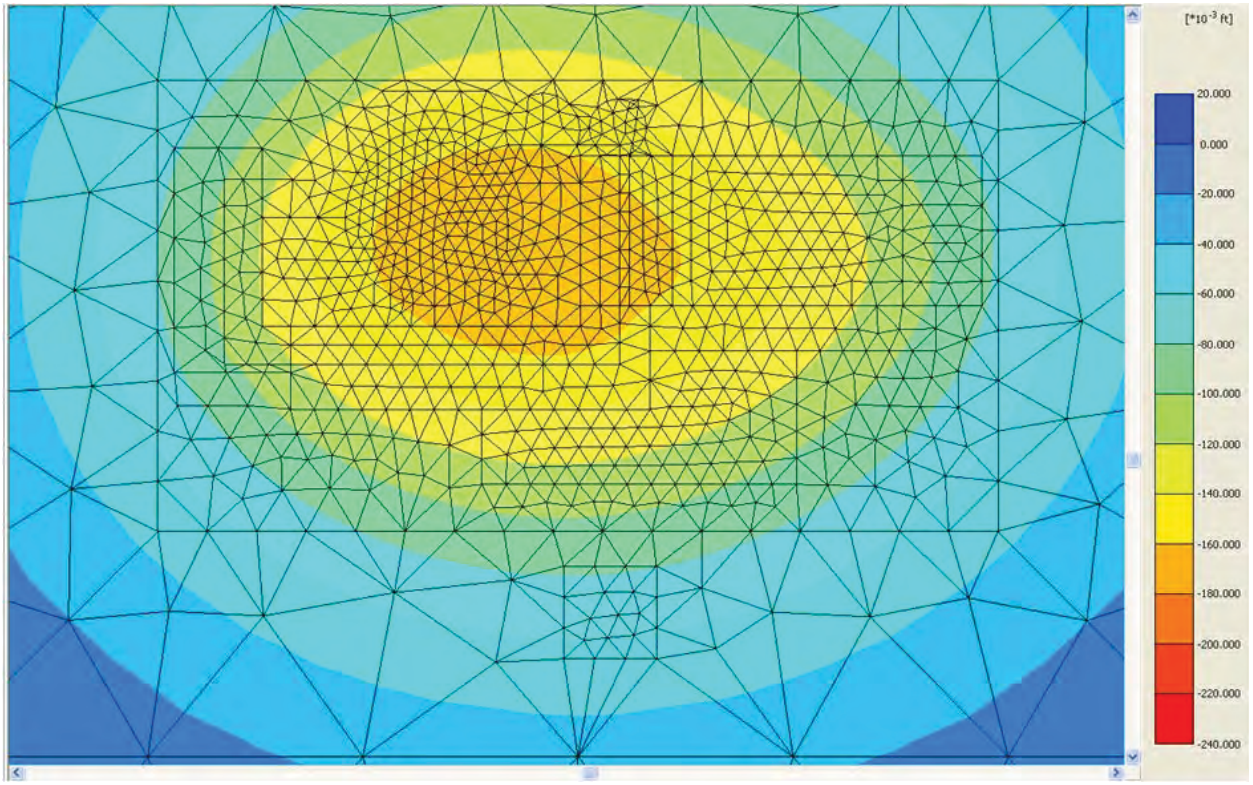

Table 3 shows the comparison between the settlement predicted by the hand calculation and PLAXIS 3D model to the DCD requirements. The lower bound and best estimate cases for the hand calculation and the PLAXIS 3D model are within the acceptable limits provided by the DCD.

Table 3

Comparison of Limits of Acceptable Settlement without Additional Evaluation

		Differential Across Nuclear Island Foundation Mat (in per 50 ft)	Total for Nuclear Island Foundation Mat (in)	Differential Between Nuclear Island and Turbine Building[1] (in)	Differential Between Nuclear Island and Other Buildings[1][2] (in)
DCD Requirement		0.5	6	3	3
Best Estimate	Plaxis 3D	0.20	2.5	0.5	1.6
	Hand Calculation	0.21	2.3	0.5	1.9
Lower Bound	Plaxis 3D	0.23	3.4	0.9	2.2
	Hand Calculation	0.25	3.1	0.8	2.6

(1) Differential settlement is measured at the center of the nuclear island and the center of adjacent structures.
(2) Maximum differential settlement occurs between NI and radwaste buildings.
(3) Settlements presented exclude the rewatering phase

The revised settlement analyses, including the hand calculation and PLAXIS 3D model, show that the predicted best estimate settlement is within the limits provided by the DCD.

This response is PLANT SPECIFIC.

References:

1. Westinghouse Electric Company, AP1000 Design Control Document (DCD), Revision 19, June 21, 2011.
2. Milovic, D., Stresses and Displacements for Shallow Foundations, Elsevier, 1992.
3. Poulos, H. G. and E.H. Davis, Elastic Solutions for Soil and Rock Mechanics, John Wiley & Sons, Inc., 1974.
4. Bowles, J. E., Foundation Analysis and Design, Fifth Edition, McGraw-Hill, Inc., 1997.

ASSOCIATED COLA REVISIONS:

FSAR Subsection 2.5.4.10.3 will be revised in a future revision as follows:

The settlement analyses consist of a hand calculation that uses stress distributions appropriate for layered systems as well as a three-dimensional finite element model using PLAXIS 3D Foundation (PLAXIS 3D). Settlement analyses use the revised best estimate material properties. These updated material properties are based on laboratory data from both the initial (Reference 257) and supplemental (Reference 290) field investigations.

~~Foundation settlements are estimated using pseudo-elastic compression methods. Based on a stress-strain model that computes settlement in discrete layers, the settlement of shallow foundations due to elastic compression of subsurface materials is estimated as:~~

~~$\delta = \Sigma (\Delta p_i h_i)/E_i$ Equation 2.5.4-21~~

~~Where,~~

~~δ= settlement~~
~~i = 1 to n, where n is the number of layers~~
~~Δp_i = vertical applied pressure at the center of layer i~~
~~h_i = thickness of layer i~~
~~E_i = elastic modulus of layer i~~

~~The stress distribution below the corner of a rectangular flexible foundation is based on a Boussinesq-type distribution (Reference 225):~~

~~$\sigma z = (p/2\pi) \{\tan^{-1} [l\ b/(z\ R3)] + (l\ b\ z/R3)(1/R12 + 1/R22)\}$ Equation 2.5.4-22~~

~~Where,~~

~~l = length of the footing~~
~~b = width of footing~~
~~z = depth below footing at which pressure is computed~~
~~R1 = (l2 + z2)0.5~~
~~R2 = (b2 + z2)0.5~~
~~R3 = (l2 + b2 + z2)0.5~~

~~Note that to calculate σz values below the midpoint of an edge and below the center of a rectangular foundation, the values of σz calculated from Equation 2.5.4-22 above are multiplied by two and four, respectively, to obtain p_i , the vertical applied pressure at the center of layer i for use in Equation 2.5.4-21.~~

The containment and auxiliary buildings (nuclear island) share the same mat foundation and are founded on lean concrete placed above rock of the Key Largo Limestone. Therefore, for settlement computations, the bottom of the foundation is taken at El. –14 feet on lean concrete. **The best estimate** ~~S~~**s**ettlement of the rock **and soil** strata is computed using the elastic modulus values tabulated in Table 2.5.4-209. ~~Settlement of the soil strata is evaluated using the strain compatible elastic moduli of the Tamiami and Peace River Formations with corresponding axial strains, as discussed later in this section.~~ The elastic modulus for the lean concrete used for settlement estimates is derived as follows:

The thickest part of lean concrete is between El. –14 feet and El. –35 feet, i.e., 21 feet thick (see Figure 2.5.4-222). The elastic modulus of lean concrete with a unit weight of **150**~~145~~ pcf can be calculated using the following equation (Reference ~~274~~**317**).

~~$E_c = 1820 \cdot f'_c{}^{0.5}$ (ksi) Equation 2.5.4-23~~

$E_c = 57,000\sqrt{f'_c}$ (psi) **Equation 2.5.4-21**

where,

f'c = specified compressive strength of concrete (~~ksi~~**psi**)

The lean concrete placed on rock is expected to have a minimum compressive strength of ~~1.5 ksi.~~**1500 psi.**

~~f'c = 1.5 ksi, then Ec = 1820·1.50.5 = 2229 ksi ≈ 321,000 ksf~~

$f'_c = 1.5\ ksi, then\ E_c = 57,000\sqrt{1500} = 2.21 * 10^6 psi \approx 318,500\ ksf$

~~The settlements under the nuclear island foundation with plan dimensions of 88 feet by 254 feet and 159 feet by 254 feet are calculated with an applied pressure of 8.9 ksf. The estimated total settlements at the center and at midpoints of the sides are largely impacted by the large foundation size and loading, and by the elastic modulus values of the soil strata. The preconsolidated soils of the Tamiami and Peace River Formations are confined below an 80-foot-thick stratum of rock, and thus a relatively low settlement estimate is expected from these dense granular and stiff fine-grained layers. Settlements at the center of the mat foundations are evaluated using the strain-compatible elastic moduli of the Tamiami and Peace River Formations with corresponding axial strains. The strain compatible evaluation is performed only for the soil strata, i.e., the Tamiami and Peace River Formations where there is a difference between the high and low strain moduli. In order to apply the elastic moduli in Equation 2.5.4-21, their values need to be equated with strain level. In this case, the modulus degradation with increasing strain is based on the recommended curves in Figure 2.5.4-233 after converting shear strain to axial strain.~~

~~For calculating settlement of structures using the elastic method, the maximum principal strain is the vertical strain (i.e., $\varepsilon_1 = \varepsilon_v$), while the minimum principal strain is assumed to be zero (i.e., $\varepsilon_3 = 0$). Because the maximum shear strain $\gamma_{max} = \varepsilon_1 - \varepsilon_3 = \varepsilon_1$ (Reference 275) and $E/E_{max} = G/G_{max}$, the elastic modulus reduction curves with respect to vertical strain should be the same as the shear modulus reduction curves with respect to the shear strain. Therefore, the strain levels in degradation curves (Figure 2.5.4-233) are interchangeable between the shear strain and axial strain without any need of correction. Thus, the same degradation curve in Figure 2.5.4-233 with G/G_{max} on the vertical axis and percent shear strain on the horizontal axis can be used to determine appropriate values of E for settlement calculations. The ratio of E/E_{max} is equivalent to G/G_{max} and the computed percent axial strain corresponds to the percent shear strain using Figure 2.5.4-233.~~

~~A trial process is followed for soil Strata 5, 6, and 7 using the degradation curves to arrive at a compatible axial strain, such that the strain for the adopted modulus and the calculated strain converge. For rock and concrete strata, the settlements computed are based on a constant (not strain dependent) elastic modulus. The results of the settlement analysis on Table 2.5.4-219 show the computed settlements at the center and edge of the nuclear island foundations with dimensions of 88 feet by 254 feet and 159 feet by 254 feet, under loading of 8.9 ksf. (Two sets of plan dimensions are used because of the irregular shape of the foundation.) Similar settlement calculations are made for the turbine, annex and radwaste buildings, and the results are presented in Table 2.5.4-219. As with the nuclear~~

~~island, settlements of the annex building are analyzed for two sets of foundation dimensions.~~

~~As noted earlier, Equation 2.5.4-22 computes the stress distribution beneath a flexible foundation, which accounts for the sometimes significant difference in computed settlement between the center of the foundation and the mid-point of the side of the foundation. In fact, the foundations of the structures listed in Table 2.5.4-219 are thick, reinforced concrete mats with appreciable structural stiffness. Thus the mean settlements listed in Table 2.5.4-219 more closely reflect the actual anticipated settlements across the whole foundation. Table 2.0-201 lists the DCD limits of acceptable settlement without need for additional evaluation. Limits for the nuclear island are 6 inches total settlement and a differential settlement across the nuclear island foundation mat of one-half inch in 50 feet. The Table 2.5.4-219 values are within the limits for total settlement. The values for differential settlement are within the limits for Case I and outside the limits for Case II. However, as noted above, the Table 2.5.4-219 values assume a flexible foundation, and the actual differential settlement across the thick, reinforced mat foundation is negligible. Table 2.0-201 also lists limits of differential settlement between the nuclear island and surrounding structures as 3 inches. The difference between the estimated settlement of the nuclear island and the settlement of the surrounding structures in Table 2.5.4-219, i.e., the differential settlement, is within the limits. As noted below, because of the nature of the soils and rock underlying the new units, post construction settlement will be negligible.~~

~~Because the construction of each unit is over a period of greater than five years, the elastic settlement estimated in Table 2.5.4-219 is essentially complete prior to the start of operation of the unit. No time-dependent consolidation settlement is anticipated. Any additional settlement after completion is considered not significant.~~

FSAR Subsection 2.5.4.10.3.1 will be added in a future revision as follows:

2.5.4.10.3.1 Hand Calculation of Settlement

In the hand calculation, vertical incremental strains are calculated assuming linear elastic properties. The resulting settlement is obtained by integrating the vertical incremental strains over the soil/rock column using Equations 2.5.4-22a through 2.5.4-22e (Reference 217).

Two cases are considered in the settlement hand calculation. The first is a best estimate case using the design stiffness for each layer. The second case acts as a sensitivity analysis by using the lower bound stiffness for two layers (the upper Tamiami and Peace River). The lower bound stiffness is defined as the 16th percentile, indicating a 16 percent probability of that or a lower stiffness occurring. Therefore, the probability of having two layers with lower bound stiffness is approximately 2.5 percent. The upper Tamiami and Peace River layers are chosen for the lower bound case because they are the layers that impact settlement the most. Average lower bound properties are given in Table 2.5.4-221.

The Key Largo Limestone and the Fort Thompson Formation form a stiff upper layer, while the layers below (upper Tamiami, lower Tamiami, and Peace River) are comprised primarily of dense, silty sands. Because of this layering, a typical

Boussinesq stress distribution may not provide realistic stress distributions, showing very high settlement in the deep sand layers. Therefore, stress distributions appropriate for layered systems are used.

For the NI, a stress distribution from Milovic (Reference 316) for a two-layered system was used with rock (Key Largo and Fort Thompson) as the first layer and soil (upper Tamiami, lower Tamiami, and Peace River) as the second layer. For the remaining buildings (turbine, first bay, annex, and radwaste), a stress distribution from Poulos and Davis (Reference 275) for a three-layered system was used with the fill as the first layer; rock (Miami Limestone, Key Largo, and Fort Thompson) as the second layer; and soil (upper Tamiami, lower Tamiami, and Peace River) as the third layer. In each case, the stress distribution is dependent on the stiffness and thickness of each layer, the area of the building, and the depth of interest. The stress distributions assume a circular foundation. Based on the layering information, Iz coefficients, defined as the percentage of the building pressure, are found.

$$\Delta\sigma_z = PI_z \qquad \text{Equation 2.5.4-22a}$$

Where,

σ_z= the vertical stress,
P= the building pressure,
and I_z = the percentage of building pressure at depth z

$$\Delta\sigma_h = \Delta\sigma_z * K_0 \qquad \text{Equation 2.5.4-22b}$$

Where,

σ_h= the horizontal stress,
and K_0= the at rest earth pressure coefficient

$$K_0 = 1 - \sin(\varphi) \qquad \text{Equation 2.5.4-22c}$$

Where,

φ= the friction angle

$$\Delta\varepsilon = \frac{1}{E}\left(\Delta\sigma_z - 2\nu'\Delta\sigma_h\right) \qquad \text{Equation 2.5.4-22d}$$

Where,

Δε= the vertical strain,
E= the Young's modulus,
and v'= Poisson's ratio

$$\Delta S = \Delta\varepsilon * \Delta z \qquad \text{Equation 2.5.4-22e}$$

Where,

ΔS= the settlement,
and Δz= the thickness

Heave is considered for the excavation below the NI. Dewatering will occur prior to the construction process to an elevation of -38 feet under the NI. Up to the construction of the lean concrete layer, pumping rates are assumed to create conditions of zero pressure in the bottom of the foundation (no buoyancy). Conservatively, these conditions are assumed during loading, i.e., the buoyancy forces acting to reduce settlement are neglected. The effects of buoyancy are calculated and reported separately.

Lastly, consolidation settlement is also considered using Equation 2.5.4-23 (Reference 217) for the lower Tamiami and Peace River layers. Consolidation settlement is found to be negligible, as expected, because the soil types at the site (upper Tamiami, lower Tamiami, and Peace River) are silty sands and are therefore not considered to be prone to consolidation type settlement. Any secondary consolidation (creep) would be even smaller than consolidation settlement, and is therefore not considered in this analysis.

$$\Delta\varepsilon = \frac{C_r}{1+e_0} * \log \frac{\sigma'_v + \Delta\sigma_z}{\sigma'_v}$$ **Equation 2.5.4-23**

Where,

$\Delta\varepsilon$= the strain,
C_r = the recompression index,
e_0= the void ratio,
σ'_v= the in-situ effective stress,
and $\Delta\sigma_z$= the vertical stress

FSAR Subsection 2.5.4.10.3.2 will be added in a future revision as follows:

2.5.4.10.3.2 PLAXIS 3D Settlement Model

In addition to the settlement hand calculation, settlement is determined using PLAXIS 3D, a Finite Element Method (FEM)-based computer code designed for geotechnical analyses. The program calculates displacements with the use of numerical integration methods. In addition to the typical capabilities of a general FEM application for elastic solids, PLAXIS 3D incorporates advanced constitutive models, (stress vs. strain relationship) that are capable of simulating the response of soils to external loading.

The PLAXIS 3D model includes the following phases:

1. **Initial conditions: Initial effective stresses for the soil column are obtained. The structural fill from El. –5 feet to El. 25.5 feet is already in place in this phase.**
2. **Dewatering: The water level, initially assumed to be at the ground surface (El. –1 feet) is lowered to El. –38 feet in the footprint of the NI. The vertical effective stresses across the depth of the soil column increase due to dewatering, causing incremental settlement.**
3. **Excavation and lean concrete placement: Upon dewatering down to El. –38 feet, the material between El. 25.5 feet and El. –35 feet is removed in the footprint of the NI and a lean concrete backfill is installed from El. –35 feet up to El. –14 feet. In the PLAXIS 3D model, the net effect of the removal of soil/rock and the addition of the lean concrete is an incremental heave due to the drop in effective stresses across the depth. In the excavation phase, the area of the Turbine Building that is founded on El. 8.25 feet is also excavated.**
4. **Construction of power block structures (excluding the NI): Loads on the footprints of the turbine, first bay, radwaste, annex, and diesel generator buildings and water tanks are applied. Effective stresses increase causing incremental settlement in this stage.**
5. **Construction of the NI: Loads are applied on the footprint of the NI. Effective stresses increase causing incremental settlement in this stage. It is important to note that the loads on the footprint of the NI are applied while the pore pressure is assumed to be zero at the bottom of the foundation.**
6. **Rewatering: The water table is redefined in the PLAXIS model to be back at El. –1 for the NI footprint, which has the effect of generating the hydrostatic pressures acting on the bottom of the NI foundation from the stage where pumping for dewatering purposes ceased. The net effect of buoyant forces is to reduce settlements as calculated in the previous phase. However, for conservative purposes, this effect is neglected.**

The actual construction sequence may involve simultaneous dewatering and excavation as well as simultaneous building construction and rewatering. The phases modeled in PLAXIS allow for determining settlements/heaves associated with each activity. Furthermore, initial conditions in the model include the backfill in place up to El. 25.5 feet. The excavation prediction, thus, includes slightly more material removal (larger heave number reported).

Nuclear Regulatory Commission RG 1.132 Appendix D states that, "Where soils are very thick, the maximum required depth for engineering purposes, denoted d_{max}, may be taken as the depth at which the change in the vertical stress during or after construction for the combined foundation loadings is less than 10% of the effective in situ overburden stress." The analysis depth of El.–450 feet, which is greater than 2B (B = the least dimension of the foundation), was assumed to be adequate to meet the aforementioned criterion. In situ initial overburden effective vertical stress at the

bottom of the model is 31,303 pounds per square foot (psf). The vertical effective stress at the bottom of the model becomes: 32,299 psf at the end of excavation, 32,694 psf at the end of loading other buildings, 33,262 psf at the end of loading the NI, and 31,781 psf at the end of the rewatering phase. The changes in effective vertical stresses are less than 10 percent of the effective in situ stress for each phase, demonstrating that the model depth is appropriate.

The plan dimensions considered in the model are 1724 feet by 1396 feet. The total displacement at the corner of the model is less than 0.1 inches, confirming that the horizontal extent of the model is appropriate.

The foundations are considered as plate elements with a thickness corresponding to the basemat thickness. The plate elements have no self weight, as the building is assumed to be inclusive of the foundation weight.

The analysis uses 15-node wedge elements. Total number of elements is 70,152 for the design mesh. The boundary conditions for the sides of the model are set to allow for the vertical displacement, and restrain the two horizontal displacement components in the x- and z- directions. The bottom of the model is restrained in the vertical and horizontal directions.

The four following sensitivity analyses are included in the PLAXIS 3D calculation:

1. **Mesh Sensitivity:**

   Four models with the following numbers of elements are considered: very coarse – 11,514, moderately coarse – 25,650, design – 70,152, and finest – 115,810. The change in mesh density for these models is focused on the loaded areas. Both vertical and horizontal meshes are varied. These models have the best estimate material properties (slightly fractured [FD1], for rock). Figure 2.5.4-260 shows the design mesh.

2. **Fracture Density:**

   Two main fracture zones are identified: slightly fractured (FD1) and moderately fractured (FD4). The zone of moderately fractured rock is significantly smaller than the zone of slightly fractured rocks as shown in Figure 2.5.4-254. The stiffness of the FD4 zone is less than the FD1 zone. However, the effect of including FD4 zone in the 3D settlement model is anticipated to be negligible, since the settlement is governed by the lower stiffness of the soil layers. An additional sensitivity run is conducted to check this assumption. FD4 zones are incorporated into the model, assuming FD4 zones for Unit 6, since an FD4 zone extends below the Unit 6 NI, and the fracture density is higher for Unit 6 than for Unit 7 (Figure 2.5.4-254). Best estimate material properties are used for soil, and FD1 properties are used for the remaining rock.

3. Soil Constitutive Behavior:

Soil layers are modeled using an elasto-plastic Mohr-Coulomb model, since the strain levels are expected to be low and within the relatively elastic range. The use of a Mohr-Coulomb model also dictates the use of the constant stiffness throughout soil layers. This assumption is justified based on the insensitivity that the shear wave velocity shows against depth for the soil layers, particularly for the upper and lower Tamiami Formations. To check this assumption, a more comprehensive Hardening Soil model is adopted for the soil layers.

The hardening soil model is a hyperbolic model developed based on the theory of plasticity. The hardening soil model accounts for the stress-dependency of the soil stiffness by increasing stiffness with increasing pressure. When the soil experiences reloading, such as foundation loading after excavation, the hardening soil model will account for the previous stress history. This is because the reloading stiffness is typically about three to five times higher than the loading stiffness. Unlike the loading portion of the stress-strain curve, the reloading portion of the stress-strain curve is linear. The reloading stiffness is used during the reloading until the stresses induced by the applied load exceed the stresses that the soil has previously experienced; at that point, PLAXIS 3D automatically switches to using the reloading portion of the hyperbolic curve.

To determine the material properties to use in the hardening soil model (triaxial stiffness E_{50}, triaxial unloading stiffness E_{ur}, and the oedometer loading stiffness E_{oed}), a calibration was done varying the material parameters, while keeping the E_u/E_i ratio constant, until the stress-strain plot from PLAXIS 3D matches the stress-strain plots from the triaxial testing results. Figures 2.5.4-261 through 2.5.4-263 show the plots of the hardening soil calibration, where all the triaxial test results from each layer are shown, along with the soil hardening based PLAXIS 3D curves at the mid-depth, top, and bottom of each layer. In addition, Figures 2.5.4-261 through 2.5.4-263 show the Mohr-Coulomb stress-strain curves obtained from the PLAXIS 3D best estimate model.

4. Lower Bound:

For the lower bound model, soil layers (upper Tamiami, lower Tamiami, and Peace River) are given lower bound stiffness values, defined as the 16th percentile, indicating a 16 percent probability of that or a lower stiffness occurring. The rock layers are given FD1 stiffness values.

FSAR Subsection 2.5.4.10.3.3 will be added in a future revision as follows:

2.5.4.10.3.3 Settlement Results

Table 2.5.4-219 shows the maximum settlement per building predicted by the hand calculation.

The following PLAXIS 3D results do not include the excavation and dewatering phases because the basemat is expected to be placed and leveled before the structural loads are applied, and excess pore pressures generated prior to basemat placement are considered to be dissipated. Therefore, monitored settlements on the basemat will not reflect the effects of dewatering and excavation. In the PLAXIS 3D model, the average heave of the NI due to excavation is estimated to be 0.5 inches.

Table 2.5.4-222 shows the results of the mesh sensitivity analysis. Maximum settlement predicted for the NI varies from the design mesh by 0.10 percent, 0.05 percent, and 0.14 percent for the coarse, moderately coarse, and finest meshes, respectfully. Based on these results, the design mesh is confirmed to be appropriate for the settlement analysis.

Table 2.5.4-223 shows the results of the fracture density, hardening soil, and lower bound sensitivity analyses for the PLAXIS 3D models. Maximum settlement predicted for the NI varies by 1.4 percent between the model without fractures and the model with FD4 fractures. This confirms that the effect of including FD4 zone in the 3D settlement model is negligible, since the settlement is governed by the lower stiffness of the soil layers. Maximum settlement predicted for the NI varies by 1.6 percent based on the type of model (Mohr-Coulomb or hardening soil), confirming that the Mohr-Coulomb best estimate model is appropriate. The maximum settlement predicted for the NI varies by 29.9 percent between the lower bound and best estimate cases, again confirming that the settlement is governed by the lower stiffness of the soil layers.

Table 2.5.4-224 shows the comparison between the settlement predicted by the hand calculation and the PLAXIS 3D model to the DCD requirements. The lower bound and best estimate cases for the hand calculation and the PLAXIS 3D model are within the acceptable limits provided by the DCD.

The sensitivity analyses presented in Tables 2.5.4-222 and 2.5.4-223 demonstrates that the best estimate model used is appropriate. Figure 2.5.4-264 shows the PLAXIS 3D total displacement output for the best estimate model after the loading of the NI. Figure 2.5.4-265 shows the PLAXIS 3D total displacement output for the best estimate model after rewatering.

FSAR Subsection 2.5.13 in will be revised in a future revision as follows:

~~274. American Association of State Highway and Transportation Officials, *LRFD Bridge Design Specification,* 2d ed., Washington, D.C., 1998.~~

316. Milovic, D., *Stresses and Displacements for Shallow Foundations*, Elsevier, 1992.

317. American Concrete Institute, *Building Code Requirements for Structural Concrete and Commentary*, ACI 318-11, 2011.

FSAR Table 2.5.4-219 will be replaced with the following revised table in a future revision:

Table 2.5.4-219
Estimated Foundation Settlements

Structure	Contact Pressure (ksf)	Subsurface	Area (ft^2)	Hand Calculation Best Estimate Maximum Settlement[2] (inch)
Reactor & Auxiliary	9.2	Lean Concrete Fill on Rock	31,318	2.3
Turbine	4.2	Compacted Fill	41,925	1.8
First Bay	3.7	Compacted Fill	4,740	0.9
Annex[1]	2.4	Compacted Fill	19,888	0.9
Radwaste	1.3	Compacted Fill	13,363	0.4

(1) Excludes annex office building.
(2) Excludes heave due to rewatering.

The following Tables will be added in a future revision:

Table 2.5.4-222

Comparison of Mesh Sensitivity Results in the Loading Phases

Maximum Settlement (inch)		Nuclear Island	Turbine Building Interior	Turbine Building Exterior	Annex Building	First Bay Building	Radwaste Building	Ancillary Water Tank	Condensate Water Tank	Diesel Generator
Load Other Buildings	Design	–	2.03	2.05	2.04	1.92	1.02	1.86	1.89	0.86
	Coarse	–	2.02	2.04	2.04	1.93	0.99	1.92	1.92	0.84
	Moderately Coarse	–	2.03	2.05	2.04	1.93	1.01	1.88	1.90	0.84
	Finest	–	2.04	2.05	2.04	1.92	1.02	1.84	1.88	0.86
Load NI(1)	Design	2.52	2.89	3.02	2.99	2.99	2.15	3.09	2.93	1.35
	Coarse	2.52	2.89	3.00	3.00	2.97	2.12	3.16	2.95	1.33
	Moderately Coarse	2.52	2.89	3.01	2.99	3.00	2.16	3.12	2.94	1.33
	Finest	2.52	2.90	3.01	2.98	2.98	2.15	3.07	2.92	1.35

(1) The loading NI phase is inclusive of the previous phase.

Table 2.5.4-223
Fracture Density, Hardening Soil, and Lower Bound Sensitivity Analyses

Maximum Settlement (inch)		Nuclear Island	Turbine Building Interior	Turbine Building Exterior	Annex Building	First Bay Building	Radwaste Building	Ancillary Water Tank	Condensate Water Tank	Diesel Generator
Load Other Buildings	Best Estimate	–	2.0	2.0	2.0	1.9	1.0	1.9	1.9	0.9
	Lower Bound	–	2.5	2.5	2.5	2.4	1.3	2.3	2.3	1.2
	Soil Hardening	–	1.9	1.9	1.9	1.8	0.9	1.7	1.7	0.8
	Fractured Zone	–	2.1	2.1	2.1	2.0	1.0	1.9	1.9	0.9
Load NI[(1)]	Best Estimate	2.5	2.9	3.0	3.0	3.0	2.1	3.1	2.9	1.3
	Lower Bound	3.4	3.7	3.9	3.8	3.9	2.9	3.9	3.8	2.0
	Soil Hardening	2.5	3.0	3.1	3.0	3.0	2.1	3.1	3.0	1.5
	Fractured Zone	2.6	3.0	3.1	3.0	3.0	2.2	3.1	3.0	1.4
Rewatering	Best Estimate	2.1	2.6	2.7	2.7	2.7	1.8	2.7	2.6	1.1
	Lower Bound	2.9	3.3	3.4	3.4	3.4	2.4	3.4	3.3	1.6
	Soil Hardening	2.3	2.8	2.9	2.9	2.9	2.0	2.9	2.8	1.4
	Fractured Zone	2.2	2.6	2.7	2.7	2.7	1.8	2.8	2.6	1.1

(1) The loading NI phase is inclusive of the previous phase.

Table 2.5.4-224
Comparison of Limits of Acceptable Settlement without Additional Evaluation

		Differential Across Nuclear Island Foundation Mat (inch per 50 feet)	Total for Nuclear Island Foundation Mat (inch)	Differential Between Nuclear Island and Turbine Building[1] (inch)	Differential Between Nuclear Island and Other Buildings[1] [2] (inch)
DCD Requirement		0.5	6	3	3
Best Estimate[3]	PLAXIS 3D	0.20	2.5	0.5	1.6
	Hand Calculation	0.21	2.3	0.5	1.9
Lower Bound[3]	PLAXIS 3D	0.23	3.4	0.9	2.2
	Hand Calculation	0.25	3.1	0.8	2.6

(1) Differential settlement is measured at the center of the NI and the center of adjacent structures.

(2) Maximum differential settlement occurs between NI and radwaste buildings.

(3) Settlements presented exclude the rewatering phase.

The following figures will be added in a future revision:

Figure 2.5.4-260 PLAXIS 3D Design Mesh

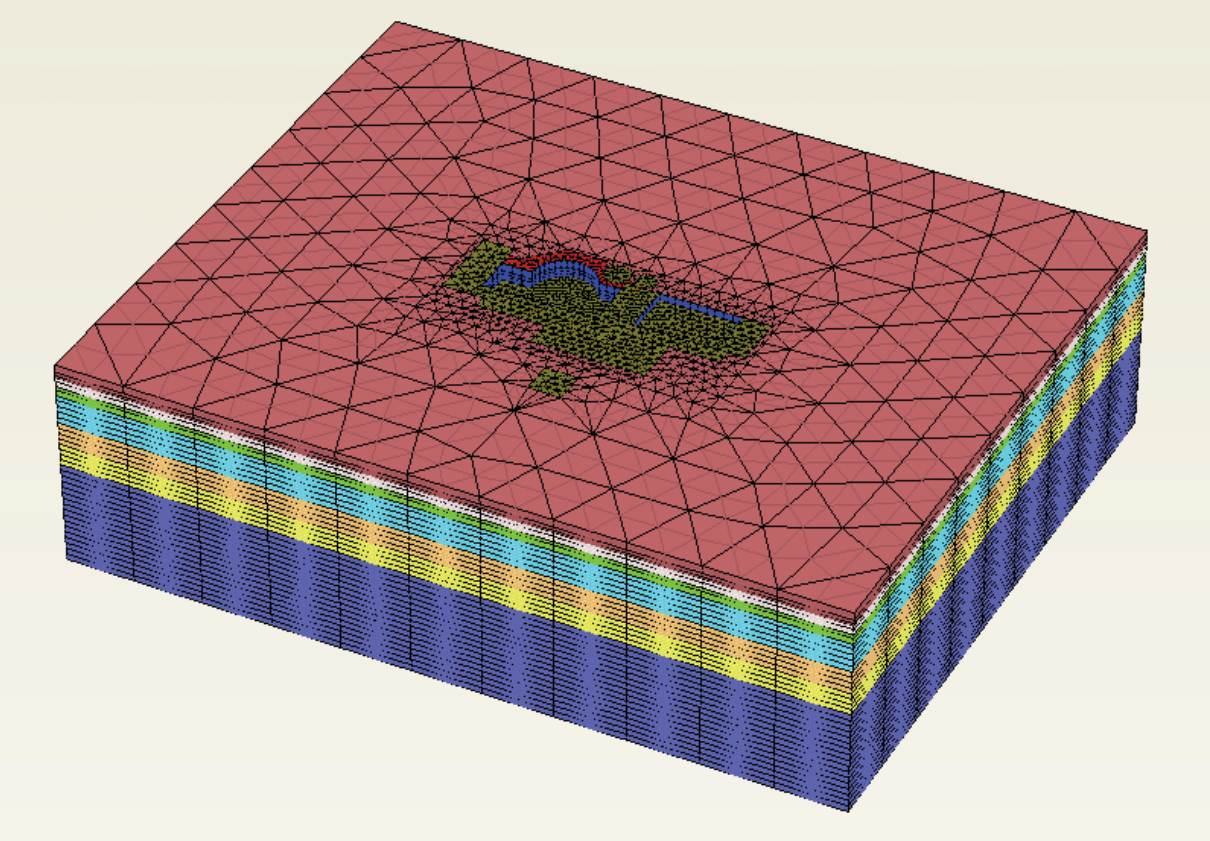

Figure 2.5.4-261 Plot of Soil Hardening Calibration for the Upper Tamiami

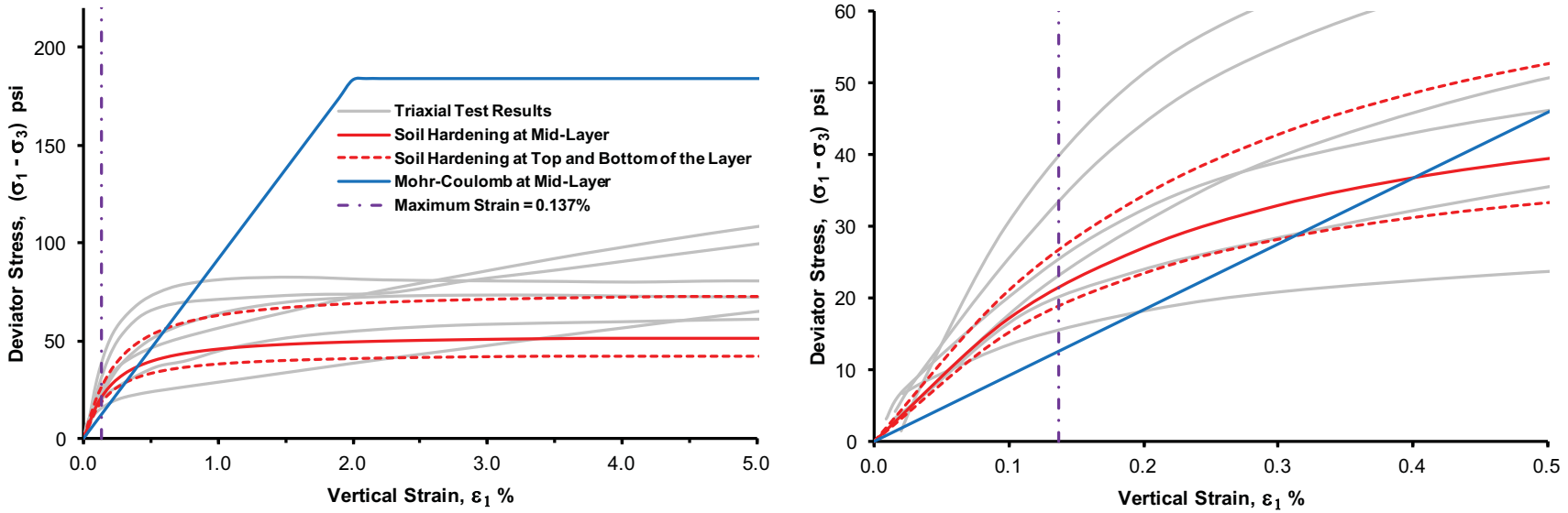

Figure 2.5.4-262 Plot of Soil Hardening Calibration for the Lower Tamiami

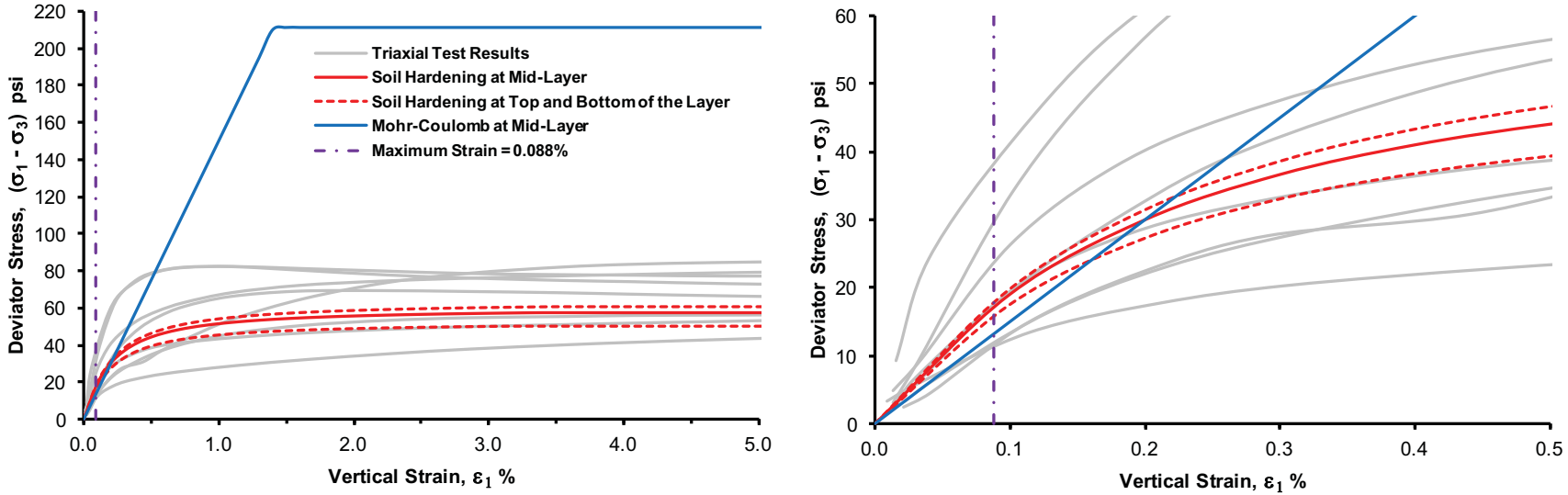

Figure 2.5.4-263 Plot of Soil Hardening Calibration for the Peace River

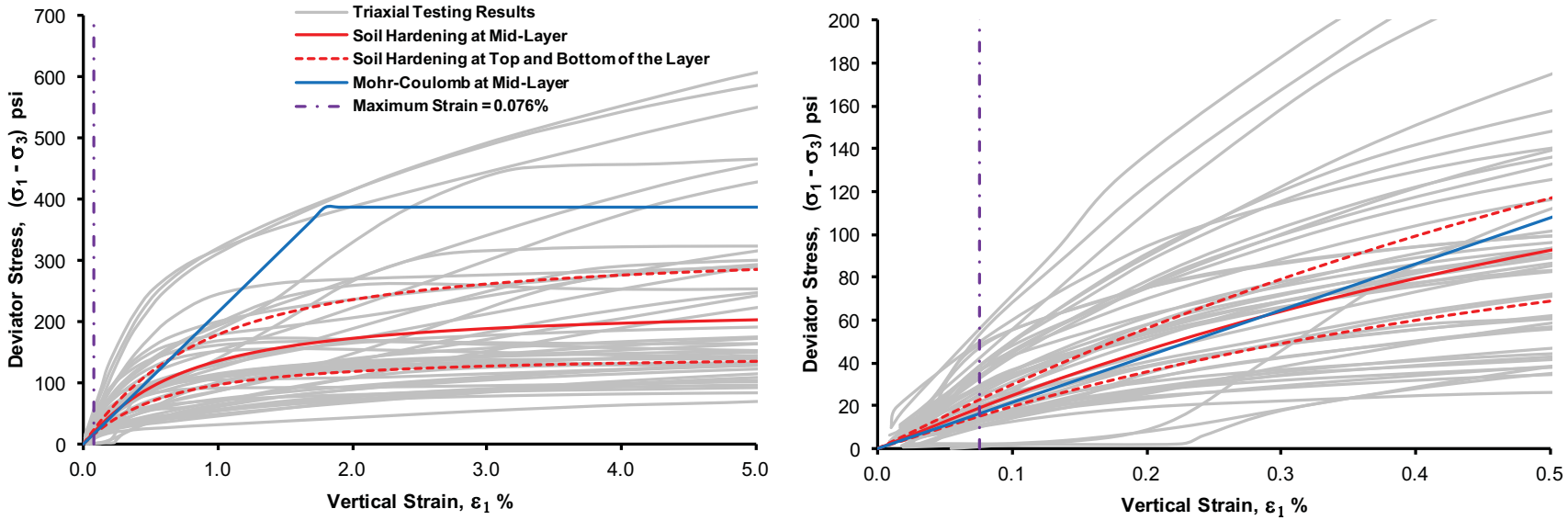

Figure 2.5.4-264 PLAXIS 3D Best Estimate Model Total Settlement After Loading

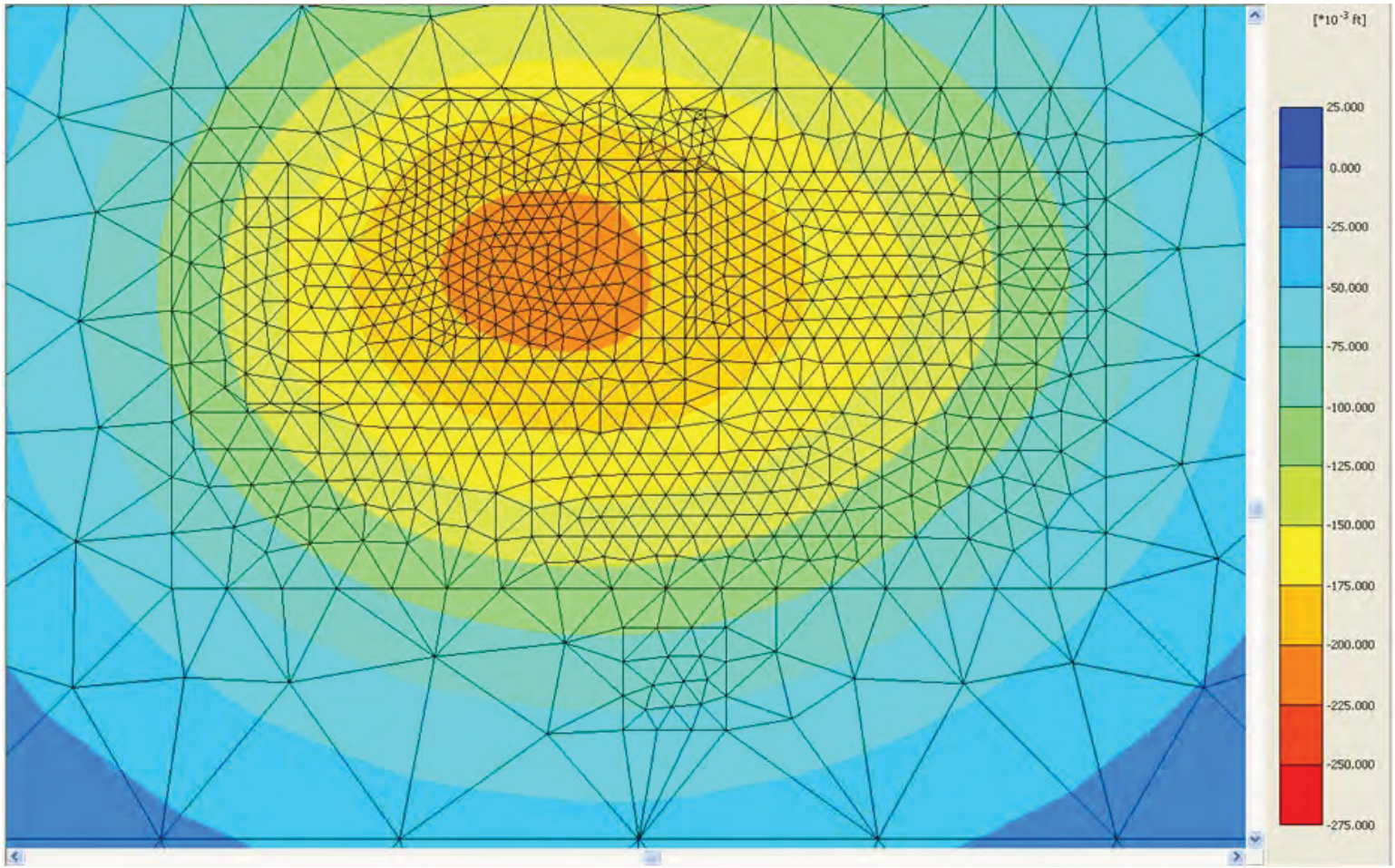

Figure 2.5.4-265 PLAXIS 3D Best Estimate Model Total Settlement After Rewatering

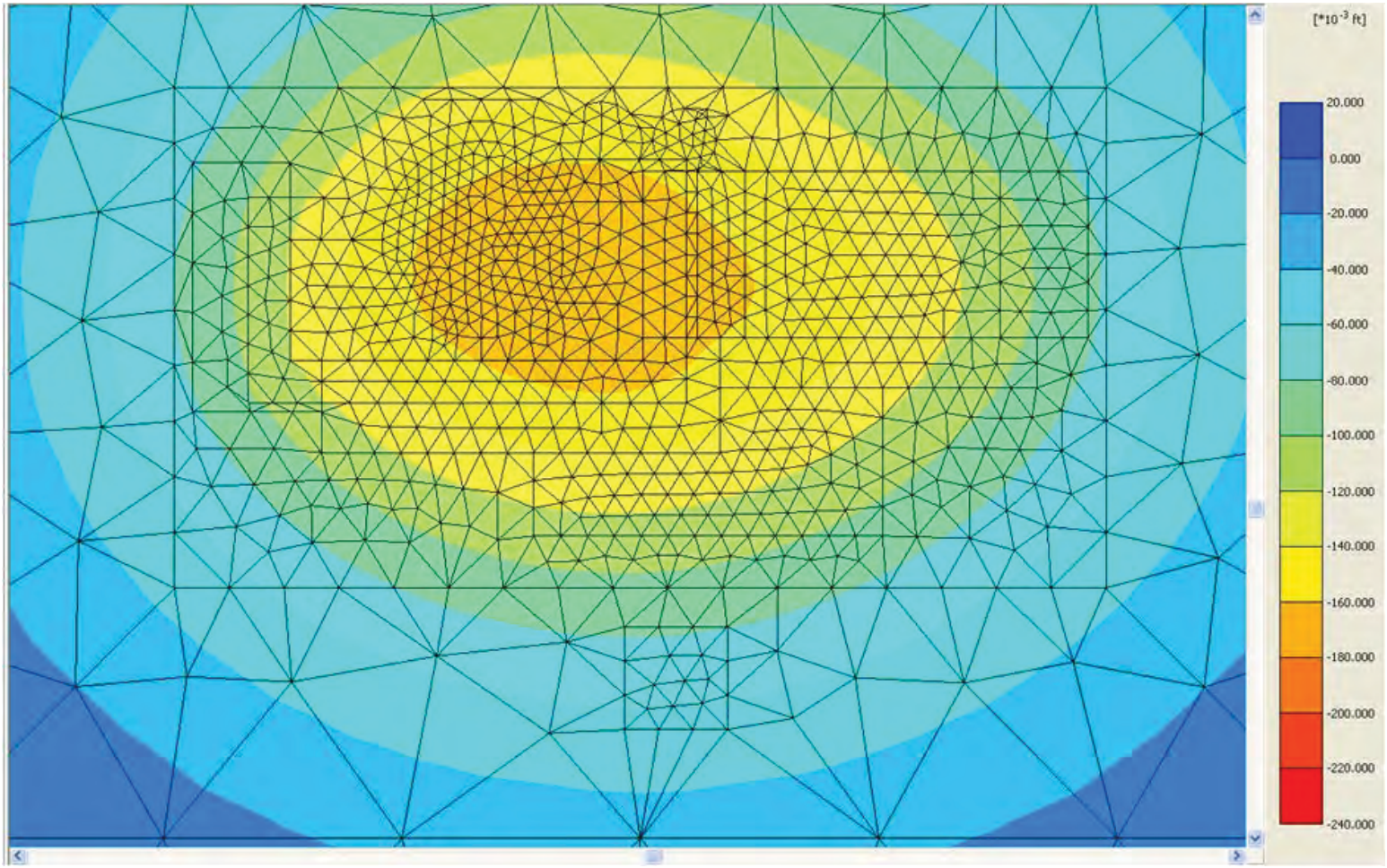

ASSOCIATED ENCLOSURES:

None

NRC RAI Letter No. PTN-RAI-LTR-040

SRP Section: 02.05.04 - Stability of Subsurface Materials and Foundations

QUESTIONS from Geosciences and Geotechnical Engineering Branch 1 (RGS1)

NRC RAI Number: 02.05.04-20 (eRAI 6006)

FSAR Subsection 2.5.4.10.3 indicates that the stress distribution used for the settlement calculation was based on Boussinesq distribution. The Boussinesq distribution is based on the assumption that the soil is a homogeneous, linear elastic, isotropic half-space media. In accordance with NUREG-0800, Standard Review Plan, Chapter 2.5.4, "Stability of Subsurface Materials and Foundations," please justify how this method is applicable for the site since a considerable variation in Elastic modulus was reported in the FSAR.

FPL RESPONSE:

The settlement calculation has been revised to use stress distributions appropriate for layered systems. For the nuclear island (NI), a stress distribution from Milovic (Reference 1) for a two-layered system was used with rock (Key Largo and Fort Thompson) as the first layer and soil (upper Tamiami, lower Tamiami, and Peace River) as the second layer. For the remaining buildings (turbine, first bay, annex, and radwaste), a stress distribution from Poulos and Davis (Reference 2) for a three layered system was used with the fill as the first layer; rock (Miami Limestone, Key Largo, and Fort Thompson) as the second layer; and soil (upper Tamiami, lower Tamiami, and Peace River) as the third layer. Since Poulos and Davis (Reference 2) only provides interface stresses and does not provide stresses for the top of the first layer or the bottom of the third layer, linear interpolation is used between the interface stresses from Poulos and Davis (Reference 2) and the top and bottom stresses from the Boussinesq case. It is appropriate to use the top and bottom stresses from Boussinesq because the top stress is equal to the building pressure and the bottom stress is very small due to the large depth. The entire Boussinesq stress distribution is not used in the settlement calculation because it is not appropriate for layered systems as it would yield a highly conservative stress profile. To show how the Boussinesq stress profile results in highly conservative stresses, it is compared to the stress distributions used from References 1 and 2 as well as the results of the finite element method (FEM) model.

<u>Nuclear Island:</u>

The Key Largo Limestone and the Fort Thompson Formation form a stiff upper layer, while the layers below (upper Tamiami, lower Tamiami, and Peace River) are comprised primarily of dense, silty sands. Because of this layering, a typical Boussinesq stress distribution may not provide realistic stress distributions, showing very high settlement in the deep sand layers. Therefore, the stress distribution for a two-layered system from Milovic (Reference 1) was used. This stress distribution is dependent on the stiffness ratio of the upper and lower layers, the thickness of the layers, the area of the building, and the depth of interest. This distribution assumes a Poisson’s ratio of 0.15 for the upper layer and 0.45 for the lower layer. The recommended Poisson’s ratios for the Key Largo and Fort Thompson formations are 0.3 and 0.34, respectively. The recommended Poisson’s ratios for the upper Tamiami, lower Tamiami, and Peace River formations are 0.3, 0.35, and 0.3, respectively. Although, the recommended Poisson’s ratios vary from the Poisson’s ratios

assumed by Milovic, the stress distribution obtained from Milovic is similar to the stress distribution obtained from the finite element model, indicating that the Poisson's ratio has a secondary effect on the stress distribution. This stress distribution assumes a circular foundation, therefore the radius and diameter of the foundation were found for a circular foundation of equivalent area to the NI.

To obtain this stress distribution, the problem is simplified as shown in Figure 1. The Key Largo and Fort Thompson layers are taken as one layer with a thickness of 80 feet, while the upper Tamiami, lower Tamiami, and Peace River layers are taken as the other layer with a thickness of 339 feet. The concrete is considered rigid with respect to the stiffness of the rock.

Figure 1 Geometry of the Two-Layered System

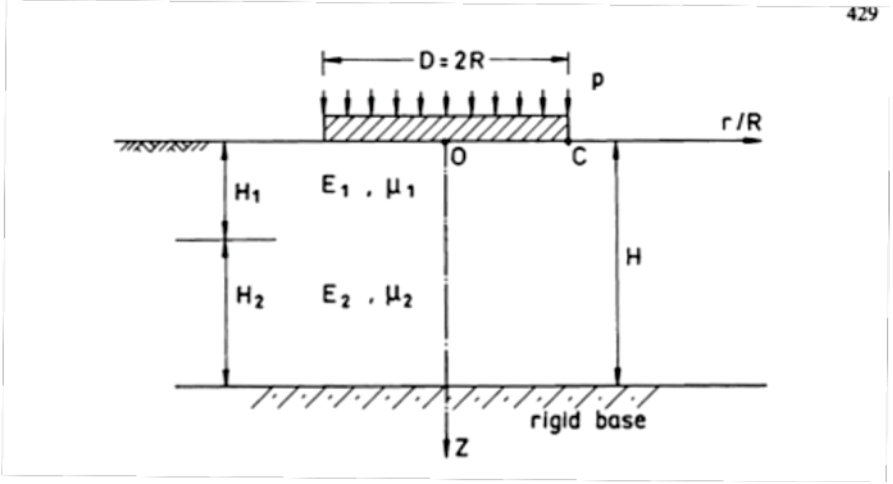

Source: Reference 1

Table 1 shows the Iz coefficients (taken as a percentage of building pressure) for the NI best estimate case.

Table 1
Iz Coefficients for the NI, H/D = 2, H_1 = 0.4D, E_1/E_2 = 10

z/D	Iz r/R = 0	Iz r/R = 1.0
0.05	0.94	0.500
0.15	0.738	0.441
0.25	0.496	0.328
0.35	0.337	0.253
0.45	0.272	0.220
0.55	0.252	0.205
0.65	0.233	0.192
0.75	0.217	0.180
0.85	0.202	0.170
0.95	0.189	0.160
1.1	0.172	0.149
1.3	0.155	0.135
1.5	0.141	0.124
1.7	0.129	0.115
1.9	0.118	0.103

Source: Reference 1

The points shown in Table 1 are plotted and a best-fit curve is generated. This curve is used to define the stress distribution below the NI. For the stress increment beneath the center of the foundation r/R = 0 is used, and for the stress increment beneath the edge of the foundation r/R = 1 is used.

Vertical incremental strains are calculated assuming linear elastic properties. The resulting settlement is obtained by integrating the vertical incremental strains over the soil/rock column.

In addition to the hand calculation described above, stress increments and settlement are modeled using the PLAXIS 3D foundation (PLAXIS 3D). PLAXIS 3D is a finite element method (FEM) based computer code designed for geotechnical analyses. The program calculates displacements with the use of numerical integration methods. In addition to the typical capabilities of a general FEM application for elastic solids, PLAXIS 3D incorporates advanced constitutive models, (stress vs. strain relationship) that are capable of simulating the response of soils to external loading.

The PLAXIS 3D model (Figure 2) includes the shield, auxiliary, radwaste, annex, annex office, and turbine buildings, as well as water tank structures. The PLAXIS 3D model developed uses the same material properties, layering information, building loads, and building areas as the hand calculation. In the PLAXIS 3D model, soil layers are modeled

using elasto-plastic Mohr-Coulomb model, since the strain levels are expected to be low and mostly within the elastic range. Therefore, the numerical finite element solution using PLAXIS 3D is considered to be comparable to the theoretical solution used by the hand calculation. For more information regarding the PLAXIS 3D settlement calculation, see the revised response to RAI 02.05.04-19.

Figure 2 PLAXIS 3D Model

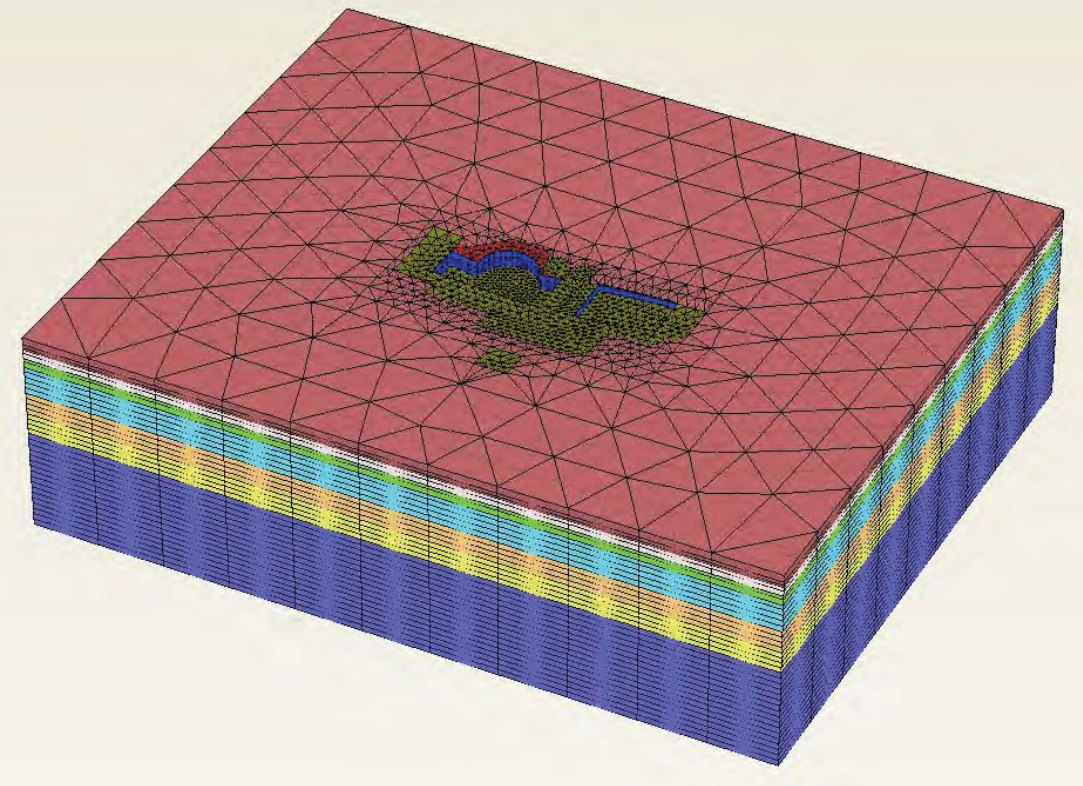

The stress distribution used from Milovic (Reference 1) is compared to the stress distribution provided by PLAXIS 3D as well as Boussinesq as shown in Figure 3.

Figure 3 Comparison of Stress Distributions

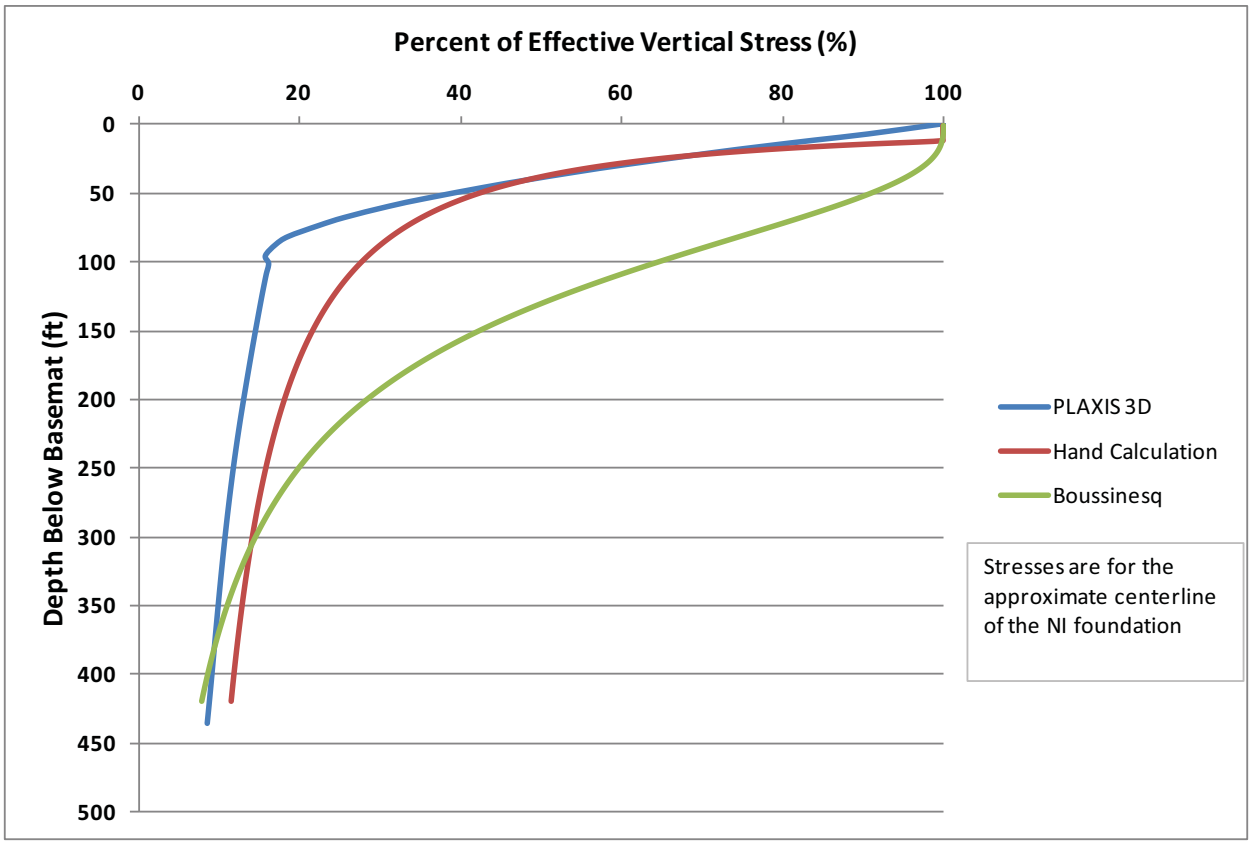

As shown in Figure 3, Boussinesq is highly conservative as it estimates higher stresses in both the rock and soil layers. The stress distribution found by using Reference 1 is similar to but more conservative than the PLAXIS 3D stress distribution. The difference between the PLAXIS 3D and the Milovic stress distributions can be attributed to the fact that PLAXIS 3D estimates the stresses based on all of the soil and rock strata, while the Milovic stress distribution approximates the system as two layers.

Turbine, First Bay, Annex, and Radwaste:

Due to the relatively more compressible fill placed on top of the Miami Limestone beneath the turbine, first bay, annex, and radwaste buildings, a stress distribution from Poulos and Davis (Reference 2) is used that is appropriate for three layered systems. The structural fill is taken as the first layer, the limestone layers (Miami Limestone, Key Largo, and Fort Thompson) are taken as the second layer, and the soils (upper Tamiami, lower Tamiami, and Peace River) are taken as the third layer.

Layer interface stresses are found from Reference 2 for the geometry shown in Figure 4.

Figure 4 Geometry of the Three-Layered System

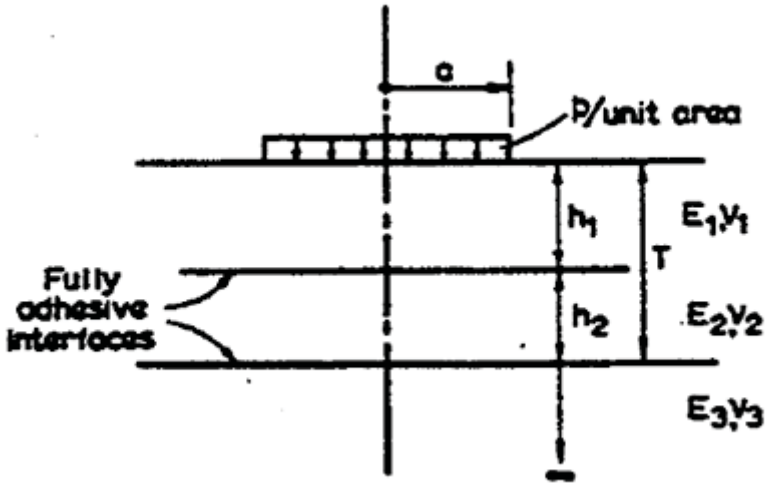

Source: Reference 2, Figure 6.17

Reference 2 provides tables with interface stresses based on the following parameters:

- $k_1 = E_1/E_2$
- $k_2 = E_2/E_3$
- $H = h_1/h_2$
- $a_1 = a/h_2$

The three-layered system has a k_1 value of 0.02. Since interface values are not provided in Poulos and Davis (Reference 2) with k_1 values as low as 0.02, extrapolation was used. Best-fit curves used for extrapolation have R^2 values higher than 0.99, suggesting that extrapolation is appropriate. Table 2 shows the interface stresses from Reference 2 with the values of H and k_2 closest to the parameters for the turbine, first bay, annex, and radwaste buildings (H = 0.25, k_2 = 20). For the table of interface stresses presented:

- σ_{z1} is the interface stress (percent of building pressure) at the upper interface
- σ_{z2} is the interface stress (percent of building pressure) at the lower interface

Table 2
Interface Stresses for Three-Layered Systems

$a_1 = 0.4$			$a_1 = 0.8$			$a_1 = 1.6$		
k_1	σ_{z1}	σ_{z2}	k_1	σ_{z1}	σ_{z2}	k_1	σ_{z1}	σ_{z2}
0.2	0.90	0.03	0.2	0.94	0.12	0.2	0.97	0.34
2	0.77	0.03	2	0.93	0.09	2	0.91	0.26
20	0.36	0.02	20	0.69	0.07	20	0.85	0.20
200	0.09	0.01	200	0.23	0.04	200	0.47	0.13

Source: Reference 2

Using extrapolation, the following values were found for $k_1 = 0.02$ (Table 3):

Table 3
Interface Stresses for $k_1 = 0.02$

a_1	σ_{z1}	σ_{z2}
0.4	0.92	0.04
0.8	0.95	0.14
1.6	0.98	0.41

Because a_1 values for the turbine ($a_1 = 1.0$) and radwaste ($a_1 = 0.6$) buildings are in between the a_1 values in Table 3, σ_{z1} and σ_{z2} were found by using interpolation. The interface stresses used for each building are shown in Table 4.

Table 4
Interface Stresses per Building for a Three-Layered System

	Turbine	First Bay	Annex	Radwaste
Upper Interface σz1	0.96	0.92	0.95	0.94
Lower Interface σz2	0.22	0.04	0.14	0.09

Since Poulos and Davis (Reference 2) only provides interface stresses and does not provide stresses for the top of the first layer or the bottom of the third layer, linear interpolation between the interface stresses from Poulos and Davis (Reference 2) and the top and bottom stresses from the Boussinesq case are then used to approximate the stress distribution.

To demonstrate that the stress distribution from Reference 2 is appropriate for the site, the stress distribution of the turbine building is compared to the stress distribution found in PLAXIS 3D as well as Boussinesq (Figure 5).

Figure 5 Comparison of Stress Distributions

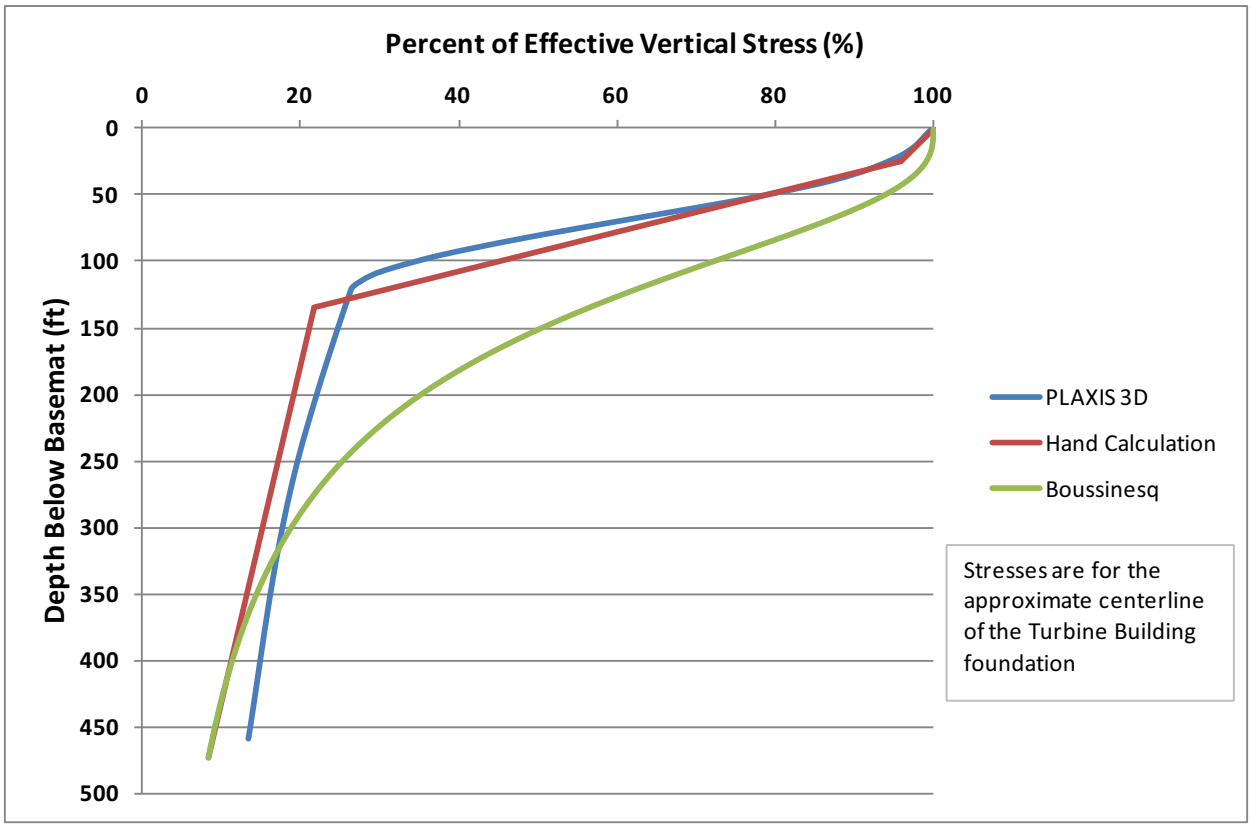

As shown in Figure 5, Boussinesq is highly conservative by estimating higher stresses in both the rock and soil layers. The stress distribution found by using Reference 2 is very similar to the PLAXIS 3D stress distribution demonstrating that it is appropriate for the settlement calculation.

Conclusion:

As shown in Figures 3 and 5, the stress distributions used for the settlement hand calculation from References 1 and 2 are similar to the stress distributions found from the PLAXIS 3D model. The Boussinesq stress distributions are shown to be highly conservative for the site and are not used.

This response is PLANT SPECIFIC.

References:

1. Milovic, D., *Stresses and Displacements for Shallow Foundations*, Elsevier, 1992.
2. Poulos, H. G. and E.H. Davis, *Elastic Solutions for Soil and Rock Mechanics*, John Wiley & Sons, Inc., 1974.

ASSOCIATED COLA REVISIONS:

Revisions associated with FSAR Subsection 2.5.4.10.3 and FSAR Table 2.5.4-219 are provided in the revised response to RAI 02.05.04-19.

ASSOCIATED ENCLOSURES:

None

NRC RAI Letter No. PTN-RAI-LTR-040

SRP Section: 02.05.04 - Stability of Subsurface Materials and Foundations

QUESTIONS from Geosciences and Geotechnical Engineering Branch 1 (RGS1)

NRC RAI Number: 02.05.04-22 (eRAI 6006)

The lateral earth pressure diagram shown in Figure 2.5.4-240 shows a plot corresponding to the dynamic lateral earth pressure. The shape of this plot appears to be consistent with the shape for dynamic pressure considering a rigid structural wall (see ASCE 4). In Section 2.5.4.10.4.2 “Seismic Lateral Earth Pressures”, the active seismic pressure was computed using the Mononobe- Okabe equation. The last sentence of the section indicates that at-rest pressure as a function of depth for below-grade walls is developed consistent with Reference 277 (ASCE-4) using the design ground motion. It is noted that the pressure developed using the ASCE-4 methodology uses the zpa value from the input motion.

Figure 2.5.2-252 shows the input motion (GMRS) developed for the site, the GMRS is located at Elevation 35. In this Figure the zpa is approximately 0.058g. However, the elevation of the GMRS is considerably lower than the surface of the soils adjacent to the basement walls that are to be evaluated for seismic lateral earth pressure. In accordance with NUREG-0800, Standard Review Plan, Chapter 2.5.4, "Stability of Subsurface Materials and Foundations," please clarify on the definition of the design ground motion, and how that motion is consistent with Appendix S to 10CFR50.

FPL RESPONSE:

FSAR Figure 2.5.2-253 and FSAR Table 2.5.2-228 show the zero period acceleration (zpa) for the GMRS as about 0.058g. This zpa value was not considered appropriate when computing lateral earth pressure because it was developed for El. -35 feet. The design response spectra (DRS) at 5% damping, calculated at the ground surface for the near nuclear island (NI) and far from NI soil sites, were considered appropriate for computing lateral earth pressure, using the envelope of low frequency (LF) and high frequency (HF) acceleration response spectra (ARS) at 10-4 and 10-5 annual probability of exceedance. These ARS envelopes and the DRS are plotted in Figures 1 and 2 for the near NI and far from NI soil sites, respectively. From Figures 1 and 2, the peak ground acceleration at the ground surface is equal to approximately 0.0824g and 0.0806g (DRS at 100 Hertz [Hz]) for the near NI and far from NI soil sites, respectively.

Regarding the computation of active seismic pressure using the Mononobe-Okabe equation, according to Seed and Whitman (FSAR Section 2.5.4 Reference 276), use of horizontal ground acceleration for design at the base level of the wall may result in underestimating the movements. FSAR Section 2.5.4 Reference 276 states that it seems best to use the acceleration at the surface of the backfill, or an average between the surface and the base of the wall. Thus, an acceleration of 0.1g rather than the peak ground acceleration of 0.0824g (near NI) or 0.0806g (far from NI), is conservatively used in the Mononobe-Okabe equation. This value is also consistent with the minimum peak ground acceleration of 0.1g as defined in the Standard Review Plan 3.7.2 Section II.2 and 10 CFR 50 Appendix S.

Similarly, for the computation of at-rest seismic pressure using ASCE 4-98 (FSAR Section 2.5.4 Reference 277), an acceleration of 0.1g, rather than the peak ground acceleration of 0.0824g (near NI) or 0.0806g (far from NI), is conservatively used.

Figure 1 5% Damping ARS at Ground Surface – Near NI, Envelope of LF and HF

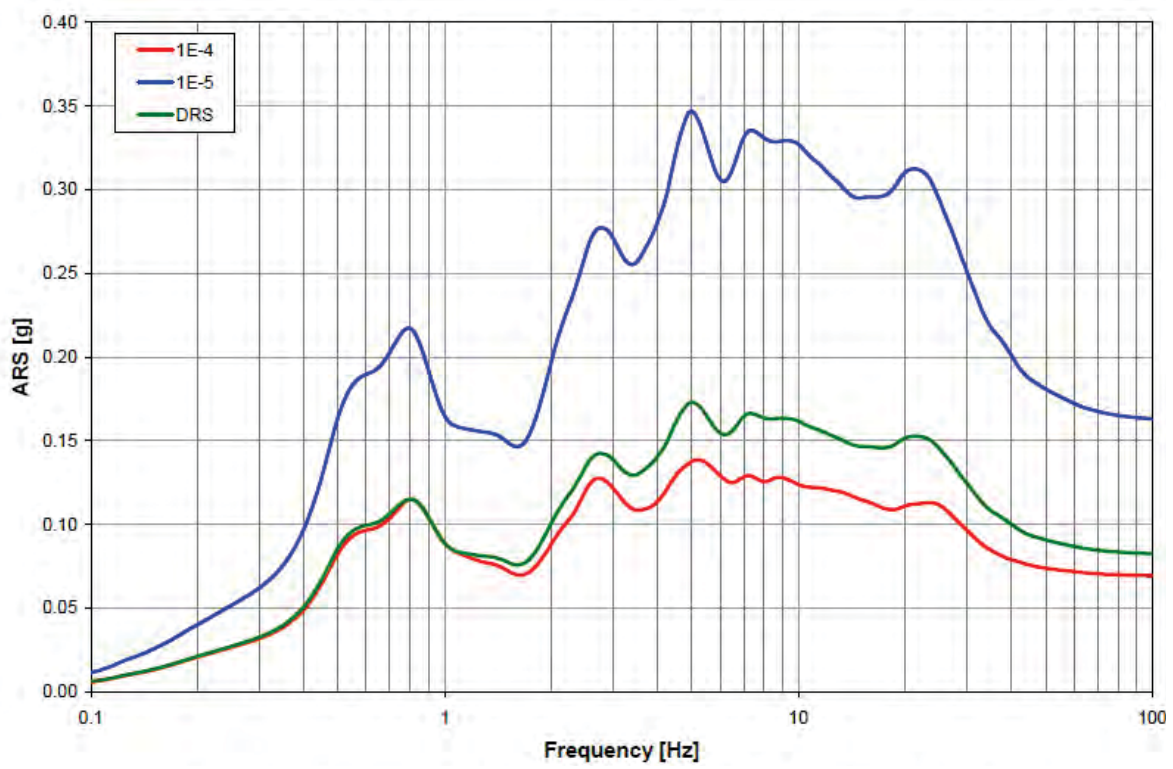

Figure 2 5% Damping ARS at Ground Surface – Far from NI, Envelope of LF and HF

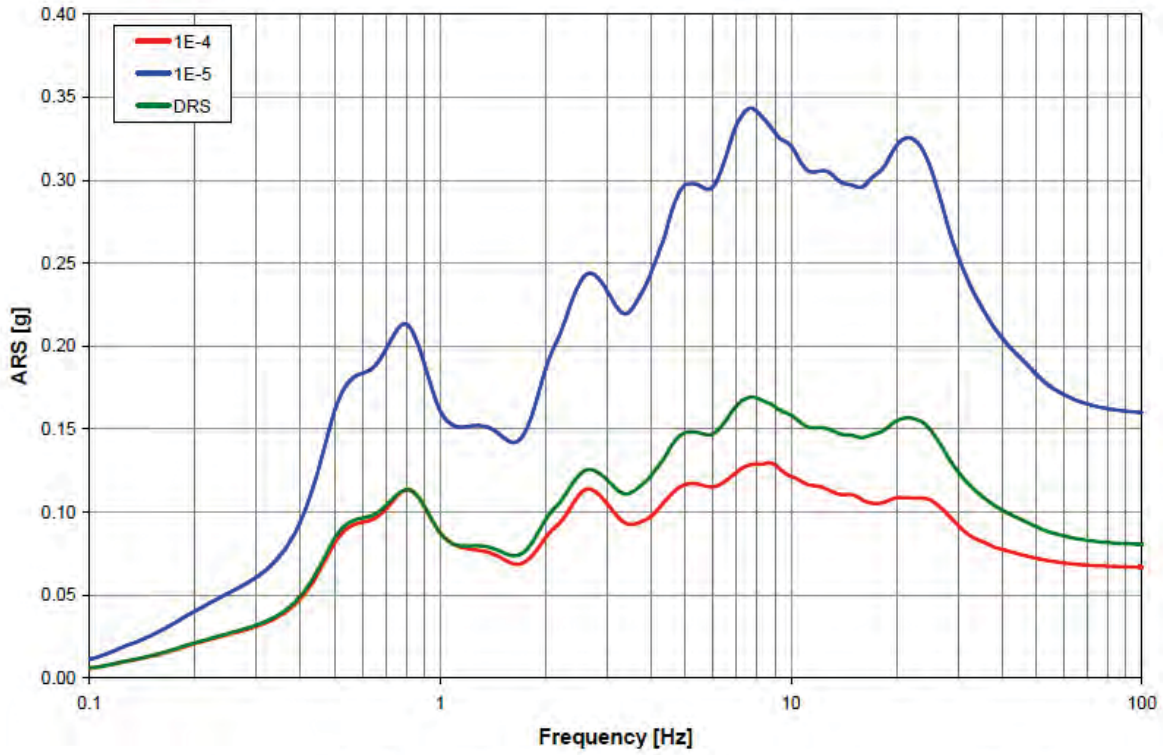

This response is PLANT SPECIFIC.

References:

None

ASSOCIATED COLA REVISIONS:

None

ASSOCIATED ENCLOSURES:

None

NRC RAI Letter No. PTN-RAI-LTR-040

SRP Section: 02.05.04 - Stability of Subsurface Materials and Foundations

QUESTIONS from Geosciences and Geotechnical Engineering Branch 1 (RGS1)

NRC RAI Number: 02.05.04-23 (eRAI 6006)

FSAR Section 2.5.4.10.4.3 states that a surcharge pressure of 500 psf was included when calculating the lateral earth pressures, however the calculation for COL static and seismic lateral earth pressures states that the adjacent building loads and the equipment loads were not considered. In accordance with NUREG-0800, Standard Review Plan, Chapter 2.5.4, "Stability of Subsurface Materials and Foundations," please describe the selection of 500 psf.

FPL RESPONSE:

As indicated in FSAR Subsection 2.5.4.10.4.3, an area-wide surcharge pressure of 500 pounds per square foot (psf) is included in the earth pressure calculations. For the active condition presented in Figure 1 and for the at-rest condition presented in Figure 2, this loading represents the temporary construction loading, and does not include the permanent adjacent building loads. As indicated in FSAR Subsection 2.5.4.10.4.3, the validity of this pressure will be reviewed during the detailed design phase. This temporary loading is conservatively twice the typical design pressure for heavy truck loading (Reference 1).

To address adjacent building loads, an additional case considering a surcharge pressure of 4000 psf is presented in Figures 3 and 4. This surcharge is adopted because it is the highest expected building bearing pressure for the buildings founded on fill around the nuclear island. This pressure will also be reviewed during the detailed design phase.

Figure 1 Active Earth Pressure Considering a 500 psf Surcharge on Fill

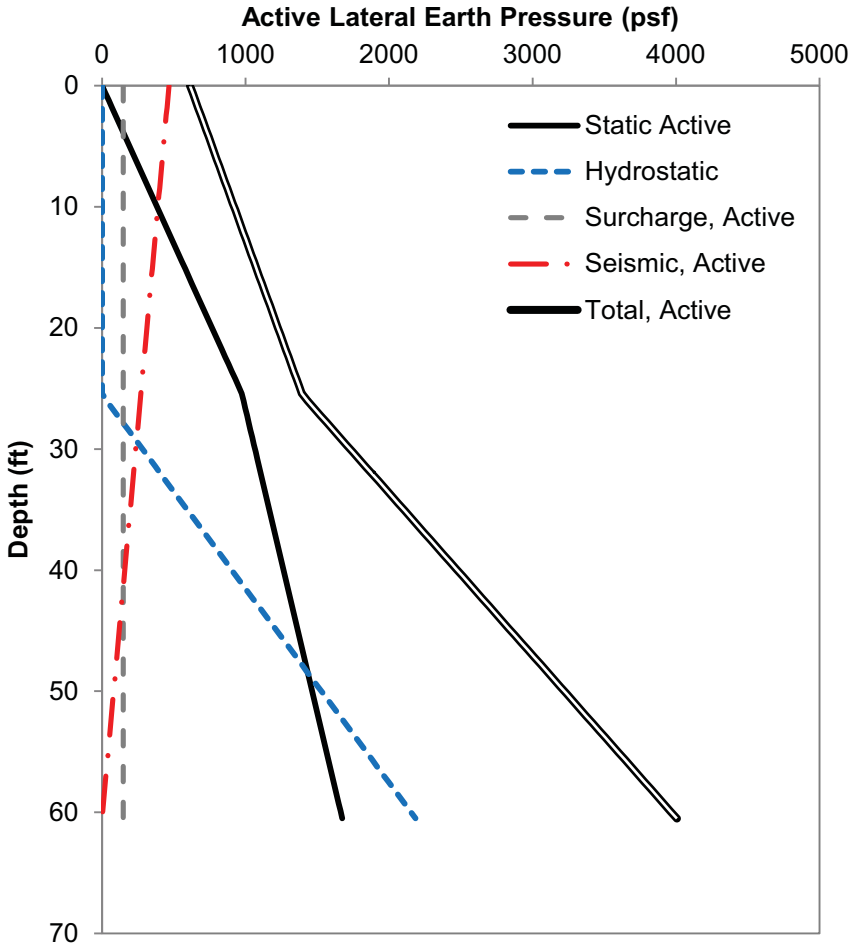

Figure 2 At-Rest Earth Pressures Considering a 500 psf Surcharge on Fill

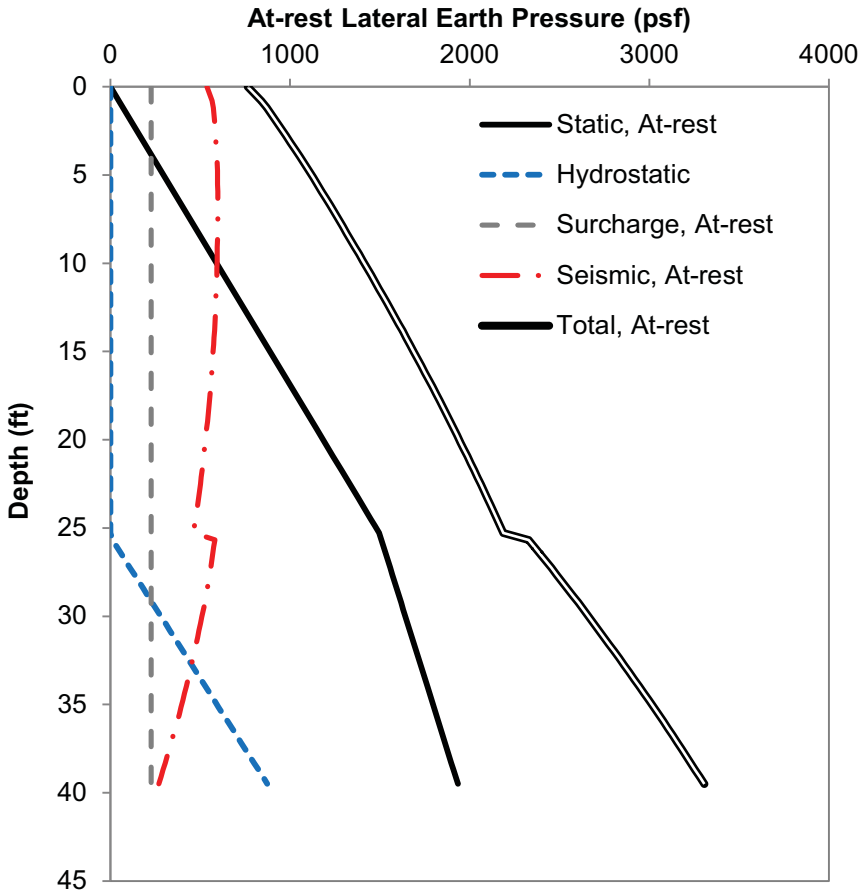

Figure 3 Active Earth Pressure Considering a 4000 psf Surcharge on Fill

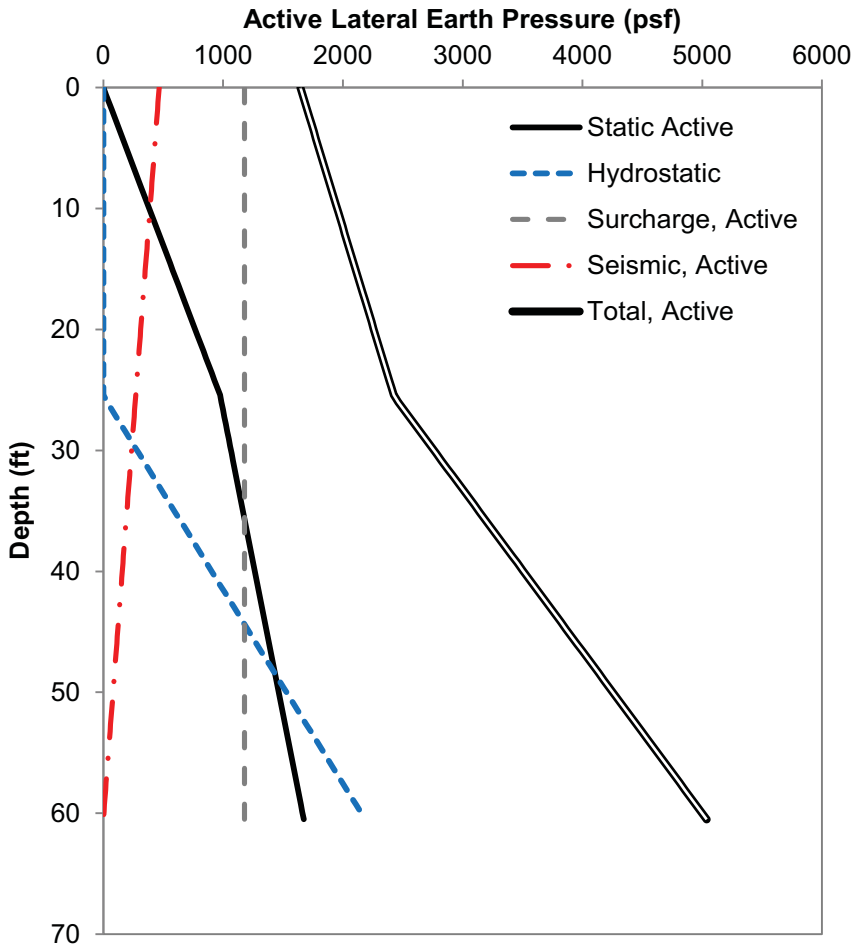

Figure 4 At-Rest Earth Pressures Considering a 4000 psf Surcharge on Fill

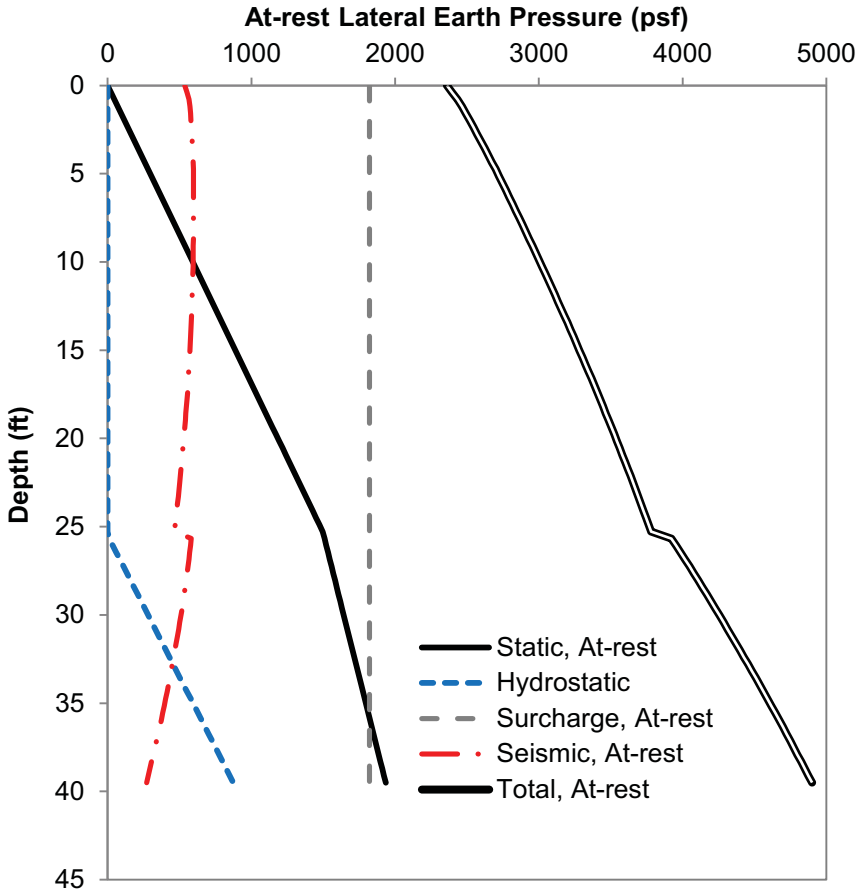

This response is PLANT SPECIFIC.

References:

1. International Code Council, *2006 International Building Code,* Table 1607.1, Items 24 and 33, January 2006.

ASSOCIATED COLA REVISIONS:

The last paragraph FSAR Subsection 2.5.4.10.4.3 will be revised in a future revision as follows:

Note that ~~a~~ surcharge pressure**s** of 500 psf **and 4000 psf are**~~is~~ included in the earth pressure calculations summarized here. The validity of ~~this~~**these** pressure**s are**~~is~~ reviewed during the detailed design phase.

FSAR Subsection 2.5.4.10.4.4, will be revised in a future revision as follows:

Using the relationships outlined above and the compacted limerock fill properties summarized in Table 2.5.4-209, sample earth pressure diagrams are developed. Compacted limerock fill properties (granular soils) used have a unit weight (γ_t) of 130 pcf and a drained friction angle (φ') of 33 degrees (refer to Table 2.5.4-209). These values apply to both structural and general fill. ~~A u~~**U**niform surcharge load**s** of 500 psf **and 4000 psf are**~~is~~ included.

FSAR Subsection 2.5.4.10.5, will be revised in a future revision as follows:

Recommended diagrams for use in calculating lateral earth pressures against walls are developed based on strata thicknesses and lateral earth pressure coefficients. Figure**s** 2.5.4-239 **(500 psf surcharge) and 2.5.4-252 (4000 psf surcharge)** show~~s~~ the diagram**s** for above grade walls where the walls can rotate or deflect away from the soil mass, known as the active case. This case considered walls extending from the highest finish grade (El. +25.5 feet) to a depth of El. –35 feet, and models active earth pressures on the diaphragm wall during the construction period.

Figure**s** 2.5.4-240 **(500 psf surcharge) and 2.5.4-253 (4000 psf surcharge)** show~~s~~ the pressure diagram**s** for below grade walls where no rotation is possible (at-rest case). This case considers walls from El. +25.5 feet to El. –14 feet, the base of the deepest structure wall.

The last paragraph FSAR Subsection 2.5.4.11 will be revised in a future revision as follows:

Subsection 2.5.4.10 also addresses criteria for static and seismic earth pressure estimation. The calculated lateral earth pressure diagrams shown on Figures 2.5.4-239**,** ~~and~~ 2.5.4-240**, 2.5.4-252, and 2.5.4-253** are best estimates, and thus contain a FOS = 1.0. In the analyses of sliding and overturning due to these lateral loads when the seismic component is included, a FOS = 1.10 is recommended.

FSAR Table 2.5.4-209 will revised in a future revision as follows:

Table 2.5.4-209
Summary of Recommended Geotechnical Engineering Parameters

Stratum[(a)]	1[(a)]	2	3	4	5	6	7	8	Fill
Description	**Muck**	**Miami**	**Key Largo**	**Ft. Thompson**	**Upper Tamiami**	**Lower Tamiami**	**Peace River**	**Arcadia**	**—**
Elevation of top of layer (ft)	–1.2	–4.5	–26.7	–49.4	–115.1	–159.0	–215.2	–452.1	—
USCS symbol	ML, MH	GM, GP-GM, SM, SW-SM, SW, SP-SM	Limestone	Limestone	SM, SP-SM	ML	SM	Limestone	—
Total unit weight, γ (pcf)	80	125	136	139	120	120	120	130	130
Natural water content, w, (%)	>80	—	—	—	—	30	—	—	33
Fines content (%)	>60	18	—	—	28	62	16	—	15
Atterberg limits									
Liquid limit, LL	—	—	—	—	—	24	—	—	—
Plastic limit, PL	—	—	—	—	—	20	—	—	—
Plasticity index, PI	—	—	—	—	—	4	—	—	—
SPT N_{60}-value (blows/ft)	~0	20	—	—	40	32	75	—	30
Undrained properties									
Undrained shear strength, s_u (ksf)	—	—	—	—	—	4.0	—	—	—
Internal friction angle, φ, (deg)	—	—	—	—	—	—	—	—	—
Drained properties									
Effective cohesion, c' (ksf)	—	—	—	—	0	1.7	0	—	—
Effective friction angle, φ' (deg)	—	—	—	—	35	20	40	—	33
Average Rock core recovery (%)	—	—	83 to 96	41 to 98	—	—	—	63 to 100	—
Average RQD (%)	—	—	54 to 81	16 to 91	—	—	—	32 to 90	—
Unconfined compressive strength, U (psi)	—	200	1,500	2,000	—	—	—	100	—
Elastic modulus (high strain), E_H	—	630 ksi	2,600 ksi	1,500 ksi	1,500 ksf	2,500 ksf	2,700 ksf	980 ksi	1,100 ksf
Elastic modulus (low strain), E_L	—	950 ksi	2,600 ksi	1,500 ksi	19,700 ksf	25,750 ksf	27,400 ksf	980 ksi	9,100 ksf
Shear modulus (high strain), G_H	—	230 ksi	1,000 ksi	550 ksi	550 ksf	900 ksf	1,000 ksf	360 ksi	420 ksf
Shear modulus (low strain), G_L	—	350 ksi	1,000 ksi	550 ksi	7,300 ksf	9,500 ksf	10,150 ksf	360 ksi	3,500 ksf
Shear wave velocity, V_S, (ft/sec)	—	3,600	5,800	4,250	1,400	1,600	1,650	3,600	860
Compression wave velocity, V_C, (ft/sec)	—	8,000	11,000	8,700	2,900	3,300	3,450	7,850	1,600
Coefficient of sliding	—	0.6	0.7	0.7	0.4	0.3	—	—	0.5
Poisson's ratio, *v'*	—	0.37	0.31	0.34	0.35	0.35	0.35	0.36	0.3
Static earth pressure coefficients									
Active, K_a	—	0.3	—	—	0.27	0.5	—	—	**0.29**
At-rest, K_o	—	0.5	—	—	0.5	0.66	—	—	**0.46**

(a) Properties of Stratum 1 (muck) are not provided as this stratum was removed prior to construction.
The values tabulated for use as design guideline only. Refer to specific boring logs, CPT logs, and laboratory test results for appropriate modifications at specific design locations.
USCS = Unified Soil Classification System (ML = silt; MH = silt of high plasticity; GM = silty gravel; GP = poorly graded gravel; SM = silty sand; SW = well graded sand; SP = poorly graded sand).

FSAR Figure 2.5.4-239 will be replaced with the following figure in a future revision:

FSAR Figure 2.5.4-239 ~~Lateral Earth Pressure Diagram: Active Case~~Active Earth Pressure Considering a 500 psf Surcharge on Fill

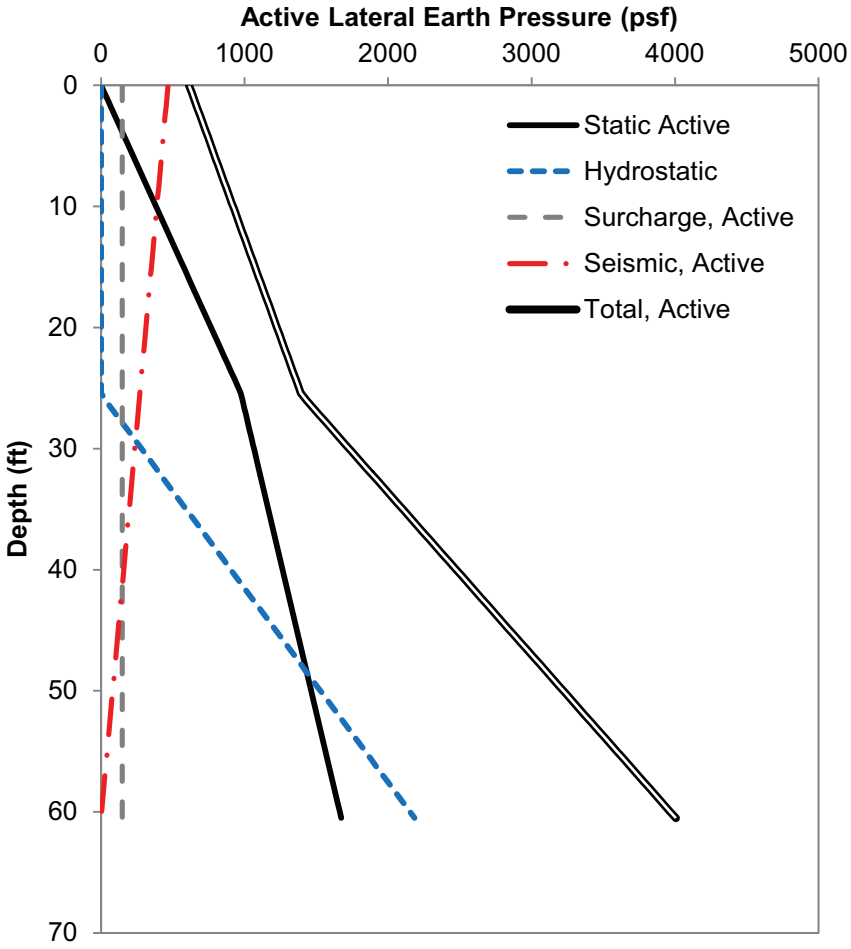

Data from Table 2.5.4-209 for compacted limerock fill.

FSAR Figure 2.5.4-240 will be replaced with the following figure in a future revision:

FSAR Figure 2.5.4-240 ~~Lateral Earth Pressure Diagram: At-Rest Case~~At-Rest Earth Pressures Considering a 500 psf Surcharge on Fill

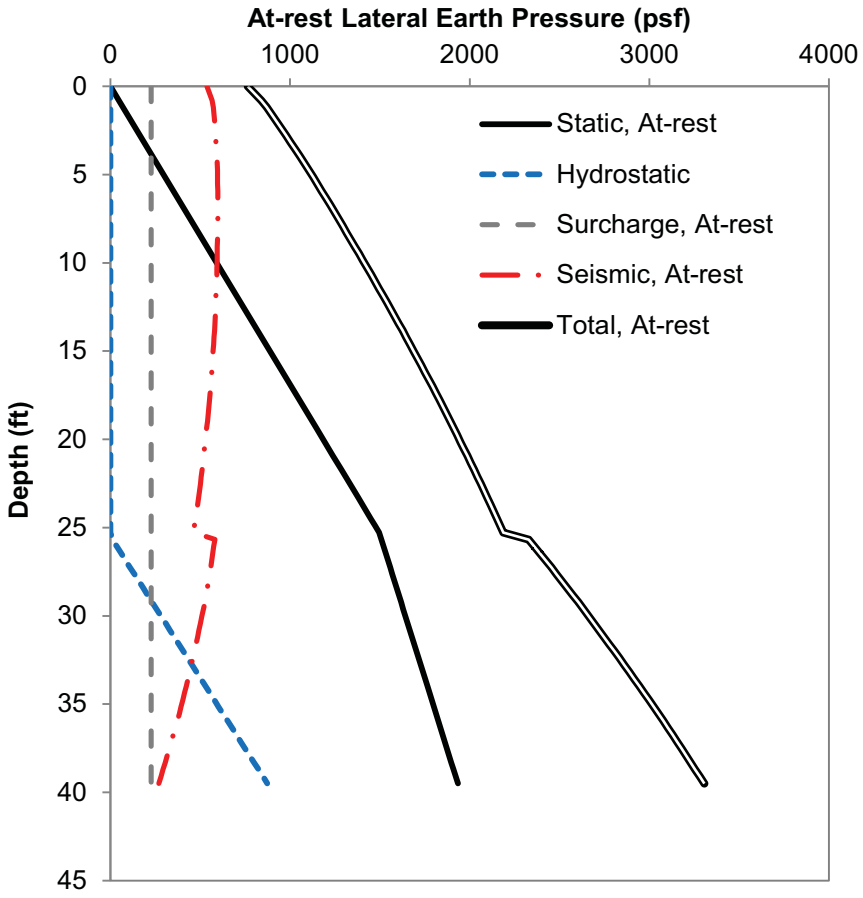

Data from Table 2.5.4-209 for compacted limerock fill.

FSAR Figures 2.5.4-252 and 2.5.4-253 will be added in a future revision:

FSAR Figure 2.5.4-252 Active Earth Pressure Considering a 4000 psf Surcharge on Fill

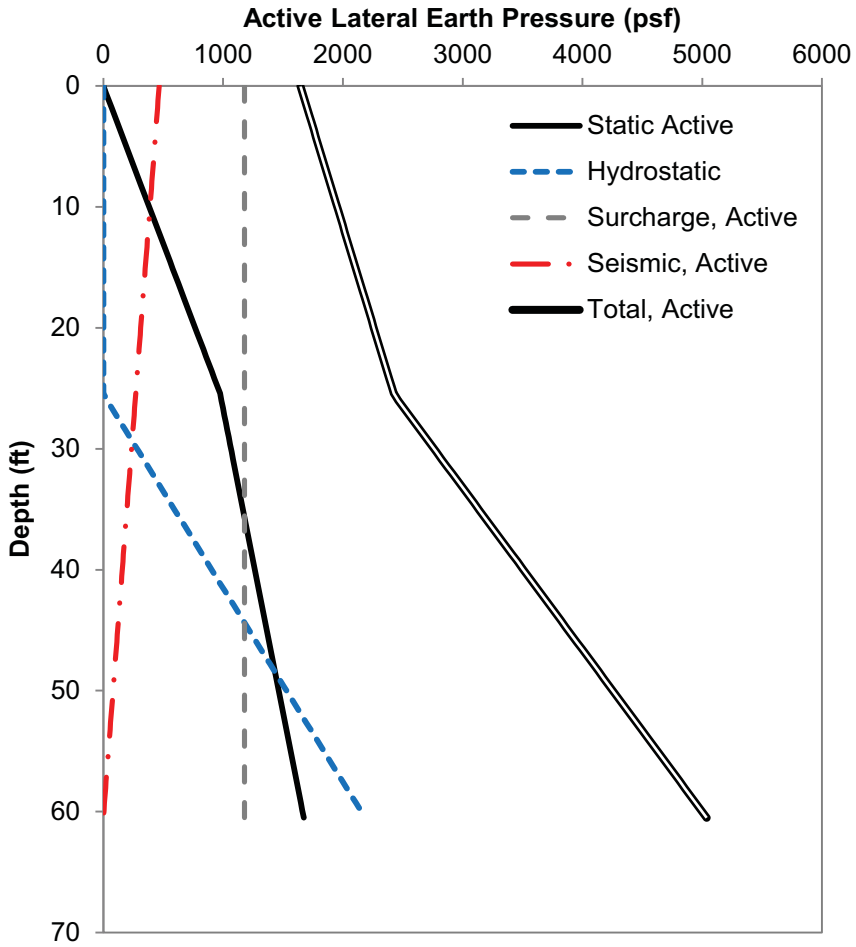

Data from Table 2.5.4-209 for compacted limerock fill.

FSAR Figure 2.5.4-253 At-Rest Earth Pressures Considering a 4000 psf Surcharge on Fill

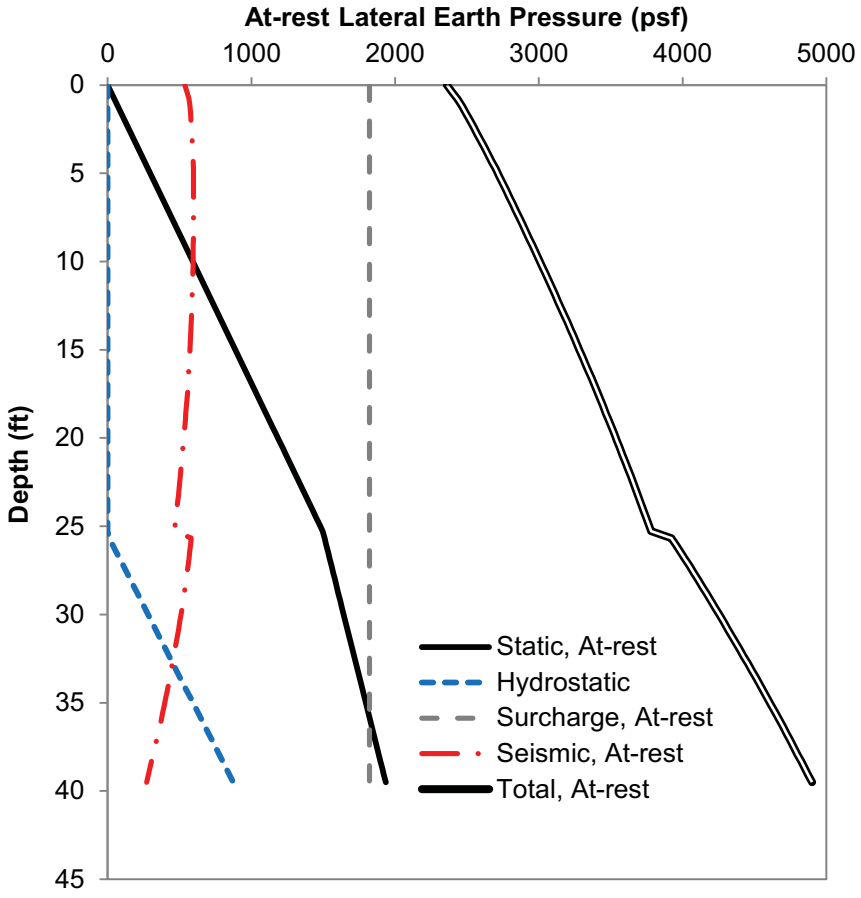

Data from Table 2.5.4-209 for compacted limerock fill.

ASSOCIATED ENCLOSURES:

None

NRC RAI Letter No. PTN-RAI-LTR-040

SRP Section: 02.05.04 - Stability of Subsurface Materials and Foundations

QUESTIONS from Geosciences and Geotechnical Engineering Branch 1 (RGS1)

NRC RAI Number: 02.05.04-24 (eRAI 6006)

FSAR Section 2.5.4.10.4 states that the active seismic lateral earth pressures were computed using the Mononobe-Okabe methodology and ASCE Standard 4- 98 was used to calculate the at-rest seismic lateral earth pressures. The calculation for COL static and seismic lateral earth pressures calculates at-rest seismic lateral earth pressures using Ostadan method. In accordance with NUREG-0800, Standard Review Plan, Chapter 2.5.4, "Stability of Subsurface Materials and Foundations," please clarify which method was ultimately used for design purposes and provide a justification regarding why ASCE Standard 4-98 was referenced in the FSAR and not Ostadan's method.

FPL RESPONSE:

NUREG-0800 Standard Review Plan, Section 3.8.1 outlines the criteria acceptable to meet the relevant requirements of the U.S. Nuclear Regulatory Commission (NRC) regulations. The subsection titled *Dynamic Soil Pressure* on page 3.8.1-14 of the Standard Review Plan provides that the dynamic lateral earth pressure be calculated in accordance with ASCE 4-98 Section 3.5.3.2.

Seismic active lateral earth pressures were calculated using the Mononobe-Okabe method (FSAR Section 2.5.4 Reference 276) as specified in ASCE 4-98 (FSAR Section 2.5.4 Reference 277) and seismic at-rest lateral earth pressures were calculated using the elastic method as specified in ASCE 4-98 (FSAR Section 2.5.4 Reference 277).

This response is PLANT SPECIFIC.

References:

None

ASSOCIATED COLA REVISIONS:

None

ASSOCIATED ENCLOSURES:

None